Influence of steady-state and transient flow conditions on the bearing capacity of shallow foundations in unsaturated soils

By

Mengxi Tan

Thesis submitted in partial fulfillment of the requirements for the

Doctorate in Philosophy degree in Civil Engineering

Department of Civil Engineering

Faculty of Engineering

University of Ottawa

ABSTRACT

Shallow foundations are widely used in different types of soils for supporting the loads from the lightly loaded superstructures of various civil infrastructures both on level and sloping ground. Design of shallow foundations in geotechnical engineering practice is widely based on the principles of saturated soil mechanics because they are relatively simple. However, the soil near the ground surface (i.e., vadose zone) in which the shallow foundations are typically placed is in an unsaturated state. The water content variation in unsaturated soils is influenced by hydrological events such as the snow melt, rainfall infiltration, evaporation, and the plant transpiration. Due to this reason, the hydro-mechanical properties (i.e., coefficient of permeability, shear strength and volume change) of unsaturated soils are sensitive to the variation in soil suction associated with water content changes. These properties in turn have a significant impact on the bearing capacity and settlement behavior of the shallow foundations. Therefore, it is rational to investigate shallow foundations' behavior extending the principles of unsaturated soil mechanics.

During the last two decades, there has been a significant interest towards investigating shallow foundations based on unsaturated soil mechanics. Laboratory, field, and model studies highlight that matric suction variation in unsaturated soils has a significant influence on the bearing capacity and settlement behavior of shallow foundations. However, the focus of most of the presently available studies in the literature consider mostly vertical loading conditions on level soil ground. There are limited studies related to the design of shallow foundations on sloping ground and subjected to inclined and eccentric loading conditions. Also, there are only few studies that consider the effect of the steady state and transient flow conditions on the foundation bearing capacity evaluation. Therefore, one of the key objectives of this thesis is directed toward developing rational tools for investigating shallow foundations considering the steady state and transient flow conditions associated with water infiltration and evaporation in unsaturated soils. Comprehensive investigation studies are undertaken to interpret the influence of the steady state and transient flow conditions on the shallow foundations related to: (i) bearing capacity on the sloping ground in different types of soils including expansive soils, and (ii) bearing capacity under the inclined and eccentric loading conditions with homogeneous

soil properties and considering spatial variation of soil properties. Succinct details related to investigated studies are summarized below:

(1) An analytical method is proposed for quantifying the bearing capacity of the shallow foundations on unsaturated soil slopes considering different rainfall infiltration conditions. The proposed method is a novel tool for considering the simultaneous influence of several parameters that include the flow rates, the infiltration duration, the foundation set-back distance and the ground water table depth on the foundation bearing capacity.

(2) Another analytical method is proposed for evaluating the foundation bearing capacity under inclined and eccentric loading considering both the steady state and transient flow conditions. Semi-empirical equations are proposed for describing the failure envelops in vertical and horizontal (V - H) loading space and in the vertical and moment (V - M) loading space. These equations are capable to describe the variation of failure envelops considering the influence of the groundwater table depth variation, internal friction angles, surface flux boundary conditions and different infiltration durations.

(3) The influence of infiltration on the combined performance of both the foundation and the slope in cracked expansive soils is evaluated with the aid of a numerical technique. A semi-empirical model that describes the elastic modulus and the matric suction is implemented into the numerical model. Bimodal soil water characteristic curve is used as a tool for understanding the influence of surface cracks in the numerical study in a simplified manner. The influence of the rainfall intensity, rainfall duration, foundation setback distance and foundation loading on the combined performance of foundation and slope were investigated. Results combined with some suggestions for rational design procedures are presented that can be useful for geotechnical engineers in practice applications.

(4) Numerical analyses are conducted for shallow foundations under vertical and combined loading subjected to different flow conditions. A numerical code procedure is exclusively developed as a part of this study to: (i) consider the variation of soil properties along with the matric suction fluctuations in the commercial software ABAQUS with the aid of a user developed subroutine USDFLD; (ii) incorporate the spatial variability of soil properties into the finite element model. Comparisons are provided between the numerical study and other methods such as the experimental investigations, the analytical methods,

and the semi-empirical equations for bearing capacity failure envelopes. In addition, comparisons are also made between the failure envelopes and the failure mechanisms contour using the model considering soil spatial variability and homogeneous soil properties.

The proposed methods in this thesis are simple to use for evaluating bearing capacity of shallow foundations that are subjected to steady state and transient state flow conditions considering two scenarios: (i) foundation on sloping ground (ii) foundation under inclined and eccentric loading. The results from the above studies reveal that it is the relationship between the soil permeability and the rainfall characteristics that mainly control the water infiltration rates. The soil suction and the effective degree of saturation are influenced by the water infiltration rates and have a significant impact on the foundation as well as the slope behavior. More importantly, the investigations undertaken in this thesis contribute towards addressing the research gaps related to the behavior of foundations in unsaturated soils. Various scenarios considered in this thesis include the influence of unsaturated flow have not been considered earlier in the literature. The results of the studies summarized in this thesis are expected to be useful for practicing geotechnical engineers in the optimal design of shallow foundations extending the principles of unsaturated soil mechanics for various soils. Moreover, the proposed methods can be used for interpreting the foundation behavior for their entire life span service. In addition, these methods can be employed to rationally explain the field-measured data and can also be used in the forensics analyses of failed slopes and shallow foundations.

ACKNOWLEDGEMENTS

The research studies presented in this thesis were conducted under the supervision of Professor Sai K. Vanapalli at the Department of Civil Engineering, University of Ottawa. I would like to express my deepest gratitude to Prof. Vanapalli for his patient guidance, continuous encouragement, and unwavering support throughout my entire doctoral study. He generously shares his extensive academic knowledge and helps me shape my academic growth to be a qualified researcher as well as a teacher. He also takes care students' physical and mental health while they are working on their research programs; I am particularly touched with the approach that he has taken especially during the COVID-19 pandemic period. I feel fortunate to be inspired by Prof. Vanapalli's philosophy both in my professional and personal life.

The financial supports received from the China Scholarship Council (CSC) – University of Ottawa joint scholarship, the Natural Sciences and Engineering Research Council of Canada (NSERC) are gratefully acknowledged. Additionally, I would like to express my appreciation to Faculty of Engineering at University of Ottawa which provides me the international experience scholarship to support my visit study at Durham University in UK.

I would like to extend my sincere thanks to my thesis committee members, Prof. Farshid Vahedifard, Prof. Siva Sivathayalan, Prof. Mamadou Fall and Prof. Julio Angel Infante Sedano. I'm also grateful to Prof. David Toll and Prof. Alexandros Petalas at Durham University for their guidance and support during my visiting study in UK.

Special thanks to the officers in Faculty of Engineering, Luc, Jean-Claude and Olga. Many thanks to my colleagues and friends: Penghai, Xiuhan, Junping, Ping, Xiaokun, Ruixia, Maha, Xinting, Xinye, Mingshu, Junjie, Yao, Aolin, Pan, Xingyi, Ziwen, Hao and Alpesh.

I am deeply indebted to my parents for their encouragement and unconditional support throughout my years of study. It is their endless love that provides me courage to overcome any difficulty and challenge. This thesis would not have been possible without their love and inspiration.

TABLE OF CONTENTS

ABSTRACT II

ACKNOWLEDGEMENTS V

TABLE OF CONTENTS VI

LIST OF TABLES X

LIST OF FIGURES XI

CHAPTER 1 1

Introduction 1

1.1 Background 1
1.2 Novelty, objectives, and methodology 5
1.3 Thesis Layout 9
1.4 Related publications 12
Reference 14

CHAPTER 2 18

Literature Review 18

2.1 Introduction 18
2.2 Shear strength background 18
2.3 Foundation on level ground of unsaturated soil 23
2.3.1 Foundation subjected to vertical loading on unsaturated soil 23
2.3.2 Foundation subjected to inclined and eccentric loadings 33
2.4 Foundation design on sloping ground 38
2.4.1 Foundation on saturated soil slope 38
2.4.2 Foundation on unsaturated soil slope 44
2.5 Summary 45
References 47

CHAPTER 3 57

Foundation bearing capacity estimation on unsaturated soil slope under transient flow condition 57

3.2 Background and governing equations ... 59
3.2.1 Shear strength and failure criterion ... 59
3.2.2 Stress equations ... 62
3.2.3 Analytical solution to suction profile under transient flow ... 63
3.3 Problem introduction ... 66
3.3.1 Problem definition ... 66
3.3.2 Boundary value problem and solution procedure ... 67
3.4 Procedure verification ... 71
3.4.1 Validation of foundation bearing capacity in saturated soil ((u_a - u_w) = 0)) ... 72
3.4.2 Comparitive studies related to effective degree of saturation, S_e and suction profiles ... 73
3.4.3 Comparative study on foundation bearing capacity in unsaturated soil ... 75
3.5 Parametric studies on foundation bearing capacity ... 76
3.5.1 Effect of rainfall characteristics-Study I ... 78
3.5.2 Effect of slope angle-Study II ... 82
3.5.3 Effect of foundation setback ratio-Study III ... 84
3.5.4 Effect of ground water table depth-Study IV ... 86
3.6 Discussion ... 90
3.7 Conclusions ... 93
References ... 95
CHAPTER 4 ... 102
Failure envelops for foundation subjected to inclined and eccentric loading considering steady state and transient flow conditions in unsaturated soils ... 102
4.1 Introduction ... 102
4.2 The slip line framework ... 106
4.2.1 Slip line equations ... 106
4.2.2 Suction profile under steady state flow ... 110
4.2.3 Suction profile under transient flow ... 111
4.2.4 The framework for slip line method ... 112
4.3 Proposed framework verification ... 115
4.3.1 Foundation subjected to inclined and eccentric loads ... 115
4.3.2 Foundation performance considering unsaturated flow conditions ... 117

4.4 Problem definition 120
4.5 Foundation with non-eccentric inclined loading 121
4.5.1 Influence of steady state flow on the bearing capacity 122
4.5.2 Influence of transient flow on the bearing capacity 129
4.6 Foundation with eccentric vertical loadings 133
4.6.1 Influence of steady state flow on the bearing capacity 134
4.6.2 Influence of transient flow on the bearing capacity 138
4.7 Proposed semi-empirical failure envelope equations 141
4.8 Comparison studies 143
4.8.1 Comparison study I 143
4.8.2 Comparison study II 144
4.9 Discussion 148
4.10 Conclusions 151
References 154
CHAPTER 5 160
Shallow foundation behavior on an expansive soil slope subjected to different infiltration conditions 160
5.1 Introduction 160
5.2 Methodology 164
5.2.1 Governing equations 164
5.2.2 Constitutive relationships 165
5.2.3 Shear strength and modulus of elasticity 167
5.2.4 Slope stability 168
5.3 Model details and validation 171
5.3.1 Model details 171
5.3.2 Model validation 177
5.4 Results 179
5.4.1 Foundation bearing capacity 179
5.4.2 Slope stability 184
5.5 Discussion and limitation of the present study 190
5.6 Conclusions 196
References 199

CHAPTER 6 204

Numerical studies on foundation behavior in unsaturated soils subjected to vertical and inclined and eccentric loading 204

6.1 Introduction 204
6.2 Methodology 207
6.2.1 Finite element model details 208
6.2.2 Soil spatial variability 212
6.2.3 Numerical modeling framework 215
6.3 Comparison studies for foundations on homogeneous soils 217
6.3.1. Comparison study I 217
6.3.2 Comparison study II 220
6.4 Comparison studies for foundation on soil with spatial variable properties 224
6.4.1 Soil saturated hydraulic conductivity 225
6.4.2 Soil effective cohesion and internal friction angle 228
6.5 Summary and conclusion 232
Reference 235

CHAPTER 7 241

Conclusions and suggestions for future work 241

7.1 Major Conclusions 241
7.1.1 State-of-the-art review 242
7.1.2 Foundation bearing capacity estimation on unsaturated soil slope under transient flow condition 242
7.1.3 Failure envelopes for foundation subjected to inclined or eccentric loading considering steady and transient state flow. 243
7.1.4 Foundation on cracked expansive soil slope subjected to rainfall infiltration 244
7.1.5 Numerical studies on foundation behavior in unsaturated soils subjected to vertical and inclined and eccentric loading 245
7.2 Suggestions for future work 246

LIST OF TABLES

Table 2.1. Summary of the foundation bearing capacity equations in unsaturated soil ... 24
Table 2.2. Summary of the experimental studies ... 27
Table 2.3 Summary of the inclination factors ... 34
Table 2.4 Summary of failure envelop equations ... 35
Table 2.5 Summary of studies on foundation on sloping ground ... 39
Table 3.1 Soil paramters information from two studies ... 73
Table 3.2 Soil properties and other information used in the comparative study ... 76
Table 3.3 Summary of parametric studies ... 77
Table 3.4 Soil properties used in the study ... 78
Table 3.5 Relative deviation of $Q/\gamma B$ of 0 day compared to that of 120 days (q / k_s =1) ... 88
Table 4.1 Summary of the bearing capacity factors ... 116
Table 4.2 Soil properties used in comparative studies ... 117
Table 4.3 Properties of the soils used in the study ... 121
Table 4.4 Details of various parameters used in the study ... 121
Table 4.5 Deviation of the bearing capacity for δ = 0° and δ = 25° ... 125
Table 4.6 Proposed semi-empirical equations ... 142
Table 4.7 Summary of the parameters used in various cases ... 146
Table 4.8 Soil properties used for comparison ... 149
Table 5.1 Soil properties ... 174
Table 6.1 Soil properties for the sand ... 220
Table 6.2 Soil properties used in the numerical model ... 221
Table 6.3 Summary of soil properties statistics ... 225

LIST OF FIGURES

Fig. 1.1 Pore water pressure distribution profiles in unsaturated soil................................ 2
Fig. 1.2 Thesis layout.. 12
Fig. 2.1 Relationship between SWCC and soil shear strength: (a) Typical soil water characteristic curve; (b) Shear strength variation of unsaturated soils 21
Fig. 2.2 Average matric suction values for footing with different sizes........................... 29
Fig. 2.3 Typical failure mechanisms.. 43
Fig. 3.1. Extended Mohr stress circle in unsaturated soil and stress state of a point *A* 62
Fig. 3.2 Definition of the problem and different failure modes....................................... 67
Fig. 3.3 Schematic diagram of iteration points in the slip line method and boundary value problem: (a) Iteration point; (b) b = 0; (c) $b \neq 0$; (d) Bearing capacity failure. 69
Fig. 3.4 Flow chart of the proposed framework... 71
Fig. 3.5 Comparison of results obtained in this study to the published literature on saturated soils.. 73
Fig. 3.6 Comparison of S_e, normalized (u_a - u_w) along with z/H_w under transient flow condition: (a) S_e along z/H_w for silt; (b) Normalized (u_a - u_w) along z/H_w for silt; (c) S_e along z/H_w for clay; (d) Normalized (u_a - u_w) along z/H_w for clay..... 74
Fig. 3.7 Comparison of results obtained using the proposed method and that in the literature: (a) Comparison of vertical stress along the foundation base; (b) Comparison of the bearing capacity of foundation.. 76
Fig. 3.8 Effect of rainfall characteristic on the normalized bearing capacity (H_w/B = 3): (a) Clay; (b) Silt 1; (c) Silt 2 79
Fig. 3.9 Critical slip surface under the influence of rainfall infiltration (b/B = 0, H_w/B = 3): (a) Level ground for clay; (b) Sloping ground for clay; (c) Level ground for silt 1; (d) Sloping ground for silt 2.. 80
Fig. 3.10 Contribution of matric suction under transient flow condition (ϕ' = 25°): (a) (u_a - u_w) S_e tan ϕ' variation with matric suction; (b) (u_a - u_w) S_e tan ϕ' variation with normalized depth; (c) matric suction with normalized depth; (d) SWCC of the three soils.. 82
Fig. 3.11 Influence of the slope angle on the normalized bearing capacity and critical slip line: (a) Clay; (b) Silt 1; (c) Silt 2; (d) Critical slip line of clay; (e) Critical slip line of silt 1; (f) Critical slip line of silt 2 83
Fig. 3.12 Effect of foundation setback ratio on the normalized bearing capacity: (a) Clay; (b) Silt 1; (c) Silt 2.. 85

Fig. 3.13 Critical slip surface with different foundation setback ratios (β = 20°, q/k_s = 1): (a) b/B = 0; (b) b/B = 1; (c) b/B = 2; (d) b/B > 3 86
Fig. 3.14 Effect of the ground water table depth on the normalized bearing capacity: (a) Clay; (b) Silt 1; (c) Silt 2 87
Fig. 3.15 Contribution of matric suction for silt 1 soil: (a) $(u_a - u_w)$ S_e tan ϕ' with suction; (b) $(u_a - u_w)$ S_e tan ϕ' with normalized depth; (c) matric suction with normalized depth; (d) SWCC of silt 1 soil.. 89
Fig. 3.16 Average soil unit weight in the slip line method 91
Fig. 3.17 Influence of the soil unit weight: (a) Clay; (b) Silt 1; (c) Silt 2 91
Fig. 4.1 Shallow foundation subjected to different loading conditions: (a) Scenario 1: Axial vertical loading; (b) Scenario 2: Inclined loading without eccentricity; (c) Scenario 3: Eccentric vertical loading 105
Fig. 4.2 Stress state of foundation subjected to inclined loading: (a) Definition of the coordinate; (b) Mohr circle associated with inclined loading.......................... 108
Fig. 4.3 Flow chart of the slip line procedure 114
Fig. 4.4 Comparison between the results from the present study and published results from the literature: (a) Foundation with inclined loading; (b) Foundation with eccentric loading. 116
Fig. 4.5 Comparison of proposed framework with published studies (a) $[S_e(u_a - u_w)]$ under steady state condition; (b) $[S_e(u_a - u_w)]$ under transient flow condition; (c) Vertical stress along foundation width under steady state condition; (d) Vertical stress under transient condition; (e) Hydrostatic condition. 118
Fig. 4.6 Influence of the loading inclination angle under steady state flow: (a) Effect of δ on Q of clay soil; (b) Influence of the q and H_w on $V - H$ loading for clay; (c) Normalized failure envelope for clay; (d) Effect of δ on Q of silt soil; (e) Influence of the q and H_w on $V - H$ loading for silt; (f) Normalized failure envelope for silt.. 124
Fig. 4.7 Influence of the soil internal friction angle: (a) Influence of the ϕ' on the Q for clay soil; (b) Effect of ϕ' on the V, H loading of clay soil; (c) Normalized failure envelope for clay; (d) Influence of the ϕ' on the Q for silt soil; (e) Effect of ϕ' on the V, H loading of silt soil; (f) Normalized failure envelope for silt 128
Fig. 4.8 Influence of the foundation bearing capacity under the transient flow condition (H_w = 8 m): (a) Effect of δ on the Q for clay; (b) V, H loading for clay; (c) Normalized failure envelope for clay; (d) Effect of δ on the Q for silt; (e) V, H loading for silt; (f) Normalized failure envelope for silt.............................. 130

Fig. 4.9 Normalized failure envelopes in the $V - H$ loading space at different H_w: (a) For clay at H_w = 4 m; (b) For clay at H_w = 8 m; (c) For silt at H_w = 4 m; (d) For silt at H_w = 8 m. ... 132
Fig. 4.10 [$S_e (u_a - u_w) \tan\phi'$] variation along the Y coordinates ... 133
Fig. 4.11 Foundation subjected to eccentric vertical loading ... 134
Fig. 4.12 Effect of the eccentric loading for steady state flow: (a) Effect of q and H_w on the V, M loading for clay; (b) Normalized failure envelope for clay; (c) Effect of q and H_w on the V, M loading for silt; (d) Normalized failure envelope for silt ... 137
Fig. 4.13 Influence of the soil internal friction angle on the $V - M$ loading space (q = -3.14×10^{-8} m/s): (a) V, M loading components in clay; (b) Normalized failure envelope for clay; (c) V, M loading components in silt; (d) Normalized failure envelope for silt ... 138
Fig. 4.14 Effect of the eccentric loading under transient flow (q_{in} = 3.14×10^{-8} m/s): (a) Effect of infiltration duration for clay; (b) H_w = 8 m for clay; (c) H_w = 4 m for clay; (d) Effect of infiltration duration for silt; (e) H_w = 8 m for silt; (f) H_w = 4 m for silt. ... 140
Fig. 4.15 Comparison of the proposed equation with the results obtained from the slip line method: (a) For clay in $V - H$ loading space; (b) For silt in $V - H$ loading space; (c) For clay in $V - M$ loading space; (d) For silt in $V - M$ loading space. ... 144
Fig. 4.16 Comparison with additional data: (a) Case 1 and 2 in $V - H$ loading space; (b) Case 1 and 2 in $V - M$ loading space; (c) Case 3 and 4 in $V - H$ loading space; (d) Case 3 and 4 in $V - M$ loading space; (e) Case 5 and 6 in $V - H$ loading space; (f) Case 5 and 6 in $V - M$ loading space; (g) Case 7 and 8 in $V - H$ loading space; (h) Case 7 and 8 in $V - M$ loading space; ... 147
Fig 4.17 Hysteretic soil water characteristic curves (modified from Jeong et al. 2018) 149
Fig 4.18 Failure envelops obtained from the drying and wetting curves (infiltration under 1×10^{-7} m/s): (a) 0 day for $V - H$ loading space; (b) 0 day for $V - M$ loading space; (c) 10 days for $V - H$ loading space; (d) 10 days for $V - M$ loading space ... 150
Fig. 5.1 Problem definition: (a) Water cycle; (b) Foundation on cracked soil slope ... 164
Fig. 5.2 Flow chart with details of steps of modelling ... 172
Fig. 5.3 Model details ... 174
Fig. 5.4 The Regina clay soil properties: (a) Grain size distribution; (b) SWCC; (c) Soil hydraulic conductivity ... 175

Fig. 5.5 Precipitation records in Regina, Canada.. 177
Fig. 5.6 Comparison between results of this study and Qi and Vanapalli (2015a): (a) PWP distribution; (b) Modulus of elasticity 178
Fig. 5.7 Bearing capacity comparison: (a) Bearing capacity determination; (b) Comparison with published studies 179
Fig. 5.8 Foundation bearing capacity for different rainfall scenarios: (a) Bearing capacity under different rainfall intensities; (b) Yielding contour corresponding to the ultimate bearing capacity; (c) Maximum shear strain contour (d) Maximum shear strain under different rainfall intensities 181
Fig. 5.9 Effect of foundation setback ratios: (a) q_1; (b) q_2; (c) q_3; (d) Yield contour; (e) Maximum shear strain contour under q_1; (f) Maximum shear strain contour under q_3 183
Fig. 5.10 CFS with various loading conditions for different rainfall scenarios: (a) Without foundation loading; (b) With ultimate bearing capacity loading; (c) With allowable bearing capacity loading.. 185
Fig. 5.11 Vertical displacement of the slope surface without foundation loading: (a) q_1; (b) q_2; (c) q_3 188
Fig. 5.12 Effect of foundation set back ratio: (a) With ultimate bearing capacity loading; (b) With allowable bearing capacity loading; (c) Critical slip surface corresponding to CFS under bearing capacity failure...................................... 189
Fig. 5.13 Comparison of the finite element stress based method and Morgenstern-Price method: (a) CFS, (b) Normal stress along the deep seated failure surface, (c) Normal stress along the surface/toe failure surface, (d) Deep seated failure comparison, (e) Comparison at 30 days of rainfall, (f) comparison at 60 days of rainfall, (g) Comparison at 90 days of rainfall 193
Fig. 5.14 PWP variation at the surface of the slope under rainfall infiltration: (a) q_1; (b) q_2; (c) q_3; (d) Relationship between the soil hydraulic conductivity and rainfall intensity 195
Fig. 6.1 Flow chart of developed USDFLD and the random field generation................ 207
Fig. 6.2 Details of the numerical model.. 208
Fig. 6.3 Mesh sensitivity results 209
Fig. 6.4 Loading paths and failure envelopes: (a) Swipe test; (b) Probe test 211
Fig. 6.5 Flow chat of the numerical modeling framework 216
Fig. 6.6 Strip footing model test setup and the corresponding numerical model: (a) Test rig; (b) Numerical model.. 218
Fig. 6.7 SWCC for the sand used in the numerical model... 219
Fig. 6.8 Comparison results between the FE analysis and the experimental study 220

Fig. 6.9 Foundation subjected to inclined and eccentric loading: (a) Inclined loading; (b) Eccentric loading 221
Fig. 6.10 SWCC of the Indian Head till... 222
Fig. 6.11 Comparison of the failure envelope obtained from various methods: (a) *V*-*H* loading space for hydrostatic condition; (b) *V*- *M* loading space for hydrostatic condition; (c) *V*- *H* loading space for transient condition; (d) *V*-*M* loading space for transient condition. 223
Fig. 6.12 Random fields of k_s: (a) Random field 1; (b) Random field 2 226
Fig. 6.13 Results comparison: (a) Section diagram; (b) Pore water pressure profile at section 1-1; (c) Pore water pressure profile at section 2-2............................... 226
Fig. 6.14 Comparison of normalized failure envelopes: (a) Normalized failure envelopes in *V*-*H* loading space (b) Normalized failure envelopes in *V*-*M* loading space.. 227
Fig. 6.15 Random fields of c' and ϕ': (a) Random field 1 of c'; (b) Random field 2 of c'; (c) Random field 1 of ϕ'; (d) Random field 2 of ϕ' 229
Fig. 6.16 Comparison of normalised failure envelopes: (a) Spatial variability of c' in $V – H$ loading space; (b) Spatial variability of c' in $V – M$ loading space; (c) Spatial variability of ϕ' in *V*- *H* loading space; (d) Spatial variability of ϕ' in *V*- *M* loading space... 230
Fig. 6.17 Comparison of PEEQ obtained from models with and without consideration of soil spatial variability: (a) Inclined loading (δ = 20°); (b) Vertical loading; (c) Eccentric loading (Eccentricity e = 0.6) 231

CHAPTER 1
Introduction

1.1 Background

Foundations typically serve as a substructure to carry different types of loads from the superstructure to the soil below safely alleviating problems associated with stability and excessive settlement. Several billions of dollars are spent annually towards the design and construction of shallow foundations in various types of soils all over the world (Tang 2018). Traditionally, design of foundation is based on shear strength parameters of saturated soils. For example, several investigators (Terzaghi 1943, Skempton 1948, Meryerhof 1963, Hansen 1970, Vesic 1973) have proposed bearing capacity equations considering saturated soil conditions that are commonly used in the design of foundations. However, more than 40% of the earth surface soil constitutes of semi-arid and arid regions where the groundwater table is at a greater depth and the soil above it is typically in a state unsaturated condition, (Fredlund 1996, Khalili et al. 2000). Due to this reason, foundations are widely constructed partly or fully in unsaturated soils for their entire service life as shown as Fig. 1.1. The design protocols that are based on the saturated soil mechanics are conservative for most scenarios that are considered in conventional engineering practice. However, it is also important to understand the foundation behavior when soils are in a state of unsaturated condition, especially considering the rigorous influence of climatic factors. Such a background is valuable to assess the service state of the foundation or slopes considering the anticipated challenges associated with global warming effects. Research studies in this direction would be able to provide rational techniques for the interpretation of the foundation behaviors on sloping ground. A comprehensive background of the principles of unsaturated soil mechanics is required for achieving this objective.

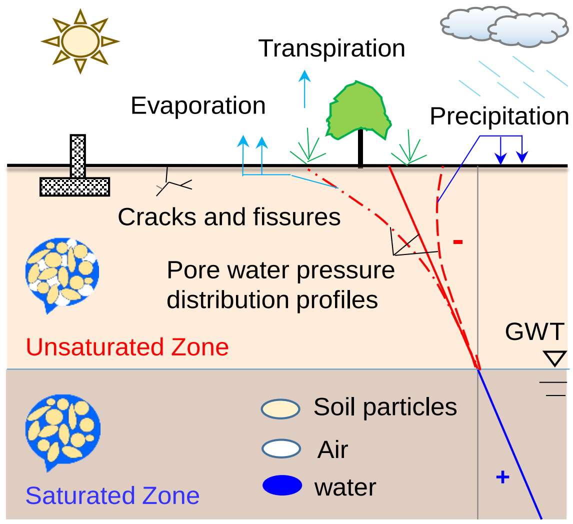

Fig. 1.1 Pore water pressure distribution profiles in unsaturated soil

The soil behavior in unsaturated conditions is significantly different from saturated soils due to the presence of more than one fluid phase (i.e., water and air in the soil as shown in Fig. 1.1). The pore water pressure (PWP) in unsaturated soil zone is negative. Typically, the pore-air phase within the unsaturated soil zone is continuous; due to this reason, the negative PWP with respect to atmospheric pressure is a positive value and is referred to as matric suction, more specific is called capillary suction (Lu 2016). In this thesis, adsorption contribution is not considered, which is of importance only in the high suction range. This is because the focus of the investigations of this thesis is limited to matric suction changes associated water content variation in the liquid phase in unsaturated soils. The matric suction variation is linear with respect to depth when it is in equilibrium condition of zero moisture flux at the ground surface (Fredlund et al. 2012, the hydrostatic line in Fig. 1.1). This is a typical initial PWP distribution profile assumption used in many studies (Zhan and Vanapalli 2012, Han et al., 2014, Tang and Senetakis 2018, Jeong et al. 2018). However, environmental factors play a vital role on the PWP distribution within the surficial unsaturated soil zone. The evaporation of water from the soil and transpiration of the vegetative cover both cause the PWP to be more negative (matric suction increases, see Fig. 1.1). However, the PWP increases (matric suction decreases) due to the influence of water infiltration associated with precipitation (see Fig. 1.1). As a result, the soil volume and shear strength will vary with the PWP variation. Shrinkage and swelling can also be found in soils that are expansive in nature due to the PWP variations. The reduction of matric suction (increasing PWP under water in filtration process) can result in the decrease in the shear strength of unsaturated soil, and the shear strength in turn will have a negative effect on the foundation bearing capacity and settlement behavior.

Research studies during the last decade suggest a likelihood of increase in the temperature and precipitation in comparison to present averages associated with global warming in several regions of the world (Chou and Lan 2012, Yoo 2013, IPCC 2018). Report of IPCC (2019) points out that the mean global land surface air temperature has increased by 1.53 ˚C (it is estimated to be in the range in 1.38 ˚C - 1.68 ˚C) from 1850-1900 to 2006-2015. The frequency and intensity of the precipitation and drought weather may increase because of the global warming (IPCC 2019). Therefore, increase in landslides, debris flow and other hazards may be associated to these likely extreme weather conditions. As a result, annual casualties and economic losses may be expected increase in future. The design of foundations for geo-infrastructures based on the conventional saturated soil mechanics do not provide reliable foundation behavior prediction both with respect to stability and settlement for the discussed extreme weather conditions. For example, several residential houses and commercial buildings were destroyed during the Pomarico landslide in the southern Italy after a prolonged rainfall in 2019 (Perrone et al. 2021). Events such as this suggest that there is an urgent need to better understand the influence of flow on the behavior of shallow foundations extending the unsaturated soil mechanics.

Several investigators have focussed to better understand and develop theoretical, experimental and numerical studies that can assist in the understanding of foundations for unsaturated soils in the past 20 years (Costa et al. 2003, Vanapalli and Mohammed 2007, Vanapalli et al. 2007, Le et al. 2013, Oh and Vanapalli 2013, Vahedifard and Robinson 2016, Kim et al. 2017, Ghasemzadeh and Akbari 2019, Vanapalli and Oh 2021). The focus of most of these studies were directed towards understanding the behavior of foundations subjected to vertical loading on level ground of unsaturated soils with a hydrostatic condition. A limited number of studies focused on the foundation behavior under inclined or eccentric loading conditions in unsaturated soils (Wuttke et al. 2013, Jin et al. 2021); however, these studies did not consider the influence of unsaturated flow conditions. In recent years, several investigators focused on the nonlinear PWP distribution profile considering climate factors and their influence on the behavior of foundations (for example, Le et al. 2013, Vo and Russell, 2016, Vahedifard and Robinson 2016, Kim et al. 2017, Ghasemzadeh and Akbari 2019, Ravichandran et al, 2021). However, these studies were undertaken only on level ground uniform soil. Proliferation of infrastructures on hilly regions can be attributed to the increasing population and urban development in the past half century. Several different types of infrastructures such as the highways, transmission towers and even residential structures are typically constructed on the sloping ground. Due to this reason, it is necessary to provide a better understanding for the behavior of foundations on unsaturated soil slopes. Furthermore, soils are typically non-uniform with varying soil properties associated with different soil layers or spatial variability. Limited studies are undertaken in the literature (Le et al. 2013, Tan et al., 2017) that consider unsaturated flow conditions in heterogeneous soils and its impact on the design of foundations. In other words, there is a lack of understanding in many areas for providing better understanding of foundation behavior on unsaturated soils. More rational methods for evaluating the foundation behavior are required considering the unsaturated flow for interpreting the foundations behavior during its entire service life span. These studies are useful forensics analysis of failed foundation or slopes considering the matric suction variation.

1.2 Novelty, objectives, and methodology

For the reasons discussed in the earlier paragraphs, one of key objectives of this thesis is directed towards developing rational tools for better understanding foundations in unsaturated soils considering the unsaturated flow conditions. In addition, comprehensive investigation studies were undertaken to interpret the unsaturated flow on the shallow foundations related to: (i) bearing capacity on the sloping ground in different types of soils including expansive soils, and (ii) bearing capacity under the inclined and eccentric loading conditions with homogeneous soil properties and considering spatial variation of soil properties.

The four objectives combined with their novelty that are addressed in this research thesis are summarized below:

(1) ***To propose a method quantifying the bearing capacity of the shallow foundation on unsaturated soil slope under rainfall infiltration condition.***

Limited studies have been conducted to interpret the shallow foundations extending the unsaturated soil mechanics behavior on sloping ground that are subjected to rainfall infiltration (Tran et al. 2019, Troncone et al, 2021, Tan and Vanapalli 2021). The behavior of these foundations can be different with that on level ground when subjected to rainfall infiltration. The study presented in this research contributes towards addressing the research gap for foundation in unsaturated soil in the literature. For this reason, the slip line method is employed coupling it with a closed-form solution to take account the vertical transient unsaturated flow conditions. To the best of the authors' knowledge, this is the first attempt in the literature to develop a novel framework combining the slip line method for the foundation bearing capacity taking account the transient flow conditions for unsaturated soils. A code procedure was developed exclusively as a part of thesis study with the aid of MATLAB. In addition, a comprehensive parametric study was conducted using the proposed framework. The proposed method is a novel tool for considering the simultaneous influence of several parameters. The influences of the flow rates, the infiltration duration, the foundation set-back distance and the ground water table depth on the foundation bearing capacity are investigated using the proposed method. The results provided a better understanding of the foundation bearing capacity variation on the sloping ground subjected to water infiltration.

(2) ***To investigate the foundation bearing capacity under the non-eccentric inclined loading and the non-inclined eccentric loading on level ground of unsaturated soils taking account the steady state flow and transient flow.***

There are many studies in the literature that propose bearing capacity equations for foundations on level ground considering unsaturated soil conditions. Most of the studies focus on vertical foundation loading conditions. However, the foundation may be subjected to the other types of loading such as the wind loading, the asymmetric structures loading and the earthquake forces. The inclined or eccentric loading is one important scenario that should be considered while assessing the foundation bearing capacity. The variation of the bearing capacity and the individual loading components variation under the steady state flow and transient flow conditions are not extensively discussed in the literature. For this reason, an improved slip line method based on the previous research study by the author was proposed in this study for evaluating the foundation bearing capacity under inclined and eccentric loading considering both the steady state flow and transient flow. The improved method incorporates the variation of the soil unit weight with the varied matric suction and can also consider the steady state flow behavior. Parametric studies were conducted, and the results were presenting in a form of failure envelop for better describe the variation of the individual components of the inclined loading or eccentric loading. Semi-empirical equations were also proposed for the failure envelops in the vertical and horizontal (V - H) loading space and in the vertical and moment (V - M) loading space. These equations are capable to describe the variation of failure envelops taking account of different soil properties and unsaturated flow conditions.

(3) ***To evaluate the influence of the water infiltration on the combined performance of the foundation and expansive soil slope system***

Shallow foundations are still used in many scenarios to transmit the loads from the lightly loaded superstructures constructed on expansive soil slopes. Water infiltration influences both the foundation and the expansive soil slope behavior. However, several research studies that are available in the literature focus on only one of the above discussed problems. The influence of infiltration on the combined performance of the foundation and the slope in cracked expansive soils has not received the attention it deserved in the literature. Therefore, the combined performance regarding the foundation bearing capacity and the slope stability was investigated in the study with the aid of a developed numerical technique in this thesis. A semi-empirical model that describes the variation of elastic modulus with respect to the matric suction is implemented into the numerical model. Bimodal soil water characteristic curve is used as a tool for understanding the influence surface cracks in the numerical study in a simplified manner. Parametric studies were also conducted to provide better understandings for the foundation and cracked expansive soil slope system subjected to rainfall infiltration for a foundation on expansive soil in Regina area, Canada.

(4) ***To predict the foundation bearing capacity and bearing capacity failure envelopes in V – H and V – M loading spaces using a proposed numerical technique taking account the soil properties variation with matric suction and the soil properties spatial variability***

Limited studies are found in the literature that focus on the foundation behavior subjected to inclined and eccentric loading taking account the unsaturated flow and soil spatial variability in unsaturated soil. Therefore, a numerical modelling framework was proposed in this research to predict the foundation bearing capacity failure envelops in $V – H$ and $V – M$ loading spaces for foundation subjected to inclined and eccentric loading. A user developed subroutine USDFLD was developed and called into the commercial software ABAQUS which made it possible to describe the soil properties variation along with the matric suction variation under unsaturated flow conditions. Moreover, code procedure was developed using MATLAB and Python to describe the soil saturated effective cohesion, effective internal friction angle and the saturated hydraulic conductivity spatial variability and incorporated them into the finite element models. Several comparison studies were conducted between the foundation bearing capacity and the failure envelops obtained from the proposed numerical framework and other methods. The comparison results from the proposed numerical framework agreed well with other methods which suggested the proposed framework could be a promising tool for the failure envelope prediction. Comparisons were also conducted between the failure envelops obtained from numerical models that consider the soil spatial variability and that consider the uniform soil properties. Results of this study suggest that different soil properties have varied influence on the foundation failure envelopes when considering the soil properties spatial variability.

1.3 Thesis Layout

The thesis consists of seven chapters in total. The thesis is structured in a format of 'a collection of manuscripts'. The layout along with the mentioned objectives is summarized in Fig. 1.2:

(1) Chapter 1 provides background related to the thesis topic along with the key objectives for the research program. The novelty of each of the objectives has been succinctly highlighted providing details of the methodology followed by the general layout.

(2) Chapter 2 presents comprehensive literature review on foundations on the level ground and the sloping ground of both saturated and unsaturated soils. The background related to the shear strength of unsaturated soils is firstly introduced. Studies related to the foundation subjected to vertical loading in unsaturated soil are summarized. In addition, the develop methods for the investigation of foundation behavior under inclined and

eccentric loadings are introduced. In addition, the influence of various parameters with respect to the foundation behavior on the sloping ground is presented. Simultaneously, the research gaps and the importance of the foundation behavior under different types of unsaturated flow conditions is succinctly summarized.

(3) Chapter 3 proposes a slip line based analytical method accounting for the bearing capacity of foundation on unsaturated soil slope subjected to transient flow condition. The method was first validated to be reliable. The influence of parameters that include the foundation setback ratio, the slope angle, the ground water table depths, the rainfall intensity, and rainfall duration were considered in the study. The combined influence of the rainfall and foundation position results are summarized considered various failure mechanisms.

(4) Chapter 4 investigates the foundation bearing capacity under the non-eccentric inclined loading and the non-inclined eccentric loading under the steady state flow and transient flow. The analytical method proposed in Chapter 3 was modified and improved for the cases investigated in this chapter. The influence of the ground water table depths, the influence of the flow rates, the infiltration duration, the loading inclination angles and the eccentricity on the individual loading components (vertical and horizontal loading in V - H loading space, vertical and moment loading in V – M loading space) were evaluated after verification of the proposed procedure. The results were presented in the form of the failure envelop in each loading space. Semi-empirical equations for describing the failure envelops were then proposed and validated considering different scenarios.

(5) Chapter 5 evaluates the combined performance of foundation and cracked expansive soil slope subjected to rainfall infiltration using a numerical technique implanted with a semi-empirical model. The numerical model was first validated with several cases which shows good agreement. The influence of the rainfall intensity, rainfall duration, foundation setback distance and loading magnitude on the foundation bearing capacity and slope stability were investigated. Relationships between the soil saturated hydraulic conductivity and the rainfall characteristics are analyzed and suggestion for design are provided based on the numerical results.

(6) Chapter 6 summarizes the developed numerical framework for investigating the foundation bearing capacity and the failure envelops in V - H and $V - M$ loading spaces. The numerical model details along with the developed code procedure for considering soil spatial variability and soil properties variation with matric suction are presented. Comparison studies are conducted between the numerical model considered uniform soil properties and the experiments, analytical method, and semi-empirical equations. In addition, comparison studies are conducted between the failure envelopes considering the soil spatial variability of the saturated effective cohesion, effective internal friction angle and the saturated hydraulic conductivity.

(7) Chapter 7 summarizes the key conclusions of various research studies undertaken in this thesis. Suggestions for future research is also succinctly summarized in this chapter.

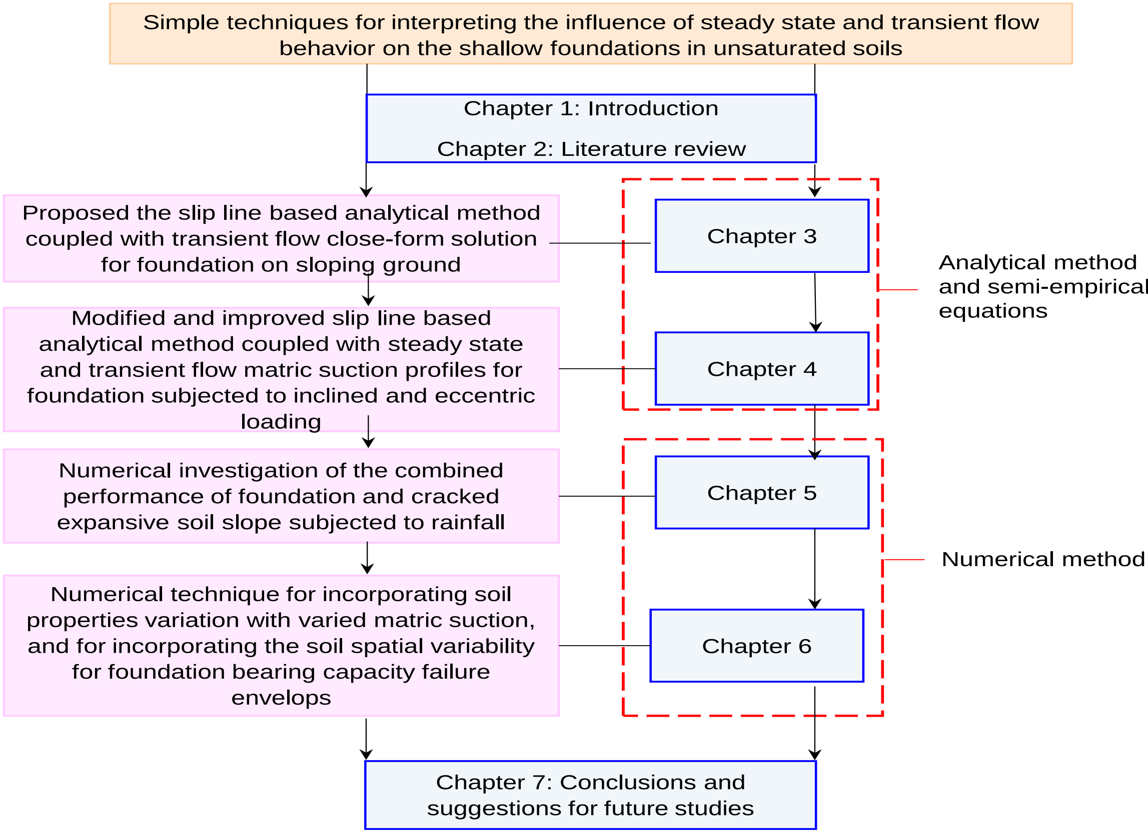

Fig. 1.2 Thesis layout

1.4 Related publications

Journal publications:

Tan, M. and Vanapalli, S.K. 2023. Failure envelops for foundation subjected to inclined and eccentric loading considering steady state and transient flow conditions in unsaturated soils. ***Computers and Geotechnics***, 157, 105315.

Tan, M. and Vanapalli, S.K. 2022. Foundation bearing capacity estimation on unsaturated soil slope under transient flow condition using slip line method. ***Computers and Geotechnics***, *148*, 104804.

Tan, M., Xinting Cheng and Sai Vanapalli. 2021. Simple Approaches for the Design of Shallow and Deep Foundations for Unsaturated Soils I: Theoretical and Experimental Studies. ***Indian Geotechnical Journal***, 1-18.

Cheng X., **Tan, M.** and Sai Vanapalli. 2021. Simple Approaches for the Design of Shallow and Deep Foundations for Unsaturated Soils II: Numerical Techniques. ***Indian Geotechnical Journal***, 1-12.

Tan, M. and Vanapalli S.K. 2023. Shallow foundation behavior on an expansive soil slope subjected to different infiltration conditions. (Revised version is under review with a journal).

Conference papers:

Tan, M., and Vanapalli, S.K. 2021. Performance estimation of a shallow foundation on an unsaturated expansive soil slope subjected to rainfall infiltration. In *MATEC Web of Conferences* (Vol. 337, p. 03009). EDP Sciences.

Reference

Chou, C., Lan, C.W., 2012. Changes in the annual range of precipitation under global warming. Journal of Climate, 25(1), 222-235. https://doi.org/10.1175/JCLI-D-11-00097.1.

Costa, Y.D., Cintra, J.C., Zornberg, J.G., 2003. Influence of matric suction on the results of plate load tests performed on a lateritic soil deposit. Geotechnical Testing Journal, 26(2), 219-227. https://doi.org/10.1520/GTJ11326J.

Fredlund, D., 1996. The emergence of unsaturated soil mechanics. *The Fourth Spencer J Buchanan Lecture*, University of Saskatchewan, SK, Canada, 1–39.

Fredlund D.G., Rahardjo H., Fredlund M.D., 2012. Unsaturated Soil Mechanics in Engineering Practice. John Wiley & Sons, Inc. https://doi.org/10.1002/9781118280492.

Ghasemzadeh, H., Akbari, F., 2019. Determining the bearing capacity factor due to nonlinear matric suction distribution in the soil. Can. J. Soil Sci., 99(4), 434-446. https://doi.org/10.1139/cjss-2019-0071.

Han, Z., Han, S., Oh, W.T., Vanapalli, S.K., 2014. Modelling the stress settlement behavior of shallow foundation in unsaturated sand using Sigma/W and Plaxis. In *67th Canadian Geotechnical Conference*, pp. 1-8. Regina, Saskatchewan: Can. Geotech. Soc.

Hansen, J.B., 1970. A revised and extended formula for bearing capacity. Bulletin, No 28, 5-11. Geoteknisk Institut (The Danish Geotechnical Institute), Copenhagen.

IPCC (Intergovernmental Panel on Climate Change), 2018. "Global Warming of 1.5°C." *An IPCC Special Report on the impacts of global warming of 1.5°C above pre-industrial levels and related global greenhouse gas emission pathways, in the context of strengthening the global response to the threat of climate change, sustainable development, and efforts to eradicate poverty.*

IPCC (Intergovernmental Panel on Climate Change), 2019. "Climate change and land." *An IPCC Special Report on climate change, desertification, land degradation, sustainable land management, food security, and green house gas fluxes in terrestrial ecosystems.*

Jeong, S., Kim, Y., Park, H., Kim, J., 2018. Effects of rainfall infiltration and hysteresis on the settlement of shallow foundations in unsaturated soil. Environmental Earth Sciences, 77(13), 1-12. https://doi.org/10.1007/s12665-018-7690-1.

Jin, L., Zhang, H., Luo, C., Feng, Q., 2021. The implementation of improved radial movement optimization to calculate the ultimate bearing capacity of strip footing on unsaturated soil under inclined loading. Arabian Journal of Geosciences, 14(17), 1-13. https://doi.org/10.1007/s12517-021-08090-3.

Khalili, N., Khabbaz, M.H., Valliappan, S., 2000. An effective stress based numerical model for hydro-mechanical analysis in unsaturated porous media. Computational Mechanics, 26(2), 174-184. https://doi.org/10.1007/s004660000165.

Kim, Y., Park, H., Jeong, S., 2017. Settlement behavior of shallow foundations in unsaturated soils under rainfall. Sustainability, 9(8), 1417. https://doi.org/10.3390/su9081417.

Le, T.M.H., Gallipoli, D., Sanchez, M., Wheeler, S., 2013. Rainfall-induced differential settlements of foundations on heterogeneous unsaturated soils. Géotechnique, 63(15), 1346-1355. https://doi.org/10.1680/geot.12.P.181.

Lu, N. 2016. Generalized soil water retention equation for adsorption and capillarity. J. Geotech. Geoenvironmental Eng., 142(10), 04016051.

Meyerhof, G.G., 1963. Some recent research on the bearing capacity of foundations. Canadian Geotechnical Journal, 1(1), 16-26. https://doi.org/10.1139/t63-003.

Oh, W.T., Vanapalli, S.K., 2013. Interpretation of the bearing capacity of unsaturated fine-grained soil using the modified effective and the modified total stress approaches. Int. J. Geomech., 13(6), 769-778. https://doi.org/10.1061/(ASCE)GM.1943-5622.0000263.

Perrone, A., Canora, F., Calamita, G., Bellanova, J., Serlenga, V., Panebianco, S., Tragni, N., Piscitelli, S., Vignola, L., Doglioni, A., Simeone, V., 2021. A multidisciplinary approach for landslide residual risk assessment: the Pomarico landslide (Basilicata Region, Southern Italy) case study. Landslides, 18(1), 353-365. https://doi.org/10.1007/s10346-020-01526-z.

Ravichandran, N., Vickneswaran, T., Marathe, S., Jella, V.S., 2021. Numerical analysis of settlement response of shallow footing subjected to heavy rainfall and flood events. Int. J. Geosci., 12(2), 138-158. https://doi.org/10.4236/ijg.2021.122009.

Skempton, A.W., 1948. The ϕ_u=0 analysis for stability and its theoretical basis. In *Proceedings of the 2nd International Conference of Soil Mechanics and Foundation Engineering*, 1, 72-77.

Tan, M.X., Vanapalli, S.K., 2021. Performance estimation of a shallow foundation on an unsaturated expansive soil slope subjected to rainfall infiltration. In MATEC Web of Conferences, 337, 03009. https://doi.org/10.1051/matecconf/202133703009.

Tan, X.H., Xie, Y., Hou, X.L., Li, P., Wang, X., 2017. Reliability analysis of shallow foundations on unsaturated soils under rainfall infiltration. In *Geo-Risk 2017*, 588-597.

Tang, Y., 2018. Numerical modelling of shallow foundations in unsaturated soils. Doctoral dissertation, University of New South Wales, Sydney.

Tang, Y., Senetakis, K., 2018. Bearing capacity equations for shallow foundations on unsaturated soils with uniform and linearly varied suction profiles. In *UNSAT 2018: The 7th International Conference on Unsaturated Soils*.

Terzaghi, K., 1943. Theoretical Soil Mechanics. John Wiley & Sons, Inc. https://doi.org/10.1002/9780470172766.

Tran, A.T.P., Kim, A.R., Cho, G.C., 2019. Numerical modeling on the stability of slope with foundation during rainfall. Geomech. Eng., 17(1), 109-118. https://doi.org/10.12989/gae.2019.17.1.109.

Troncone, A., Pugliese, L., Lamanna, G., Conte, E., 2021. Prediction of rainfall-induced landslide movements in the presence of stabilizing piles. *Eng. Geol.*, 288, 106143. https://doi.org/10.1016/j.enggeo.2021.106143.

Vahedifard, F., Robinson, J.D., 2016. Unified method for estimating the ultimate bearing capacity of shallow foundations in variably saturated soils under steady flow. *J. Geotech. Geoenviron. Eng.*, 142(4), 04015095. https://doi.org/10.1061/(ASCE)GT.1943-5606.0001445.

Vanapalli, S.K., Mohamed, F.M., 2007. Bearing capacity of model footings in unsaturated soils. In *Experimental Unsaturated Soil Mechanics*, 483-493. Springer, Berlin, Heidelberg.

Vanapalli, S.K., Oh, W.T., 2021. Analytical and numerical methods for prediction of the bearing capacity of shallow foundations in unsaturated soils. Soils and Rocks, 44(3), e2021066521. https://doi.org/10.28927/SR.2021.066521.

Vanapalli, S.K., Oh, W.T., Puppala, A.J., 2007. Determination of the bearing capacity of unsaturated soils under undrained loading conditions. In *Proceedings of the 60th Canadian Geotechnical Conference*. pp. 21-24. Alliston, ON: Can. Geotech. Soc.

Vesić, A.S., 1973. Analysis of ultimate loads of shallow foundations. Journal of the Soil Mechanics and Foundations Division, 99(1), 45-73. https://doi.org/10.1061/JSFEAQ.0001846.

Vo, T., Russell, A.R., 2016. Bearing capacity of strip footings on unsaturated soils by the slip line theory. Comput. Geotech., 74, 122-131. https://doi.org/10.1016/j.compgeo.2015.12.016.

Wuttke, F., Kafle, B., Lins, Y., Schanz, T., 2013. Macroelement for statically loaded shallow strip foundation resting on unsaturated soil. International Journal of Geomechanics, 13(5), 557-564. https://doi.org/10.1061/(ASCE)GM.1943-5622.0000254.

Yoo, C., 2013. Effect of rainfall on performance of geosynthetic reinforced soil wall using stress-pore pressure coupled analysis. In *Geo-Congress 2013: Stability and Performance of Slopes and Embankments III*, 566-573.

Zhan, Y.G., Vanapalli, S.K., 2012. Some aspects on numerical modeling of model footing test on saturated and unsaturated sands. Electronic Journal of Geotechnical Engineering, 17(9.57), 8-76.

CHAPTER 2

Literature Review[1]

2.1 Introduction

In this chapter, a brief introduction on the shear strength of unsaturated soils is provided because there is a strong relationship of this property with the soil bearing capacity. This is followed with a comprehensive literature review about the studies related to the bearing capacity of shallow foundations on level ground of unsaturated soils. A discussion is then provided related to the behavior of foundation on sloping ground and the failure mechanisms. The research needs related to the behavior of shallow foundations in unsaturated soils are discussed based on the state-of-the art research summarized from the literature.

2.2 Shear strength background

The shear strength of soil is a key factor in the design of several geo-infrastructures. Many scholars provide insight into the unsaturated soil shear strength and the foundation bearing capacity. In this section, a succinct summary related to the shear strength behavior of unsaturated background is provided.

Bishop (1959) extended the Terzaghi (1943) shear strength equation to describe the effective shear strength of unsaturated soil, which is given below.

[1] Part of the contents are published as journal article:
Tan, M., Cheng, X. & Vanapalli, S. 2021. Simple Approaches for the Design of Shallow and Deep Foundations for Unsaturated Soils I: Theoretical and Experimental Studies. *Indian Geotech J*, 51, 97–114.

$$\tau = c' + \left[\left(\sigma_n - u_a \right) + \chi \left(u_a - u_w \right) \right] \tan \phi' \tag{2.1}$$

where τ is shear strength of unsaturated soil, c' and ϕ' are the effective shear strength parameters, χ is a parameter related to the degree of saturation; terms (σ_n - u_a) and (u_a - u_w) are the stress state variables: net normal stress and matric suction. This equation is simple; however, it has some limitations. For example, the parameter χ, determined from shear strength results is different for volume change behavior of unsaturated soils for the same set of stress state variables. For this reason, several researchers suggested use of two independent stress state variables to eliminate the use of parameter χ and reliably interpret the unsaturated soil behavior (Fredlund et al. 1978).

Fredlund et al. (1978) proposed the shear strength equation for unsaturated soil in terms of two independent stress state variables, which is shown as Eq. 2.2

$$\tau = c' + \left(\sigma_n - u_a \right) \tan \phi' + \left(u_a - u_w \right) \tan \phi^b \tag{2.2}$$

where ϕ^b is the angle of shearing resistance relative to an increase in matric suction. This equation is well established in the literature and provides a rational interpretation of the shear strength behavior of unsaturated soils.

The simple approaches proposed later by Vanapalli et al. (1996) and Fredlund et al. (1996) for predicting the unsaturated soil shear strength are widely used in the literature. In these approaches (Eq. 2.3a and 2.3b), shear strength is predicted using the effective shear strength parameters (i.e., $c'$and ϕ') and the soil water characteristic curve (SWCC).

$$\begin{aligned} &\tau = c' + \left(\sigma_n - u_a \right) \tan \phi' + \left(u_a - u_w \right) (S^{\kappa}) \tan \phi' \\ &\tan \phi^b = S^{\kappa} \tan \phi' \end{aligned} \tag{2.3a}$$

$$\begin{aligned} &\tau = c' + \left(\sigma_n - u_a \right) \tan \phi' + \left(u_a - u_w \right) (\frac{\theta - \theta_r}{\theta_s - \theta_r}) \tan \phi' \\ &\tan \phi^b = \left(\frac{\theta - \theta_r}{\theta_s - \theta_r} \right) \tan \phi' \end{aligned} \tag{2.3b}$$

where θ is the volumetric water content of the soil, θ_s and θ_r are respectively the saturated and residual volumetric water contents, S is degree of saturation. The fitting parameter κ varies for different soils and is strongly related to the plasticity index, I_p (Vanapalli and Fredlund 2000, Oliveira and Marinho 2003, Garven and Vanapalli 2006). In Eq. 2.3a and 2.3b, $[c' + (\sigma_n - u_a) \tan \phi']$) represents the saturated shear strength. The terms, $[(u_a - u_w) S^\kappa \tan \phi']$ and $[(u_a - u_w) ((\theta - \theta_s) / (\theta_s - \theta_r) \tan \phi')]$ respectively in Eq. 2.3a and Eq. 2.3b, represent the contribution of the matric suction towards the shear strength.

Several researchers (Khalili and Khabbaz 1998, Lee et al. 2003, Tekinsoy et al. 2004, Sheng et al. 2008) proposed simple approaches for predicting or estimating the unsaturated soil shear strength, which typically have forms of Eq. 2.1 or Eq. 2.2. Comprehensive description of the other unsaturated soil shear strengths equations can be found in Vanapalli and Fredlund (2000) and Vanapalli (2009).

Fig. 2.1 shows the shear strength variation along with the matric suction. As a stress state variable, suction contributes to shear strength along the wetted area of contact of soil particles or aggregates. SWCC reflects the relationship between the soil water content (volumetric water content, gravimetric water content or degree of saturation) and the soil suction. Fig. 2.1a shows a typical drying SWCC for fine-grained soil. Three key stages, namely boundary effect zone, transition effect zone and residual zone of saturation can be identified in the figure. All the soil pores are filled with water in the boundary effect zone and the soil is in a state of saturated condition, despite soil suction. The value of matric suction at which air enters the largest pores of soil is referred to as the air-entry value. The soil water content starts to reduce rapidly (i.e., desaturates) with a further increase in the matric suction after the air-entry value. The water menisci area which is continuous within the soil particles or aggregates in the boundary effect zone becomes discontinuous during the soil desaturation process in the transition zone as shown in Fig. 2.1a. The desaturation phase in the transition effect zone is typically associated with the movement of water in the liquid phase. In the residual zone of saturation, significantly large suction changes are necessary to achieve even there is small change in the water content. The water content reduction in this zone is mostly in the vapor phase as there are no continuous paths for the water to flow in the liquid phase. In other words, the water menisci are typically negligible in the residual zone.

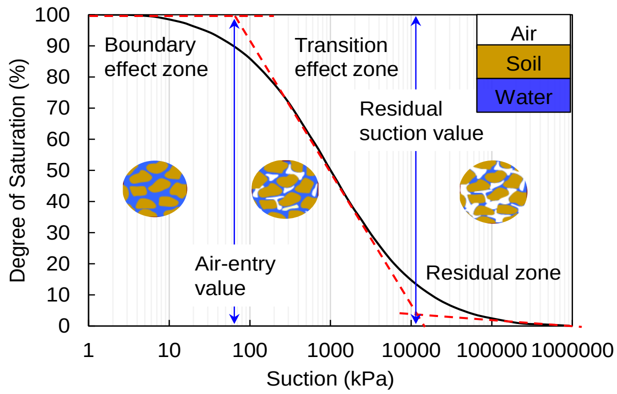

(a)

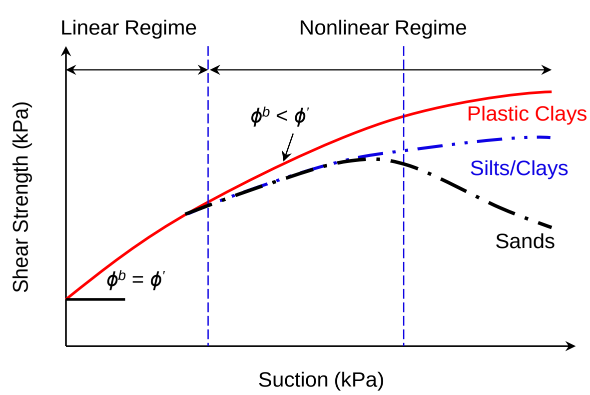

(b)

Fig. 2.1 Relationship between SWCC and soil shear strength: (a) Typical soil water characteristic curve; (b) Shear strength variation of unsaturated soils

Therefore, the shear strength increases linearly in the boundary effect zone (i.e., tan ϕ^b = tan ϕ') when the matric suction is lower than the air entry value shown in Fig. 2.1b. In this zone the soil is in a state of saturated condition and the matric suction is effectively transmitted along the entire wetted area of contact of particles. Due to this reason, the value of ϕ^b is equal to the angle of shearing resistance ϕ'. However, there will be a non-linear increase in shear strength as the suction increases which is associated with a decrease in the degree of saturation. In this zone, matric suction acts along the discontinuous wetted area of contact of soil particles within the transition effect zone. Therefore, the angle of shearing resistance with respect to suction ϕ^b is less than the angle of shearing resistance ϕ'. In the residual zone of saturation, sand desaturates at a relatively fast rate and has a low water content (i.e., low degree of saturation). In other words, there is a limited wetted area of contact. Due to this reason, suction may not be transmitted effectively to all the soil particles at their contact points (Vanapalli et al. 1996). Therefore, shear strength in coarse-grained soils typically decreases. However, fine-grained soils such as clays may not have a well-defined residual state. Considerable water (in the form of adsorbed water) in clay at residual stage may still be available to transmit suction effectively. Due to this reason, the shear strength of clays typically increases in the residual zone of saturation. However, increase of shear strength of certain fine-grained soils such as silts decreases gradually over a large suction range (Escario and Juca, 1989). These results suggest that the nonlinear shear strength behavior of unsaturated soils should be considered in the rational design of geotechnical infrastructure. The trends in the variation of the bearing capacity of foundation in unsaturated soil may be consistent with the shear strength behavior (Mohamed 2014).

2.3 Foundation on level ground of unsaturated soil

Background with respect to the foundation behavior under vertical loading is first summarized in this section. Later, the foundation behavior under combined loading is summarized.

2.3.1 Foundation subjected to vertical loading on unsaturated soil

In the last quarter century, several researchers focus has been directed towards proposing equations for interpreting the bearing capacity taking account influence of matric suction to facilitate the design of foundation of unsaturated soils (Oloo et al., 1997, Vanapalli and Mohammed, 2007, Oh and Vanapalli, 2011, 2013, 2018, Vahedifard and Robinson, 2016, Vo and Russell, 2016, Kim et al., 2017, Tang et al., 2017, Ghasemzadeh and Akbari, 2019, Ravichandran et al., 2021, Vanapalli and Oh, 2021, Anand and Sarkar 2022). Table 2.1 summarizes the various bearing capacity equations proposed in the published literature using different methods. In all equations, the contribution of matric suction is included into the Terzaghi's (1943) bearing capacity equation.

$$q_{\mathrm{ult(sat)}} = c' N_{\mathrm{c}} + \gamma D_{\mathrm{f}} N_{\mathrm{q}} + 0.5 B \gamma N_{\gamma} \tag{2.4}$$

where $q_{\mathrm{ult(sat)}}$ is the ultimate bearing capacity for saturated soil, c' is the effective cohesion of soil, B is the width of footing, γ is soil unit weight, N_{c}, N_{q}, N_{γ} are the bearing capacity factors, D_{f} is the footing embedment depth.

Different characterizations of the contribution from matric suction beneath the foundation have been proposed among these studies. Most of the studies were directed to understand the foundation behavior of unsaturated soils considering hydrostatic condition. Oloo et al. (1997) proposed the equation (Eq. 2.5 in Table 2.1) to estimate the bearing capacity of surface footing for unsaturated fine-grained soils extending the effective stress approach. The equation is based on the bilinear shear strength failure envelope of unsaturated soil (Gan et al. 1988). This bilinear assumption may result in the discrepancies when the matric suction value is higher than the air-entry value. This is due to the nonlinear behavior of foundation bearing capacity with matric suction value greater than the air-entry value as per the discussions in the previous section.

Table 2.1. Summary of the foundation bearing capacity equations in unsaturated soil

Number (No.)	Bearing capacity equations	References
Eq. 2.5	$q_{\mathrm{ult(unsat)}}=\left[\begin{array}{l} c'+(u_{\mathrm{a}}-u_{\mathrm{w}})_{\mathrm{b}}\tan\phi' \\ \quad +\left[(u_{\mathrm{a}}-u_{\mathrm{w}})-(u_{\mathrm{a}}-u_{\mathrm{w}})_{\mathrm{b}}\right]\tan\phi^{\mathrm{b}}\end{array}\right]N_{\mathrm{c}}+0.5B\gamma N_{\gamma}$	Oloo et al. (1997)
Eq. 2.6	$q_{\mathrm{ult(unsat)}}=\left[\begin{array}{l} c'+(u_{\mathrm{a}}-u_{\mathrm{w}})_{\mathrm{b}}(1-S^{\psi})\tan\phi' \\ \quad +(u_{\mathrm{a}}-u_{\mathrm{w}})_{\mathrm{AVR}}S^{\psi}\tan\phi'\end{array}\right]N_{\mathrm{c}}\xi_{\mathrm{c}}+\gamma D_{\mathrm{f}}N_{\mathrm{q}}\xi_{\mathrm{q}}+0.5B\gamma N_{\gamma}\xi_{\gamma}$ $\psi=-0.0031(I_{\mathrm{p}})^2+0.34(I_{\mathrm{p}})+1$	Vanapalli and Mohammed (2007)
Eq. 2.7	$q_{\mathrm{ult(unsat)}}=\left[\dfrac{q_{\mathrm{u(unsat)}}}{2}\right]\left[1+0.2\left(\dfrac{B}{L}\right)\right]N_{\mathrm{cunsast}}$ $c_{\mathrm{u(unsat)}}=\dfrac{q_{\mathrm{u(unsat)}}}{2}$	Vanapalli et al. (2007)
Eq. 2.8	$q_{\mathrm{ult(unsat)}}=\left[\begin{array}{l} c'+(u_{\mathrm{a}}-u_{\mathrm{w}})_{\mathrm{b}}(1-S_{\mathrm{e,AVR}})\tan\phi' \\ \quad +\left[(u_{\mathrm{a}}-u_{\mathrm{w}})S_{\mathrm{e}}\right]_{\mathrm{AVR}}\tan\phi'\end{array}\right]N_{\mathrm{c}}\xi_{\mathrm{c}}+q_0N_{\mathrm{q}}\xi_{\mathrm{q}}+0.5B\bar{\gamma}N_{\gamma}\xi_{\gamma}$	Vahedifard and Robinson (2016)
Eq. 2.9	$q_{\mathrm{ult(unsat)}}=\left[c'+(u_{\mathrm{a}}-u_{\mathrm{w}})\chi\tan\phi'\right]N_{\mathrm{c}}d_{\mathrm{c}}+\gamma D_{\mathrm{f}}N_{\mathrm{q}}d_{\mathrm{q}}+0.5B(\gamma-\rho)N_{\gamma}d_{\gamma}$ $\chi=\begin{cases}1, \text{ for } \dfrac{(u_{\mathrm{a}}-u_{\mathrm{w}})}{(u_{\mathrm{a}}-u_{\mathrm{w}})_{\mathrm{b}}}\le 1 \\ \left(\dfrac{(u_{\mathrm{a}}-u_{\mathrm{w}})}{(u_{\mathrm{a}}-u_{\mathrm{w}})_{\mathrm{b}}}\right)^{-0.55}, \text{ for main drying curve } \dfrac{(u_{\mathrm{a}}-u_{\mathrm{w}})}{(u_{\mathrm{a}}-u_{\mathrm{w}})_{\mathrm{b}}}>1\end{cases}$	Tang et al. (2017)

Eq. 2.10	$q_{\text{ult(unsat)}} = \left[c' + (u_a - u_w)_b (\tan\phi' - \tan\phi^b)\right] N_c \xi_c + q_0 N_q \xi_q + 0.5 B \gamma N_\gamma \xi_\gamma + (u_a - u_w) N_s \tan\phi^b \xi_s$	Ghasemzadeh and Akbari (2019)
Eq. 2.11	Uniform suction with depth $q_{\text{all(unsat)}} = \left[c' + (u_a - u_w)\tan\phi^b\right] M_c + \gamma D_f M_q + 0.5 B \gamma M_\gamma$ Linear suction with depth $q_{\text{all(unsat)}} = \left[c' + (u_a - u_w)_0 (1 - D/D_W)\tan\phi^b\right] M_c + \gamma D_f M_q + 0.5 B \gamma M_\gamma$	Zhang et al. (2019)
Eq. 2.12	$q_{\text{ult(unsat)}} = \left[c' + (u_a - u_w) S^\psi \tan\phi'\right] N_c \xi_c + 0.5 B \gamma N_\gamma$	Vanapalli and Oh (2021)

Note: $q_{\text{ult(unsat)}}$ = ultimate bearing capacity for unsaturated soil; S = degree of saturation; S_e = effective degree of saturation; $c_{\text{u(unsat)}}$ = unsaturated soil cohesion under undrained condition. $\overline{\gamma}$ = modified average unit weight; q_0 = soil surcharge load above the base of the foundation; N_c, N_q, $(u_a - u_w)_b$ = air-entry value; $(u_a - u_w)_{AVR}$ = average matric suction; ξ_c, ξ_q, ξ_γ = shape factors; Ψ = fitting parameter. χ = effective stress parameter; $q_{\text{all(unsat)}}$ = allowable bearing capacity for unsaturated soil; M_c, M_q, M_γ = allowable bearing capacity factors. $c_{\text{u(unsat)}}$ is equal to $q_{\text{u(unsat)}}/2$

Vanapalli and Mohammed (2007) proposed the equation (Eq. 2.6 in Table 2.1) that overcomes the limitation of the equation proposed by Oloo et al. (1997) using the modified effective stress approach. The equation was originally proposed for surface square footing. There is a smooth transition between this equation and Eq. 2.4 used for unsaturated and saturated soils. This equation can be used as a tool to predict the nonlinear variation of the bearing capacity with respect to matric suction using the effective shear strength parameters of saturated soil (i.e., c' and ϕ') and the *SWCC*. The term $S^\Psi \tan\phi'$ describes the shear strength contribution with respect to matric suction towards the bearing capacity. However, it may underestimate the bearing capacity when the matric suction value is greater than the residual suction value when the bearing capacity convergences to the certain value (Oh and Vanapalli 2013). The average matric suction in the stress bulb zone (typically 1.5B to 2B beneath the foundation) has been used to interpret the foundation bearing capacity in the equation. To overcome the limitation of the Eq. 2.6, Vanapalli and Oh (2021) proposed a modified bearing capacity equation (Eq. (2.12)) for the suction value in the residual zone of SWCC.

Oh and Vanapalli (2011) also proposed a methodology using Eq. 2.6 to evaluate the foundation stress versus settlement relationship. This method was developed by assuming the stress and settlement relationship in the elastic and plastic zones as two straight lines (i.e., linear). The slope of the elastic line is equal to the modulus of elasticity of the soil. Oh et al. (2009) proposed Eq. 2.13 for the prediction of the modulus of elasticity considering about the matric suction.

$$E_{\mathrm{unsat}} = E_{\mathrm{sat}}\left[1+\alpha\frac{\left(u_{\mathrm{a}}-u_{\mathrm{w}}\right)}{\left(P_{a}/101.3\right)}\left(S^{\beta}\right)\right] \tag{2.13}$$

where E_{unsat} and E_{sat} are the elastic modulus of unsaturated soil and saturated soil respectively. P_a is the atmosphere pressure (101.3kPa). α and β are fitting parameters, β = 1 for coarse grained soil (Oh et al. 2009) and $\beta = 2$ (Vanapalli and Oh 2010) for fine grained soil. α value is related to the ratio of footing size to soil particle size and the plasticity index, I_{p} (Oh et al. 2009, Vanapalli and Oh 2010).

Several researchers focused on the bearing capacity of unsaturated soils using different theoretical methods combined with numerical computation techniques (Jahanandish et al. 2010, Ghasemzadeh and Akbari 2019, Zhang et al. 2019). For example, Jahanandish et al. (2010) used the stress characteristics method extended to zero extension lines method in the bearing capacity investigation. The method is achieved by combining the effective stress concept and the plasticity equations. The study also provides a design chart related to the bearing capacity factor, N_{γ}. Other methods such as the discretization technique (Du et al. 2021), limit analysis (Anand and Sarkar 2021) and the improved radial movement optimization method (Jin et al. 2019) are also modified for using in the unsaturated soils.

Several researchers performed experimental studies (see Table 2.2) to investigate the bearing capacity of unsaturated soils. The results of these studies suggest that the matric suction significantly influences the foundation load-displacement behavior and hence influence the foundation performance. The bearing capacity increased almost linearly with matric suction prior to the air-entry value. The variation trend of the bearing capacity is like that of the shear strength shown in Fig. 2.1. The foundation bearing capacity in unsaturated soils is observed to be several times higher than that of saturated soil. The increase in bearing capacity depends on the type of soil and its initial water content condition. For example, bearing capacity under unsaturated condition is 10 times greater than saturated condition from model footing tests on silt (Oloo 1994). For sandy type of soil, the increase was observed to between 5 to 7 times from experimental studies by Mohamed and Vanapalli (2006), Vanapalli and Mohamed (2013).

Table 2.2. Summary of the experimental studies

Experiments	Soil	Suction range (kPa)	Foundation shape	Reference
Model footing test	Botkin Pit silt Indian Head till	Silt: 25 - 200 Till: 38 - 400	Square 30 mm × 30 mm Circular Diameter: 30 mm	Oloo (1994)
Plate load test (PLT)	Silt	-	Square 0.5 m × 0.5 m 1 m × 1 m 2 m × 2 m	Larson (1997)
PLT	Collapsible clay	-	Circular Diameter: 0.8 m	Conciani et al. (1998)

In-situ PLT	Residual soil	-	Circular Diameter: 0.3 m, 0.45m, 0.6m Square 0.4 m × 0.4 m 0.7 m × 0.7 m 1.0 m × 1.0 m	Consoli et al. (1998)
In-situ PLT	Lateritic soil	0 – 31	Circular Diameter: 0.8 m	Costa et al. (2003)
PLT	Expansive soil	-	Square 0.2 m × 0.2 m	Xu (2004)
Model footing test	Coarse grained soil (Unimin (7030) sand)	0 – 8	Square 100 mm × 100 mm, 150 mm × 150 mm	Mohamed and Vanapalli (2006) Vanapalli and Mohamed (2013)
In-situ PLT	Lean clay deposit	0 - 80	Circular steel plate Diameter: 0.31m	Rojas et al. (2007)
Model footing test (Undrained condition)	Indian Head till	0 – 205	Square 50 mm × 50 mm	Vanapalli et al. (2007) Oh and Vanapalli (2013)
Model footing test	Huston sand	0 - 6	Strip	Lins et al. (2009)
Cone penetration test (CPT)	Poorly graded fine sand (according to USCS)	0 - 8	-	Mohamed et al. (2010)
Small-scale footing test	Poorly graded unsaturated sand	0 - 6	Strip	Wuttke et al. (2013)
In-situ PLT, Standard penetration test (SPT), CPT	Dark-grey silty sand underneath the septic sand	0 - 8	Square (PLT) 0.2 m × 0.2 m	Mohamed and Vanapalli (2015)

Laboratory PLT	Silt sand mixtures	0 – 23.4	Circular steel plate Diameter: 0.15 m	Tang et al. (2018)

In some of these methods, the average matric suction in the stress bulb zone beneath the footings is used for estimating the bearing capacity. For example, the average matric suction value from tensiometer readings between the bottom of the test pit to a depth equal to the circular plate diameter is used in Costa et al. (2003). However, the average matric suction may be influenced by the footing size (Oh and Vanapalli 2013). As shown in Fig. 2.2, a footing with a relatively smaller size (B_1) will have a relatively small stress bulb zone beneath the foundation and a higher average matric suction. Other representative suction value can also be used; for example, a suction value at 0.1m depth from the circular plate is used in the PLT by Rojas et al. (2007); Vahedifard and Robinson (2016) made integration of the average matric suction in the stress bulb zone. Studies by Costa et al. (2003) and Rojas et al. (2007) show that the matric suction has a significant influence on the bearing capacity regardless of the procedure used for selection of the representative matric suction. In addition to the bearing capacity, the studies by Rojas et al. (2007) and Costa et al. (2003) also suggest that the matric suction significantly influences the stiffness of the soil.

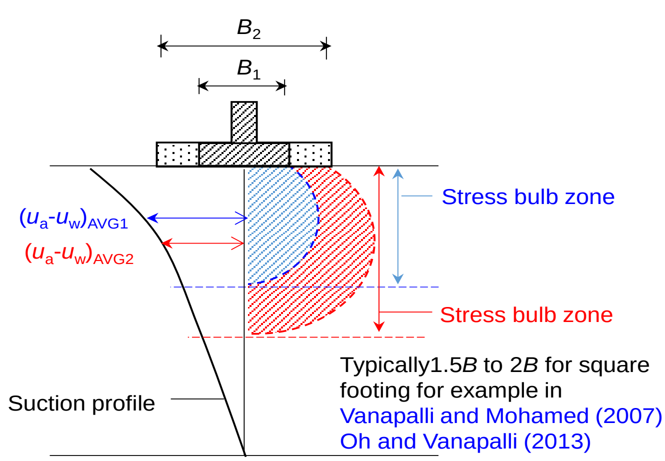

Fig. 2.2 Average matric suction values for footing with different sizes

Experimental studies are expensive and time consuming in comparison to numerical studies. One of key advantage of numerical studies is that they are simple to perform even considering complex scenarios (e.g., different soil properties). Several researchers conducted investigations using the finite element methods (Oh and Vanapalli (2011), Zhan and Vanapalli (2012), Han et al. (2014), Akbari et al. (2020)) to evaluate the influence of soil properties on the foundation performance. Results of Zhan and Vanapalli (2012), Oh and Vanapalli (2018) suggest that the foundation vertical pressure increases with increasing modulus of elasticity, cohesion, Poisson's ratio and dilatancy angle at the same vertical settlement condition.

In recent years, there has been interest to take account of influence of climate factors on the performance of foundations by several investigators. The evaporation and infiltration conditions typically lead to non-linear suction distribution in the soil below the foundation as mentioned in Chapter 1. The matric suction distribution under both steady state and transient state exhibits uncertainty. The suction profiles vary with the water content change associated with the unsaturated flow behavior. Incorporating the suction variation into the time-dependent foundation behavior introduces complexity; however, such studies are valuable.

For example, Vahedifard and Robinson (2016) studied the shallow foundation bearing capacity with nonlinear suction profiles under steady flow condition. A method (Eq. 2.8 in Table 2.1) has been proposed to estimate the foundation bearing capacity taking account the variations in depth of water table and the steady flow condition. The average matric suction within the stress bulb zone below the foundation was estimated using the numerical integration of differential elements. Due to the integration of the area in the stress bulb zone, the equation can provide relatively accurate average matric suction compared to that obtained under the average value of the matric suction between the surface and the depth of stress bulb zone. Therefore, the equation can provide rigorous bearing capacity estimation under steady flow condition compared to other equations.

Vo and Russell (2016) investigated the bearing capacity of strip footing extending the slip line theory. The non-uniform suction profile has been considered in this approach for steady state evaporation and infiltration conditions. Results of the study suggest that the depth of the ground water table, the flow rates and soil types influence the suction contribution towards the bearing capacity.

In addition to the bearing capacity investigation under steady state flow, the bearing capacity and settlement behavior under rainfall was investigated by several investigators. Kim et al. (2017) and Jeong et al. (2018) studied the bearing capacity and settlement of shallow foundation under the influence of rainfall infiltration with the aid of PlAXIS 2D. The soil properties such as the shear strength and modulus of elasticity are sensitive to the matric suction changes associated with rainfall. In other words, rainfall intensity is a key factor that will influence the foundation bearing capacity and settlement behavior. Studies by both these investigators suggest a higher bearing capacity for soils with a lower coefficient of permeability during rainfall infiltration period. Higher rainfall intensity contributes to a greater vertical settlement. The ground water position near the ground surface also influences the settlement changes during the rainfall period.

Jeong et al. (2018) also investigated the influence of hysteresis effects associated with wetting and drying conditions respectively for infiltration and evaporation conditions. Comparisons were provided between the results based on a numerical model using the drying SWCC curve and wetting SWCC curve of Dogye weathered granite soil. Results show similar trends in settlement behavior; however, the settlement was about 5% greater using the wetting SWCC curve.

Le et al. (2013) conducted coupled hydro-mechanical finite element analysis to investigate the rainfall induced differential settlements of foundations in unsaturated soils. The variability of soil properties is modelled using the Monte Carlo simulation. Results showed that highest risk of differential settlement occurred at a transient phase of infiltration. The differential settlements are typically underestimated when the soil random heterogeneity and the unsaturated condition are not considered simultaneously.

Mahmoudabadi and Ravichandran (2019) proposed a procedure based on finite difference method considering the site-specific rainfall and water table data effect. Monte Carlo simulations has been used to generate different rainfall intensities and ground water table level. The average matric suction in the influence zone has been calculated based on the generated rainfall and ground water table data. Comparisons were provided between the settlement of different size foundations under saturated and unsaturated conditions. The deviation was substantial and is approximately 87 %. The above results show the necessity to consider about the rainfall induced bearing capacity reduction and settlement of foundations.

In all the studies discussed in the earlier paragraphs the contribution from matric suction beneath the foundation has been investigated. The studies in general suggest rainfall characteristics, the soil properties, the initial ground water table have combined impact on the foundation performance. The matric suction is the predominant factor that influence the foundation bearing capacity and settlement behavior in unsaturated soils. The average matric suction is typically estimated and used for the foundation performance evaluation. However, such an assumption using average matric suction for different water infiltration or evaporation conditions may not be reliable because matric suction variation is time-dependent under the transient flow conditions. Only a few studies provide a comprehensive investigation of the foundation bearing capacity and the settlement considering the time-dependent variation of matric suction (Kim et al. 2017, Jeong et al. 2018, Mahmoudabadi and Ravichandran 2019). In addition to matric suction, there can be other sources of uncertainty that may influence the foundation stability. Limited studies (Tan et al. 2017) that are found in the literature with respect to the reliability analysis of foundation in unsaturated soils considering the varying flow conditions. The understanding related to the time-dependent variation of matric suction on the bearing capacity will provide a better explanation of the anticipated foundation behavior at various stages during the entire service life considering the influence of steady state and transient flow behavior.

2.3.2 Foundation subjected to inclined and eccentric loadings

Several researchers investigated the influence of inclined and eccentric loading on the bearing capacity of saturated soils (Meyerhof 1953, 1963, Michalowski and You 1998; Hjiaj et al. 2004; Patra et al. 2012a, 2012b; Krabbenhoft et al. 2014; Ganesh et al. 2016). Traditionally, inclination of the load is considered by incorporating inclination factors into the conventional Terzaghi bearing capacity equation. Table 2.3 provides a summary of classic inclination factors that are widely used in geotechnical engineering. For the eccentric loading, the effective rule method (Meyerhof 1953) and the reduction factor method (Purkayastha and Char 1977, Patra et al. 2012a, 2012b) are two widely used methods for evaluating the foundation bearing capacity. The effective rule method assumes that the foundation is subjected to central vertical loading with a foundation width reduced by twice the eccentricity to the original foundation width. The reduction factor method typically determines the bearing capacity of foundation subjected eccentric loading from the central vertical loading.

Table 2.3 Summary of the inclination factors

References	i_c	i_q	i_γ
Meyerhof (1963)	$\left(1-\frac{\alpha}{90°}\right)^2$	$\left(1-\frac{\alpha}{90°}\right)^2$	$\left(1-\frac{\alpha}{\phi'}\right)^2$
Hansen (1970)	$\frac{i_q N_q - 1}{N_q - 1}$	$(1-0.5\tan\alpha)^5$	$(1-0.7\tan\alpha)^5$
Vesic (1975)	$\frac{i_q N_q - 1}{N_q - 1}$	$(1-\tan\alpha)^2$	$(1-\tan\alpha)^3$
Loukidis et al. (2008)	-	-	$\left(1-0.94\frac{\tan\alpha}{\tan\phi'}\right)^{(1.5\tan\phi'+0.4)^2}$

Many researchers in recent years have extended the failure envelope method (Gourvenec and Randolph 2003; Taiebat and Carter 2000, 2002; Du et al. 2022; Fathipour et al. 2022). The foundation is considered unsafe if the combination of loads is outside the failure envelope. The inclined load can be treated as a combination of the vertical load, *V* and horizontal load, *H*. Similarly, the eccentric load can be considered as a moment load, *M* taking account of vertical load and the eccentricity. Typically, the failure envelop is presented in a normalized version. There are mainly two methods for the normalizing. The first method is to normalize the loading in each direction with the vertical ultimate bearing capacity, V_{max}. For example, the horizontal loading can be normalized as H / V_{max}. The moment loading is typically normalized as M / BV_{max} with the foundation width included to keep the dimensional homogeneity. The second method is to normalize the loading with the ultimate bearing capacity in the same direction. For example, the horizontal loading can be normalized as H / H_{max}. Table 2.4 summarizes the failure envelop equations that proposed by many scholars for foundation subjected to V, H, M combined loadings with the first method listed followed by the second method.

Table 2.4 Summary of failure envelop equations

References		Equations
Gottardi and Butterfield (1993)	VH	$\left(\frac{H}{V_{max}}\right)=0.48\left(\frac{V}{V_{max}}\right)\left[1-\left(\frac{V}{V_{max}}\right)\right]$
	VM	$\left(\frac{M}{BV_{max}}\right)=0.36\left(\frac{V}{V_{max}}\right)\left[1-\left(\frac{V}{V_{max}}\right)\right]$
Loukidis et al. (2008)	VH	$\left(\frac{H}{V_{max}}\right)=\frac{\tan\phi}{0.94}\left(\frac{V}{V_{max}}\right)\left[1-\left(\frac{V}{V_{max}}\right)^{1/(1.5\tan\phi+0.4)^2}\right]$
Tang et al. (2014)	VH	$\left(\frac{H}{V_{max}}\right)=1.04\left(\frac{V}{V_{max}}\right)\left[1-\left(\frac{V}{V_{max}}\right)^{1/3}\right]$
	VM	$\left(\frac{M}{BV_{max}}\right)=0.52\left(\frac{V}{V_{max}}\right)\left[1-\left(\frac{V}{V_{max}}\right)^{0.5}\right]$
Zheng et al. (2019)	VH	$\left(\frac{H}{V_{max}}\right)=\frac{\tan\phi}{0.88}\left(\frac{V}{V_{max}}\right)\left[1-\left(\frac{V}{V_{max}}\right)^{1/(1.56\tan\phi+0.45)^2}\right]$
Pham et al. (2019)	VM	$\left(\frac{M}{BV_{max}}\right)=0.63\left(\frac{V}{V_{max}}\right)\left[1-\left(\frac{V}{V_{max}}\right)^{0.8}\right]$
Pham et al. (2020)	VH	$\left(\frac{H}{V_{max}}\right)=\frac{\tan\phi}{0.76}\left(\frac{V}{V_{max}}\right)\left[1-\left(\frac{V}{V_{max}}\right)^{1/(1.7\tan\phi+0.4)^2}\right]$
Pham et al. (2022)	VM	$\left(\frac{M}{BV_{max}}\right)=0.55\left(\frac{V}{V_{max}}\right)\left[1-\left(\frac{V}{V_{max}}\right)^{\lambda}\right]$ $\lambda=0.98\frac{\ln\left(\left(\frac{c}{\gamma B}\right)+1\right)+0.18}{\ln\left(\left(\frac{c}{\gamma B}\right)+1\right)+0.36}$

	VH $$\left(\frac{H}{V_{\max}}\right)=\frac{\tan\phi}{0.76}\left(\frac{V}{V_{\max}}\right)\left[1-\left(\frac{V}{V_{\max}}\right)^{1/(1.7\tan\phi+0.4)^2}\right]\mu+\frac{1}{\pi+2}\left(1-\left(\frac{V}{V_{\max}}\right)^{7.4}\right)\nu$$ $$\mu=\frac{1.16\tan\phi-0.064}{\tan\phi+0.04}\left(0.135\ln\left(\left(\frac{c}{\gamma B}\right)+1\right)+1\right)$$ $$\nu=\frac{(\pi+2)\left(\frac{c}{\gamma B}\right)}{\left(\frac{c}{\gamma B}\right)N_c+0.5N_\gamma}$$
Du et al. (2022)	*MH* $$\frac{\left(\frac{M}{BV_{\max}}\cos\theta-\frac{H}{V_{\max}}\sin\theta\right)^2}{a^2}+\frac{\left(\frac{M}{BV_{\max}}\sin\theta+\frac{H}{V_{\max}}\cos\theta\right)^2}{b^2}=1$$ $$a=l_1\left(\frac{V}{V_{\max}}\right)\left[1-\left(\frac{V}{V_{\max}}\right)^{m_1}-\frac{n_1}{l_1}\right]+n_1$$ $$b=l_2\left(\frac{V}{V_{\max}}\right)\left[1-\left(\frac{V}{V_{\max}}\right)^{m_2}-\frac{n_2}{l_2}\right]+n_2$$ $$\theta=l_3\left(\frac{V}{V_{\max}}\right)+m_3\left(\frac{V}{V_{\max}}\right)+n_3$$ θ = deflection angle of the ellipse; a = length of the semiaxis of ellipse corresponding to the *M*-axis, and *b* = length of the semiaxis of ellipse corresponding to the *H*-axis. l_n, m_n, and n_n are the equation fitting coefficients.
Bransby and Randolph (1998)	*VHM* $$f=\left(\frac{V}{V_{\max}}\right)^2+\left[\left(\frac{M^*}{M_{\max}}\right)^m+\left(\frac{H}{H_{\max}}\right)^n\right]^{1/p}-1$$ *m*, *n*, *p* are fitting parameters $$f=\left(\frac{V}{V_{\max}}\right)^{2.5}-\left(1-\frac{H}{H_{\max}}\right)^{1/3}\left(1-\frac{M^*}{M_{\max}}\right)+\frac{1}{2}\left(\frac{M^*}{M_{\max}}\right)\left(\frac{H}{H_{\max}}\right)^5$$ for the soil non-homogeneity factor: k/s_{uo} = 6
Ukritchon et al. (1998)	*VM* $$\frac{V}{Bs_u}=\alpha_1\left\{1-\alpha_2\left(\frac{2e}{B}\right)-\alpha_3\left(\frac{2e}{B}\right)^2\right\}$$ Eccentricity ratio: $e/B = (M/(B^2s_u))/(V/(Bs_u))$ α_1, α_2, α_3 are fitting parameters related to $H/(Bs_u)$.
Bransby and Randolph (1999)	*VHM* $$f=\left(\frac{V}{V_{\max}}\right)^{2.5}-\left(1-\frac{H}{H_{\max}}\right)^{1/3}\left(1-\frac{M^*}{M_{\max}}\right)+\frac{1}{2}\left(\frac{M^*}{M_{\max}}\right)\left(\frac{H}{H_{\max}}\right)^5$$

Yun and Bransby (2007)	*HM*	$f=\left(\frac{M^*}{M_{\max}}\right)^2+\left(\frac{H}{H_{\max}}\right)^2-1$
Taiebat and Carter (2000)	*VHM*	$f=\left(\frac{V}{V_{\max}}\right)^2+\left[\left(\frac{M}{M_{\max}}\right)\left(1-\alpha_1\left(\frac{HM}{H_{\max}\lvert M\rvert}\right)\right)\right]^2+\left\lvert\left(\frac{H}{H_{\max}}\right)^3\right\rvert-1$ α_1 is fitting parameter depends on the soil profile: for homogeneous soil, $\alpha_1 = 0.3$.
Vulpe et al. (2014)	*HM*	$f=\left(\left\lvert\frac{H}{H_{\max}}\Big/h^*\right\rvert\right)^{\alpha}+\left(\frac{M}{M_{\max}}\Big/m^*\right)^{\alpha}+2\beta\frac{\frac{H}{H_{\max}}\frac{M}{M_{\max}}}{h^*m^*}=1$ $h^*=1-\left(\frac{V}{V_{\max}}\right)^q$, $m^*=1-\left(\frac{V}{V_{\max}}\right)^p$, p, q are fitting parameters
Liu et al. (2014)	*VM*	$\left(\frac{V}{V_{\max}}\right)=\left(1-\left(\frac{M}{M_{\max}}\right)\right)^p$, p is fitting parameter.

Compared to the traditional methods that are based on linear superposition of the load inclination and eccentricity or using independent reduction factors; the failure envelope method is advantageous as it explicitly considers the interaction of the *V*, *H*, and *M* and indicates the failure based on the changes that arise for each of the load components (Gottardi and Butterfield, 1993; Gourvenec and Barnett 2011). This method can incorporate the influence of the foundation embedment depths, soil shear strengths profiles, and the soil internal friction angle into the failure envelops (Gourvenec and Randolph 2003).

The equations in Table 2.4 can only be used for foundations in saturated soils. Limited research studies focus on foundations in unsaturated soils that are subjected to the inclined and eccentric loading (Wuttke et al. 2013, Fathipour et al. 2022, Li and Jiang 2022). Wuttke et al. (2013) conducted a small-scale footing test on unsaturated sandy soil and an elastoplastic strain-hardening microelement for the strip foundation on unsaturated soil formulated for static loading. Jin et al. (2021) employed the improved radial movement optimization method to investigate the foundation behavior in unsaturated soils under inclined loading. Results show the foundation bearing capacity exhibited a strong nonlinear reduction trend with the increasing loading inclination angle.

2.4 Foundation design on sloping ground

In this section, first foundation behavior on saturated soil slope ground will be summarized. Later, several parameters that influence the foundation and slope system stability on unsaturated soil slope ground will be discussed. In addition, different failure mechanisms corresponding to the various parameters will be presented.

2.4.1 Foundation on saturated soil slope

Table 2.5 summarizes studies carried out by various investigators using different methods for the foundation on sloping ground. Most of the early studies focused on strip foundations using cohesionless soil because of ease in design, construction, and testing time (e.g., Shields et al. 1977, Bauer et al. 1981, Castelli and Lentini 2012). In recent years, several investigators have developed analytical and numerical methods to provide insight into the foundation behavior on slopes. These studies suggest that foundation behavior on slopes is influenced by several additional parameters compared to level ground conditions. The studies reveal that the slope geometry, soil properties, foundation setback distance, foundation embedment depth, foundation loading condition all influence the foundation-slope system (see Table 2.5). In many of these studies, the ultimate bearing capacity of foundation on slope is investigated extending a dimensionless form such as $q/\gamma B$ or the bearing capacity factors. Design charts or equations have been provided to correlate the bearing capacity factors with different influence parameters mentioned above.

Table 2.5 Summary of studies on foundation on sloping ground

Method	Foundation	Soil type	Parameters	Solution provided	References
Laboratory test	Strip	Sand-fill slope	Embedment depths (*H*), relative density (D_r)	Bearing capacity factors	Shields et al. (1977)
Laboratory test	Rough-base strip	Sand	Foundation widths (*B*), load inclination	Scale factor, inclination factor	Bauer et al. (1981)
Centrifuge experiments	Model footing	Cohesionless soil	Slope geometry, H/B, ϕ, footing aspect ratio (B/L), β, b/B	Bearing capacity factors	Gemperline (1988)
Laboratory test, energy dissipation method (numerical analysis)	Strip	Coarse sand backfill	ϕ	Bearing capacity, slip surface	Yang et al. (2007)
Laboratory test, limit equilibrium method	Strip	Sandy slope	b	Bearing capacity	Castelli and Lentini (2012)
Laboratory test	Strip	Sandy slope	b, β, D_r, B	Bearing capacity	Keskin and Laman (2013)
Laboratory test	Strip	Sandy slope	Eccentrically load	Bearing capacity and failure mechanism	Cure et al. (2014)

Theoretical method	Strip	Cohesive soil, Cohesionless soil	Embedment ratio (H/B), slope angle (β), ϕ, setback ratio (b/B, b:setback distance)	Bearing capacity factors	Meyerhof (1957)
Theoretical method (Stress characteristics)	Strip	Cohesionless soil	β, ϕ, H/B	Bearing capacity factors	Graham et al. (1988)
Theoretical method	Strip	Clay, Sand	β, b/B,H/B	$q/\gamma B$	Narita and Yamaguchi (1990)
Limit analysis with discontinuity layout optimization	Strip	c'- ϕ' soil	ϕ, β, B/H, $\gamma H/c'$	Bearing capacity factors, reduction factors	Leshchinsky (2015)
Limit analysis with discontinuity layout optimization	Spread footing	c'- ϕ' soil	ϕ, β, $\gamma H/c'$, b/B	reduction factors	Leshchinsky and Xie (2017)
Theoretical method	Strip	Cohesive soil	H/B, c, ϕ, β, b/B, slope height (V)	$q/\gamma B$	Yang et al. (2019)
Upper bound	Strip	Clay	V/B, β, b/B, $c_u/(\gamma B)$	Bearing capacity factors	Georgiadis (2010a)
Upper bound limit analysis, finite element analysis	Strip	Clay	Inclined loading, $c_u/(\gamma B)$, β, b/B, V/B	Bearing capacity factors	Georgiadis (2010b)

Finite element analysis	Strip	Cohesionless soil	Inclined loading, b/B	Normalized failure load	Baazouzi et al. (2016)
Finite element analysis	Square	Cohesionless soil	b/B, H/B, ϕ, β, B, E	Bearing capacity	Acharyya and Dey (2017)
Discontinuity layout optimization (DLO)	Strip	c - ϕ soil	b/B, H/B, ϕ, β, $c/(\gamma B)$	Bearing capacity factors	Zheng et al. (2018)
Lower bound limit analysis	Strip	c - ϕ soil	β, b/B, ϕ, dilative coefficient	Bearing capacity factors	Halder et al. (2019)

Several researchers investigated the influence of the foundation setback distance, b, or the setback ratio (b/B) impact on the foundation bearing capacity (Meyerhof, 1957, Gemperline, 1988, Narita and Yamaguchi, 1990, Castelli and Lentini, 2012, Georgiadis 2010a, 2010b, Baazouzi et al. 2016, Acharyya and Dey 2017, Halder et al. 2019). Typically, the normalized bearing capacity will increase with an increase in the foundation setback ratio until a specific foundation setback ratio. This specific foundation setback ratio is defined as the critical setback ratio. The critical setback ratio also depends on the slope angle, soil properties and the ratio of the foundation width over the slope height (Georgiadis 2010a, Zheng et al. 2018). The slope with a higher slope angle requires a higher critical foundation setback distance. This is because of less area of soil that is available on slope with a higher slope angle for shear strength mobilization and provide resistance to the foundation loading. In construction manual such as AASHTO (2012) and Chinese code design for building foundation (Academy of Building Research 2011), the slope angle and soil properties also have been considered with the foundation setback ratio in the design chart. For example, an equation (Eq. 2.14) has been provided for the foundation setback ratio in Chinese code design for building foundation.

$$b \geq 3.5B - \frac{H}{\tan\beta} \tag{2.14}$$

For foundation located on the slope with a constant setback distance, a lower foundation bearing capacity factor are derived with a higher normalized slope height. The critical foundation setback ratio will also increase with an increase in the normalized slope height. Different slope angle, soil properties will also have impact on the normalized foundation bearing capacity. The normalized bearing capacity is lower at a higher slope angle when the slope heights are the same (Zhang et al. 2018, Yang et al. 2019). An interesting phenomenon has been highlighted by Georgiadis (2010a) based on their study under undrained condition for a slope angle of 30˚; for such a scenario, when the soil normalized strength influence factor ($c_u/\gamma B$) is increased to a specific value, the foundation normalized bearing capacity was not influenced by the normalized slope height. Therefore, different foundation position combined with the slope geometry may contribute to variations in the foundation bearing capacity.

Based on the published studies, failure mechanisms of the foundation slope system under different conditions can be generally classified under four different types (Meyerhof 1957, Georgiadis 2010a, 2010b, Leshchinsky 2015, Zhou et al. 2018, Dey et al. 2019, Halder et al. 2019, Li et al. 2020). Fig. 2.3 shows these failures: foundation bearing capacity failure (Failure ①), face failure (Failure ②, ③), toe failure (Failure ④) and deep-seated failure (Failure ⑤). The toe failure (Failure ④) can be considered as a special case of the face failure. Parameters such as the foundation setback ratio, slope height and angle, soil properties that were discussed earlier have an impact on these types of failure mechanisms (Georgiadis 2010a, Zheng et al. 2018, Yang et al. 2019). For example, the toe failure is common to see on the slope with a small height (Georgiadis 2010a). Beyond the critical height, the soil failure plain will extend to the sloping ground (Failure ② and ③ in Fig. 2.3, Georgiadis 2010a). This condition is typically observed with small foundation setback ratio. While the foundation bearing capacity failure is commonly found with greater foundation setback ratio.

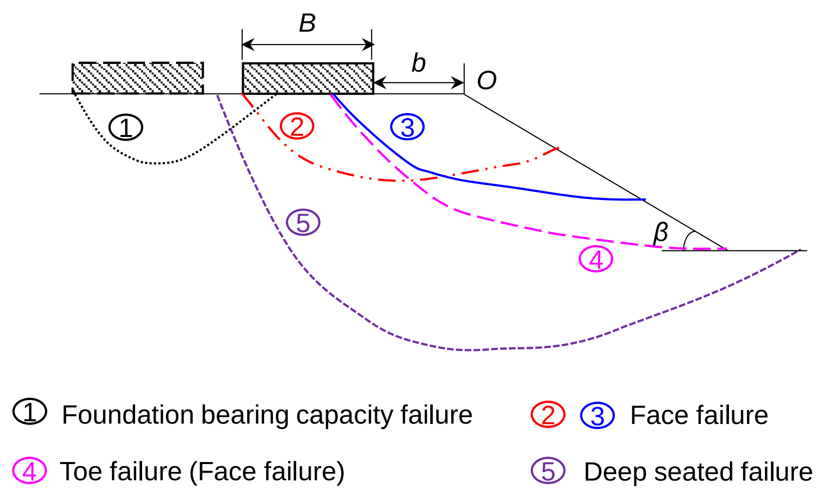

Fig. 2.3 Typical failure mechanisms

In summary, the influence of different parameters that influence the foundation behavior on slope is addressed in this section. Foundation setback ratio, foundation embedment depth, foundation loading conditions, slope geometry including slope height, angle, and soil properties all influence the foundation and slope system. The various failure mechanisms such as the foundation bearing capacity failure, the slope face failure for foundation on sloping ground depend on different parameters combinations. The above studies are all conducted on soil under saturated condition. However, as mentioned above, the matric suction has a significant influence on the foundation bearing capacity. The variation of the matric suction under the unsaturated flow may have a different impact compared to that in saturated soil.

2.4.2 Foundation on unsaturated soil slope

Currently, only a limited number of studies in the literature focus on the foundation behavior on sloping ground that in the state of unsaturated condition. Though foundation bearing capacity on unsaturated soil is relatively higher in comparison to saturated soil condition, environmental factors such as the infiltration and evaporations condition significantly influence their performance. Tran et al. (2019) and Troncone et al. (2021) carried out study of slope reinforced with a pile foundation subjected to rainfall infiltration. Shallow slope face failures are the main types of the failure during rainfall according to the study by Tran et al. (2019). The study indicated that the rainfall intensity, duration, soil properties and structures do influence the combined system. However, both studies focus on the slope stability taking account of rainfall infiltration rather than the foundation behavior. Talukdar et al. (2018) investigated the anthropogenic activities on the slope due to seepage. Results of this study suggest that the construction of structures without proper protection especially for scenarios with a shallow ground water table triggers slope failures during rainy season; such a behavior can be attributed to the seepage behavior that will aggravate the progressive failure. Tan and Vanapalli (2021) conducted hydro-mechanical modeling to investigate a foundation on a clay type of soil subjected to rainfall infiltration; the bearing capacity along with the factor of safety of the slope are presented under the transient flow. Different failure mechanisms are found with the increasing rainfall duration. The results reflect more uncertainty for the foundations on sloping ground due to infiltration of rainfall water. Therefore, it is of important to take account of the influence of environmental factors on the behavior of foundations in unsaturated soil slopes.

2.5 Summary

In this chapter, the studies related to foundation on level ground in unsaturated soils were summarized followed by studies for foundation on sloping ground with soil under saturated and unsaturated conditions. All the studies suggest that the matric suction is a key parameter that significantly influences the foundation behavior. The matric suction has a significant impact on the soil shear strength and other soil properties which in turn influence the foundation behavior in unsaturated soils. This also reflects the necessity to take account the unsaturated flow into the foundation performance evaluation. Based on the comprehensive literature, the following key conclusions are summarized.

(1) Several researchers investigated the behavior of foundations in unsaturated soils on level ground; however, studies related to the foundation behavior taking account of inclined and eccentric loading is rather limited. No studies have been found to the author's best knowledge that addresses the unsaturated flow for foundation subjected to inclined and eccentric loading and for foundation on non-homogeneous soil.

(2) The foundation behavior on slopes in saturated soils has been studied comprehensively. The foundation setback ratio, embedment depth, foundation loading conditions, slope height and angle, and soil properties all have influence on the foundation and slope system. However, only a few studies are reported in the literature with respect foundation behavior in unsaturated soil slopes taking account the above parameters and the unsaturated flow behavior. The combined performance of the foundation and the

unsaturated soil slope subjected to water infiltration is still awaiting in the literature to the best of the author’s knowledge.

(3) Determination of foundation behavior taking account of the influence of various parameters based on experimental methods is time consuming and expensive. Numerical and analytical methods facilitate in investigating the influence of several parameters to assess the behavior of foundations in unsaturated soils considering complex scenarios: for example, the climate influences. There is a need for developing new models that can provide a better understanding for foundation behavior under different unsaturated flow conditions taking account influence of several parameters efficiently.

References

AASHTO (American Association of State Highway and Transportation Officials), 2014. AASHTO LRFD Bridge Design Specifications. 7th ed., customary U.S. units. Washington, DC: AASHTO.

Acharyya, R., Dey, A., 2017. Finite element investigation of the bearing capacity of square footings resting on sloping ground. INAE Letters, 2(3), 97-105. https://doi.org/10.1007/s41403-017-0028-6.

Akbari G.A., Sadeghi, H., Saheb, S., Lamei, A., 2020. Bearing capacity of shallow foundations on unsaturated soils: Analytical approach with 3D numerical simulations and experimental validations. Int. J. Geomech., 20(3), 04019181. https://doi.org/10.1061/(ASCE)GM.1943-5622.0001589.

Anand, A., Sarkar, R., 2021. A comprehensive investigation on bearing capacity of shallow foundations on unsaturated fly ash slopes adopting finite element limit analysis. Eur. J. Environ. Civ., 1-27. https://doi.org/10.1080/19648189.2021.1967200.

Anand, A., Sarkar, R., 2022. Probabilistic investigation on seismic bearing capacity of shallow foundation on unsaturated fly ash deposit. In *Ground Characterization and Foundations* (pp. 459-470). Springer, Singapore.

Baazouzi, M., Benmeddour, D., Mabrouki, A., Mellas, M., 2016. 2D numerical analysis of shallow foundation rested near slope under inclined loading. Procedia Engineering, 143, 623-634. https://doi.org/10.1016/j.proeng.2016.06.086.

Bauer, G.E., Shields, D.H., Scott, J.D., Gruspier, J.E., 1981. Bearing capacity of footing in granular slope. In *Proceedings of 11th International Conference on Soil Mechanics and Foundation Engineering*, 2, 33–36.

Bishop, A.W., 1959. The principle of effective stress. Technisk Ukeblad, 39, 859-863.

Bransby, M.F., and Randolph, M.F. 1998. Combined loading of skirted foundations. Géotechnique, 48(5), 637-655.

Bransby, M.F., and Randolph, M.F. 1999. The effect of embedment depth on the undrained response of skirted foundations to combined loading. Soils and foundations, 39(4), 19-33.

Castelli, F., Lentini, V., 2012. Evaluation of the bearing capacity of footings on slopes. International Journal of Physical Modelling in Geotechnics, 12(3), 112-118. https://doi.org/10.1680/ijpmg.11.00015.

Chinese Academy of Building Research, 2011. GB 50007-2011 Code for Design of Building Foundation. Beijing: China Architecture & Building Press.

Conciani, W., Soares, M.M., Futai, M.M., 1998. Plate load tests with suction measurements. In *Problematic soils*, 301-304.

Consoli, N.C., Schnaid, F., Milititsky, J., 1998. Interpretation of plate load tests on residual soil site. Journal of Geotechnical and Geoenvironmental Engineering, 124(9), 857-867. https://doi.org/10.1061/(ASCE)1090-0241(1998)124:9(857).

Costa, Y.D., Cintra, J.C., Zornberg, J.G., 2003. Influence of matric suction on the results of plate load tests performed on a lateritic soil deposit. Geotechnical Testing Journal, 26(2), 219-227. https://doi.org/10.1520/GTJ11326J.

Cure, E., Sadoglu, E., Turker, E., Uzuner, B.A., 2014. Decrease trends of ultimate loads of eccentrically loaded model strip footings close to a slope. Geomechanics and Engineering, 6(5), 469-485. https://doi.org/10.12989/gae.2014.6.5.469.

Dey, A., Acharyya, R., Alammyan, A., 2021. Bearing capacity and failure mechanism of shallow footings on unreinforced slopes: a state-of-the-art review. International Journal of Geotechnical Engineering, 15(10), 1284-1297. https://doi.org/10.1080/19386362.2019.1617480.

Du, D., Zhuang, Y., Sun, Q., Yang, X., Dias, D., 2021. Bearing capacity evaluation for shallow foundations on unsaturated soils using discretization technique. Comput. Geotech., 137, 104309. https://doi.org/10.1016/j.compgeo.2021.104309.

Du, Y., Sheng, Q., Fu, X., Chen, H., Li, G., 2022. New model for predicting the bearing capacity of large strip foundations on soil under combined loading. Int. J. Geomech., 22(5), 04022055. https://doi.org/10.1061/(ASCE)GM.1943-5622.0002389.

Escario, V., Juca, J.F.T., Coppe, M.S., 1989. Strength and deformation of partly saturated soils. In *Proceedings of 12th International Conference on Soil Mechanics and Foundation Engineering*, 43-46.

Fathipour, H., Payan, M., Chenari, R.J., Fatahi, B., 2022. General failure envelope of eccentrically and obliquely loaded strip footings resting on an inherently anisotropic granular medium. Computers and Geotechnics, 146, 104734. https://doi.org/10.1016/j.compgeo.2022.104734.

Fredlund, D.G., Morgenstern, N.R., Widger, R.A., 1978. The shear strength of unsaturated soils. Canadian Geotechnical Journal, 15(34), 313-321. https://doi.org/10.1139/t78-029.

Fredlund, D.G., Xing. A., Fredlund, M.D., Barbour, S.L., 1996. Relationship of the unsaturated soil shear strength to the soil-water characteristic curve. Canadian Geotechnical Journal, 33(3), 440-448. https://doi.org/10.1139/t96-065.

Gan, J.K.M., Fredlund, D.G., Rahardjo, H., 1988. Determination of the shear strength parameters of an unsaturated soil using the direct shear test. Canadian Geotechnical Journal, 25(3), 500-510. https://doi.org/10.1139/t88-055.

Ganesh, R., Khuntia, S., Sahoo, J.P., 2017. Bearing capacity of shallow strip foundations in sand under eccentric and oblique loads. Int. J. Geomech., 17(4), 06016028. https://doi.org/10.1061/(ASCE)GM.1943-5622.0000799.

Garven, E.A., Vanapalli, S.K., 2006. Evaluation of empirical procedures for predicting the shear strength of unsaturated soils. In *Proceedings of 4th International Conference on Unsaturated Soils*, Carefree, Arizona, United States. American Society of Civil Engineers Geotechnical Special Publication, 147(2), 2570-2581. https://doi.org/10.1061/40802(189)219.

Gemperline, M.C., 1988. Centrifugal modeling of shallow foundations. In *Soil Properties Evaluation from Centrifugal Models and Field Performance*, 45-70. Reston, VA: American Society of Civil Engineers.

Georgiadis, K., 2010a. Undrained bearing capacity of strip footings on slopes. Journal of Geotechnical and Geoenvironmental Engineering, 136(5), 677-685. https://doi.org/10.1061/(ASCE)GT.1943-5606.0000269.

Georgiadis, K., 2010b. The influence of load inclination on the undrained bearing capacity of strip footings on slopes. Computers and Geotechnics, 37(3), 311-322. https://doi.org/10.1016/j.compgeo.2009.11.004.

Ghasemzadeh, H., Akbari, F., 2019. Determining the bearing capacity factor due to nonlinear matric suction distribution in the soil. Can. J. Soil Sci., 99(4), 434-446. https://doi.org/10.1139/cjss-2019-0071.

Gottardi, G., and Butterfield, R. 1993. On the bearing capacity of surface footings on sand under general planar loads. Soils and Foundations, 33(3), 68–79.

Gourvenec, S., Randolph, M., 2003. Effect of strength nonhomogeneity on the shape of failure envelopes for combined loading of strip and circular foundations on clay. Géotechnique, 53(6), 575–586. https://doi.org/10.1680/geot.2003.53.6.575.

Graham, J., Andrews, M., Shields, D.H., 1988. Stress characteristics for shallow footings in cohesionless slopes. Canadian Geotechnical Journal, 25(2), 238-249. https://doi.org/10.1139/t88-028.

Halder, K., Chakraborty, D., Dash, S.K., 2018. Bearing capacity of a strip footing situated on soil slope using a non-associated flow rule in lower bound limit analysis. In *Geotechnical Earthquake Engineering and Soil Dynamics V: Numerical Modeling and Soil Structure Interaction*, 454-463. Reston, VA: American Society of Civil Engineers. https://doi.org/10.1061/9780784481479.047.

Han, Z., Han, S., Oh, W.T., Vanapalli, S.K., 2014. Modelling the stress settlement behavior of shallow foundation in unsaturated sand using Sigma/W and Plaxis. In *Proceedings of the 67th Canadian Geotechnical Conference*, 1-8. Regina, Saskatchewan: Can. Geotech. Soc.

Hansen, J.B., 1970. A revised and extended formula for bearing capacity. Bulletin, No 28, 5-11. Geoteknisk Institut (The Danish Geotechnical Institute), Copenhagen.

Hjiaj, M., Lyamin, A. V., Sloan, S.W., 2004. Bearing capacity of a cohesive-frictional soil under non-eccentric inclined loading. Computers and Geotechnics, 31(6), 491-516. https://doi.org/10.1016/j.compgeo.2004.06.001.

Jahanandish, M., Habibagahi, G., Veiskarami, M., 2010. Bearing capacity factor, N_γ, for unsaturated soils by ZEL method. Acta Geotechnica, 5(3), 177-188. https://doi.org/10.1007/s11440-010-0122-3.

Jeong, S., Kim, Y., Park, H., Kim, J., 2018. Effects of rainfall infiltration and hysteresis on the settlement of shallow foundations in unsaturated soil. Environmental Earth Sciences, 77(13), 1-12. https://doi.org/10.1007/s12665-018-7690-1.

Jin, L.X., Zhang, H.C., Feng, Q.X., 2019. Application of improved radial movement optimization for calculating the upper bound of ultimate bearing capacity of shallow foundation on unsaturated soil. Comput. Geotech., 109, 82-88. https://doi.org/10.1016/j.compgeo.2019.01.016.

Jin, L.X., Zhang, H.C., Luo, C., Feng, Q.X., 2021. The implementation of improved radial movement optimization to calculate the ultimate bearing capacity of strip footing on unsaturated soil under inclined loading. Arabian Journal of Geosciences, 14(17), 1-13. https://doi.org/10.1007/s12517-021-08090-3.

Keskin, M.S., Laman, M., 2013. Model studies of bearing capacity of strip footing on sand slope. KSCE Journal of Civil Engineering, 17(4), 699-711. https://doi.org/10.1007/s12205-013-0406-x.

Khalili, N., Khabbaz, M.H., 1998. A unique relationship for χ for the determination of the shear strength of unsaturated soils. Géotechnique, 48(5), 681-687. https://doi.org/10.1680/geot.52.1.76.40832.

Kim, Y., Park, H., Jeong, S., 2017. Settlement behavior of shallow foundations in unsaturated soils under rainfall. Sustainability, 9(8), 1417. https://doi.org/10.3390/su9081417.

Krabbenhoft, S., Damkilde, L., Krabbenhoft, K., 2014. Bearing capacity of strip footings in cohesionless soil subject to eccentric and inclined loads. Int. J. Geomech., https://doi.org/10.1061/(ASCE)GM.1943-5622.0000332.

Larsson, R., 1997. Investigations and load tests in silty soils. Results from a series of investigations in silty soils in Sweden. Report No. 54, Swedish Geotechnical Institute.

Le, T.M.H., Gallipoli, D., Sanchez, M., Wheeler, S., 2013. Rainfall-induced differential settlements of foundations on heterogeneous unsaturated soils. Géotechnique, 63(15), 1346-1355. https://doi.org/10.1680/geot.12.P.181.

Lee, S.J., Lee, S.R., Kim, Y.S., 2003. An approach to estimate unsaturated shear strength using artificial neural network and hyperbolic formulation. Computers and Geotechnics, 30(6), 489-503. https://doi.org/10.1016/S0266-352X(03)00058-2.

Leshchinsky, B., 2015. Bearing capacity of footings placed adjacent to c'- ϕ' slopes. Journal of Geotechnical and Geoenvironmental Engineering, 141(6), 04015022. https://doi.org/10.1061/(ASCE)GT.1943-5606.0001306.

Leshchinsky, B., Xie, Y., 2017. Bearing capacity for spread footings placed near c'-ϕ' slopes. Journal of Geotechnical and Geoenvironmental Engineering, 143(1), 06016020. https://doi.org/10.1061/(ASCE)GT.1943-5606.0001578.

Li, C., Jiang, P., 2022. Oblique and eccentric bearing capacity of embedded strip footings using the method of rigorous characteristics. International Journal for Numerical and Analytical Methods in Geomechanics, 46(9), 1685-1704. https://doi.org/10.1002/nag.3363.

Li, C., Zhou, A., Jiang, P., 2020. Eccentric bearing capacity of embedded strip footings placed on slopes. Comput. Geotech., 119, 103352. https://doi.org/10.1016/j.compgeo.2019.103352.

Lins, Y., Schanz, T., Vanapalli, S.K., 2009. Bearing capacity and settlement behavior of a strip footing on an unsaturated coarse-grained soil. In *Proceedings of the 4th Asia-Pacific Conference on Unsaturated Soils*.

Liu, R., Wang, L., Ding, H.Y., Lian, J.J., and Li, B R. 2014. Failure envelopes of large-diameter shallow buried bucket foundation in undrained saturated soft clay under combined loading conditions. Chinese journal of geotechnical engineering, 36(1), 146-154.

Loukidis, D., Chakraborty, T., Salgado, R., 2008. Bearing capacity of strip footings on purely frictional soil under eccentric and inclined loads. Canadian Geotechnical Journal, 45(6), 768-787. https://doi.org/10.1139/T08-015.

Mahmoudabadi, V., Ravichandran, N., 2019. Design of shallow foundation considering site-specific rainfall and water table data: Theoretical framework and application. International Journal of Geomechanics, 19(7), 04019063. https://doi.org/10.1061/(ASCE)GM.1943-5622.0001432.

Meyerhof, G.G., 1953. The bearing capacity of foundations under eccentric and inclined loads. In *Proceedings of the 3rd International Conference on Soil Mechanics and Foundation Engineering (ICSMFE)*, Vol. 1, 440-445. London: International Society of Soil Mechanics and Geotechnical Engineering.

Meyerhof, G.G., 1957. The ultimate bearing capacity of foundations on slopes. In *Proceedings of the 4th International Conference on Soil Mechanics and Foundation Engineering (ICSMFE)*, Vol. 1, 384-386. London: International Society of Soil Mechanics and Geotechnical Engineering.

Meyerhof, G.G., 1963. Some recent research on the bearing capacity of foundations. Can. Geotech. J., 1(1), 16–26. https://doi.org/10.1139/t63-003.

Michalowski, R.L., You, L., 1998. Effective width rule in calculations of bearing capacity of shallow footings. Computers and Geotechnics, 23(4), 237-253. https://doi.org/10.1016/S0266-352X(98)00024-X.

Mohamed, F.M.O., 2014. Bearing capacity and settlement behaviour of footings subjected to static and seismic loading conditions in unsaturated sandy soils. Doctoral dissertation, Université d'Ottawa/University of Ottawa, Ottawa.

Mohamed, F.M.O., Vanapalli, S.K., 2006. Laboratory investigations for the measurement of the bearing capacity of an unsaturated coarse-grained soil. In *Proceedings of the 59th Canadian Geotechnical Conference*, 1-4. Vancouver, BC: Can. Geotech. Soc.

Mohamed, F.M.O., Vanapalli, S.K., 2015. Bearing capacity of shallow foundations in saturated and unsaturated sands from SPT–CPT correlations. International Journal of Geotechnical Engineering, 9(1), 2-12. https://doi.org/10.1179/1939787914Y.0000000082.

Mohamed, F.M.O., Vanapalli, S.K., Saatcioglu, M. 2010. Comparison of bearing capacity of unsaturated sands using cone penetration tests (CPT) and plate load tests (PLT). In *Unsaturated Soils*, 1183–1188. Barcelona: CRS Press.

Narita, K., Yamaguchi, H., 1990. Bearing capacity analysis of foudations on slopes by use of log-spiral sliding surfaces. Soils and Foundations, 30(3), 144-152. https://doi.org/10.3208/sandf1972.30.3_144.

Oliveira, O.M., Marinho, F.A.M., 2003. Unsaturated shear strength behaviour of a compacted residual soil. In *Proceedings of Asian Conference on Unsaturated Soils: Unsaturated Soil Geotechnical and Geoenvironmental Issues*, 237-242. Osaka, Japan.

Oloo, S.Y., 1994. A bearing capacity approach to the design of low-volume-traffic roads. Doctoral dissertation, University of Saskatchewan, Saskatoon.

Oloo, S.Y., Fredlund, D.G., Gan, J.K., 1997. Bearing capacity of unpaved roads. Can. Geotech. J., 34(3), 398-407. https://doi.org/10.1139/t96-084.

Oh, W.T., Vanapalli, S.K., 2011. Modelling the applied vertical stress and settlement relationship of shallow foundations in saturated and unsaturated sands. Canadian Geotechnical Journal, 48(3), 425-438. https://doi.org/10.1139/T10-079.

Oh, W.T., Vanapalli, S.K., 2013. Interpretation of the bearing capacity of unsaturated fine-grained soil using the modified effective and the modified total stress approaches. Int. J. Geomech., 13(6), 769-778. https://doi.org/10.1061/(ASCE)GM.1943-5622.0000263.

Oh, W.T., Vanapalli, S.K., 2018. Modeling the stress versus settlement behavior of shallow foundations in unsaturated cohesive soils extending the modified total stress approach. Soils and Foundations, 58(2), 382-397. https://doi.org/10.1016/j.sandf.2018.02.008.

Oh, W.T., Vanapalli, S.K., Puppala, A.J., 2009. Semi-empirical model for the prediction of modulus of elasticity for unsaturated soils. Canadian Geotechnical Journal, 46(8), 903-914. https://doi.org/10.1139/T09-030.

Patra, C., Behara, R., Sivakugan, N., Das, B., 2012a. Ultimate bearing capacity of shallow strip foundation under eccentrically inclined load, Part I. International Journal of Geotechnical Engineering, 6(3), 343-352. https://doi.org/10.3328/IJGE.2012.06.03.343-352.

Patra, C., Behara, R., Sivakugan, N., Das, B., 2012b. Ultimate bearing capacity of shallow strip foundation under eccentrically inclined load, Part II. International Journal of Geotechnical Engineering, 6(4), 507-514. https://doi.org/10.3328/IJGE.2012.06.04.507-514.

Pham, Q. N., Ohtsuka, S., Isobe, K., Fukumoto, Y., and Hoshina, T. 2019. Ultimate bearing capacity of rigid footing under eccentric vertical load. Soils and Foundations, 59(6), 1980-1991.

Pham, Q. N., Ohtsuka, S., Isobe, K., and Fukumoto, Y. 2020. Limit load space of rigid footing under eccentrically inclined load. Soils and Foundations, 60(4), 811-824.

Pham, Q. N., Ohtsuka, S., Isobe, K., and Fukumoto, Y. 2022. Limit load space of rigid strip footing on cohesive-frictional soil subjected to eccentrically inclined loads. Computers and Geotechnics, 151, 104956.

Purkayastha, R.D., and Char, R.A. 1977. Stability analysis for eccentrically loaded footings. J. Geotech. Eng., 103(6), 647–651. https://doi.org/10.1061/AJGEB6.0000441.

Ravichandran, N., Vickneswaran, T., Marathe, S., Jella, V.S., 2021. Numerical analysis of settlement response of shallow footing subjected to heavy rainfall and flood events. Int. J. Geosci., 12(2), 138-158. https://doi.org/10.4236/ijg.2021.122009.

Rojas, J.C., Salinas, L.M., Sejas, C., 2007. Plate-load tests on an unsaturated lean clay. In *Experimental Unsaturated Soil Mechanics*, 445-452. Springer, Berlin, Heidelberg.

Sheng, D., Gens, A., Fredlund, D.G., Sloan, S.W., 2008. Unsaturated soils: From constitutive modelling to numerical algorithms. Computers and Geotechnics, 35(6), 810-824. https://doi.org/10.1016/j.compgeo.2008.08.011.

Shields, D.H., Scott, J.D., Bauer, G.E., Deschenes, J.H., Barsvary, A.K., 1977. Bearing capacity of foundation near slopes. In *Proceedings of the 10th International Conference on Soil Mechanics and Foundation Engineering (ICSMFE)*, Vol. 1, 715–720. Tokyo, Japan: Japanese Society of Soil Mechanics and Foundation Engineering.

Taiebat, H.A., Carter, J.P., 2000. Numerical studies of the bearing capacity of shallow foundations on cohesive soil subjected to combined loading. Géotechnique, 50(4), 409-418. https://doi.org/10.1680/geot.2000.50.4.409.

Taiebat, H.A., Carter, J.P., 2002. Bearing capacity of strip and circular foundations on undrained clay subjected to eccentric loads. Géotechnique, 52(1), 61–64. https://doi.org/10.1680/geot.2002.52.1.61.

Talukdar, P., Bora, R., Dey, A., 2018. Numerical investigation of hill slope instability due to seepage and anthropogenic activities. Indian Geotechnical Journal, 48(3), 585–594. https://doi.org/10.1007/s40098-017-0272-4.

Tan, M.X., Vanapalli, S.K., 2021. Performance estimation of a shallow foundation on an unsaturated expansive soil slope subjected to rainfall infiltration. In *Proceedings of the 3rd Pan-American Conference on Unsaturated Soils: MATEC Web of Conferences*, 337, 03009. https://doi.org/10.1051/matecconf/202133703009.

Tan, X.H., Xie, Y., Hou, X.L., Li, P., Wang, X., 2017. Reliability analysis of shallow foundations on unsaturated soils under rainfall infiltration. In *Geo-Risk 2017: Reliability-Based Design and Code Developments*, 588-597. Denver, Colorado: the Geo-Institute of ASCE. https://doi.org/10.1061/9780784480700.

Tang, C., Phoon, K.K., and Toh, K.C. 2015. Effect of footing width on N_γ and failure envelope of eccentrically and obliquely loaded strip footings on sand. Canadian Geotechnical Journal, 52(6), 694-707.

Tang, Y., Taiebat, H.A., Senetakis, K., 2017. Effective stress based bearing capacity equations for shallow foundations on unsaturated soils. Journal of GeoEngineering, 12(2), 59-64. https://doi.org/10.6310/jog.2017.12(2).2.

Tang, Y., Vo, T., Taiebat, H.A., Russell, A.R., 2018. Influences of suction on plate load tests on unsaturated silty sands. Journal of Geotechnical and Geoenvironmental Engineering, 144(8), 04018043. https://doi.org/10.1061/(ASCE)GT.1943-5606.0001897.

Tekinsoy, M.A., Kayadelen, C., Keskin, M.S., Söylemez, M., 2004. An equation for predicting shear strength envelope with respect to matric suction. Computers and Geotechnics, 31(7), 589-593. https://doi.org/10.1016/j.compgeo.2004.08.001.

Terzaghi, K., 1943. Theoretical Soil Mechanics. John Wiley & Sons, Inc. https://doi.org/10.1002/9780470172766.

Tran, A.T.P., Kim, A.R., Cho, G.C., 2019. Numerical modeling on the stability of slope with foundation during rainfall. Geomech. Eng., 17(1), 109-118. https://doi.org/10.12989/gae.2019.17.1.109.

Troncone, A., Pugliese, L., Lamanna, G., Conte, E., 2021. Prediction of rainfall-induced landslide movements in the presence of stabilizing piles. Eng. Geol., 288, 106143. https://doi.org/10.1016/j.enggeo.2021.106143.

Ukritchon, B., Whittle, A.J., and Sloan, S.W. 1998. Undrained limit analyses for combined loading of strip footings on clay. Journal of Geotechnical and Geoenvironmental Engineering, 124(3), 265-276.

Vahedifard, F., Robinson, J.D., 2016. Unified method for estimating the ultimate bearing capacity of shallow foundations in variably saturated soils under steady flow. J. Geotech. Geoenviron. Eng., 142(4), 04015095. https://doi.org/10.1061/(ASCE)GT.1943-5606.0001445.

Vanapalli, S.K., 2009. Shear strength of unsaturated soils and its applications in geotechnical engineering practice. In *Proceedings of Asia-Pacific Conference on Unsaturated Soils*, 579-598. New Castle, Australia.

Vanapalli, S.K., Fredlund, D.G., 2000. Comparison of empirical procedures to predict the shear strength of unsaturated soils uses the soil-water characteristic curve. In *Geo-Denver 2000: Advances in Unsaturated Geotechnics*, 195-209. Denver, Colorado: American Society of Civil Engineers. https://doi.org/10.1061/40510(287)13.

Vanapalli, S.K., Fredlund, D.G., Pufahl, D.E., Clifton, A.W., 1996. Model for the prediction of shear strength with respect to soil suction. Canadian Geotechnical Journal 33(3), 379-392. https://doi.org/10.1139/t96-060.

Vanapalli, S.K., Mohamed, F.M., 2007. Bearing capacity of model footings in unsaturated soils. In *Experimental Unsaturated Soil Mechanics*, 483-493. Springer, Berlin, Heidelberg.

Vanapalli, S.K., Mohamed, F.M., 2013. Bearing capacity and settlement of footings in unsaturated sands. Int. J. Geomate, 5(1), 595-604. https://doi.org/10.21660/2013.9.3k.

Vanapalli, S.K., Oh, W.T., 2010. A model for predicting the modulus of elasticity of unsaturated soils using the soil-water characteristic curve, International Journal of Geotechnical Engineering, 4(4), 425-433. https://doi.org/10.3328/IJGE.2010.04.04.425-433.

Vanapalli, S.K., Oh, W.T., 2021. Analytical and numerical methods for prediction of the bearing capacity of shallow foundations in unsaturated soils. Soils and Rocks, 44(3), e2021066521. https://doi.org/10.28927/SR.2021.066521.

Vanapalli, S.K., Oh, W.T., Puppala, A.J., 2007. Determination of the bearing capacity of unsaturated soils under undrained loading conditions. In *Proceedings of the 60th Canadian Geotechnical Conference*, 21-24. Alliston, ON: Can. Geotech. Soc.

Vesić, A., 1975. Bearing capacity of shallow foundations. In: Foundation engineering handbook (1st edn.), Winterkorn, H.F., Fang, H.Y. (eds), Chapter 3. New York, NY: Van Nostrand Reinhold.

Vo, T., Russell, A.R., 2016. Bearing capacity of strip footings on unsaturated soils by the slip line theory. Computers and Geotechnics, 74, 122-131. https://doi.org/10.1016/j.compgeo.2015.12.016.

Vulpe, C., Gourvenec, S., and Power, M. 2014. A generalised failure envelope for undrained capacity of circular shallow foundations under general loading. *Géotechnique Letters*, *4*(3), 187-196.

Wuttke, F., Kafle, B., Lins, Y., Schanz, T., 2013. Macroelement for statically loaded shallow strip foundation resting on unsaturated soil. International Journal of Geomechanics, 13(5), 557-564. https://doi.org/10.1061/(ASCE)GM.1943-5622.0000254.

Xu, Y., 2004. Bearing capacity of unsaturated expansive soils. Geotechnical and Geological Engineering, 22(4), 611-625. https://doi.org/10.1023/B:GEGE.0000047043.29898.17.

Yang, S., Leshchinsky, B., Cui, K., Zhang, F., Gao, Y., 2019. Unified approach toward evaluating bearing capacity of shallow foundations near slopes. J. Geotech. Geoenviron. Eng., 145(12), 04019110. https://doi.org/10.1061/(ASCE)GT.1943-5606.0002178.

Yang, X.L., Wang, Z.B., Zou, J.F., Li, L., 2007. Bearing capacity of foundation on slope determined by energy dissipation method and model experiments. Journal of Central South University of Technology, 14(1), 125-128. https://doi.org/10.1007/s11771-007-0025-0.

Yun, G., and Bransby, M.F. 2007. The horizontal-moment capacity of embedded foundations in undrained soil. Canadian Geotechnical Journal, 44(4), 409-424.

Zhan, Y.G., Vanapalli, S.K., 2012. Some aspects on numerical modeling of model footing test on saturated and unsaturated sands. Electronic Journal of Geotechnical Engineering, 17, 2833-2850.

Zhang, C., Gao, B., Yan, Q., Zhao, J., Wu, L., 2019. Development of allowable bearing capacity for strip foundations in unsaturated soils. Comput. Geotech., 114, 103138. https://doi.org/10.1016/j.compgeo.2019.103138.

Zheng, G., Yu, X., Du, J., Yin, X., Zhou, H., Yang, X., 2018. Numerical analysis of ultimate bearing capacity of strip footings near slopes. Rock and Soil Mechanics, 39(10), 3812-3820. (In Chinese). https://doi.org/10.16285/j.rsm.2017.0257.

Zheng, G., Zhao, J., Zhou, H., and Zhang, T. 2019. Ultimate bearing capacity of strip footings on sand overlying clay under inclined loading. Computers and Geotechnics, 106, 266-273.

Zhou, H., Zheng, G., Yin, X., Jia, R., Yang, X., 2018. The bearing capacity and failure mechanism of a vertically loaded strip footing placed on the top of slopes. Comput. Geotech., 94, 12-21. https://doi.org/10.1016/j.compgeo.2017.08.009.

CHAPTER 3

Foundation bearing capacity estimation on unsaturated soil slope under transient flow condition[2]

3.1 Introduction

Design of foundations for the various infrastructure constructed on hilly regions are typically based on the assumption that the soil is in a state of saturated condition. However, foundations for most of the infrastructure in many scenarios is above the groundwater table during their entire service life. Natural soils, especially in semi-arid and arid regions that constitute 40% of the earth's surface are typically in an unsaturated state condition (e.g., Khalili et al. 2000, Fredlund et al., 2012). Several investigators during the last quarter century have significantly contributed to the design of shallow foundations, extending the mechanics of unsaturated soils (e.g., Oloo et al., 1997, Xu, 2004, Vanapalli and Mohammed, 2007, Oh and Vanapalli, 2011, 2013, 2018, Tang et al., 2017, Ghasemzadeh and Akbari, 2019, Zhang et al., 2019, Akbari et al., 2020, Cascone et al., 2021, Vanapalli and Oh, 2021). The conventional Terzaghi (1943) and Skempton (1948) bearing capacity equations are modified in these studies to interpret the influence of matric suction on the bearing capacity.

In recent years, several investigators have contributed to better understand the influence of environmental effects on the foundation bearing capacity in unsaturated soils

[2] The contents presented in this chapter are published as a journal article:
Tan, M., & Vanapalli, S. K. (2022). Foundation bearing capacity estimation on unsaturated soil slope under transient flow condition using slip line method. *Computers and Geotechnics*, *148*, 104804. https://doi.org/10.1016/j.compgeo.2022.104804.

(Vahedifard and Robinson, 2016, Vo and Russell, 2016, Kim et al., 2017, Jeong et al., 2019, Mahmoudabadi and Ravichandran, 2019, Anand and Sarkar, 2021, Du and Ye, 2021, Ravichandran et al., 2021). Most of these studies were directed to understand the foundation behavior on a level ground considering steady state conditions. The soil hydraulic and mechanical behavior are nonlinear and sensitive to matric suction fluctuations especially under transient condition. Incorporating the influence of matric suction changes on the foundation behavior under transient condition is time-dependent and is associated with uncertainties. Comprehensive research studies in this direction are lacking in the literature. For example, Tran et al. (2019) and Troncone et al. (2021) conducted studies of slope reinforced with a pile foundation subjected to rainfall infiltration. Tan and Vanapalli (2021) investigated the shallow foundation behavior on a clay soil slope considering the influence of rainfall infiltration. Results of the above studies suggest that the rainfall intensity and its duration along with the soil properties influence the foundation-slope system. In addition, the foundation setback distance, the slope angle and the foundation loading conditions also significantly influence both the foundation and the slope system. However, the influence of these parameters was investigated only for saturated soils (Meyerhof, 1957, Georgiadis, 2010a, 2010b, Leshchinsky, 2015, Zhou et al., 2018, Dey et al., 2019, Halder et al., 2019, Jin et al., 2020, Li et al., 2020, Li et al., 2021).

For this reason, the focus of the present study is directed towards providing a comprehensive understanding of the bearing capacity of shallow foundations on unsaturated soil slopes considering the transient flow conditions. The slip line method has been used in the recent literature for interpreting the behavior of both foundations and slopes (Vo and Russell, 2016, 2017, 2020, Li and Jiang, 2019, Cascone et al., 2021, Li et al., 2021). In this study, slip line method is employed coupling it with a closed-form solution to take account the vertical transient unsaturated flow conditions. To the best of the authors' knowledge, this is the first attempt to develop a novel framework combining the slip line method for the foundation bearing capacity taking account the transient flow conditions for unsaturated soils. In addition, a comprehensive parametric study is conducted using the proposed framework. The influence of the rainfall infiltration characteristics, slope angle, β, foundation setback distance, b, ground water table depth, H_w, and varying soil properties on different types of soils are considered in the parametric study. Coding for the proposed framework is developed using MATLAB, which has the advantage of integrating programming along with the visualization aids. The proposed framework provides a valuable tool to estimate the foundation bearing capacity on both level and sloping ground under transient flow conditions. The results presented in the study are useful for the practicing engineers for rational interpretation of the foundation performance taking of various parameters including the vertical transient flow conditions.

3.2 Background and governing equations

The failure criterion is first presented in this section along with the details related to the induced slip lines. The closed-form solution is then introduced to take account the vertical transient unsaturated flow.

3.2.1 Shear strength and failure criterion

The following assumptions are made in this study:

(i) The shallow strip foundation is assumed as a rigid structure and is considered weightless.

(ii) The mechanical behavior of the soil can be reasonably evaluated using the Mohr-Coulomb (MC) failure criterion.

(iii) The interface between the foundation material and the soil is assumed smooth for achieving conservative estimations.

(iv) The ground water table is assumed parallel to the ground surface which is widely used in analytical methods (Zhan et al. 2013, Gongze Shi 2019).

In this study, Vanapalli et al. (1996) equation is used in the evaluation of the contribution of the matric suction towards the soil shear strength. This equation uses the effective shear strength parameters and the soil water characteristic curve (SWCC), which is summarized below.

$$\tau = c' + \left(\sigma_{\mathrm{n}} - u_{\mathrm{a}}\right)\tan\phi' + \left(u_{\mathrm{a}} - u_{\mathrm{w}}\right)\left(\frac{\theta_{\mathrm{w}} - \theta_{\mathrm{r}}}{\theta_{\mathrm{s}} - \theta_{\mathrm{r}}}\right)\tan\phi' \tag{3.1}$$

where τ is the shear strength of unsaturated soil; c' is the effective cohesion; ϕ' is the effective internal friction angle; (σ_n - u_a) and (u_a - u_w) are the net normal stress and matric suction, respectively. θ_w is the volumetric water content of the soil, θ_s and θ_r are the saturated and residual volumetric water contents, respectively. The term [(u_a - u_w) ((θ_w - θ_s) / (θ_s - θ_r) tan ϕ')] in Eq. (3.1) represents the contribution of the matric suction towards the shear strength. This can also be expressed as [(u_a - u_w) S_e tan ϕ'], where S_e, is the effective degree of saturation, which is defined as [(S - S_r) / (1 - S_r)] or in the term of [(θ_w - θ_s) / (θ_s - θ_r)]; S and S_r are the degree of saturation and the residual degree of saturation, respectively. As the change of the effective internal friction angle with respect to the matric suction is typically negligible for conventional soils (Fredlund and Rahardjo, 1993; Vanapalli et al. 1996; Tan et al. 2021), the apparent cohesion, c_a can also be used to describe the matric suction contribution and can be written using one of the equations below:

$$c_a = c' + (u_a - u_w)\left(\frac{\theta_w - \theta_r}{\theta_s - \theta_r}\right)\tan\phi' \quad (3.2a)$$

$$c_a = c' + (u_a - u_w)\left(\frac{S - S_r}{1 - S_r}\right)\tan\phi' \quad (3.2b)$$

Fig. 3.1 shows the extended Mohr-Coulomb (MC) envelope for interpreting the shear strength of unsaturated soils highlighting the terms introduced in the earlier paragraphs. The MC failure criterion can then be expressed as Eqs. (3.3 – 3.5) where u_a is equal to the atmospheric pressure and used as a reference for measurement of other stresses in the soil.

$$\sigma_x = (1 + \sin\phi'\cos 2\theta)\sigma_e' - c'\cot\phi' - S_e(u_a - u_w) \quad (3.3)$$

$$\sigma_y = (1 - \sin\phi'\cos 2\theta)\sigma_e' - c'\cot\phi' - S_e(u_a - u_w) \quad (3.4)$$

$$\tau_{xy} = \tau_{yx} = \sin\phi'\sin 2\theta\sigma_e' \quad (3.5)$$

where σ_x, σ_y are the normal stresses in the *X*- and *Y*- directions, respectively; τ_{xy} is the shear stress; θ is the angle between the major principal stress direction and the *X*- axis; σ_e' is the effective equivalent stress, $\sigma_e' = \sigma_m' + c_a \cot\phi'$, σ_m' is the effective mean stress.

Study by Sheng et al. (2011) shows Eq. (3.1) may be sensitive to the residual suction value especially for some clayey soils. However, this equation provides reasonable predictions for shear strength behavior when matric suctions values are influenced by the water movement in unsaturated soils (i.e., this typically forms the boundary effect and transition zones in an unsaturated soil that can be identified from the SWCC) (Vanapalli et al., 1996). There are also other shear strength equations in the literature that provide good estimations of the contribution of matric suction based on the effective stress equation (e.g., Bishop, 1959, Khalili and Khabbaz, 1998, Lu and Likos, 2006). These equations can also be introduced into Eqs. (3.3 – 3.5) to describe the matric suction contribution (e.g., Vo and Russel, 2016).

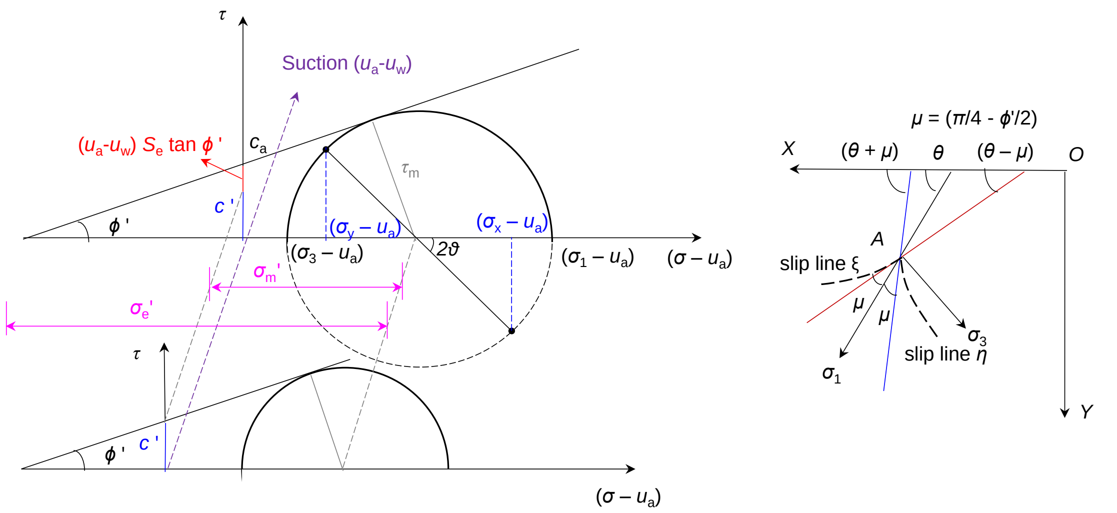

Fig. 3.1. Extended Mohr stress circle in unsaturated soil and stress state of a point *A*

3.2.2 Stress equations

Eq. (3.6) and Eq. (3.7) are widely used equilibrium equations under the plane strain conditions.

$$\frac{\partial \sigma_x}{\partial x} + \frac{\partial \tau_{xy}}{\partial y} = 0 \tag{3.6}$$

$$\frac{\partial \sigma_y}{\partial y} + \frac{\partial \tau_{xy}}{\partial x} = \gamma \tag{3.7}$$

where γ is soil unit weight. By substituting Eqs. (3.3 – 3.5) into Eq. (3.6) and Eq. (3.7), Eq. (3.8) and Eq. (3.9) can be obtained:

$$(1+\sin\phi'\cos 2\theta)\frac{\partial \sigma_e'}{\partial x} - \frac{\partial\left(c'\cot\phi' + S_e\left(u_a - u_w\right)\right)}{\partial x} + \sin\phi'\sin 2\theta\frac{\partial \sigma_e'}{\partial y} - 2\sigma_e'\sin\phi'\left(\sin 2\theta\frac{\partial \theta}{\partial x} - \cos 2\theta\frac{\partial \theta}{\partial y}\right) = 0 \tag{3.8}$$

$$(1-\sin\phi'\cos 2\theta)\frac{\partial\sigma_e'}{\partial y}-\frac{\partial\left(c'\cot\phi'+S_{\mathrm{e}}\left(u_{\mathrm{a}}-u_{\mathrm{w}}\right)\right)}{\partial y}+\sin\phi'\sin 2\theta\frac{\partial\sigma_e'}{\partial x}+2\sigma_e'\sin\phi'\left(\sin 2\theta\frac{\partial\theta}{\partial y}+\cos 2\theta\frac{\partial\theta}{\partial x}\right)=\gamma \tag{3.9}$$

After simplifications, the two families of characteristics (ξ line and η line) are obtained using Eqs. (3.10) and (3.11), respectively:

$$\xi\ Line\ \begin{cases} \dfrac{dy}{dx}=\tan(\theta-\mu) \\ d\sigma_{\mathrm{e}}'-2\sigma_{\mathrm{e}}'\tan\phi' d\theta=\left[\gamma+\dfrac{\partial\left(S_{\mathrm{e}}\left(u_{\mathrm{a}}-u_{\mathrm{w}}\right)\right)}{\partial y}\right]\bullet\left[\left(-\tan\phi'\right)dx+dy\right] \end{cases} \tag{3.10}$$

$$\eta\ Line\ \begin{cases} \dfrac{dy}{dx}=\tan(\theta+\mu) \\ d\sigma_{\mathrm{e}}'+2\sigma_{\mathrm{e}}'\tan\phi' d\theta=\left[\gamma+\dfrac{\partial\left(S_{\mathrm{e}}\left(u_{\mathrm{a}}-u_{\mathrm{w}}\right)\right)}{\partial y}\right]\bullet\left[\tan\phi' dx+dy\right] \end{cases} \tag{3.11}$$

where $\mu = (\pi/4 - \phi'/2)$, μ is the angle between the tangent of the slip lines and the direction of the major principal stress (see Fig. 3.1).

3.2.3 Analytical solution to suction profile under transient flow

One-dimensional form of Richards' equation for the transient flow in an unsaturated soil is summarized below:

$$\frac{\partial\theta_{\mathrm{w}}}{\partial t}=\frac{\partial}{\partial y_{\mathrm{LC}}}\left[k\frac{\partial(\psi+y_{\mathrm{LC}})}{\partial y_{\mathrm{LC}}}\right] \tag{3.12}$$

where t is the time; k is the hydraulic conductivity; ψ is the suction head; y_{LC} is the vertical coordinate with the upward direction positive starting from the ground water level. It should be noted that the coordinate transformation is conducted by incorporating y_{LC} into the coordinate system of the slip line procedure (e.g., $y_{\mathrm{LC}} = H_{\mathrm{w}} - y$ for level ground; H_{w} is the ground water table depth measured from the ground surface). Great efforts have been made by various scholars (Philip 1957, Broadbridge and White, 1988, Srivastava and Yeh

1991) to obtain the analytical solutions for the above highly nonlinear equation. In this Chapter, the analytical solution of matric suction with different time intervals and positions are obtained based on the solutions suggested by Srivastava and Yeh (1991). The solutions by Srivastava and Yeh (1991) are validated in the literature for estimation of the slope stability (Zhan et al., 2013) and 2*D* and 3*D* earth pressure (Shahrokhabadi et al. 2019, Li and Yang 2020). The advantages and disadvantages associated with the assumption of using 1D flow compared to 2D flow will be discussed in a later section.

The relationship between the hydraulic conductivity and the soil volumetric water content is described using the model proposed by Gardner (1958) as follow:

$$k = k_s e^{-\alpha\psi} \tag{3.13}$$

$$\theta_w = \theta_r + (\theta_s - \theta_r)e^{-\alpha\psi} \tag{3.14}$$

where k_s is the saturated hydraulic conductivity. α is a parameter that represents the reduction rate of SWCC (Zhan and Ng, 2004). There are also other good models for describing the soil hydraulic conductivity, for example, the van Genuchten model (1980). However, the Gardner's model is used in this study because it is simple and has an exponential form for obtaining the closed-form solution of the matric suction. By substituting Eqs. (3.13) and (3.14) into Eq. (3.12), the linearized Richards' equation can be obtained as:

$$\frac{\alpha(\theta_s - \theta_r)}{k_s}\frac{\partial k}{\partial t} = \frac{\partial^2 k}{\partial y_{LC}} - \alpha\frac{\partial k}{\partial y_{LC}} \tag{3.15}$$

One initial and two boundary conditions are involved in this study to solve the partial differential equation (i.e., Eq. 3.15). Extending the assumptions in the studies by Srivastava and Yeh (1991), Shahrokhabadi et al. (2019), Li and Yang (2020), a constant surface infiltration flux and a stationary water table is assumed. This is achieved by using a linear distribution suction profile to describe the steady state condition prior to the infiltration with a prescribed initial surface flux, q_{ini} equal zero. In addition, the matric suction in the soil is initially set as zero at the ground water table. The following dimensionless factors are defined for simplification purposes in the remainder of the discussions in this study:

$$Y_{\text{LC}} = ay_{\text{LC}},\ K = \frac{k}{k_{\text{s}}},\ L = aH_{\text{w}}, Q = \frac{q}{k_{\text{s}}},\ Q_{\text{ini}} = \frac{q_{\text{ini}}}{k_{\text{s}}}, T = \frac{ak_{\text{s}}t}{\theta_{\text{s}} - \theta_{\text{r}}}$$

q is the surface influx of the rainfall. Eq. (3.15) can then be rewritten as

$$\frac{\partial K}{\partial T} = \frac{\partial^2 K}{\partial Y_{\text{LC}}^2} + \frac{\partial K}{\partial Y_{\text{LC}}} \tag{3.16}$$

The initial conditions and the boundary conditions can be described using the equations below:

Initial condition with $T = 0$: $K(Y_{\text{LC}}, 0) = e^{-Y_{\text{LC}}} = K_0(Y_{\text{LC}})$ (3.17a)

For $Y_{\text{LC}} = 0$, $(u_{\text{a}} - u_{\text{w}}) = 0$ at the ground water table: $K(0,\ T) = 1$ (3.17b)

For $Y_{\text{LC}} = L$ at the ground surface: $\left[\frac{\partial K}{\partial Y_{\text{LC}}} + K\right]_{Y_{\text{LC}} = L} = Q$ (3.17c)

Eq. (3.16) can be solved employing the Laplace transformation technique with the above initial and boundary conditions. The solution for this relationship can be expressed as

$$K = Q - (Q-1)\,\mathrm{e}^{-Y_{\text{LC}}} - 4\left(Q - Q_{\text{ini}}\right) e^{\frac{(L - y_{LC})}{2}} e^{-\frac{T}{4}} \sum_{n=1}^{\infty} \frac{\sin(\lambda_{\text{n}} Y_{\text{LC}}) \sin(\lambda_{\text{n}} L)\, \mathrm{e}^{-\lambda_{\text{n}}{}^2 T}}{1 + \frac{L}{2} + 2\lambda_{\text{n}}{}^2 L} \tag{3.18}$$

where λ_{n} is the n*th* root of the pseudo-periodic characteristic equation as shown in Eq. (3.19).

$$\tan\ (\lambda_{\text{n}} L) + 2\lambda_{\text{n}} = 0 \tag{3.19}$$

The expression of the matric suction and the effective degree of saturation, S_e can be obtained as Eqs. (3.20) and (3.21) using the K solution along with Eqs. (3.13) and (3.14).

$$\left(u_{\mathrm{a}} - u_{\mathrm{w}}\right) = -\frac{\gamma_{\mathrm{w}} \ln(K)}{a} \tag{3.20}$$

$$S_{\mathrm{e}} = K \tag{3.21}$$

3.3 Problem introduction

The problem is first defined introducing the different failure modes that typically arise in slope stability analyses. The associated boundary value problems are summarized. The procedure for obtaining the solution to the slip line problems previously described is then discussed in this section.

3.3.1 Problem definition

Fig. 3.2 shows a typical strip foundation located on the top of an unsaturated soil slope. In this study, the effect of the soil deformation on the soil slope associated with matric suction is assumed negligible. One-side failure mechanism that is typically applied (Li et al., 2021) is extended in this study to estimate the ultimate bearing capacity of shallow foundations on sloping ground. For foundation on the slope, there are mainly four types of failure mechanisms: (i) foundation bearing capacity failure, (ii) slope face failure, (iii) toe failure, and (iv) the deep-seated failure (See Fig. 3.2). The deep-seated failure is also considered as a global slope failure. Foundation bearing capacity failure occurs when the foundation setback distance, b, is large enough; the bearing capacity of the foundation is almost equal to that on the level ground. Toe failure can be treated as a special case of the face failure when the slope height is equal to the sliding height.

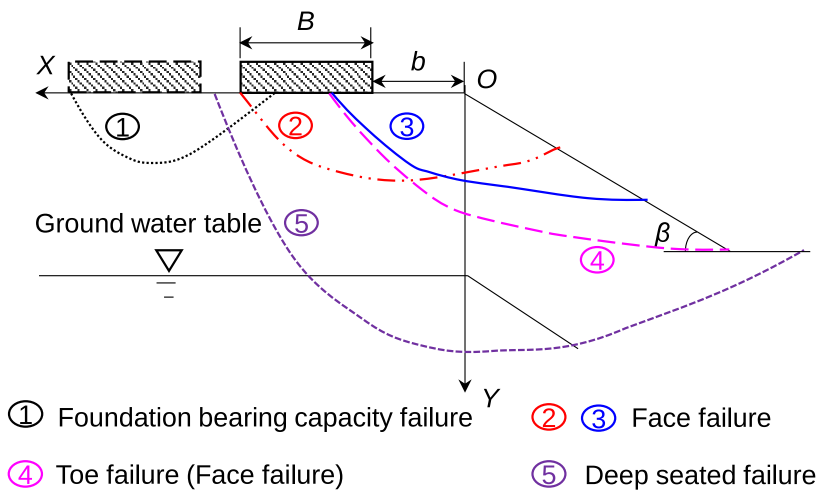

Fig. 3.2 Definition of the problem and different failure modes

3.3.2 Boundary value problem and solution procedure

Finite difference method is employed to discretize the slip line equations (i.e., Eqs. (3.10) and (3.11)). After discretizing, the expression for the four components x, y, θ and σ_e' of a point on the slip line are obtained and summarized below (Eq. (3.22 – 3.25)):

$$x = \frac{x_1 \tan(\theta_1 - \mu) - x_2 \tan(\theta_2 + \mu) + y_2 - y_1}{\tan(\theta_1 - \mu) - \tan(\theta_2 + \mu)} \tag{3.22}$$

$$\begin{aligned} y &= \tan(\theta_1 - \mu)(x - x_1) + y_1 \\ y &= \tan(\theta_2 + \mu)(x - x_2) + y_2 \end{aligned} \tag{3.23}$$

$$\theta = \frac{\left[\gamma + \dfrac{\partial\left[S_e(u_a - u_w)\right]}{\partial y}\right]\left[y_1 - y_2 + (2x - x_1 - x_2)\tan\phi'\right] + 2\left(\sigma_{e1}'\theta_1 + \sigma_{e2}'\theta_2\right)\tan\phi' + \sigma_{e2}' - \sigma_{e1}'}{2\left(\sigma_{e1}' + \sigma_{e2}'\right)\tan\phi'} \tag{3.24}$$

$$\begin{aligned} \sigma_e' &= \left[\gamma + \frac{\partial\left[S_e(u_a - u_w)\right]}{\partial y}\right]\left[y - y_1 - (x - x_1)\tan\phi'\right] + 2\sigma_{e1}'\tan\phi'(\theta - \theta_1) + \sigma_{e1}' \\ \sigma_e' &= \left[\gamma + \frac{\partial\left[S_e(u_a - u_w)\right]}{\partial y}\right]\left[y - y_2 + (x - x_2)\tan\phi'\right] - 2\sigma_{e2}'\tan\phi'(\theta - \theta_2) + \sigma_{e2}' \end{aligned} \tag{3.25}$$

where x_1, y_1, θ_1, σ_{e1}' and x_2, y_2, θ_2, σ_{e2}' describe the coordinates and stress states of the previous iteration points on slip line ξ and slip line η, respectively (see Fig. 3.3a).

The matric suction profiles obtained in the previous section can be incorporated into the above Eqs. (3.22) to (3.25) with a unified coordinate system in Fig. 3.2 (i.e., extending coordinate transformation discussions introduced earlier).

Boundary value problem is incorporated with the above finite difference equations. Figs. 3.3b, 3.3c and 3.3d describe different failure modes examples with the three different boundary value problems: Cauchy boundary value problem, degenerative Riemann boundary value problem and the mixed boundary value problem. The mobilized soil zone can be divided into passive zone, transition zone and the active zone as shown in Fig. 3.3b. By solving the corresponding boundary value problems, the stress state of the soil can be obtained in each zone. The initial boundary will start from the passive zone with no other surcharge at the ground surface. The soil surface is divided into several uniform grids with a length of dx. Details about parameters of the grids related to the accuracy of the calculation will be illustrated later. The initial stress state of each point at the soil surface in the passive zone can be written as

$$\begin{aligned}
&\sigma_e' = \frac{c'\cot\phi' + S_e\left(u_a - u_w\right)}{1-\sin\phi'} \\
&\theta = \pi \text{ level ground} \\
&\theta = \pi - \beta \text{ sloping ground}
\end{aligned} \tag{3.26}$$

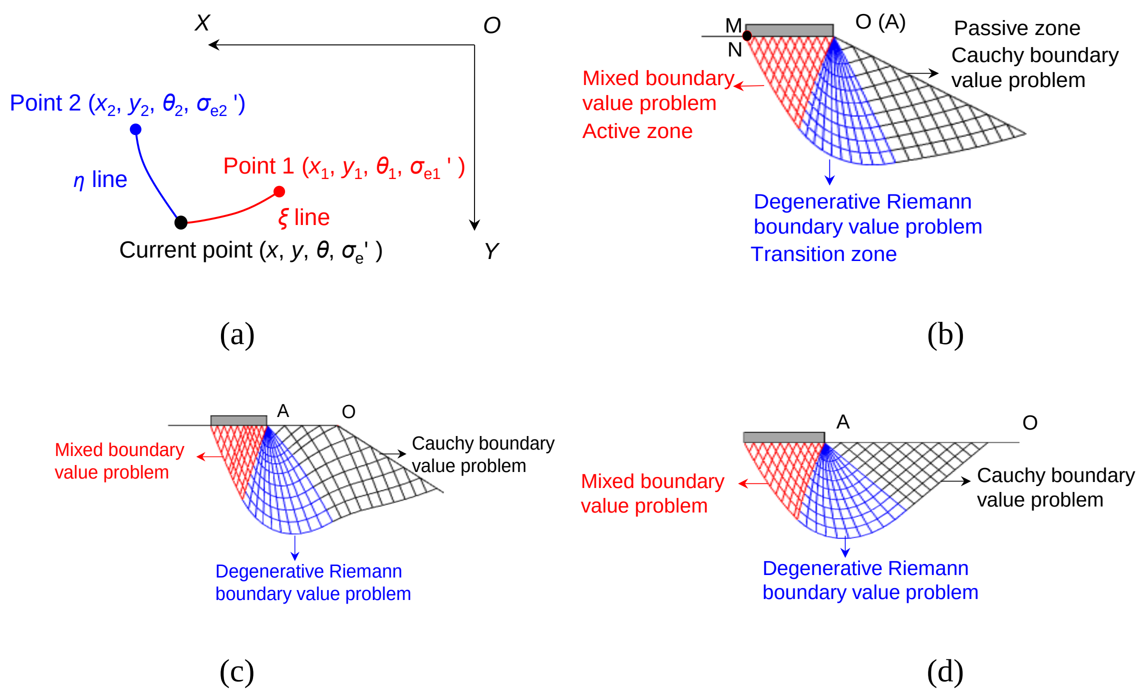

Fig. 3.3 Schematic diagram of iteration points in the slip line method and boundary value problem: (a) Iteration point; (b) b = 0; (c) $b \neq 0$; (d) Bearing capacity failure.

The iterative method based on Eqs. (3.22-3.25) can be applied to solve the problem. After solving the Cauchy boundary value problem, the slip line between the passive zone and the transition zone can be used as an initial boundary condition in the degenerative Riemann boundary value problem. High stress gradients are developed at the singularity point (Point A in Figs. 3.3b, 3.3c and 3.3d) of the footing edge. The major principal stress direction changes abruptly at this point. Therefore, the point is treated as a characteristic line as all the points on the line converge into this point of singularity. The iteration technique is similar to that described for the Cauchy boundary value problem. For the active zone below the foundation, the foundation base and the slip line obtained from the degenerative Riemann boundary value problem are used as the initial boundary condition for the mixed boundary value problem. The $\sigma_e{}'$ at the foundation base can be obtained extending this approach after the iterations terminate. The vertical stress of each grid points at the foundation base can then be expressed using the obtained $\sigma_e{}'$ as Eq. (3.27). The total foundation bearing capacity can be obtained based on Eq. (3.28).

$$q_{\mathrm{b}} = \sigma_e^{'}\left(1+\sin\phi'\right) - c'\cot\phi' - S_{\mathrm{e}}\left(u_{\mathrm{a}} - u_{\mathrm{w}}\right) \tag{3.27}$$

$$Q = \int_0^x q_{\mathrm{b}} dx \tag{3.28}$$

The flow chart in Fig. 3.4 summarizes the MATLAB program procedure. Several algorithms can be used for adjusting the grid parameters such as the hybrid algorithm by Powell (1970) and Martin (2004). In addition to the hybrid algorithm, a golden section search (GSS) algorithm is also developed to adjust the grid parameters for use in the present study. An initial value of *dx* is used as input into the slip line iteration procedure (e.g., 0.3) for the first iteration. The initial coordinate of the points on the slip line in the three zones mentioned above can then be obtained. The iteration direction will be determined based on the comparison of the *X*-coordinates of point N and point M (the foundation edge) (Fig. 3.3b). The foundation bearing capacity will be output information when the relative deviation between the *X*-coordinates of point N and point M is less than 0.001 (Fig. 3.3b). If this is not achieved, adjustment procedure via iteration may be activated again. Each adjustment iteration involves recalculation of the three boundary value problems. The different failure modes can also be determined based on the critical slip line position for different input soil slope and foundation position parameters.

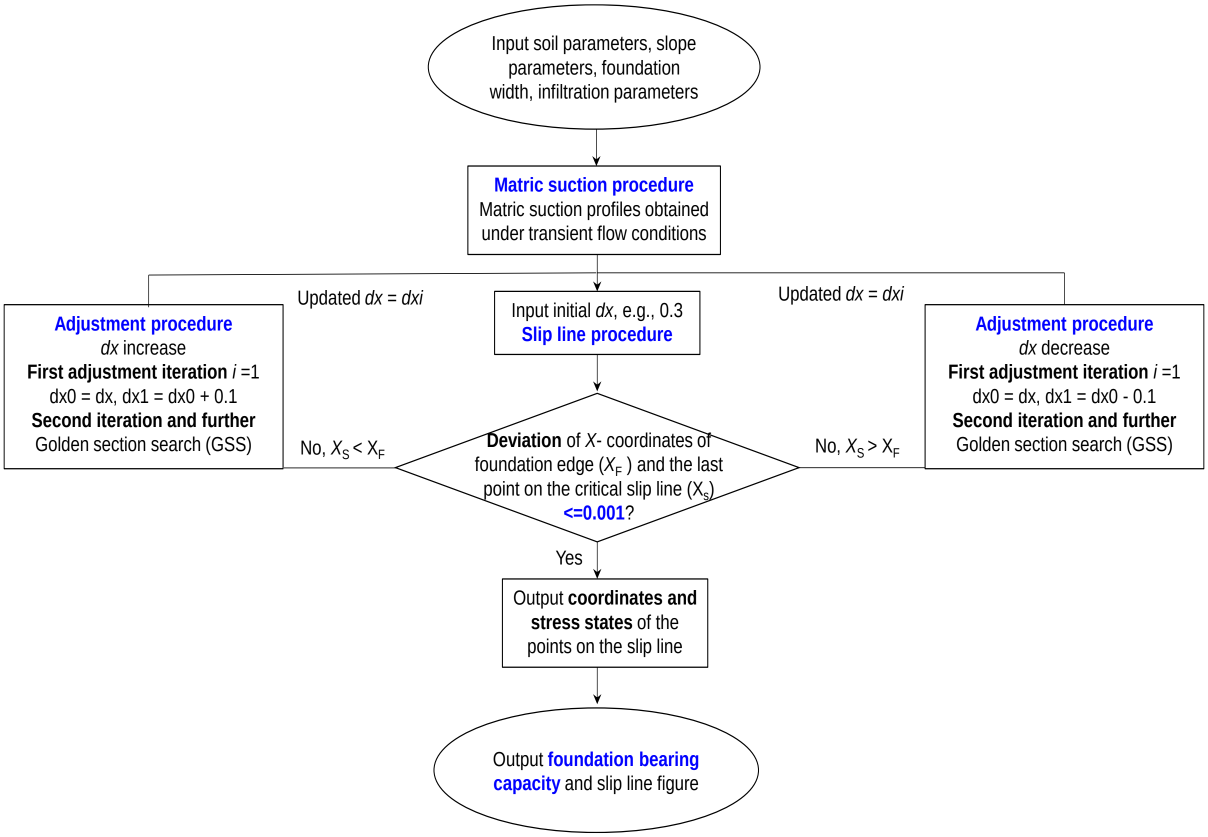

Fig. 3.4 Flow chart of the proposed framework

3.4 Procedure verification

A comparative study has been conducted to evaluate the proposed framework for the following:

(1) *Validation of the foundation bearing capacity in a saturated soil*.

This part of the study provides confidence from comparisons between existing bearing capacity related data in the literature and that obtained from the proposed framework. Both foundation on level and sloping ground are involved in the validation study.

(2) *Comparative study of the matric suction profiles under transient flow condition*. This part of the study provides details of a proposed procedure in simulating the non-uniform matric suction for transient flow conditions.

(3) *Comparative study of the foundation bearing capacity in unsaturated soils with different matric suction profiles*.

3.4.1 Validation of foundation bearing capacity in saturated soil ((u_a - u_w) = 0))

The comparative study is first conducted for evaluating foundation performance in a saturated soil extending Meyerhof (1951) bearing capacity equation. A foundation width of two meters and soil unit weight of 20 kN/m^3 are used.

Meyerhof (1951) proposed the general version of surface foundation bearing capacity equation as shown in Eq. (3.29).

$$Q_M = c' N_c + 0.5 B \gamma N_\gamma \tag{3.29}$$

where N_c, N_γ are the bearing capacity factors. The total bearing capacity Q_M and N_γ obtained from this study are compared with the published data using theoretical method (e.g., limit analysis (LA), limit equilibrium analysis (LEA), discontinuity layout optimization (DLO) and radial movement optimization (RMO)) and model experiment (ME) (Meyerhof, 1957, Chen, 1975, Saran et al., 1989, Michalowski, 1997, Soubra 1999, Martin 2004, EI Sawwaf, 2005, Leshchinsky, 2015, Zhou et al. 2018, Yang et al. 2019, Jin et al., 2020). Validation is conducted for foundation on level and sloping ground with different soil friction parameters (ϕ' = 10°, 30°,40°, 42°) and slope angles (β = 0°, 15°, 20°, 30°). Good comparisons are found between all the results obtained from the proposed procedure and that from the literature (Fig. 3.5). Most of the relative deviations are less than 15%. This good agreement provides confidence of the proposed method in estimating the foundation bearing capacity on both level and sloping ground for saturated soils.

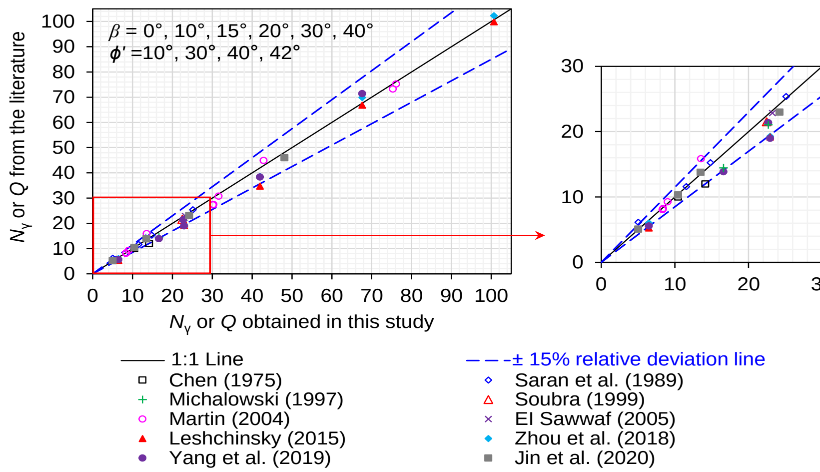

Fig. 3.5 Comparison of results obtained in this study to the published literature on saturated soils

3.4.2 Comparitive studies related to effective degree of saturation, S_e and suction profiles

The calculation procedure for the suction profile and effective degree of saturation, S_e variations under the vertical transient flow condition are evaluated in this section. Two studies with silt (Shahrokhabadi et al., 2019) and clay (Li and Yang, 2020) listed in Table 3.1 are used for comparison purposes.

Table 3.1 Soil paramters information from two studies

	θ_s	θ_r	k_s (m/s)	α (kPa^{-1})	γ (kN/m^3)	References
Study 1 – Silt	0.45	0.1	1.0×10^{-7}	0.5	20	Shahrokhabadi et al. (2019)
Study 2 – Clay	0.58	0.05	5.0×10^{-8}	0.13	20	Li and Yang (2020)

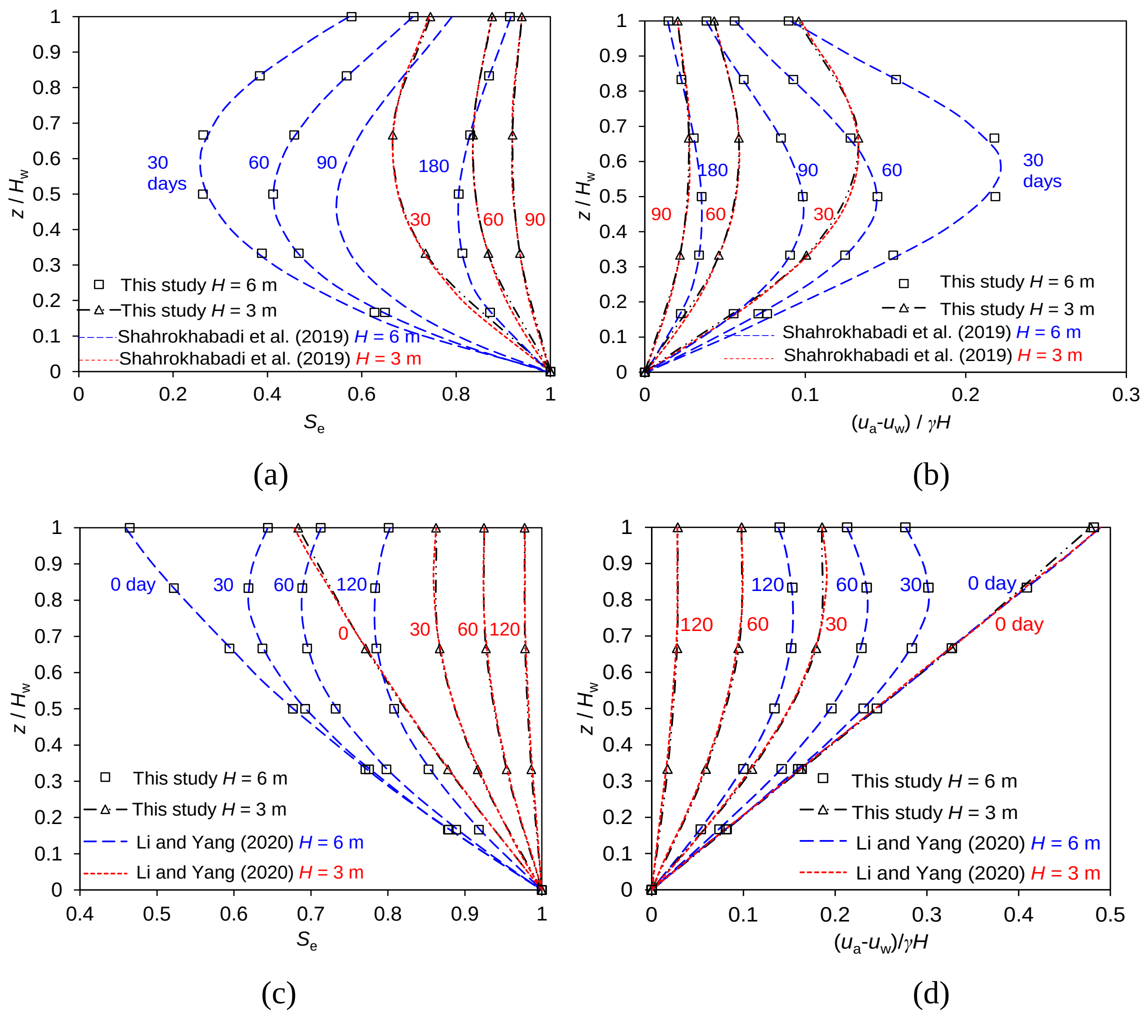

Fig. 3.6 Comparison of S_e, normalized (u_a - u_w) along with z/H_w under transient flow condition: (a) S_e along z/H_w for silt; (b) Normalized (u_a - u_w) along z/H_w for silt; (c) S_e along z/H_w for clay; (d) Normalized (u_a - u_w) along z/H_w for clay.

Two ground water table depths, H_w = 6 m and H_w = 3 m, are considered for providing comparisons of the results. The ratio of the surface infiltration flux over the saturated soil hydraulic conductivity (q/k_s) is set as one which represents an extreme infiltration condition (Shahrokhabadi et al. 2019). Fig. 3.6a and 3.6c present the S_e variation along with the normalized depth (z/H_w, z is the distance to the ground water table) under rainfall for silt and clay, respectively. Fig. 3.6b and 3.6d illustrate the corresponding normalized suction profiles along with z/H_w in silt and clay. The results obtained from the procedure in this study are consistent with that in the study 1 and study 2 for silt and clay, respectively. The peak value for the normalized suction profile in Fig. 3.6b for silt at rainfall duration t = 30 days is about 0.22 at a normalized depth of 0.6. This value is reduced to about 0.09 at z/H_w = 0.45 for a rainfall duration of 90 days. These variations under rainfall infiltration also agrees well with the two studies. The matric suction decreases as expected due to the rainwater infiltration. The reduction rate is related to different soil properties for the same rainfall characteristics as shown in Fig. 3.6. These results suggest the proposed procedure can provide reliable results for the matric suction variations associated with water content changes under the transient flow conditions.

3.4.3 Comparative study on foundation bearing capacity in unsaturated soil

The objective of this study is to evaluate the framework of the slip line procedure ((Eq. (3.22-3.25, 3.27, 3.28)) with different matric suction profiles in estimating the foundation bearing capacity. The vertical stress distribution (q_b in Eq. 3.27) along the foundation width and the corresponding foundation bearing capacity (Q in Eq. 3.28) are compared to the studies conducted by Vo and Russell (2016) and Hou et al. (2020). The matric suction profiles provided in the two studies are used. The soil properties and other information are summarized in Table 3.2. The vertical stress along the foundation width and the corresponding bearing capacity obtained from the proposed procedure are presented in Fig. 3.7a and 3.7b, respectively. Four ground water table depths were considered in this comparative study. In general, there is a relatively good agreement for the vertical stress variation along the foundation for both study 3 and study 4 in Fig. 3.7a. The corresponding bearing capacity obtained using the proposed procedure also agrees well with that in Study

3 and Study 4 in Fig. 3.7b. The maximum relative deviation between the bearing capacity obtained from the proposed method and that in Study 3 and Study 4 is 7.2%.

Table 3.2 Soil properties and other information used in the comparative study

	***c'* (kPa)**	***ϕ'* (°)**	***γ* (kN/m³)**	***H_w* (m)**	***B* (m)**	**Suction profiles**	**Method**	**References**
Study 3 – Silt	-	25	19.8	10	2	$(u_a - u_w) = 23 - 1.1\,z$	Slip line	Vo and Russell (2016)
Study 4 - *c'*- *ϕ'* soil	10	30	17	2, 3, 4	7	$(u_a - u_w) = 6.2\,z$	Slip line	Hou et al. (2020)

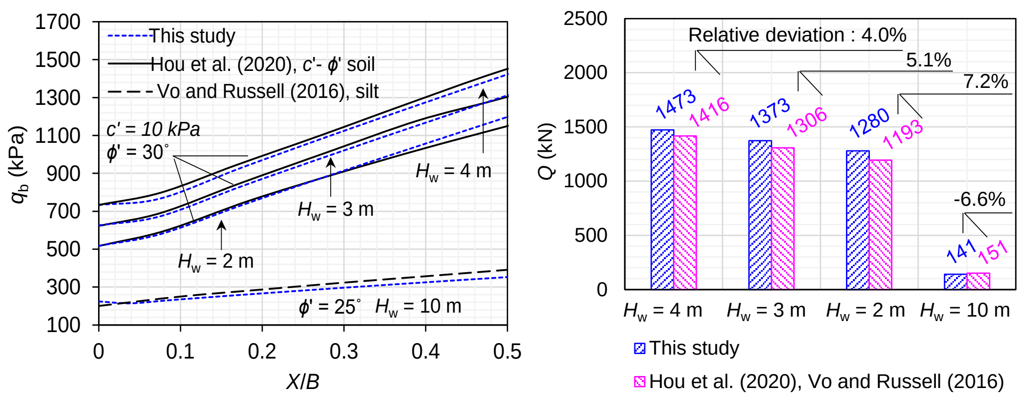

(a) (b)

Fig. 3.7 Comparison of results obtained using the proposed method and that in the literature: (a) Comparison of vertical stress along the foundation base; (b) Comparison of the bearing capacity of foundation

3.5 Parametric studies on foundation bearing capacity

Parametric studies are conducted using the proposed procedure to investigate the bearing capacity of foundation on unsaturated soil. The influence of the rainfall characteristics, slope angle, foundation setback ratio, ground water table depth is considered. The parameters range of each of parameters investigated are summarized in Table 3.3. The bearing capacity is investigated on clay and two silty soils within all the four studies. The properties of the soils are summarized in Table 3.4. The soil properties are obtained from the published data in Shahrokhabadi et al. (2019) and Aubertin et al. (2009). Similar to the assumptions used in Vo and Russell (2016), the soil unit weight is set as 20 kN/m^3 for all these example problems for simplicity. The soil unit weight will also have some influence on the bearing capacity that will be discussed later. A foundation width of 2 m is used for all the parametric studies. Results are presented to highlight the change in the normalized bearing capacity (Q / γB) of foundation. This normalized bearing capacity is similar to the normalized vertical stress (σ_y / γB) discussed in Vo and Russell (2016).

Table 3.3 Summary of parametric studies

Parametric studies	**Study I-rainfall characteristics**	**Study II-slope angle**	**Study III-foundation set-back ratio**	**Study IV-ground water table depth**
Normalized Rainfall infiltration rate (q/k_s)	0.5, 1	1	1	1
Rainfall duration (t, days)	0, 30, 60, 90, 120	0, 30, 60, 90, 120	0, 30, 60, 90, 120	0, 30, 60, 90, 120
Slope angle (β)	0°, 20°	10°, 15°, 20°, 25°, 30°	0°, 20°	0°, 20°
Foundation setback ratio (b/B)	0, ∞ (Level ground)	0, ∞	0, 0.5, 1, 1.5, 2, 3, ∞	0, ∞
Normalized ground water depth (H_w/B)	3	3	3	1.5, 3

Table 3.4 Soil properties used in the study

Soil	Clay	Silt 1	Silt 2
Cohesion, c' (kPa)	6	3.6	3.6
Soil internal friction angle, ϕ' (°)	25	25	25
Fitting parameter, α (kPa^{-1})	0.13	0.5	0.3
Saturated hydraulic conductivity, k_s (m/s)	5.0×10^{-8}	1.0×10^{-7}	1.0×10^{-7}
Saturated volumetric water content, θ_s	0.58	0.45	0.38
Residual volumetric water content, θ_r	0.1	0.1	0.06

3.5.1 Effect of rainfall characteristics-Study I

Fig. 3.8 summarizes the influence of rainfall infiltration rate and rainfall duration on the normalized foundation bearing capacity with H_w/B = 3. A higher q/k_s results in a lower normalized bearing capacity. For the clay in Fig. 3.8a, there is an obvious decrease in the bearing capacity with an increase in the rainfall duration when q/k_s = 1 compared to q/k_s = 0.5. For foundation on level ground, the relative deviation of the normalized bearing capacity prior to rainfall and that after 120 days of rainfall is about 28.8% under q/k_s = 1. The variation of the normalized bearing capacity of two silts along with the rainfall duration are different. When the rainfall infiltration rate is higher, the normalized bearing capacity of silt 1 in Fig. 3.8b has an increase during the early rainfall period and starts to drop after 30 days of rainfall. The normalized bearing capacity of silt 2 in Fig. 3.8c is constant during the period of early rainfall and starts to drop from 17.26 to 13.34 for the level ground. Same trends are observed for the sloping ground. The variation trend of the normalized bearing capacity with rainfall duration under q/k_s = 0.5 is also distinct with that under q/k_s = 1 for the two silt soils. The variations are not as obvious as observed for scenario with higher q/k_s. The reason for the variation will be illustrated later.

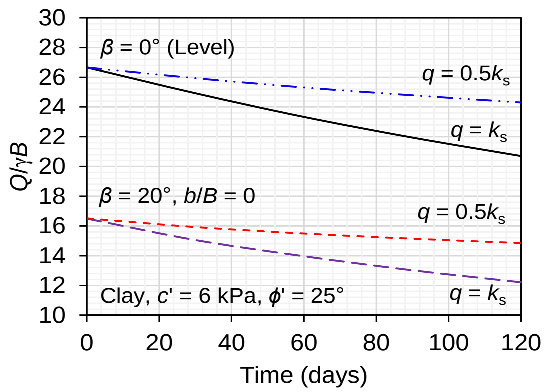

(a)

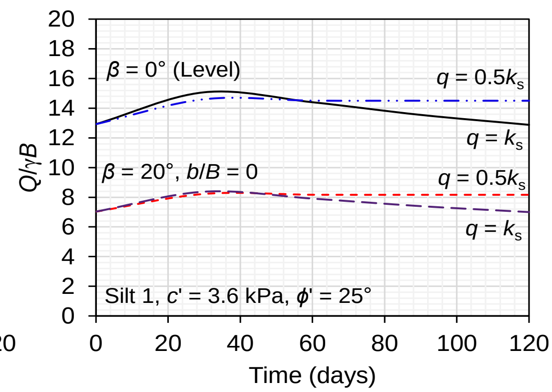

(b)

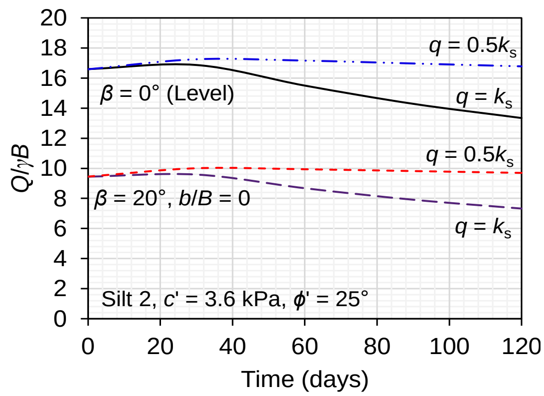

(c)

Fig. 3.8 Effect of rainfall characteristic on the normalized bearing capacity (H_w/B = 3): (a) Clay; (b) Silt 1; (c) Silt 2

The critical slip surface correspond to Fig. 3.8 are shown in Fig. 3.9. The critical slip line reflects that the foundation failure mechanism on level ground, the face failure mechanism on sloping ground are the dominant failure mechanisms in the parametric study in this section. Though the types of the failure mechanisms have no variation under the water infiltration, the critical slip surface has some variation with the infiltration. The critical slip surface in clay shrinks inward with the longer rainfall duration in Figs. 3.9a and 3.9b. While for the silt 1 in Fig. 3.9c, less soil is mobilized prior to rainfall compared to that (i.e., 30 and 60 days) after the rainfall. This critical slip line of 0 day also corresponds to the relatively lower normalized foundation bearing capacity in Fig. 3.8b at 0 day. Similar trends in the critical slip line variation can be observed in Fig. 3.8c and Fig. 3.9d for silt 2.

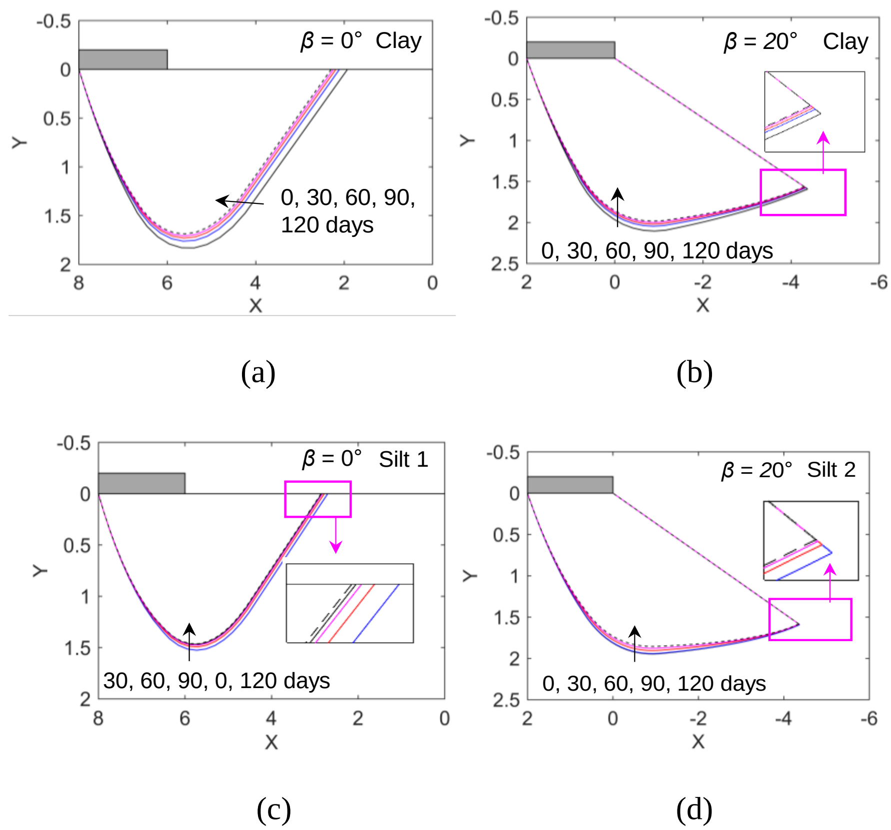

Fig. 3.9 Critical slip surface under the influence of rainfall infiltration (b/B = 0, H_w/B = 3): (a) Level ground for clay; (b) Sloping ground for clay; (c) Level ground for silt 1; (d) Sloping ground for silt 2

The reason for the above phenomenon may be attributed to the contribution of matric suction along with the SWCC (last term in Eq. (3.1), $(u_a - u_w)$ $((\theta - \theta_s) / (\theta_s - \theta_r) \tan \phi')$ or $(u_a - u_w)$ $S_e \tan \phi'$)) under the transient flow conditions. The contribution of $[(u_a - u_w)*S_e*\tan(\phi')]$ in clay and two silts along with matric suction are shown in Fig. 3.10a. Its variation and matric suction change with respect to normalized depth are respectively, shown in Fig. 3.10b and 3.10c. The SWCCs of three soils are shown in Fig. 3.10d. For the clay in Fig. 3.10a, the contribution of $[(u_a - u_w)*S_e*\tan(\phi')]$ at point A, prior to the rainfall is 12.6 kPa. The matric suction in the soil decreases due to an increase in the soil water content associated with the rainwater infiltration (see Fig. 3.10c). After 60 days of rainfall, the contribution of $[(u_a - u_w)*S_e*\tan(\phi')]$ drops to about 8.2 kPa at Point A1 in Fig. 3.10a. From Point A to Point A1 and even after Point A1, the contribution value continues to decrease. This explains why the normalized bearing capacity of clay soil decreases during the rainfall. However, from Fig. 3.10a, the contribution of $[(u_a - u_w)*S_e*\tan(\phi')]$ in silt 1 and silt 2 are not monotonically decreasing under rainfall infiltration. The variation trends of the normalized bearing capacity shown in Fig. 3.8b and 3.8c are similar to those in Fig. 3.10a. The contribution value at point B is slightly lower than that at point B1 that corresponds to 60 days rainfall period.

Similarly, with Fig. 3.10, the influence of the infiltration influx on the normalized bearing capacity can also be explained. The normalized bearing capacity of clay under q = 0.5 k_s keeps decreasing in Fig. 3.8a; this behavior is consistent with the trend from Point A to Point A05 in Fig. 3.10a. However, the changes in normalized bearing capacity of silt 1 and silt 2 is not obvious when q = 0.5 k_s, showing only a slight increase (From Point B to point B05 for silt 1 soil in Fig. 3.10a). The same explanation also works for the critical slip line variation. The critical slip line reflects the most possible failure plane. The shrink of the critical slip line is related to the reduction of the shear strength due to loss of $[(u_a - u_w)*S_e*\tan(\phi')]$ contribution. Therefore, bearing capacity and the corresponding critical slip surface is sensitive to the $[(u_a - u_w)*S_e*\tan(\phi')]$ contribution caused by the water content change under transient flow conditions. This further reflects that not only the rainfall characteristics influences the foundation bearing capacity, but also the soil properties and the soil type will have an impact on the foundation bearing capacity, under different rainfall infiltration conditions.

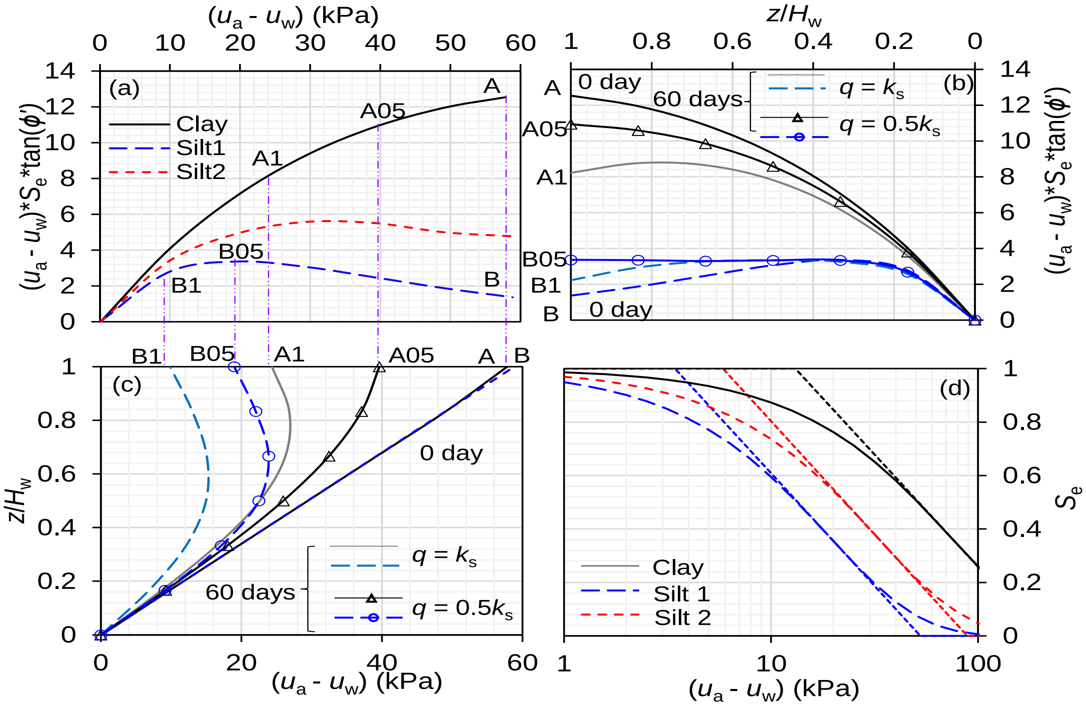

Fig. 3.10 Contribution of matric suction under transient flow condition (ϕ' = 25°): (a) (u_a - u_w) S_e tan ϕ' variation with matric suction; (b) (u_a - u_w) S_e tan ϕ' variation with normalized depth; (c) matric suction with normalized depth; (d) SWCC of the three soils

3.5.2 Effect of slope angle-Study II

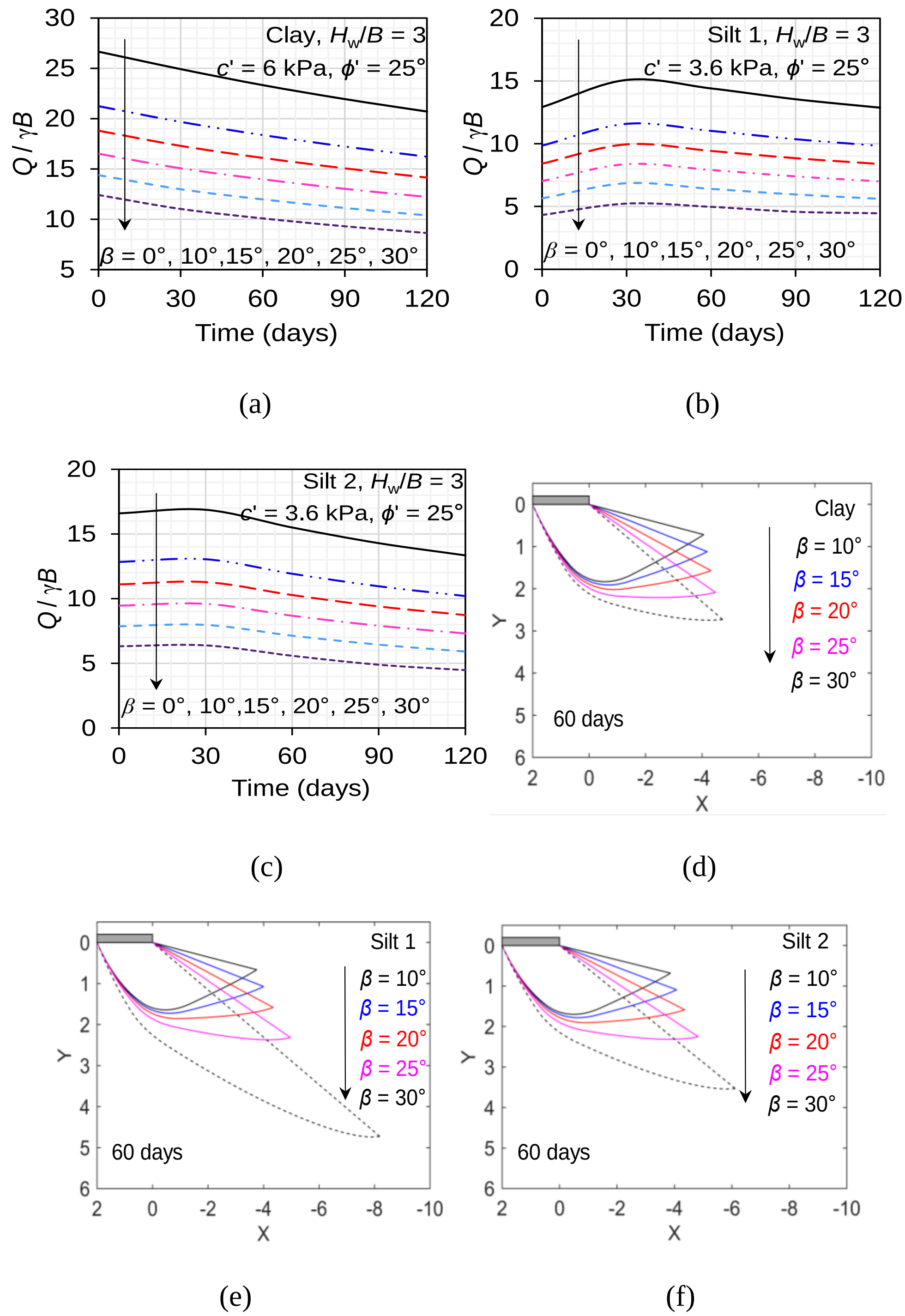

Fig. 3.11 Influence of the slope angle on the normalized bearing capacity and critical slip line: (a) Clay; (b) Silt 1; (c) Silt 2; (d) Critical slip line of clay; (e) Critical slip line of silt 1; (f) Critical slip line of silt 2

Fig. 3.11 summarizes the influence of the slope angle on the foundation normalized bearing capacity and the critical slip surface. The slope angle has a significant effect on the normalized bearing capacity as well as the critical slip surface of foundations on all the three soils. As β increases from 0° to 30°, $Q/\gamma B$ of clay, silt 1 and silt 2 drop by average values of 56.38%, 65.80%, 64.05% respectively. The reduction of the normalized bearing capacity is due to the insufficient resistance provided by the soil on the sloping ground compared to that on the level ground. This also can be seen in the critical slip surface in Figs. 3.11d, 3.11e and 3.11f. The slip surface extends downward with an increasing slope angle. A higher soil stress concentration is mobilized near the footing edge for β = 10° compared to β = 20°. The slope face failure is the predominant failure mechanism for different slope angles based on the critical slip surface in Fig. 3.11. The foundation bearing capacity failure is found only for β = 0° (Level ground) in this section. Similar trends in normalized bearing capacity variation along with the infiltration duration can be observed under each slope angle. The discussion of the corresponding critical slip line variation along with the rainfall duration is not provided in this section, as the change is similar as in the previous section.

3.5.3 Effect of foundation setback ratio-Study III

Fig. 3.12 summarizes the influence of the foundation setback distance. For all the three soils, the normalized bearing capacity increases with an increase in the foundation setback ratio. This behavior can be attributed to the increased soil resistance associated with a large foundation setback distance. The critical setback can be defined as the setback distance of foundation at which the behavior of the foundation on slope is the same as that on the level ground. The critical b/B of foundation on clay, silt 1 and silt 2 soil are respectively around

3 and 2 in the early water infiltration duration. Fig. 3.12b and 3.12c also suggest that the critical setback ratio decreases slightly for longer rainfall duration. This means the water infiltration has an impact on the foundation behavior irrespective of the foundation setback ratio.

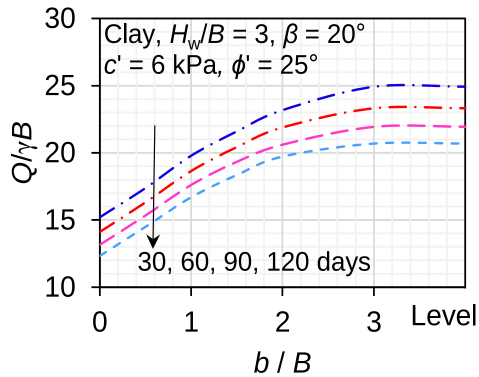

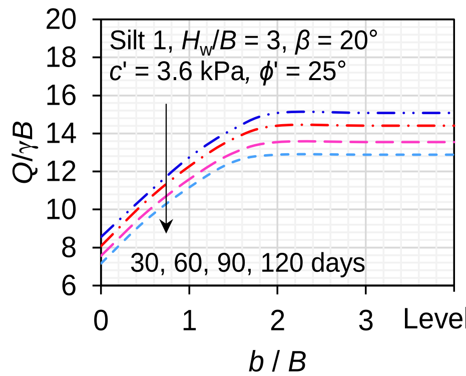

(a) (b)

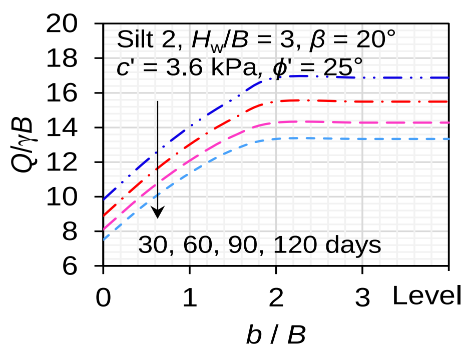

(c)

Fig. 3.12 Effect of foundation setback ratio on the normalized bearing capacity: (a) Clay; (b) Silt 1; (c) Silt 2

The critical slip surfaces under different setback ratios are shown in Fig. 3.13 with silt 1, as an example. The critical slip surface will not be developed further to the sloping ground surface when the foundation setback ratio is large enough. For example, when b/B increases from 0 to 2, the critical slip surface moves upward along the sloping surface in

Figs. 3.13a, 3.13b and 3.13c. When b/B is larger than 3, the critical slip surface extends into the level ground. The corresponding failure mechanism varies from the face failure (Figs. 3.13a, 3.13b and 3.13c) to the bearing capacity failure (Fig. 3.13d) with an increase in the setback ratio. The critical setback ratio marks the transition from the face failure to the bearing capacity failure under each rainfall durations.

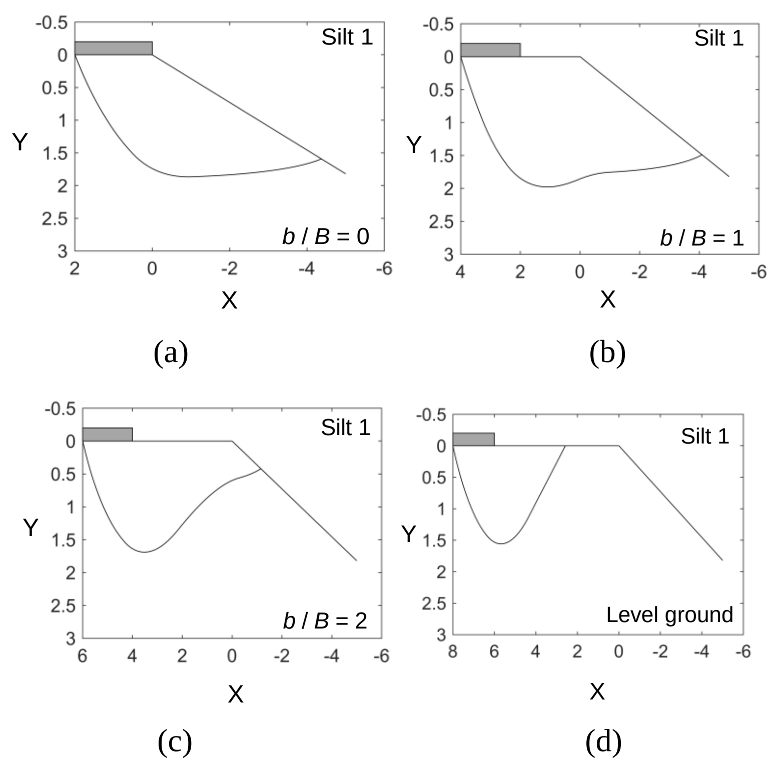

Fig. 3.13 Critical slip surface with different foundation setback ratios (β = 20°, q/k_s = 1): (a) b/B = 0; (b) b/B = 1; (c) b/B = 2; (d) b/B > 3

3.5.4 Effect of ground water table depth-Study IV

Fig. 3.14 summarizes the ground water table depth effect with H_w / B = 1.5 and H_w / B = 3 for the three soils. The normalized bearing capacity decreased markedly when H_w / B is reduced from 3 to 1.5 for the clay soil through the whole infiltration duration. However, for the two silts, the reduction will occur after a specific infiltration time. When H_w / B =

1.5, the normalized bearing capacity for all the three soils are reduced with an increasing infiltration duration. Only silt 1 shows a relative constant normalized bearing capacity value during early rainfall days. This behavior is different from that for the H_w / B = 3 condition for the two silts.

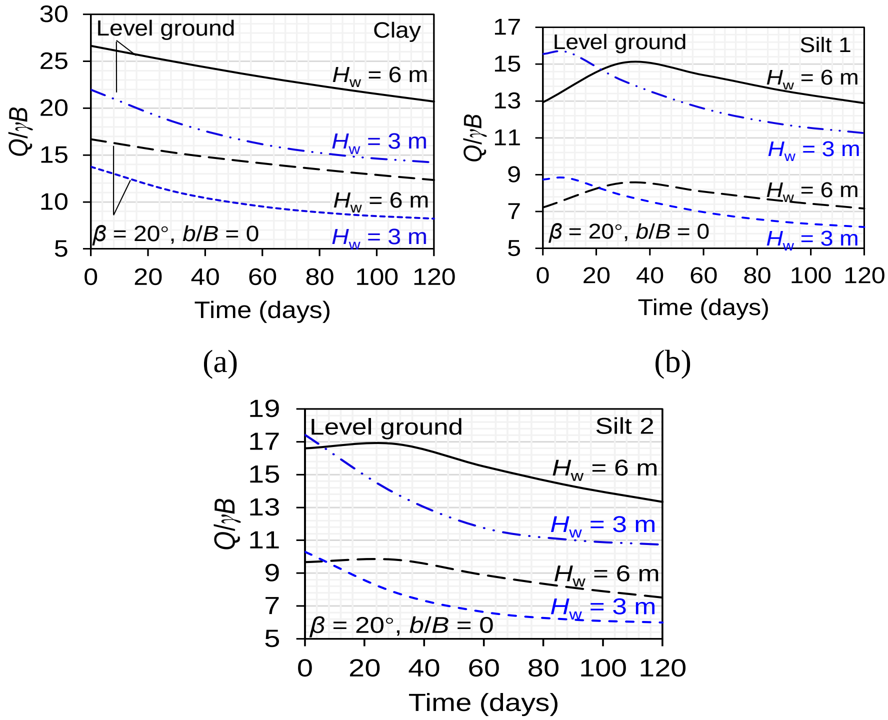

(a) (b)

(c)

Fig. 3.14 Effect of the ground water table depth on the normalized bearing capacity: (a) Clay; (b) Silt 1; (c) Silt 2

The relative deviation of the normalized bearing capacity prior to rainfall and that after rainfall of 120 days are summarized in Table 3.5. It can be observed that the relative deviation increases when H_w / B reduces from 3 to 1.5. A relative reduction of 54.7% has been found for normalized bearing capacity on level clay soil ground during 120 days of rainfall under H_w / B = 1.5. This is much higher than the relative deviation of 28.8% under

H_w / B = 3. The normalized bearing capacity reduction of two silty soils is also obvious under H_w / B = 1.5 than that under H_w / B = 3 shown in Table 3.5. Same phenomenon is also found for foundation on the three soils on the sloping ground. Results reflects the ground water table depth will influence the variation of the normalized foundation bearing capacity under rainfall infiltration.

Table 3.5 Relative deviation of $Q/\gamma B$ of 0 day compared to that of 120 days (q / k_s =1)

	Clay	**Silt 1**	**Silt 2**
H_w/B = 3, level	28.8%	0.4%	24.4%
H_w/B = 3, β = 20°	35.3%	0.8%	28.8%
H_w/B = 1.5, level	54.7%	38.2%	62.2%
H_w/B = 1.5, β = 20°	67.6%	41.9%	72.0%

The reason for the above phenomenon may be attributed to the matric suction contribution that is highlighted in Fig. 3.15. Fig. 3.15a provides details of the [(u_a - u_w)*S_e*tan(ϕ')] along with the matric suction using the results of silt 1. This behavior is consistent with the results discussed using Fig. 3.10. The contribution arising from [(u_a - u_w)*S_e*tan(ϕ')] has a significant effect on the normalized bearing capacity of foundation under the transient flow condition. For shallow ground water table depth, for example, H_w / B = 1.5, the initial [(u_a - u_w)*S_e*tan(ϕ')] contribution starts from point B as shown in Fig. 3.15a. As the rainwater infiltrates into the soil, matric suction decreases (Fig. 3.15c) and the effective degree of saturation, S_e increases as shown in Fig. 3.15d. The combined influence of matric suction and effective degree of saturation, S_e results in an increase in the normalized bearing capacity during the early rainfall days in Fig. 3.15a. After a specific matric suction, the contribution from the [(u_a - u_w)*S_e*tan(ϕ')] reduced with the decreasing matric suction (e.g., reduced to B60 point after 60 days of rainfall). The different variation trend of the [(u_a - u_w)*S_e*tan(ϕ')] from A to A60 under H_w / B = 3 and B to B60 under H_w / B = 1.5 is the predominant factor that influence the foundation normalized bearing capacity. These results also suggest that the initial matric suction distribution also influences the bearing capacity under the transient flow conditions. This discussion suggests that not only the matric suction will influence the bearing capacity, but also the initial ground water table, soil properties, soil types and rainfall characteristics will influence the foundation bearing capacity during rainfall.

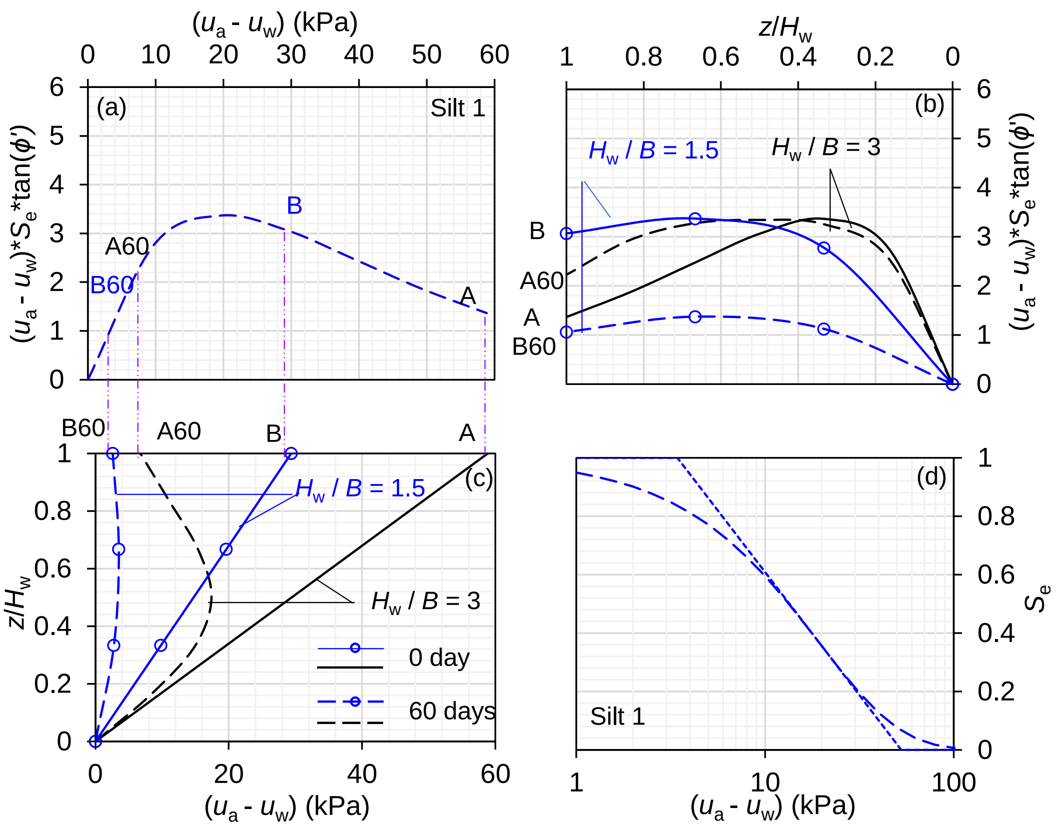

Fig. 3.15 Contribution of matric suction for silt 1 soil: (a) (u_a - u_w) S_e tan ϕ' with suction; (b) (u_a - u_w) S_e tan ϕ' with normalized depth; (c) matric suction with normalized depth; (d) SWCC of silt 1 soil

3.6 Discussion

In practice, the soil unit weight varies with changes in the water content. Typically, the dry soil unit weight, γ_d and saturated soil unit weight, γ_{sat} are respectively used for soil above and below the ground water table. Some researchers have used the average unit weight in the analytical analysis for simplicity purposes (Vahedifard and Robinson, 2016, Cascone et al., 2021). Fig. 3.16 shows the procedure used by Cascone et al. (2021) for estimating the average unit weight. The average unit weight can be used in the slip line method in the iteration process for evaluating the stress state of point 3 from point 1 and point 2; point 1 and point 2 are the previous iteration points of point 3 on the slip line. It should be noted that there would be a variation in the soil unit weight associated with the fluctuation in the soil water content. The soil moist unit weight can be calculated using Eq. (3.30):

$$\gamma = \gamma_w \frac{G_s + eS}{1 + e} \tag{3.30}$$

where γ_w is the unit weight of water, G_s is the specific gravity, e is the void ratio. For the clay, silt 1 and silt 2 soil in this study, the estimated soil unit weight variation associated with the changes in matric suction fluctuation (due to water content variations) is approximately in the range of 15 kN/m^3 to 20 kN/m^3. Fig. 3.17 illustrates the influence of soil unit weight on the foundation bearing capacity. For the bearing capacity obtained on level ground, the maximum relative difference between soil unit weight of 20 kN/m^3 and 15 kN/m^3 is less than 13% for all the three soils. This difference further reduces to values less than 10% for foundation on sloping ground (b/B = 0). The variation in soil unit weight contributes to some complexities in the iteration computations, especially for the transient flow conditions. Therefore, it is reasonable to assume a constant value that is an average soil unit weight in the bearing capacity estimation, for simplification purposes. Such an approach was also followed by several researchers in the recently published studies (Vo and Russell, 2016, Hou et al. 2020, Cascone et al., 2021 and Du et al., 2021).

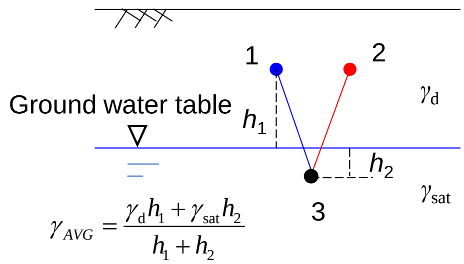

Fig. 3.16 Average soil unit weight in the slip line method

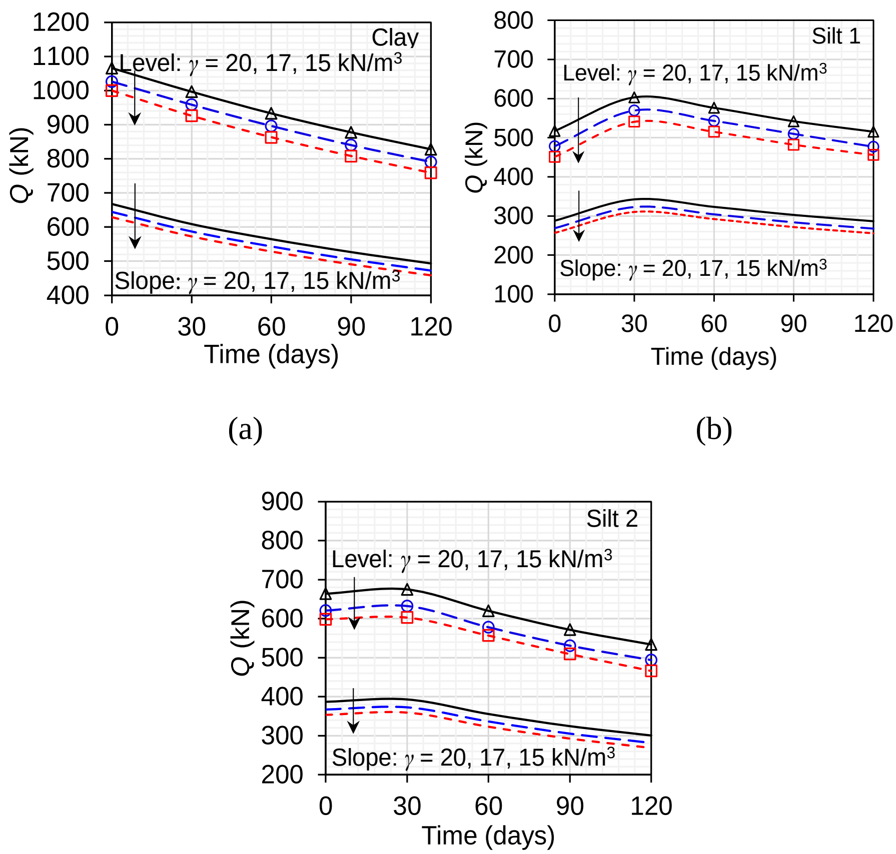

(a) (b)

(c)

Fig. 3.17 Influence of the soil unit weight: (a) Clay; (b) Silt 1; (c) Silt 2

Several other factors such as the matric suction contribution to the slope stability and slope deformation are not considered in the analysis. These factors are also important to evaluate the foundation performance during its life span. In practice, the slope stability and the foundation bearing capacity do not use the same partial factors in the design (Eurocode 7, 2004, CFEM, Canadian Geotechnical Society, 2006, Pantelidis and Griffiths, 2015). Many studies have provided valuable results on the slope stability taking account of rainfall infiltration (Zhan and Ng, 2004, Rahardjo et al. 2007, 2010, Xu et al. 2021). Insight into the effect of these factors towards the foundation bearing capacity on the sloping ground is expected to provide a valuable understanding. It can be used in the rational design of foundations taking account of the influence of climate factors. More in-situ tests and experiments data are expected to further explain the combined influence of the foundation and slope system under the climate influence.

Similar to other theoretical studies, the present study is based on certain assumptions and simplifications. The matric suction profile in this study is determined considering transient flow behavior in the vertical direction. There may be some variations or other deviations with the matric suction values encountered in real practice. Hydraulic response of two-dimensional flow is likely to be slower than the one-dimensional flow (Li et al., 2013, Lu and Godt, 2013). The matric suction near the slope face or sharp boundaries obtained by one-dimensional flow may have deviations in comparison to two-dimensional flow behavior (Shahrokhabadi et al., 2019). The foundation bearing capacity obtained with a higher foundation setback ratio condition will have less deviation compared to that obtained from a small foundation setback ratio due to the 1D flow assumption in this study. However, 1D flow is commonly used in the infiltration analysis for estimating the slope stability (Collins et al., 2004, Ali et al., 2014, Qi and Vanapalli, 2015) and earth pressure estimation (Shahrokhabadi et al., 2019, Li and Yang, 2020). Several other investigators (Lee et al., 2011; Zhan et al., 2013, Li et al., 2013) also validated that the vertical flow plays a more dominant role in the singled layered homogeneous soil; the simplified vertical seepage infiltration model provides comparable results in comparison to the two-dimensional slope stability analysis.

3.7 Conclusions

The bearing capacity of foundation on sloping ground under vertical transient flow conditions is investigated using an analytical framework proposed in this study. The analytical framework is based on the slip line method incorporated with the suction profile obtained by a closed-form solution assuming vertical transient flow conditions. The framework is a first attempt in the literature to combine the slip line method with the transient flow condition towards the evaluation of the foundation bearing capacity to the best of the authors' knowledge. Parametric studies extending the proposed framework suggest that the $[(u_a - u_w)*S_e*\tan(\phi')]$ contribution is the predominant factors that influence the foundation bearing capacity. This contribution under the transient flow condition varies depending on the rainfall characteristics, type of soil, soil properties and the initial ground condition. Overall, the infiltration flux and duration have a relative negative effect on the performance of the foundation. The rise of the ground water table depth and increase of the slope angle will contribute to a decrease in the foundation bearing capacity. In addition, the foundation setback distance needs to be taken care of in the design maintaining a critical setback distance. The proposed framework can be used by geotechnical engineers to evaluate the foundation bearing capacity on both level and sloping ground taking account of the transient flow conditions in unsaturated soils during the entire service life span. The method can be extended as a tool in forensic studies to reliably assess the shallow foundations failures.

References

Akbari G.A., Sadeghi, H., Saheb, S. and Lamei, A., 2020. Bearing Capacity of Shallow Foundations on Unsaturated Soils: Analytical Approach with 3D Numerical Simulations and Experimental Validations. Int. J. Geomech., 20, 3, 04019181. https://doi.org/10.1061/(ASCE)GM.1943-5622.0001589.

Ali, A., Huang, J., Lyamin, A.V., Sloan, S.W., Cassidy, M.J., 2014. Boundary effects of rainfall-induced landslides. Comput. Geotech., 61, 341-354. https://doi.org/10.1016/j.compgeo.2014.05.019.

Anand, A., Sarkar, R. 2021. A comprehensive investigation on bearing capacity of shallow foundations on unsaturated fly ash slopes adopting finite element limit analysis. Eur. J. Environ. Civ., 1-27. https://doi.org/10.1080/19648189.2021.1967200.

Aubertin, M., Cifuentes, E., Apithy, S.A., Bussière, B., Molson, J. and Chapuis, R.P., 2009. Analyses of water diversion along inclined covers with capillary barrier effects. Can. Geotech. J., 46, 10, 1146-1164. https://doi.org/10.1139/T09-050.

Bishop A.W., 1959. The principle of effective stress. Teknisk Ukeblad. 39:859–863.

Broadbridge, P., White, I., 1988. Constant rate rainfall infiltration: A versatile nonlinear model, 1. Analytical solution. Water Resour. Res. 24, 1, 145–154. https://doi.org/10.1029/WR024i001p00145.

Canadian Geotechnical Society, 2006. Canadian foundation engineering manual (The 4th edition). Vancouver, B.C.: Canadian Geotechnical Society.

Cascone, E., Biondi, G., Casablanca, O., 2021. Groundwater effect on bearing capacity of shallow strip footings. Comput. Geotech. 139, 104417. https://doi.org/10.1016/j.compgeo.2021.104417.

Chen, W.F., 1975. Limit analysis and soil plasticity. Amsterdam, Netherlands: Elsevier.

Collins, B. D., Znidarcic, D., 2004. Stability analyses of rainfall induced landslides. J. Geotech. Geoenviron. Eng., 130, 4, 362-372. https://doi.org/10.1061/(ASCE)1090-0241(2004)130:4(362).

Dey, A., Acharyya, R., Alammyan, A., 2019. Bearing capacity and failure mechanism of shallow footings on unreinforced slopes: a state-of-the-art review. Int. J. Geotech. Eng., 1-14. https://doi.org/10.1080/19386362.2019.1617480.

Du, J., Ye, F., 2021. The bearing capacity of strip footings adjacent to the crest of unsaturated soil slopes. Environ. Earth Sci., 80, 664. https://doi.org/10.1007/s12665-021-09955-2.

Du, D., Zhuang, Y., Sun, Q., Yang, X., Dias, D., 2021. Bearing capacity evaluation for shallow foundations on unsaturated soils using discretization technique. Comput. Geotech., 137, 104309. https://doi.org/10.1016/j.compgeo.2021.104309.

El Sawwaf, M., 2005. Strip footing behavior on pile and sheet pile stabilized sand slope. J. Geotech. Geoenviron. Eng. 131, 6, 705–715. https://doi.org/10.1061/(ASCE)1090-0241(2005)131:6(705).

Eurocode 7, EN 1997-1, 2004. Geotechnical design—part 1: general rules. European Committee for Standardization, Brussels.

Fredlund, D.G., Rahardjo, H., Fredlund, M.D., 2012. Unsaturated Soil Mechanics in Engineering Practice, Wiley, Chichester, U.K.

Fredlund, D.G., Rahardjo, H. 1993. Soil mechanics for unsaturated soils. John Wiley & Sons.

Gardner, W.R., 1958. Some steady state solutions of the unsaturated moisture flow equation with application to evaporation from a water table. Soil Sci. 85, 4, 228–232. https://doi.org/10.1097/00010694-195804000-00006.

Georgiadis, K., 2010a. Undrained bearing capacity of strip footings on slopes. J. Geotech. Geoenviron. Eng., 136, 5: 677–685. https://doi.org/10.1061/(ASCE)GT.1943-5606.0000269.

Georgiadis, K., 2010b. An upper-bound solution for the undrained bearing capacity of strip footings at the top of a slope. Géotechnique, 60, 10, 801-806. https://doi.org/10.1680/geot.09.T.016.

Ghasemzadeh, H., Akbari, F., 2019. Determining the bearing capacity factor due to nonlinear matric suction distribution in the soil. Can. J. Soil Sci., 99, 4, 434-446. https://doi.org/10.1139/cjss-2019-0071.

Shi G.Z., 2019. Calculation of bearing capacity of unsaturated soil foundation based on slip line method.

Halder, K., Chakraborty, D., Kumar Dash, S., 2019. Bearing capacity of a strip footing situated on soil slope using a non-associated flow rule in lower bound limit analysis. Int. J. Geotech. Eng., 13, 2, 103-111. https://doi.org/10.1080/19386362.2017.1325119.

Hou C.Q., Shi G.Z., Sun Z.B. Xi, Y., 2020. Calculation of bearing capacity of unsaturated soil strip foundation based on slip line theory. J. Yangtze River Scientific Res. Inst., 37, 6. https://doi.org/10.11988/ckyyb.20190112.

Jeong, S., Kim, Y., Park, H. 2019. Influences of rainfall infiltration and hysteresis SWCC of unsaturated soil on settlement of shallow foundations. Jpn. Geotech. Soc. spec. publ., 7, 2, 569-575. https://doi.org/10.3208/jgssp.v07.088.

Jin, L., Feng, Y., Zhang, H., Feng, Q., 2020. The use of improved radial movement optimization to calculate the ultimate bearing capacity of a nonhomogeneous clay foundation adjacent to slopes. Comput. Geotech., 118, 103338. https://doi.org/10.1016/j.compgeo.2019.103338.

Khalili, N., Khabbaz, M.H., 1998. A unique relationship for χ for the determination of the shear strength of unsaturated soils. Géotechnique, 48, 5, 681-687. https://doi.org/10.1680/geot.1998.48.5.681.

Khalili, N., Khabbaz, M.H., Valliappan, S., 2000. An effective stress based numerical model for hydro-mechanical analysis in unsaturated porous media. Comput. Mech., 26, 2, 174-184. https://doi.org/10.1007/s004660000165.

Kim, Y., Park, H., Jeong, S., 2017. Settlement behavior of shallow foundations in unsaturated soils under rainfall. Sustainability, 9, 8, 1417. https://doi.org/10.3390/su9081417.

Leshchinsky, B., 2015. Bearing capacity of footings placed adjacent to c'-ϕ' slopes. Geotech. Geoenviron. Eng., 141, 6, 04015022. https://doi.org/10.1061/(ASCE)GT.1943-5606.0001306.

Lee, L.M., Kassim, A., Gofar, N., 2011. Performances of two instrumented laboratory models for the study of rainfall infiltration into unsaturated soils. Eng. Geol., 117(1-2), 78-89. https://doi-org.proxy.bib.uottawa.ca/10.1016/j.enggeo.2010.10.007.

Li, C., Guan, Y., Jiang, P., Han, X., 2021. Oblique bearing capacity of shallow foundations placed near slopes determined by the method of rigorous characteristics. Géotechnique, 1-13. https://doi.org/10.1680/jgeot.20.P.355.

Li, C., Jiang, P., 2019. Ultimate load of nonhomogeneous slopes determined by using the method of characteristics. Eng. Geol., 261, 105281. https://doi.org/10.1016/j.enggeo.2019.105281.

Li, C., Zhou, A., Jiang, P., 2020. Eccentric bearing capacity of embedded strip footings placed on slopes. Comput. Geotech., 119, 103352. https://doi.org/10.1016/j.compgeo.2019.103352.

Li, W.C., Lee, L.M., Cai, H., Li, H.J., Dai, F.C., Wang, M.L., 2013. Combined roles of saturated permeability and rainfall characteristics on surficial failure of homogeneous soil slope. Eng. Geol., 153, 105-113. http://dx.doi.org/10.1016%2Fj.enggeo.2012.11.017.

Li, Z.W., Yang, X.L., 2020. Three-dimensional active earth pressure under transient unsaturated flow conditions. Comput. Geotech., 123, 103559. https://doi.org/10.1016/j.compgeo.2020.103559.

Lu, N., Godt, J.W., 2013. Hillslope hydrology and stability. Cambridge University Press.

Lu, N., Likos, W.J., 2006. Suction stress characteristic curve for unsaturated soil. J. Geotech. Geoenviron. Eng., 132, 2, 131-142. https://doi.org/10.1061/(ASCE)1090-0241(2006)132:2(131).

Mahmoudabadi, V., Ravichandran, N., 2019. Design of shallow foundation considering site-specific rainfall and water table data: theoretical framework and application. Int. J. Geomech., 19, 7, 04019063. https://doi.org/10.1061/(ASCE)GM.1943-5622.0001432.

Martin, C.M., 2004. ABC User Manual.

Meyerhof, G.G., 1951. The ultimate bearing capacity of foundations. Géotechnique, 2, 301. https://doi.org/10.1680/geot.1951.2.4.301.

Meyerhof, G.G., 1957. The ultimate bearing capacity of foundation on slopes. Proc. 4th Int. Conf. on Soil Mechan. Found. Eng. I: 384–386.

Michałowski R.L., 1997. An estimate of the influence of soil weight on bearing capacity using limit analysis. Soils Found., 37, 4, 57-64. https://doi.org/10.3208/sandf.37.4_57.

Oh, W.T., Vanapalli, S.K., 2011. Modelling the applied vertical stress and settlement relationship of shallow foundations in saturated and unsaturated sands. Can. Geotech. J., 48, 3, 425-438. https://doi.org/10.1139/T10-079.

Oh, W.T., Vanapalli, S.K., 2013. Interpretation of the bearing capacity of unsaturated fine-grained soil using the modified effective and the modified total stress approaches. Int. J. Geomech., 13, 6, 769-778. https://doi.org/10.1061/(ASCE)GM.1943-5622.0000263.

Oh, W.T., Vanapalli, S.K., 2018. Modeling the stress versus settlement behavior of shallow foundations in unsaturated cohesive soils extending the modified total stress approach. Soils Found., 58, 2, 382-397. https://doi.org/10.1016/j.sandf.2018.02.008.

Oloo, S.Y., Fredlund, D.G., Gan, J.K., 1997. Bearing capacity of unpaved roads. Can. Geotech. J., 34, 3, 398-407. https://doi.org/10.1139/t96-084.

Pantelidis, L., Griffiths, D.V., 2015. Footing on the crest of slope: slope stability or bearing capacity? In Engineering Geology for Society and Territory-Volume 2, 1231-1234. Springer, Cham. https://doi.org/10.1007/978-3-319-09057-3_215.

Philip, J.R., 1957. Theory of infiltration: 1. The infiltration equation and its solution. Soil Sci., 83, 345–357. http://dx.doi.org/10.1097/00010694-195705000-00002.

Powell, M.J.D., 1970. A hybrid method for nonlinear algebraic equations. In Numerical methods for nonlinear algebraic equations (ed. P. Rabinowitz), 87-114. London: Gordon and Breach.

Rahardjo, H., Ong, T.H., Rezaur, R.B., Leong, E.C., 2007. Factors controlling instability of homogeneous soil slopes under rainfall. J. Geotech. Geoenviron. Eng., 133, 12, 1532-1543. https://doi.org/10.1061/(ASCE)1090-0241(2007)133:12(1532).

Rahardjo, H., Nio, A.S., Leong, E.C., Song, N.Y., 2010. Effects of groundwater table position and soil properties on stability of slope during rainfall. J. Geotech. Geoenviron. Eng., 136(11), 1555-1564. https://doi.org/10.1061/(ASCE)GT.1943-5606.0000385.

Ravichandran, N., Vickneswaran, T., Marathe, S., Jella, V.S., 2021. Numerical Analysis of Settlement Response of Shallow Footing Subjected to Heavy Rainfall and Flood Events. Int. J. Geosci., 12, 2, 138-158. https://doi.org/10.4236/ijg.2021.122009.

Qi, S., Vanapalli, S.K., 2015. Hydro-mechanical coupling effect on surficial layer stability of unsaturated expansive soil slopes. Comput. Geotech., 70, 68-82. https://doi.org/10.1016/j.compgeo.2015.07.006.

Saran S, Sud V.K., Handa S.C., 1989. Undrained bearing capacity of footings adjacent to slopes. J. Geotech. Eng., 115, 4, 553–73. https://doi.org/10.1061/(ASCE)0733-9410(1989)115:4(553).

Shahrokhabadi, S., Vahedifard, F., Ghazanfari, E., Foroutan, M., 2019. Earth pressure profiles in unsaturated soils under transient flow. Eng. Geol., 260, 105218. https://doi.org/10.1016/j.enggeo.2019.105218.

Sheng, D., Zhou, A., Fredlund, D.G., 2011. Shear strength criteria for unsaturated soils. Geotech. Geol. Eng., 29, 2, 145-159. https://doi.org/10.1007/s10706-009-9276-x.

Skempton A.W., 1948. The $\phi_u = 0$ analysis for stability and its theoretical basis. Proc. 2nd Int. Conf. Soil Mechan. Found. Eng., 1, 72-77.

Soubra, A.H., 1999. Upper-bound solutions for bearing capacity of foundations. J. Geotech. Geoenviron. Eng., 125, 1, 59-68. https://doi.org/10.1061/(ASCE)1090-0241(1999)125:1(59).

Srivastava, R., Yeh, T.C.J., 1991. Analytical solutions for one dimension, transient infiltration toward the water table in homogeneous and layered soils. Water Resour. Res., 27, 5, 753–762. https://doi.org/10.1029/90WR02772.

Tan, M., Cheng, X., Vanapalli, S., 2021. Simple Approaches for the Design of Shallow and Deep Foundations for Unsaturated Soils I: Theoretical and Experimental Studies. Indian Geotech. J., 51, 1, 97-114. https://doi.org/10.1007/s40098-021-00501-2.

Tan, M.X., Vanapalli, S.K., 2021. Performance estimation of a shallow foundation on an unsaturated expansive soil slope subjected to rainfall infiltration. In MATEC Web of Conferences. 337, 03009. https://doi.org/10.1051/matecconf/202133703009.

Tang, Y., Taiebat, H.A. and Russell, A.R., 2017. Bearing capacity of shallow foundations in unsaturated soil considering hydraulic hysteresis and three drainage conditions. Int. J. Geomech., 17,6, 04016142. https://doi.org/10.1061/(ASCE)GM.1943-5622.0000845.

Terzaghi, K. 1943. Theoretical soil mechanics. New York: Wiley. http://dx.doi.org/10.1002/9780470172766.

Tran, A.T.P., Kim, A.R., Cho, G.C., 2019. Numerical modeling on the stability of slope with foundation during rainfall. Geomech. Eng., 17, 1, 109-118. https://doi.org/10.12989/gae.2019.17.1.109.

Troncone, A., Pugliese, L., Lamanna, G., Conte, E., 2021. Prediction of rainfall-induced landslide movements in the presence of stabilizing piles. Eng. Geol., 106143. https://doi.org/10.1016/j.enggeo.2021.106143.

Vahedifard, F. and Robinson, J.D. 2016. Unified method for estimating the ultimate bearing capacity of shallow foundations in variably saturated soils under steady flow. J. Geotech. Geoenviron. Eng., 142, 4, 04015095. https://doi.org/10.1061/(ASCE)GT.1943-5606.0001445.

Vanapalli, S.K., Mohamed, F.M., 2007. Bearing capacity of model footings in unsaturated soils. Experimental Unsaturated Soil Mechanics, 483-493. Springer, Berlin, Heidelberg.

Vanapalli, S.K., Fredlund, D.G., Pufahl, D.E., Clifton, A.W., 1996. Model for the prediction of shear strength with respect to soil suction. Can. Geotech. J. 33, 3, 379-392. https://doi.org/10.1139/t96-060.

Vanapalli, S.K., Oh, W.T., 2021. Analytical and numerical methods for prediction of the bearing capacity of shallow foundations in unsaturated soils. Soils and Rocks, 44, 3, e2021066521. https://doi.org/10.28927/SR.2021.066521.

Vo, T., Russell, A.R., 2016. Bearing capacity of strip footings on unsaturated soils by the slip line theory. Comput. Geotech., 74, 122-131. https://doi.org/10.1016/j.compgeo.2015.12.016.

Vo, T., Russell, A.R., 2017. Stability charts for curvilinear slopes in unsaturated soils. Soils Found., 57, 4, 543-556. https://doi.org/10.1016/j.sandf.2017.06.005.

Vo, T., Russell, A.R., 2020. Contours of saturated and unsaturated overhanging slopes at limiting equilibrium condition. Int. J. Numer. Anal. Methods Geomech., 44, 1, 93-116. https://doi.org/10.1002/nag.3008.

Xu, J., Zhao, X., Li, P., Zhang, M., 2021. Stability of a 3D unsaturated vertical cut slope subjected to variable rainfall infiltration. Comput. Geotech., 134, 104110. https://doi.org/10.1016/j.compgeo.2021.104110

Xu, Y. 2004. “Bearing capacity of unsaturated expansive soils.” Geotech. Geol. Eng., 22(4), 611-625.

Yang, S., Leshchinsky, B., Cui, K., Zhang, F., Gao, Y., 2019. Unified approach toward evaluating bearing capacity of shallow foundations near slopes. J. Geotech. Geoenviron. Eng., 145, 12, 04019110. https://doi.org/10.1061/(ASCE)GT.1943-5606.0002178.

Zhan, T.L., Ng, C.W., 2004. Analytical analysis of rainfall infiltration mechanism in unsaturated soils. Int. J. Geomech., 4, 4, 273-284. https://doi.org/10.1061/(ASCE)1532-3641(2004)4:4(273).

Zhan, T.L., Jia, G.W., Chen, Y.M., Fredlund, D.G., Li, H., 2013. An analytical solution for rainfall infiltration into an unsaturated infinite slope and its application to slope stability analysis. Int. J. Numer. Anal. Methods Geomech., 37, 12, 1737-1760. https://doi.org/10.1002/nag.2106.

Zhang, C., Gao, B., Yan, Q., Zhao, J., Wu, L., 2019. Development of allowable bearing capacity for strip foundations in unsaturated soils. Comput. Geotech., 114, 103138. https://doi.org/10.1016/j.compgeo.2019.103138.

Zhou H., Zheng G., Yin X., Jia R., Yang X., 2018. The bearing capacity and failure mechanism of a vertically loaded strip footing placed on the top of slopes. Comput. Geotech., 94, 12–21. https://doi.org/10.1016/j.compgeo.2017.08.009.

CHAPTER 4

Failure envelops for foundation subjected to inclined and eccentric loading considering steady state and transient flow conditions in unsaturated soils[3]

4.1 Introduction

Foundations are often subjected to inclined, eccentric or their combined loadings due to the wind, earth pressures, and earthquakes. In certain scenarios inclined or eccentric loadings also arise in the asymmetric structures. There will be a significant reduction in the bearing capacity of foundations associated with inclined or and eccentric loadings (Ganesh et al. 2017). Several investigators (Meyerhof 1951, 1953, 1963; Hansen 1970; Vesic 1975) introduced the inclination factors and the effective width rule to quantify the inclined or eccentric loading on the bearing capacity. The inclination factors were originally proposed for the axially loaded foundation bearing capacity equation (Terzaghi 1943). The effective width rule was suggested by Meyerhof (1953) to account for eccentric loading by reducing the foundation width with twice the eccentricity, *e*. Both the methods are widely accepted and practiced in conventional geotechnical engineering practice.

Over the years, many studies contributed towards rigorous understanding related to the bearing capacity of inclined and eccentrically loaded foundations (Michalowski and You 1998; Hjiaj et al. 2004; Patra et al. 2012a, 2012b; Krabbenhoft et al. 2014; Ganesh et al. 2017, Fathipour et al. 2022a, Li and Jiang 2022). An alternative method, which is referred

[3] The contents presented in this chapter are published as a journal article:
Tan, M., & Vanapalli, S. K. (2023). Failure envelops for foundation subjected to inclined and eccentric loading considering steady state and transient flow conditions in unsaturated soils. *Computers and Geotechnics*, *157*, 105315.

to as the failure envelope method was also extended by several researchers (Gourvenec and Randolph 2003; Taiebat and Carter 2000, 2002; Du et al. 2022; Fathipour et al. 2022a; Fathipour et al. 2022b; Ko et al. 2022) to describe the foundation behavior under the combined loading. The foundation is considered unsafe if the combination of the loads is outside the failure envelope. The inclined load can be treated as a combination of the vertical load, V and horizontal load, H. Similarly, the eccentric load can be considered as a moment load, M taking account of vertical load and the eccentricity. Compared to the traditional methods that are based on linear superposition of the load inclination and eccentricity or using independent reduction factors; the failure envelope method is advantageous as it explicitly considers the interaction of the V, H, and M and indicates the failure based on the changes that arise for each of the load components (Gottardi and Butterfield, 1993; Gourvenec and Barnett 2011). Moreover, other parameters such as the foundation embedment depth, soil shear strength profiles can also be incorporated into the failure envelope (Gourvenec and Randolph 2003).

The above discussed methods provide acceptable results for determining the foundation bearing capacity under different loading conditions for saturated soils. However, in many scenarios the foundations are above the ground water table where the soil is in a state of unsaturated condition during their entire design life. Most of the studies for foundations in unsaturated soils focus on the behavior of foundations that are subjected only to axial vertical loads (Vo and Russell 2016; Tang et al. 2017, 2022; Ghasemzadeh and Akbari, 2019; Akbari Garakani et al. 2020; Tan et al. 2021; Cheng et al. 2021; Anand and Sarkar 2022). Some studies (Vahedifard and Robinson 2016, Mahmoudabadi and Ravichandran 2019; Ravichandran et al. 2021; Anand and Sarkar 2022; Fathipour et al. 2022b; Tan and

Vanapalli 2022) recently investigated the foundation behavior under steady or transient state flow conditions in unsaturated soils. The results of these studies highlight how the foundation bearing capacity is influenced by different flow conditions in unsaturated soils. The behavior of foundations is mainly influenced by matric suction, which varies due to the water infiltration and evaporation conditions. Consequently, there is a significant variation of the shear strength and the foundation bearing capacity of unsaturated soils.

To date, only limited studies were undertaken in the literature to understand the behavior of foundations that are subjected to inclined and eccentric loading conditions in unsaturated soils (Wuttke et al. 2013, Jin et al. 2021, Fathipour et al. 2022b). Jin et al. (2021) recently employed an improved radial movement optimization method to investigate the foundation behavior in unsaturated soils considering inclined loading conditions. As expected, the results show that the matric suction and its profiles influence the foundation bearing capacity. Fathipour et al. (2022b) investigated the strip footings subjected to combined $V-H-M$ loading under steady state flow conditions in unsaturated soils using the lower bound finite element limit analysis. Results highlight the failure envelopes change due to the variations in flow characteristics associated with infiltration and evaporation conditions. However, rigorous studies are necessary for better understanding the foundation behavior subjected to the inclined and the eccentric loadings considering the influence of steady and transient state flow behavior in unsaturated soils.

In this study, the bearing capacity of a surface foundation placed on unsaturated clay and silt that is subjected to inclined or eccentric loading are investigated considering different flow conditions. Fig. 4.1 presents three different scenarios considered in this study. Scenario 1 represents the foundation under axial vertical loading. Scenario 2 and Scenario

3 show the foundation subjected to non-eccentric inclined loading and the eccentric vertical loading, respectively.

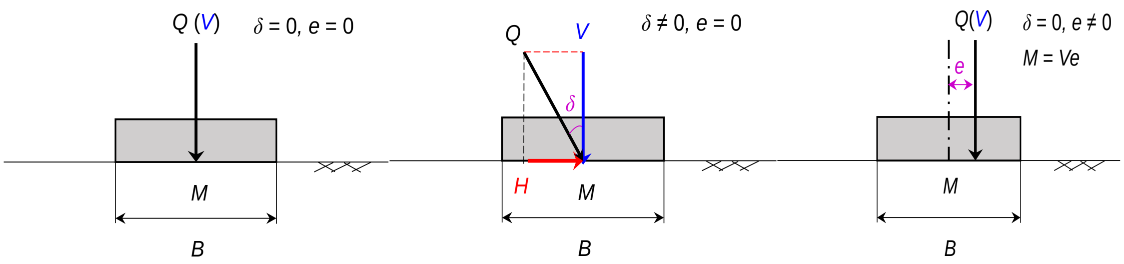

Fig. 4.1 Shallow foundation subjected to different loading conditions: (a) Scenario 1: Axial vertical loading; (b) Scenario 2: Inclined loading without eccentricity; (c) Scenario 3: Eccentric vertical loading

Firstly, an analytical method is proposed for the three different scenarios shown in Fig. 4.1 based on the slip line theory coupled with the analytical solution for both steady state and transient flow conditions. The proposed method is validated using the results from the published literature. The influence of four key parameters that include the effect of the influx or outflux, water infiltration durations, ground water table depths, soil internal friction angles on the bearing capacity of foundation with inclined and eccentric loads were investigated. The results are presented in the form of the failure envelopes.

Based on the parametric studies results from the proposed analytical method, semi-empirical equations are proposed for foundation subjected to the inclined or eccentric loading respectively in the $V – H$ loading space and V- M loading space. These equations can predict the shape and size of the failure envelopes as a function of the matric suction, foundation width and other basic soil properties. The proposed semi-empirical equations are first examined using the results obtained from the parametric studies by the introduced slip line method. Later, for further examination of the proposed semi-empirical equations, failure envelopes obtained with additional parameters which were not used in the parametric study were investigated. The proposed semi-empirical equations can be implemented as a simple calculation tool to build the failure envelopes efficiently using only limited information for both saturated and unsaturated soils.

The analytical method (i.e., modified slip line method) and the semi-emprical equations proposed in this Chapter are useful tools for the geotechnical engineers in the analyzing of foundations considering the influnece of different flow conditions in unsaturated soils. The proposed method can be used as a tool for more accurate forensic studies related to the behavior of foundations in general.

4.2 The slip line framework

4.2.1 Slip line equations

In this method, the soil is assumed to be a rigid-plastic material that obeys the Mohr-Coulomb yield criterion due to the plasticity zone of the soil is presented by the slip line method. In addition, foundation can be considered as a weightless rigid body. The weight of the foundation can be considered as surcharge loading. The foundation and the soil interface are also considered to be rough and the loading inclination angle, δ, is less than the internal friction angle, ϕ', of the soil. When $\delta = \phi'$, the surface footing starts to slide along the interface (Michalowski 2001). In addition, deformation associated with variation in matric suction is not considered in the slip line method. Based on the studies discussed in the literature (e.g., Michalowski 2001, Li and Jiang, 2022), it is reasonable to assume a one-side failure mechanism for foundation under inclined or eccentric load as shown in

Fig. 4.2a. The coordinate axes are presented in Fig. 4.2a with the origin (O) at the right edge of the foundation.

There are many models (e.g., Vanapalli et al. 1996, Khalili and Khabbaz, 1998, Lu and Likos, 2006) that provide reasonably good predictions of the contribution of matric suction towards the shear strength. In this study, the shear strength model (Eq. (4.1)) proposed by Vanapalli et al. (1996) is used; the three stress components used for the slip line solution can be expressed as Eqs. (4.2 – 4.4) with reference to Fig. 4.2b,

$$\tau = c' + \left(\sigma_{\mathrm{n}} - u_{\mathrm{a}}\right)\tan\phi' + \left(u_{\mathrm{a}} - u_{\mathrm{w}}\right)S_{\mathrm{e}}\tan\phi' \tag{4.1}$$

$$\sigma_x = (1+\sin\phi'\cos 2\theta)\sigma_{\mathrm{e}}' - c'\cot\phi' - S_{\mathrm{e}}\left(u_{\mathrm{a}} - u_{\mathrm{w}}\right) \tag{4.2}$$

$$\sigma_y = (1-\sin\phi'\cos 2\theta)\sigma_{\mathrm{e}}' - c'\cot\phi' - S_{\mathrm{e}}\left(u_{\mathrm{a}} - u_{\mathrm{w}}\right) \tag{4.3}$$

$$\tau_{xy} = \tau_{\mathrm{yx}} = \sin\phi'\sin 2\theta\sigma_{\mathrm{e}}' \tag{4.4}$$

where τ represents the unsaturated soil shear strength. S_e is the effective degree of saturation ($S_e = (S - S_r) / (S_0 - S_r)$ or $S_e = (\theta_w - \theta_s) / (\theta_s - \theta_r)$); S (θ_w) and S_r (θ_r) are the degree of saturation (volumetric water content) and the residual degree of saturation (residual water content), respectively; θ_s is the saturated soil volumetric water content; ($u_a - u_w$) refers to the matric suction; u_a is the atmospheric pressure and is considered as the reference pressure. Σ_x, σ_y refer to the normal stresses in the X- and Y- directions, respectively; σ_e', σ_m' represent the effective equivalent stress and the effective mean stress as shown in Fig. 4.2b, respectively; τ_{xy} refer to the shear stress; θ is the rotation angle from the direction of the major principal stress, σ_1, to the positive X- axis with counter-clockwise as positive. For foundation under inclined loading, the value of θ beneath the foundation can be expressed as Eq. (4.5). Fig. 4.2b provides more details of derivation of Eq. (4.5) that is based on the

Pole method. The plane PR in the Mohr's circle in the figure provides the details of σ_1 acting on surface (Li et al. 2013).

$$\theta = \frac{\pi}{2} + \frac{\delta}{2} + \frac{1}{2}\sin^{-1}\frac{\sin\delta}{\sin\phi'} \tag{4.5}$$

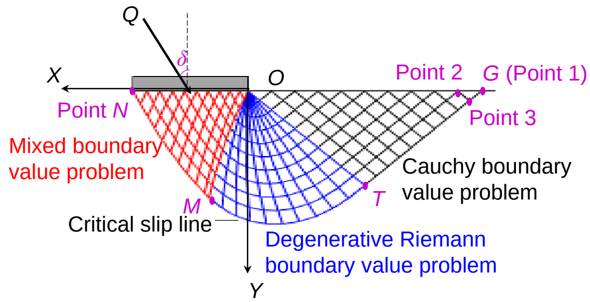

(a)

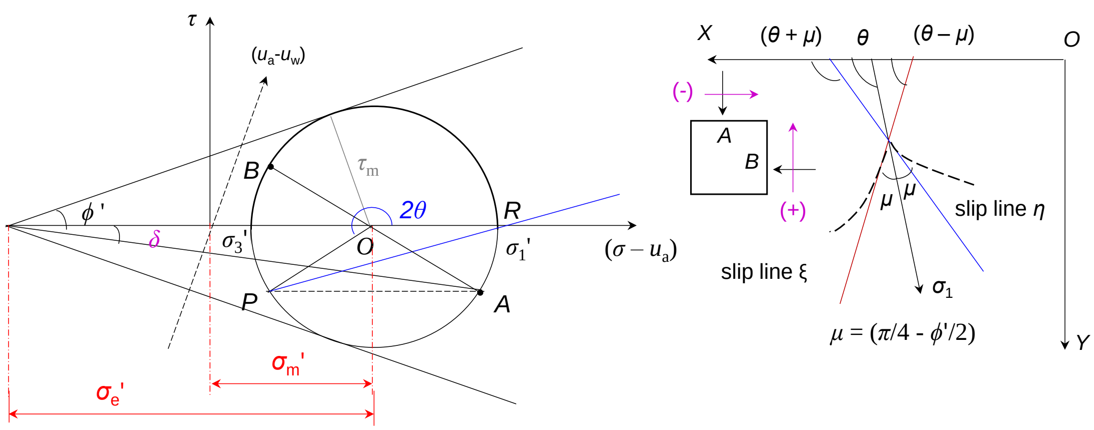

(b)

Fig. 4.2 Stress state of foundation subjected to inclined loading: (a) Definition of the coordinate; (b) Mohr circle associated with inclined loading.

The static equilibrium equations for a plane strain problem can be expressed as follows:

$$\frac{\partial \sigma_x}{\partial x} + \frac{\partial \tau_{xy}}{\partial y} = 0 \tag{4.6}$$

$$\frac{\partial \sigma_y}{\partial y} + \frac{\partial \tau_{xy}}{\partial x} = \gamma \tag{4.7}$$

where *x*, *y* are the *X* coordinate and *Y* coordinate, respectively. It should be noted that the soil unit weight, γ is not constant due to changes in water content associated with different flow conditions. The soil moist unit weight can be expressed as Eq. (4.8).

$$\gamma = \gamma_{\mathrm{w}} \frac{G_{\mathrm{s}} + e_{\mathrm{v}}\left[S_{\mathrm{e}}S_0 - (1-S_{\mathrm{e}})S_{\mathrm{r}}\right]}{1+e_{\mathrm{v}}} \tag{4.8}$$

where γ_{w} is the water unit weight; G_{s} is the specific gravity of soil; e_{v} is the void ratio and can be expressed using the γ_{w}, G_{s}, and the saturated soil unit weight, γ_{sat}. As a result, the soil unit weight in this study can be derived as Eq. (4.9), which is also used by Sun et al. (2019) for the slope stability estimation under steady state infiltration conditions.

$$\gamma = \frac{\left(\gamma_{\mathrm{sat}} - \gamma_{\mathrm{w}}\right)G_{\mathrm{s}} + \left[S_{\mathrm{e}}(S_0 - S_{\mathrm{r}}) + S_{\mathrm{r}}\right]\left(G_{\mathrm{s}}\gamma_{\mathrm{w}} - \gamma_{\mathrm{sat}}\right)}{G_{\mathrm{s}} - 1} \tag{4.9}$$

By substituting the stress components (Eqs. (4.2 – 4.4)) into the equilibrium equations (Eqs. 4.6 and 4.7), two families of the characteristic equations for ξ and η lines (Eqs. 4.10 and 4.11) can be formed after simplification as given below:

$$\xi\ Line \begin{cases} \dfrac{dy}{dx} = \tan(\theta - \mu) \\ d\sigma_{\mathrm{e}}' - 2\sigma_{\mathrm{e}}' \tan\phi' d\theta = \left[\gamma + \dfrac{\partial\left(S_{\mathrm{e}}\left(u_{\mathrm{a}} - u_{\mathrm{w}}\right)\right)}{\partial y}\right] \bullet \left[\left(-\tan\phi'\right)dx + dy\right] \end{cases} \tag{4.10}$$

$$\eta\ Line \begin{cases} \dfrac{dy}{dx} = \tan(\theta + \mu) \\ d\sigma_{\mathrm{e}}' + 2\sigma_{\mathrm{e}}' \tan\phi' d\theta = \left[\gamma + \dfrac{\partial\left(S_{\mathrm{e}}\left(u_{\mathrm{a}} - u_{\mathrm{w}}\right)\right)}{\partial y}\right] \bullet \left[\tan\phi' dx + dy\right] \end{cases} \tag{4.11}$$

where μ is the inclination between the direction of σ_1 and the tangent of slip lines as shown in Fig. 4.2b. These two equations can be solved using the finite difference method. More details about the procedure are discussed in a later section.

4.2.2 Suction profile under steady state flow

In the recently published literature, a few theoretical approaches have been developed to account for the suction-induced effect on the bearing capacity of foundation considering one dimensional vertical flow conditions (Vahedifard et al. 2015; Vahedifard and Robinson 2016; Vo and Russell 2016; Sun et al. 2019). In this study, Gardner's model (1958) (Eqs. (4.12 and 4.13)) that is widely used is employed for obtaining the suction profiles under both steady state and transient state unsaturated vertical flow.

$$k = k_{\mathrm{s}} e^{-\alpha\psi} \tag{4.12}$$

$$\theta_{\mathrm{w}} = \theta_{\mathrm{r}} + (\theta_{\mathrm{s}} - \theta_{\mathrm{r}}) e^{-\alpha\psi} \tag{4.13}$$

where k is the soil hydraulic conductivity. K_{s} represents the soil saturated hydraulic conductivity. A refers to the soil water characteristic curve (SWCC) reduction rate (Zhan and Ng, 2004). Ψ represents the suction head. The suction profile for such a scenario can be presented as Eq. (4.14) by combining the Gardner's model and the Darcy's law (Lu and Likos 2004).

$$(u_{\mathrm{a}} - u_{\mathrm{w}}) = -\frac{1}{\alpha} \ln\left[\left(1 + \frac{q}{k_{\mathrm{s}}}\right) e^{-\alpha\gamma_{\mathrm{w}}(H_{\mathrm{w}} - y)} - \frac{q}{k_{\mathrm{s}}}\right] \tag{4.14}$$

where q represents the vertical influx or outflux. Q is negative for infiltration condition and is positive for evaporation condition under the steady state flow case. H_{w} is the depth from the ground surface to the ground water table. The corresponding effective degree of saturation, S_e can be expressed as Eq. (4.15) based on the Gardner's model.

$$S_{\mathrm{e}} = e^{\frac{1}{\gamma_{\mathrm{w}}}\ln\left[\left(1+\frac{q}{k_{\mathrm{s}}}\right)e^{-\alpha\gamma_{\mathrm{w}}(H_{\mathrm{w}}-y)}-\frac{q}{k_{\mathrm{s}}}\right]} \tag{4.15}$$

4.2.3 Suction profile under transient flow

Richards' equation is commonly used to describe the transient unsaturated flow behavior (Shahrokhabadi et al. 2019). The method suggested by Srivastava and Yeh (1991) is extended in this study to obtain the closed-form solution for the Richards' equation to describe the time-dependent matric suction variation. This method can be used in the slope stability analysis, the earth pressure investigation and the foundation bearing capacity analysis (Zhan et al., 2013; Shahrokhabadi et al. 2019; Tan and Vanapalli 2022).

The analytical solution of matric suction profiles under transient state flow can be obtained by linearizing the Richards' equation (Eq. (4.16)) using the Gardner's model (Eqs. (4.12) and (4.13)).

$$\frac{\partial \theta_{\mathrm{w}}}{\partial t} = \frac{\partial}{\partial (H_w - y)}\left[k\frac{\partial(\psi + H_w - y)}{\partial (H_w - y)}\right] \tag{4.16}$$

where t represents the time. Eq. (4.16) can be transformed to the linear equation as Eq. (4.17).

$$\frac{\alpha(\theta_{\mathrm{s}} - \theta_{\mathrm{r}})}{k_{\mathrm{s}}}\frac{\partial k}{\partial t} = \frac{\partial^2 k}{\partial\left(H_{\mathrm{w}} - y\right)} - \alpha\frac{\partial k}{\partial\left(H_{\mathrm{w}} - y\right)} \tag{4.17}$$

Eq. (4.17) generally can be solved using two boundary conditions and one initial condition. The lower boundary is assumed at the stationary ground water table with zero matric suction. The upper boundary is assumed at the ground surface with constant infiltration influx, q. It should be noted for transient flow, q is positive for the infiltration condition which is different from the steady state flow. The initial matric suction distribution is obtained by performing a steady state flow analysis with a zero influx, in this study. The lower and upper boundaries and the initial condition can be written as Eqs. (4.18 – 4.20), respectively.

$$\text{Lower boundary: } K(0,\ T) = 1 \tag{4.18}$$

$$\text{Upper boundary: } \left[\frac{\partial K}{\partial Y^*} + K\right]_{Y^*=L} = Q \tag{4.19}$$

$$\text{Initial condition: } K(Y^*, 0) = e^{-Y^*} = K_0(Y^*) \tag{4.20}$$

where $Y^* = a(H_w - y)$, $K = \dfrac{k}{k_s}$, $L = aH_w$, $Q = \dfrac{q}{k_s}$, $T = \dfrac{ak_s t}{\theta_s - \theta_r}$ are the dimensionless parameters used for simplification purposes.

By using the Laplace's transformation technique, a dimensionless soil hydraulic conductivity ratio can be expressed as below:

$$K = k/k_s = Q - (Q-1)e^{-Y^*} - 4Qe^{\frac{(L-Y^*)}{2}} e^{-\frac{T}{4}} \sum_{n=1}^{\infty} \frac{\sin(\lambda_n Y^*)\sin(\lambda_n L)\,\mathrm{e}^{-\lambda_n^2 T}}{1 + \frac{L}{2} + 2\lambda_n^2 L} \tag{4.21}$$

where λ_n is the n*th* positive root of the characteristic equation (Eq. (4.22)).

$$\tan(\lambda_n L) + 2\lambda_n = 0 \tag{4.22}$$

The matric suction and the effective degree of saturation, S_e can be obtained by the combined solution of Eq. (4.21) and the Gardner's model (Eq. (4.12) and Eq. (4.13)).

$$(u_a - u_w) = -\frac{\gamma_w \ln(K)}{a} \tag{4.23}$$

$$S_e = K \tag{4.24}$$

4.2.4 The framework for slip line method

The framework for the slip line method developed in the MATLAB is summarized in Fig. 4.3. The suction profiles under the steady state flow or the transient flow conditions are first obtained after inputting the required parameters. The obtained suction profiles were incorporated into the slip line procedure. The iteration of the slip line procedure is based on discretizing the slip line equations (i.e., Eqs. (4.10) and (4.11)) using the finite difference method; three boundary value problems, namely Cauchy boundary value problem, degenerative Riemann boundary value problem and the mixed boundary value problem (see Fig. 4.2a), are considered in the iteration. For construction of the slip line field, the numerical iteration will be initiated with the Cauchy boundary value problem. The soil surface (i.e., OG in Fig. 4.2a) is divided into several grids with an initial uniform size. The information of these iteration points including the coordinates (i.e., x, y) and the stress state (i.e., σ_e', θ) are known at the soil surface OG for the present study. The Point 3 (i.e., intersection point of the two slip lines) in Fig. 4.2a can then be obtained based on information of previous iteration Point 1 and Point 2 on the two families of slip line. Then the slip line field are built in zone OTG in Fig. 4.2a. The points on the slip line OT can be considered as the new iteration boundary for zone OMT. The singularity point O is treated as a slip line such that all the iteration points on this slip line is converged into this point. The stress state variation for this singularity point depends on the stress state of O in zone OTG and that in zone OMN at the soil surface beneath the foundation. The slip line field in zone OMT can be built considering the degenerative Riemann boundary value problem with boundary O and OT. As mentioned earlier, the direction of the major principal stress at the soil surface (i.e., Line ON) beneath the foundation can be obtained using Eq. (4.5).

The OM and ON boundaries can be used to initiate the slip line construction in zone OMN considering the mixed boundary value problem.

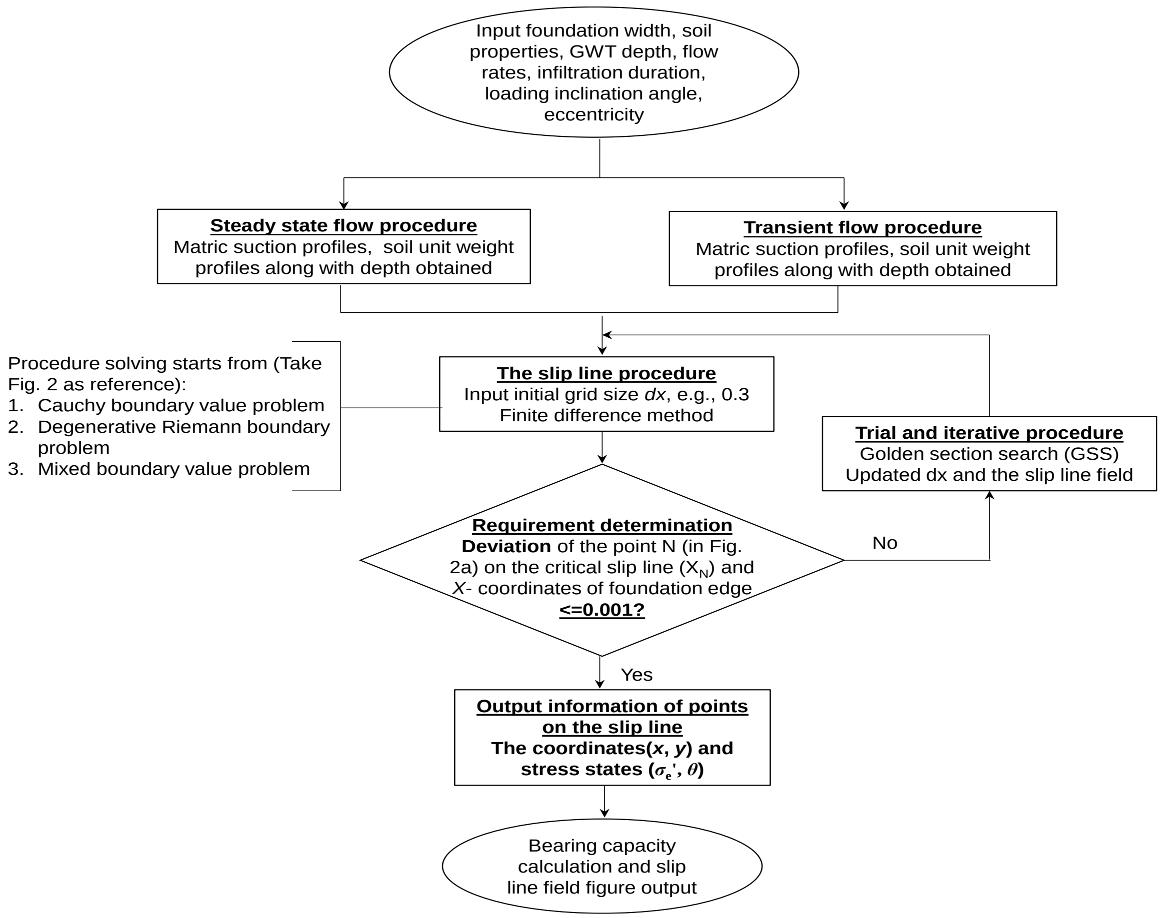

Fig. 4.3 Flow chart of the slip line procedure

After the information (i.e., x, y, σ_e', θ) for all the points on the slip line are obtained, the accuracy of the slip line field is examined by a developed trial and iterative procedure. This procedure is activated based on the Golden Section search method. Details about the Golden Section search method available in Tan and Vanapalli (2022) and are not repeated here. The slip line field in the three zone will be recalculated in this procedure until the last point (i.e., Point N in Fig. 4.2a) on the critical slip line (the outer slip line as shown in Fig.

4.2a) has a deviation equal 0.001 or less with the point at the left edge of the foundation base. The vertical stress and the shear stress are subsequently obtained based on Eq. (4.3) and Eq. (4.4) with the obtained points information along the foundation base. For the inclined loading condition, the vertical loading component and the horizontal loading component can then be derived by integrating the vertical stress and the shear stress along the foundation base, respectively. The vertical loading component of eccentric loading is also obtained by a method that is similar for obtaining the vertical loading component of inclined loading. The moment loading component can be obtained by multiplying the vertical loading with the eccentricity.

4.3 Proposed framework verification

In this section, results obtained from the proposed slip line procedure detailed in the previous section are compared with the published data from the literature for providing validations. These comparisons highlight two key aspects that are relevant to the present study. First, the feasibility and accuracy of the proposed framework in obtaining the foundation bearing capacity subjected to inclined and eccentric loadings in saturated soils are examined using the published studies. Later, comparisons are undertaken for foundation vertical stress along the foundation width and the bearing capacity in unsaturated soils considering the unsaturated flow conditions.

4.3.1 Foundation subjected to inclined and eccentric loads

Equation (Eq. (4.25)) proposed by Meyerhof (1963) is widely used in the determination of surface foundation bearing capacity in saturated soils.

$$q_{\mathrm{b}} = \frac{Q}{B'} = c' N_{\mathrm{c}} i_{\mathrm{c}} + \frac{1}{2}\gamma B' N_{\gamma} i_{\gamma} \tag{4.25}$$

where N_c, N_γ represent the bearing capacity factors. I_c, i_γ are the inclination factors. Several researchers proposed inclination factors (Meyerhof 1963; Hansen 1970; Vesic 1975) to take account the inclination loading (see Table 4.1).

Table 4.1 Summary of the bearing capacity factors

References	N_c	N_q	N_γ	i_c	i_q	i_γ
Meyerhof (1963)	$(N_q-1)\cot\phi'$	$e^{\pi\tan\phi'}\tan^2(\pi/4+\phi'/2)$	$(N_q-1)\tan(1.4\phi')$	$\left(1-\frac{\alpha}{90°}\right)^2$	$\left(1-\frac{\alpha}{90°}\right)^2$	$\left(1-\frac{\alpha}{\phi'}\right)^2$
Hansen (1970)	$(N_q-1)\cot\phi'$	$e^{\pi\tan\phi'}\tan^2(\pi/4+\phi'/2)$	$1.5(N_q-1)\tan(\phi')$	$\frac{i_q N_q-1}{N_q-1}$	$(1-0.5\tan\alpha)^5$	$(1-0.7\tan\alpha)^5$
Vesic (1975)	$(N_q-1)\cot\phi'$	$e^{\pi\tan\phi'}\tan^2(\pi/4+\phi'/2)$	$2(N_q+1)\tan(\phi')$	$\frac{i_q N_q-1}{N_q-1}$	$(1-\tan\alpha)^2$	$(1-\tan\alpha)^3$

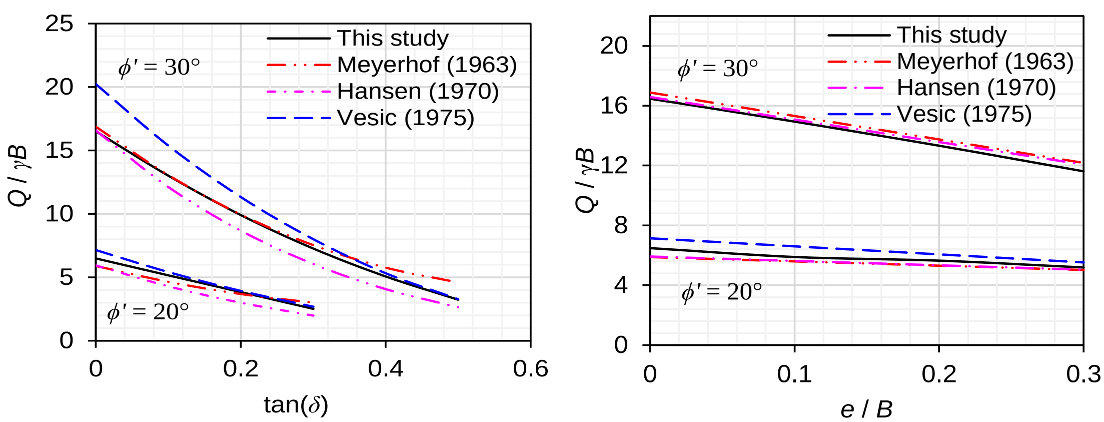

(a) (b)

Fig. 4.4 Comparison between the results from the present study and published results from the literature: (a) Foundation with inclined loading; (b) Foundation with eccentric loading.

In this comparative study, the soil cohesion is set as 6 kPa and the soil unit weight is assumed to be a constant value of 20 kN/m^3. These values are reasonable for the fine-grained soils investigated in this study. Results calculated from different inclination factors (i.e., Meyerhof 1963; Hansen 1970; Vesic 1975) along the Eq. (4.25) and that from this study by the slip line method are presented in Fig. 4.4. There is a reasonably good agreement between all the four different methods for saturated soils. These results provide confidence with respect to the reliability of the proposed method for the determination of foundation bearing capacity for inclined and eccentric loading conditions.

4.3.2 Foundation performance considering unsaturated flow conditions

In this section, the foundation bearing capacity and vertical stress along the foundation width obtained from the proposed slip line framework considering the hydrostatic, steady state and transient unsaturated flow are compared with the results from published studies. Two experimental studies (Wuttke et al. 2013, Shwan 2015) and three different approaches proposed by Vo and Russell (2016); Hou et al. (2020); Tan and Vanapalli (2022) respectively, are used for providing these comparisons. Soil properties used in the comparative studies are summarized in Table 4.2.

Table 4.2 Soil properties used in comparative studies

References	c' (kPa)	ϕ' (°)	γ (kN/m^3)	H_w (m)	k_s (m/s)	q (m/s)	Comparison purpose
Wuttke et al. (2013)	0.01	46.9	17.65	-	-	-	Hydrostatic
Shwan (2015)	2	36.8	19.33	-	-	-	Hydrostatic
Vo and Russell (2016)	_	25	17	10	1.0×10^{-7}	q_{in}: -3.14×10^{-8}	Infiltration Steady state
Hou et al. (2020)	10	30	19.8	1, 4	1.0×10^{-7}	q_{out}: 1.15×10^{-8}	Evaporation Steady state
Tan and Vanapalli (2022)	6	25	20	6	5×10^{-8}	q_{in}: 5×10^{-8}	Infiltration Transient state

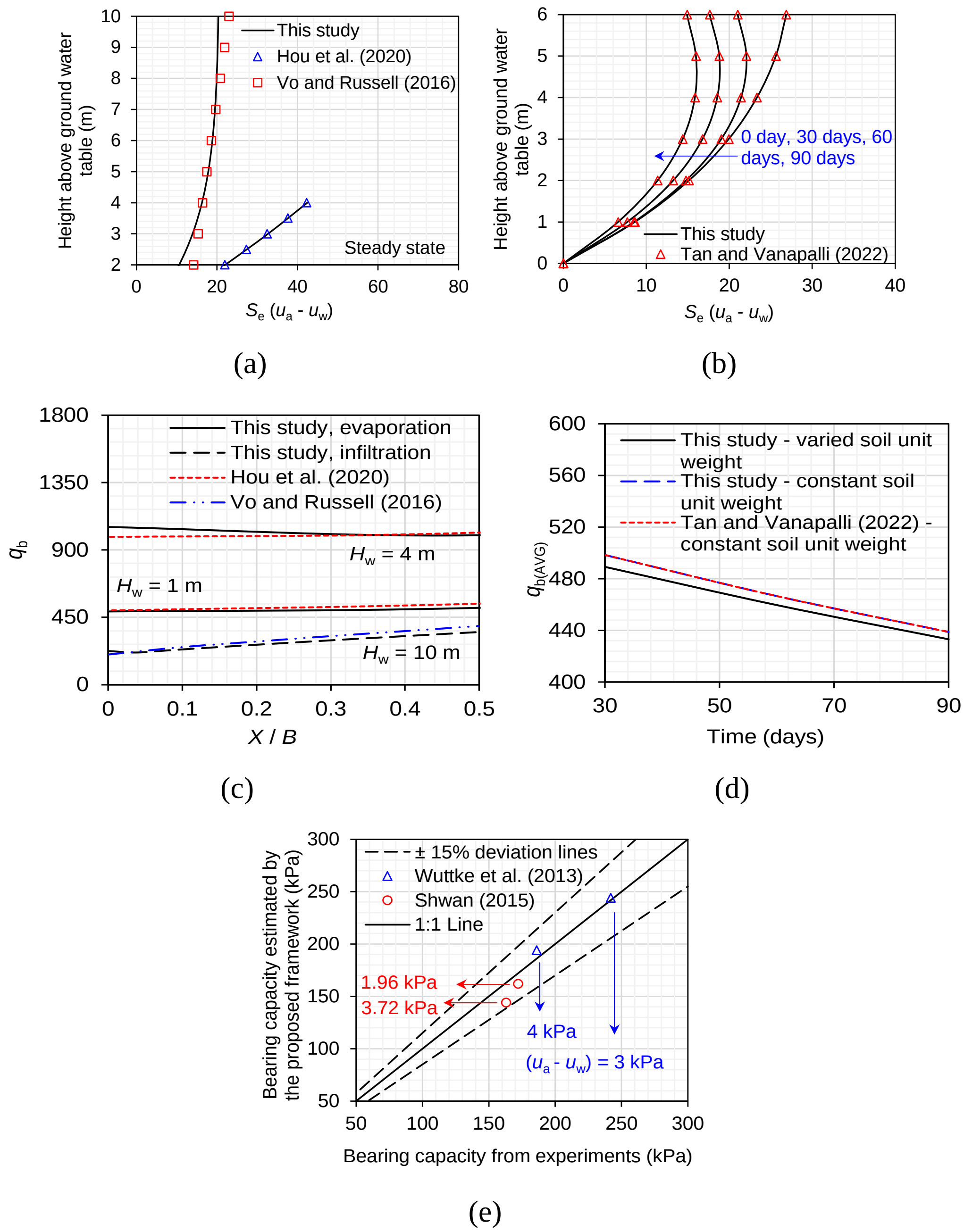

Fig. 4.5 Comparison of proposed framework with published studies (a) [$S_e(u_a - u_w)$] under steady state condition; (b) [$S_e(u_a - u_w)$] under transient flow condition; (c) Vertical stress along foundation width under steady state condition; (d) Vertical stress under transient condition; (e) Hydrostatic condition.

Fig. 4.5a and 4.5b show the good consistency of the [S_e (u_a – u_w)] profiles obtained from the proposed framework and that from Vo and Russell (2016), Hou et al. (2020) and Tan and Vanapalli (2022). Fig. 4.5c presents results of the vertical stress along the foundation width, q_b, under steady state unsaturated flow. A good agreement can be observed between the results obtained from the slip line procedure in comparison to published results in the literature for both evaporation and infiltration conditions. Fig. 4.5d shows the average q_b variation with respect to time for the transient flow condition. In an earlier study by Tan and Vanapalli (2022), a constant soil unit weight was used. In this study, both the constant soil unit weight and the varying soil unit weight taking account of water content changes are used for providing comparisons: (i) verifying the accuracy of the results from the proposed procedure; (ii) providing comparisons using the varying soil unit weight and the constant soil unit weight. The differences between the results obtained considering the variations in the soil unit weight and the constant soil unit weight is not significant (see Fig. 4.5d). However, conservative results can be obtained by taking account the soil unit weight variation into account.

The comparison results of the proposed framework and two model footing tests of strip foundation are presented in Fig. 4.5e. The foundation widths used in Wuttke et al. (2013) and Shwan (2015) are respectively 79mm and 25 mm. The average matric suction in between the foundation base to a depth of 1.5*B* is provided by Wuttke et al. (2013). Then the matric suction and the effective degree of saturation profile used in the proposed framework are estimated based on the given average matric suction and the SWCC fitting parameters. The Fredlund and Xing (1994) equation (Eq. 4.26) was used in Wuttke et al. (2013) with fitting parameters α_f = 2.4 kPa, n_f = 9.95 and m_f = 1.4.

$$S_{\mathrm{e}} = \left(\ln\left\{e + \left[\left(u_{\mathrm{a}} - u_{\mathrm{w}}\right)/\alpha_{\mathrm{f}}\right]^{n_{\mathrm{f}}}\right\}\right)^{-m_{\mathrm{f}}} \tag{4.26}$$

where e is the natural logarithm number.

As soil unit weight is not given in Wuttke et al. (2013) it is assumed to be the same value as in Yuan and Du (2020) who conducted comparisons using the experimental results from Wuttke et al. (2013). For the experiment conducted by Shwan (2015), the matric suction value and the corresponding effective degree of saturation that were provided were incorporated into the slip line procedure directly.

Good agreement (i.e., deviation values less than 15% in Fig. 4.5e) of the bearing capacity of strip foundations obtained from the proposed slip line procedure and that from the experimental studies provides more confidence for the proposed framework in determining the foundation bearing capacity. Results summarized in Fig. 4.5 suggest that the results obtained from the proposed slip line method are reliable and reasonable. The method therefore can be used for determination of the foundation bearing capacity for the inclined and eccentric loading conditions considering the different unsaturated flow conditions in unsaturated soils.

4.4 Problem definition

Earlier studies in the literature suggest that the influence of the steady state flow rate in a coarse-grained unsaturated soil is insignificant (e.g., Vahedifard and Robinson 2016). For this reason, investigations are undertaken using two different soils; namely, clay and silt that represent fine-grained soils to study the influence of steady and transient state flow conditions. The clay and silt properties summarized in Table 4.3 are obtained from published studies (Vahedifard and Robinson 2016; Tan and Vanapalli 2022), respectively.

The foundation with an inclined loading without eccentricity (Scenario 1 and 2 in Fig. 4.1) is first investigated followed by the foundation that is subjected to eccentric vertical loading (Scenario 1 and 3 in Fig. 4.1). The steady state and transient flow conditions are considered for both the inclined and eccentric loading cases. The effect of the ground water table depth, the flow rates, and the soil internal friction angle to the foundation bearing capacity and the corresponding failure envelopes are investigated. The range of these parameters are summarized in Table 4.4.

Table 4.3 Properties of the soils used in the study

Properties	Clay	Silt
Specific gravity, G_s	2.71	2.67
Effective cohesion, c' (kPa)	10	5
Saturated soil unit weight, γ_{sat} (kN/m^3)	20	20
Fitting parameters, α (kPa^{-1})	0.005	0.01
Saturated hydraulic conductivity, k_s (m/s)	5.0×10^{-8}	1×10^{-7}
Saturated volumetric water content, θ_s	0.58	0.38
Residual volumetric water content, θ_r	0.1	0.06

Table 4.4 Details of various parameters used in the study

Parametric studies	Range	Investigated condition
Ground water table depth, H_w (m)	4 m, 8 m	$\phi' = 30^o$ Steady state: q_{in}: -3.14×10^{-8} m/s $q_{out:}$ 1.15×10^{-8} m/s Transient state: 3.14×10^{-8} m/s
Flow rates, q (m/s)	Steady state: q_{in}: -3.14×10^{-8} m/s $q_{out:}$ 1.15×10^{-8} m/s Transient state: q_{in}: 3.14×10^{-8} m/s	$\phi' = 30^o$ $H_w = 4$ m, $H_w = 8$ m
Soil internal friction angle, ϕ' (°)	10º, 20º, 30º	$H_w = 8$ m Steady state: q_{in}: -3.14×10^{-8}

4.5 Foundation with non-eccentric inclined loading

4.5.1 Influence of steady state flow on the bearing capacity

4.5.1.1 Effect of the flow rates and ground water table depths

The results summarized in Fig. 4.6 highlight the effect of the loading inclination on the foundation bearing capacity along with different ground water tables and flow rates. Fig. 4.6a and Fig. 4.6d show the total ultimate bearing capacity variation along with the inclination for clay and silt, respectively. The obvious reduction trend is found in the two figures for the bearing capacity with an increase in the loading inclination angle. The relative deviation between the foundation bearing capacity for the axial loading and that for an inclination angle of 25° is presented in Table 4.5. The bearing capacity of foundation for both soils have a reduction of approximately 65% to 75% for loading inclination angle that increases from 0° to 25°.

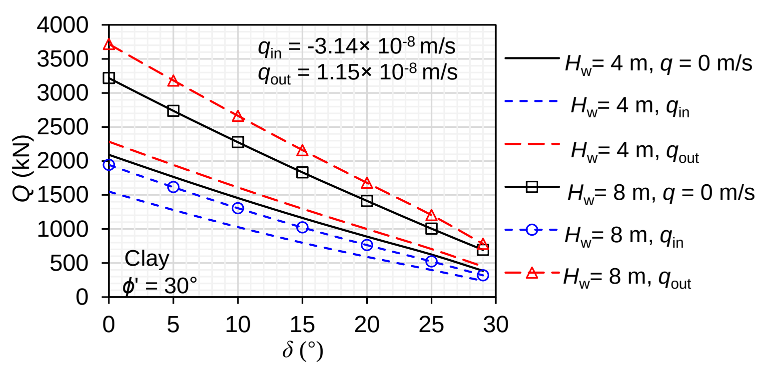

(a)

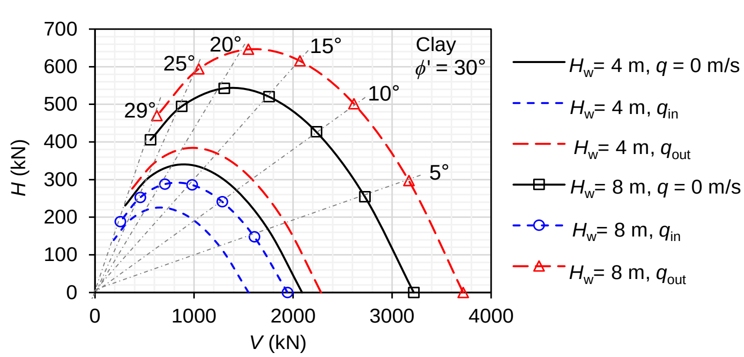

(b)

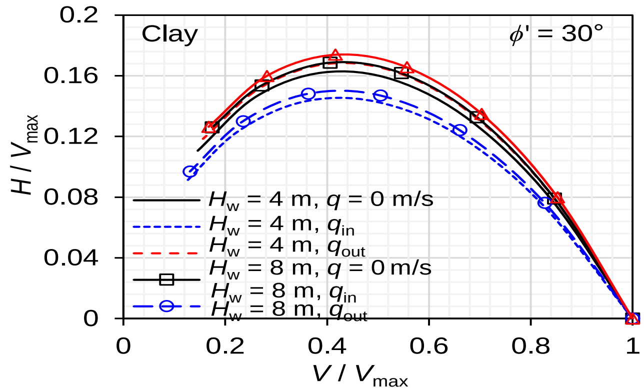
Clay
ϕ' = 30°
H / V_max
V / V_max
H_w = 4 m, q = 0 m/s
H_w = 4 m, q_in
H_w = 4 m, q_out
H_w = 8 m, q = 0 m/s
H_w = 8 m, q_in
H_w = 8 m, q_out

(c)

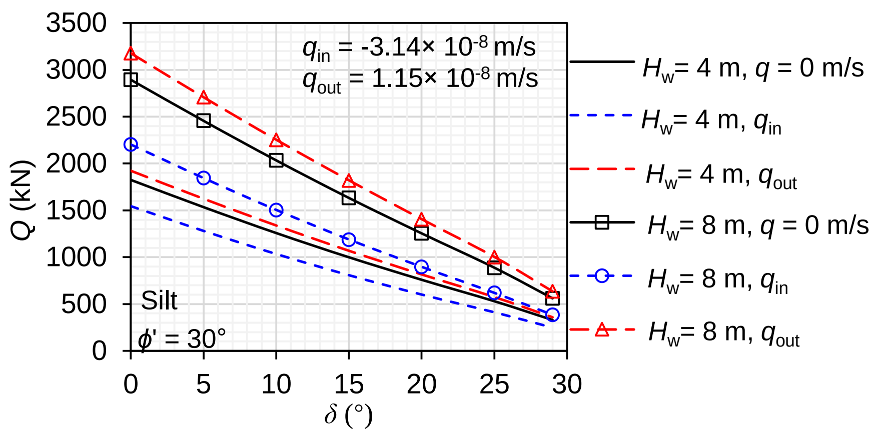
q_in = -3.14× 10^-8 m/s
q_out = 1.15× 10^-8 m/s
Silt
ϕ' = 30°
Q (kN)
δ (°)
H_w= 4 m, q = 0 m/s
H_w= 4 m, q_in
H_w= 4 m, q_out
H_w= 8 m, q = 0 m/s
H_w= 8 m, q_in
H_w= 8 m, q_out

(d)

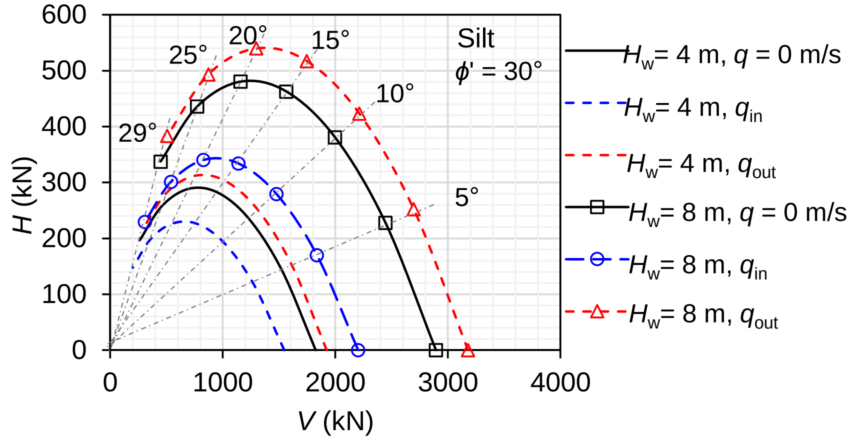
Silt
ϕ' = 30°
29°
25°
20°
15°
10°
5°
H (kN)
V (kN)
H_w= 4 m, q = 0 m/s
H_w= 4 m, q_in
H_w= 4 m, q_out
H_w= 8 m, q = 0 m/s
H_w= 8 m, q_in
H_w= 8 m, q_out

(e)

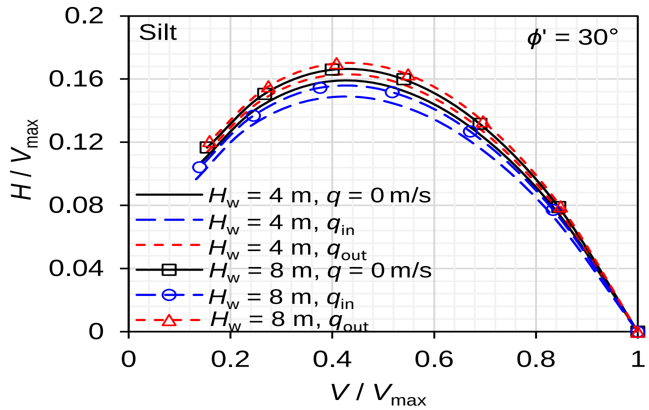

(f)

Fig. 4.6 Influence of the loading inclination angle under steady state flow: (a) Effect of δ on Q of clay soil; (b) Influence of the q and H_w on $V – H$ loading for clay; (c) Normalized failure envelope for clay; (d) Effect of δ on Q of silt soil; (e) Influence of the q and H_w on $V – H$ loading for silt; (f) Normalized failure envelope for silt.

This relative deviation value is also influenced by the variations in the ground water table depth and the flow rates. For a given flow rate, the relative deviation value of the bearing capacity between two inclination angles (i.e., 0° and 25°) is slightly lower at a ground water table level depth that is deeper from the ground surface (see Table 4.5). However, for a given ground water table depth, the relative deviation value increases for the infiltration condition and decreases for flow scenarios that represent evaporation conditions. For example, the relative deviation value for clay at H_w = 4 m under q = 0 m/s is 70.19%; this value drops to 68.78% at H_w = 8 m. The value 70.19% increases to 74.45% at H_w = 4 m when subjected to infiltration with $q = -3.14 \times 10^{-8}$ m/s. Such a behavioral trend may be attributed to the matric suction and the corresponding effective degree of saturation, S_e (i.e., due to the last term in Eq. (4.1), [$S_e (u_a – u_w) \tan\phi'$]). The variation of the

[S_e ($u_a - u_w$) tanϕ'] will be explained together with the transient flow condition, in a later section. The above results suggest that the negative effect of the loading inclination angle is alleviated to a certain extent for higher matric suction values that results from the initial ground water table depth and the flow rates.

The inclined loading can be considered as the combined loading of the horizontal and vertical loads. In addition to the total ultimate bearing capacity, the influence of the flow rates and the ground water table depths on the individual loadings are shown in Figs. 4.6b and 4.6e for the two types of soils. For a given inclination loading angle, δ, both the horizontal and the vertical loadings increase for the flow behavior representing evaporation condition and decrease for the flow behavior associated with infiltration condition. Moreover, a deeper ground water table contributes towards higher horizontal and vertical loadings for constant δ. The matric suction contributes not only towards the vertical loading but also to the horizontal loading.

Table 4.5 Deviation of the bearing capacity for δ = 0° and δ = 25°

Soil	H_w (m)	q = 0 m/s	$q = -3.14 \times 10^{-8}$ m/s	$q = 1.15 \times 10^{-8}$ m/s
Clay	4	70.19%	74.45%	69.09%
	8	68.78%	73.15%	67.63%
Silt	4	71.04%	73.32%	70.13%
	8	69.34%	71.94%	68.47%

The different soil types also have a significant impact on the bearing capacity variation as shown in Figs. 4.6b and 4.6e for clay and silt. However, similar trend is observed for both the clay and silt for the variation of the horizontal and vertical loading components with the loading inclination angle. For a given ground water table depth or the constant flow rate, there is a continuous reduction in vertical loading with increasing δ, while the horizontal loading increases with the δ until reaching a maximum value at a specific loading inclination angle and then starts decrease. This is reasonable as the vertical loading component contribution is the predominant loading for low values of δ. The resistance along the soil and foundation interface is the main factor that influences the horizontal loading at large inclination angles. The foundation starts to slide when δ is equal to the ϕ' as per the earlier discussions.

The normalized failure envelopes for the two soils are shown In Figs. 4.6c and 4.6f, respectively. The normalized horizontal bearing capacity is defined as H / V_{max} (V_{max} represents the ultimate vertical bearing capacity for foundation under only vertical loading) and the normalized vertical bearing capacity is defined as V / V_{max}. The normalized failure envelope shape for each parameter is approximately the same and falls in a narrow band that typically exhibits a parabolic form. The failure envelop variation is insignificant if the bearing capacity is normalized. For values of $\delta \leq 5°$, the normalized failure envelopes variation for different ground water tables or various flow rates are not obvious compared to values of δ that are higher. The vertical loading is the predominant loading component for the lower loading inclination angle and most contribution of the matric suction is towards the vertical loading at this stage. Overall, the failure envelope expands for foundation for evaporation condition and shrinks for foundation for infiltration condition. The maximum value of the normalized horizontal bearing capacity drops from 0.169 to 0.150 for q = 0 m/s to q = -3.14 × 10^{-8} m/s for the clay soil at H_w = 8m; and that for the silt drops from 0.166 to 0.155. The maximum values for all the conditions are found at V / V_{max}

values between 0.43 to 0.45 at inclination loading in the range of 15° to 20°. This range is consistent with the result of 20° presented by Fathipour et al. (2022b) for a clay. In addition to the influence of the flow rates on the failure envelope, expansion of the failure envelope is also observed for shallow ground water table depth. The reason for the failure envelopes variation for different flow rates and the ground water table depths can be attributed to the contribution arising from [$S_e (u_a - u_w) \tan\phi'$].

4.5.1.2 Effect of the soil internal friction angle

All the results summarized are conducted for soils with an internal friction angle of 30°. The internal friction angle typically has an impact on the foundation bearing capacity for the inclined loading and the corresponding failure envelopes (Loukidis et al. 2008; Zheng et al. 2019; Jin et al. 2021). In this study, the influence of the internal friction angle is investigated for only steady state with infiltration condition because the variation of the effective internal friction angle with respect to the matric suction can be typically neglected (Fredlund and Rahardjo 1993). Figs. 4.7a and 4.7d respectively illustrates the total ultimate bearing capacity of foundation on clay and silt soil with respect to the loading inclination angle under different internal friction angles. It is obvious that the internal friction angle contributes significantly towards the ultimate bearing capacity. Q at $\phi' = 30°$ is more than seven times of that for Q at $\phi' = 10°$ for clay under vertical loading. The value for the silt is much higher (i.e., almost nine times).

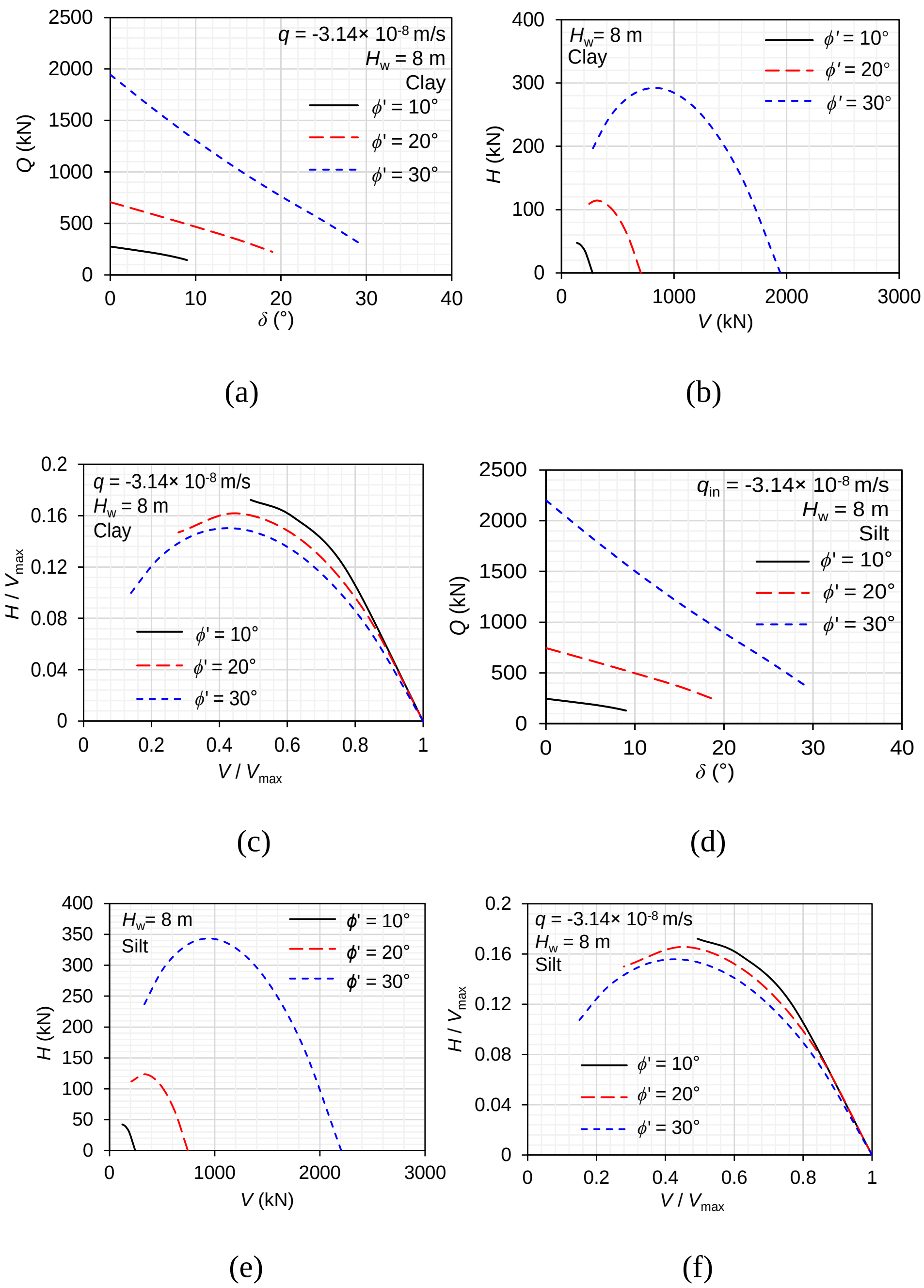

Fig. 4.7 Influence of the soil internal friction angle: (a) Influence of the ϕ' on the Q for clay soil; (b) Effect of ϕ' on the V, H loading of clay soil; (c) Normalized failure envelope for clay; (d) Influence of the ϕ' on the Q for silt soil; (e) Effect of ϕ' on the V, H loading of silt soil; (f) Normalized failure envelope for silt

The variations of the vertical and horizontal loading components are summarized In Figs. 4.7b and 4.7e. The $V - H$ loading envelope expands significantly with a higher soil internal friction angle, and both the maximum horizontal and vertical loading obviously increase. For example, the maximum horizontal bearing capacity obtained for the internal friction angle of 30° is about 2.5 times of that obtained for an internal friction angle of 20° for clay as shown in Fig. 4.7b; this is even higher, which is almost three times for the silt (see Fig. 4.7e). However, the normalized failure envelopes show a different variation trend in Figs. 4.7c and 4.7f. The envelope expands for soil with a lower internal friction angle. The reason for this behavior may be attributed to the higher vertical maximum bearing capacity obtained for a higher internal friction angle (V_{max}). The horizontal bearing capacity is normalized with this relatively higher vertical bearing capacity and the normalized value is therefore lower than that obtained for a soil with lower internal friction angle. This variation trend is also consistent with the published studies for saturated soils (Loukidis et al. 2008; Pham et al. 2020).

4.5.2 Influence of transient flow on the bearing capacity

Fig. 4.8 presents the foundation bearing capacity variation with respect to the loading inclination under the vertical transient flow condition ($q_{in} = 3.14 \times 10^{-8}$ m/s). As expected, the loading inclination has a negative effect on the total bearing capacity for both clay and silt for any given rainfall duration (see Figs. 4.8a and 4.8d). For a given δ, Q continues to decrease with an increase in the infiltration duration; however, the rate of decrease value is dependent on the type of soil. For δ = 10°, the reduction of the bearing capacity for foundation on clay prior to infiltration and that for 30 days is 35.7%; while the reduction for foundation for silt is about 20%.

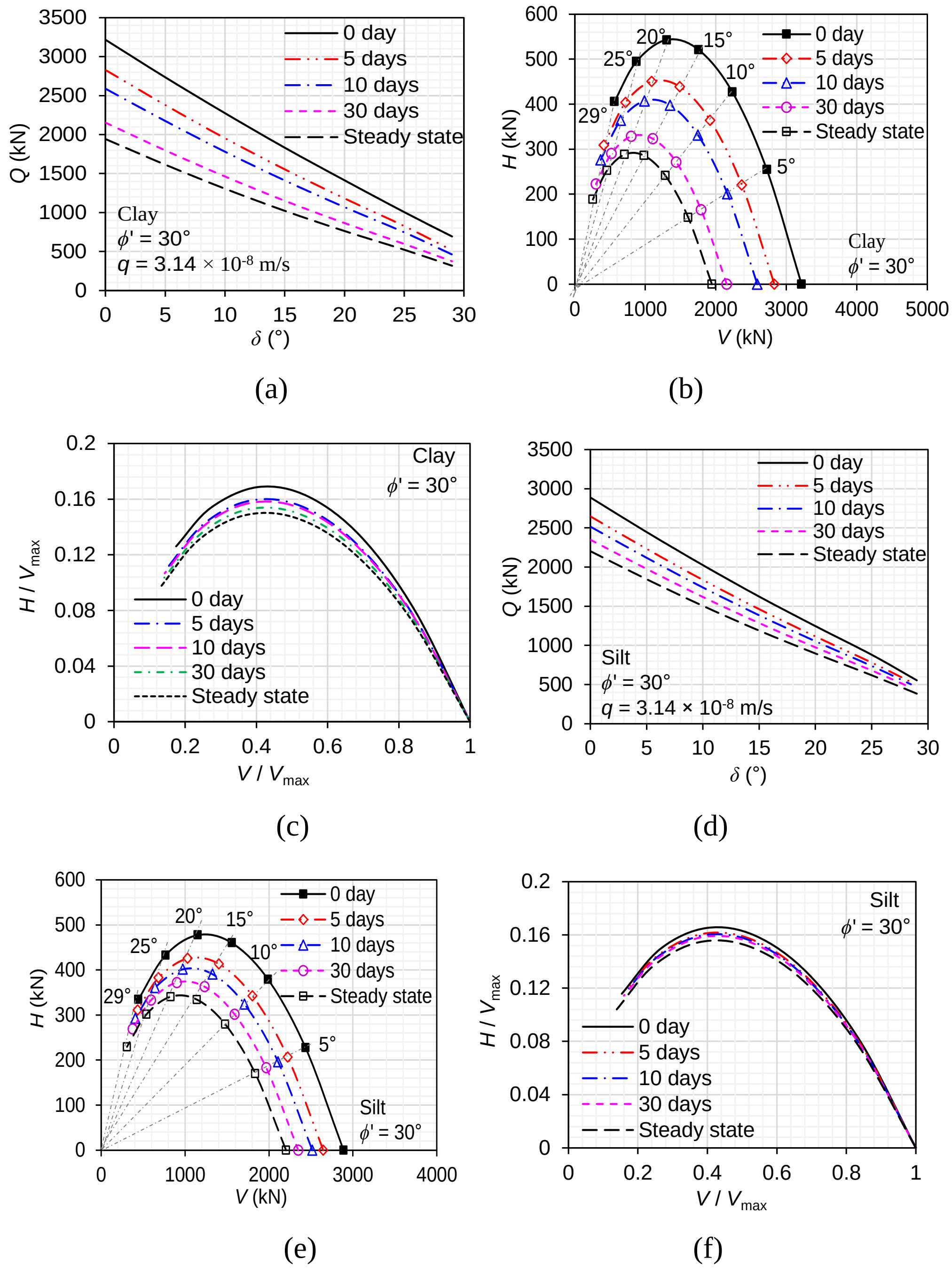

Fig. 4.8 Influence of the foundation bearing capacity under the transient flow condition (H_w = 8 m): (a) Effect of δ on the Q for clay; (b) V, H loading for clay; (c) Normalized failure envelope for clay; (d) Effect of δ on the Q for silt; (e) V, H loading for silt; (f) Normalized failure envelope for silt.

The transient flow impact on the vertical and horizontal loading components are shown in Figs. 4.8b and 4.8e. The V – H loading envelope shrinks with an increase in the infiltration duration. The shape of the V – H loading envelope is observed to be consistent with that of the steady state condition. The horizontal loading increases with an increase in the loading inclination angle; however, it drops after reaching a certain maximum value at a specific loading inclination angle. The maximum value of the horizontal loading inclination angles is between 15° and 20° for both the steady state and the transient state flow conditions for the two soils. The normalized failure envelopes in the V – H loading space in Figs. 4.8c and 4.8f for different rainfall durations also shrink with an increase in the infiltration duration. However, the variation is limited to a narrow band, especially for the silt. This means the infiltration influence is more obvious on the foundation subjected to the inclined loading on clay soil compared to the silt soil.

Fig. 4.9 summarizes the ground water table influence on the normalized failure envelope in V – H loading space under transient flow condition. Generally, after normalizing the bearing capacity, the failure envelop variation between the two ground water table depths are not significant. However, for shallow ground water table depth, infiltration duration required is less to achieve a similar failure envelope as for the steady state condition. Moreover, the deviation of the failure envelopes for different infiltration durations is small when the ground water table depth is shallow. This is more obvious for silt at H_w = 4 m compared to clay. For loading inclination angles that are typically low (e.g., $\delta \leq 5°$), the normalized failure envelope almost has no variation.

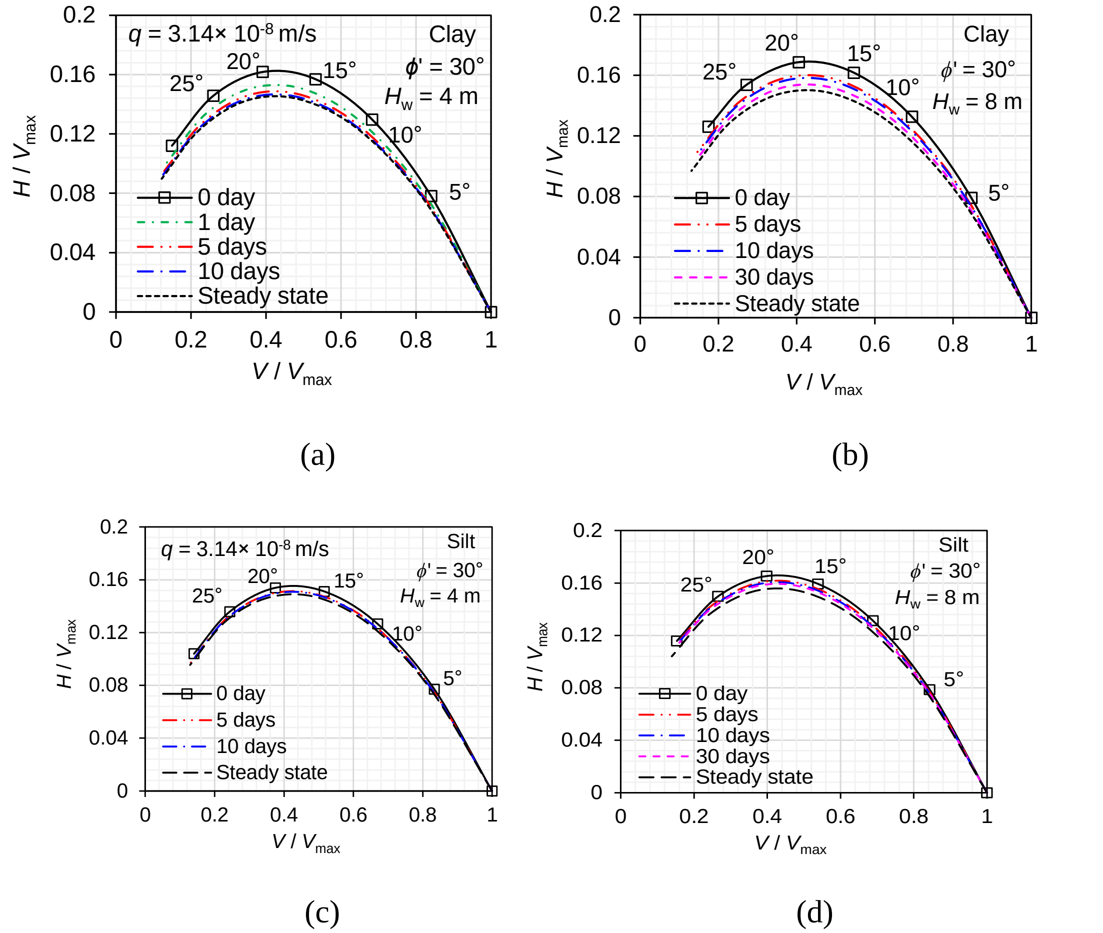

Fig. 4.9 Normalized failure envelopes in the V – H loading space at different H_w: (a) For clay at H_w = 4 m; (b) For clay at H_w = 8 m; (c) For silt at H_w = 4 m; (d) For silt at H_w = 8 m.

Fig. 4.10 illustrates the reason for the foundation bearing capacity variation and the envelope variation with respect to the variations in unsaturated flow conditions. The term $[S_e\,(u_a - u_w)\tan\phi']$ (from Eq. (4.1) which is the shear strength contribution) along with the Y axis is shown in Fig. 4.10 for clay, as an example. The increase $[S_e\,(u_a - u_w)\tan\phi']$ contributes directly to the shear strength of the soil and consequently provide a higher foundation bearing capacity for the evaporation condition. With increasing infiltration duration, $[S_e\,(u_a - u_w)\tan\phi']$ keeps decreasing and therefore results in a reduction of both the horizontal loading and vertical loading. Results summarized in Vahedifard and Robinson (2016) and Tan and Vanapalli (2022) for the foundations respectively under the steady state and transient flow conditions also indicate that the [S_e $(u_a - u_w)$ $\tan\phi$'] is the key factor that influences the bearing capacity variation. This term is influenced by the initial ground water table depth (or the initial suction profiles), the soil properties, and the flow rates. In summary, the foundation bearing capacity is influenced by not only the soil properties, but also the loading condition and the unsaturated flow conditions.

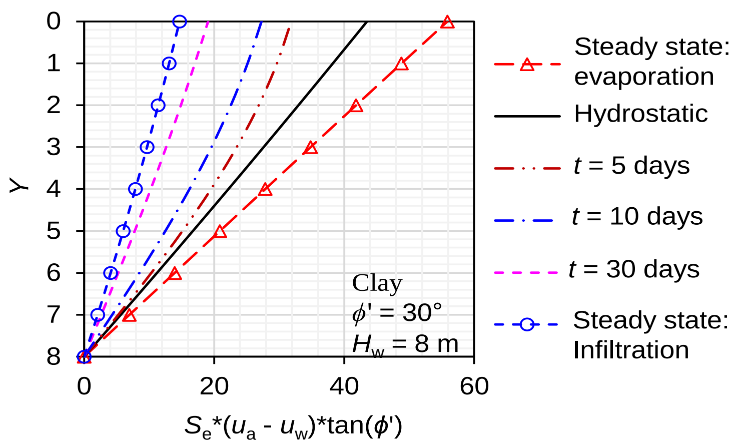

Fig. 4.10 [S_e $(u_a - u_w)$ $\tan\phi$'] variation along the Y coordinates

4.6 Foundation with eccentric vertical loadings

A schematic diagram of foundation subjected to eccentric loading is shown in Fig. 4.11. The effective width rule is used in the slip line procedure following the discussions summarized in the earlier sections. The effective width rule assumes the contact pressure along the foundation base is identical to the axially loaded foundation but with a reduced width as shown in Fig. 4.11b. It should be noted that the deformation cannot be considered using this method combined with the slip line method. However, this approach can be extended for reliable foundation bearing capacity determination (e.g., Michalowski and You 1998, Taiebat and Carter 2002, Krabbenhoft et al. 2012).

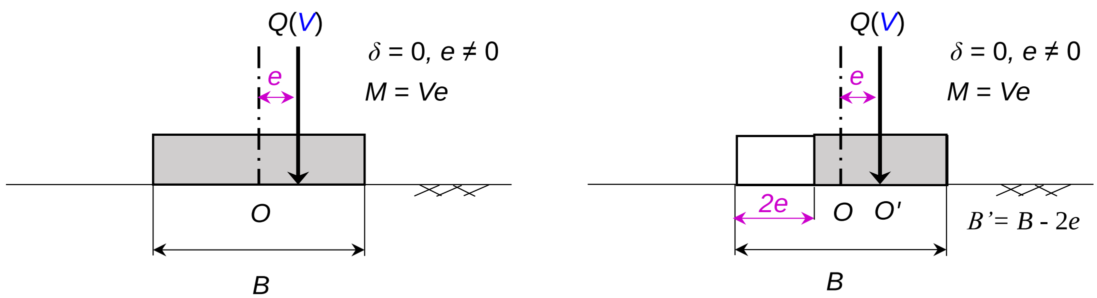

Fig. 4.11 Foundation subjected to eccentric vertical loading

4.6.1 Influence of steady state flow on the bearing capacity

Fig. 4.12 summarizes the effect of the eccentricity ratio (*e* / *B*) on the foundation bearing capacity and the corresponding normalized failure envelope for the steady state flow condition. Figs. 4.12a and 4.12c illustrate the variation of the vertical loading and the moment loading component with respect to the *e* / *B* for clay and silt, respectively. The variation of the vertical and the moment loading for the two soils are similar. The vertical loading is observed to decrease proportionally as the *e* / *B* increases. The moment loading is related to two components: namely, the eccentricity and eccentric vertical load. It is the total contribution of these two components that lead to the moment loading which increases initially with an increase in the *e* / *B* and then reduces with a further increase in the *e* / *B* values. The maximum value of the moment loading is obtained at *e* / *B* around 0.2 ~ 0.25. In addition, the maximum value of the moment is achieved at V / V_{max} around 0.48 to 0.5 from the normalized failure envelope shown in Figs. 4.12b and 4.12d.

4.6.1.1 Effect of the flow rates and ground water table depths

Fig. 4.12 highlights the influence of the flow rates and the ground water table depths on the bearing capacity and the failure envelope variation. The higher vertical and moment loading components can be observed for the evaporation conditions or at a deeper ground water table. These observations are consistent with that for foundation under the inclined loading. The normalized failure envelopes in Figs. 4.12b and 4.12d shrink under the infiltration condition. However, the variation value of each failure envelop under different flow rate or ground water table are not as significant as that without normalized bearing capacity. For eccentricity ratios of $e / B \leq 0.1$, the impact of the flow rates and the ground water table depth almost have no impact on the normalized failure envelope. At this stage, the vertical loading is the predominant loading that controls the soil failure. The matric suction mainly contributes to the vertical loading. The maximum vertical load is relatively large and the variation of the V / V_{max} and the corresponding moment load, ($M = V * e$) is not obvious. Though the normalized failure envelopes for both clay and the silt fall in a narrow band, the variation range of the normalized failure envelope for clay is wider compared to silt. Moreover, for both the soils at a large e / B (i.e., $e / B > 0.4$), the variation of both the loading and the normalized failure envelope for different flow rates and the ground water table can be neglected. At this stage, the vertical loading and the moment loading components are small; due to this reason, the contribution arising from the matric suction and its further variations can be ignored. This value ($e / B > 0.4$) is not safe for most of the foundations as it exceeds the recommended design standards as suggested in several geotechnical manuals (e.g., Eurocode 7 by CEN 2004; Canadian Foundation Engineering Manual (CFEM) of CGS 2006).

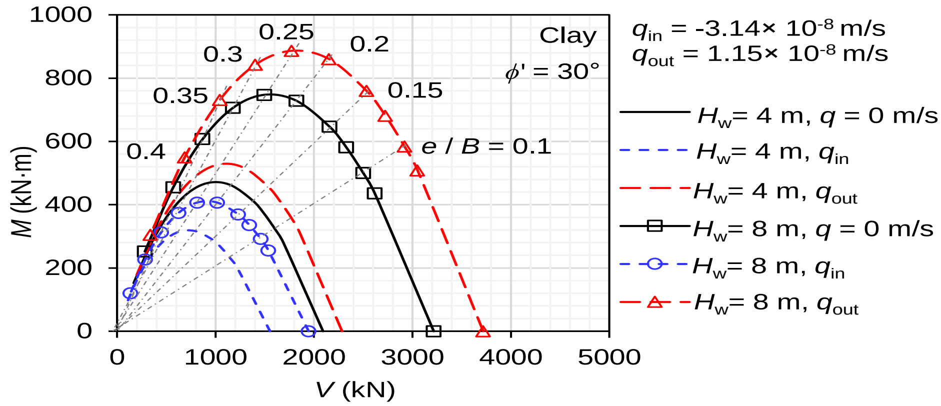
Clay
$\phi' = 30°$
q_{in} = -3.14× 10^{-8} m/s
q_{out} = 1.15× 10^{-8} m/s
0.25
0.2
0.3
0.35
0.15
0.4
e / B = 0.1
H_w= 4 m, q = 0 m/s
H_w= 4 m, q_{in}
H_w= 4 m, q_{out}
H_w= 8 m, q = 0 m/s
H_w= 8 m, q_{in}
H_w= 8 m, q_{out}
M (kN·m)
V (kN)

(a)

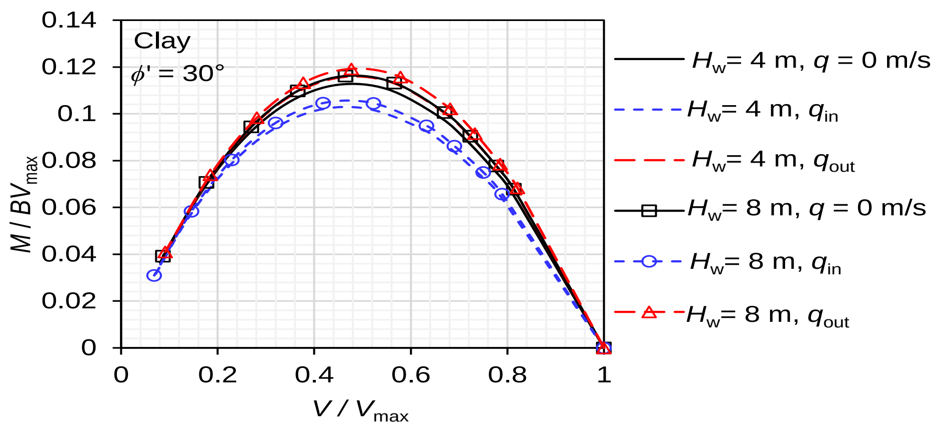
Clay
$\phi' = 30°$
H_w= 4 m, q = 0 m/s
H_w= 4 m, q_{in}
H_w= 4 m, q_{out}
H_w= 8 m, q = 0 m/s
H_w= 8 m, q_{in}
H_w= 8 m, q_{out}
M / BV_{max}
V / V_{max}

(b)

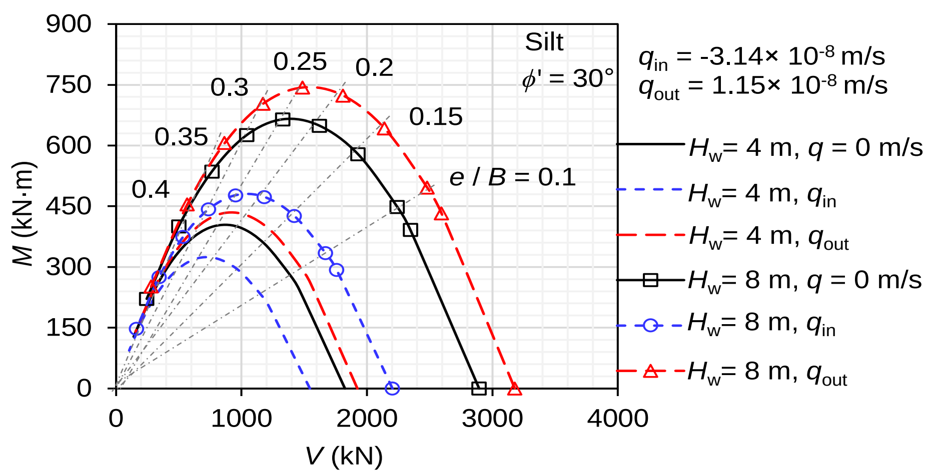
Silt
$\phi' = 30°$
q_{in} = -3.14× 10^{-8} m/s
q_{out} = 1.15× 10^{-8} m/s
0.25
0.2
0.3
0.35
0.15
0.4
e / B = 0.1
H_w= 4 m, q = 0 m/s
H_w= 4 m, q_{in}
H_w= 4 m, q_{out}
H_w= 8 m, q = 0 m/s
H_w= 8 m, q_{in}
H_w= 8 m, q_{out}
M (kN·m)
V (kN)

(c)

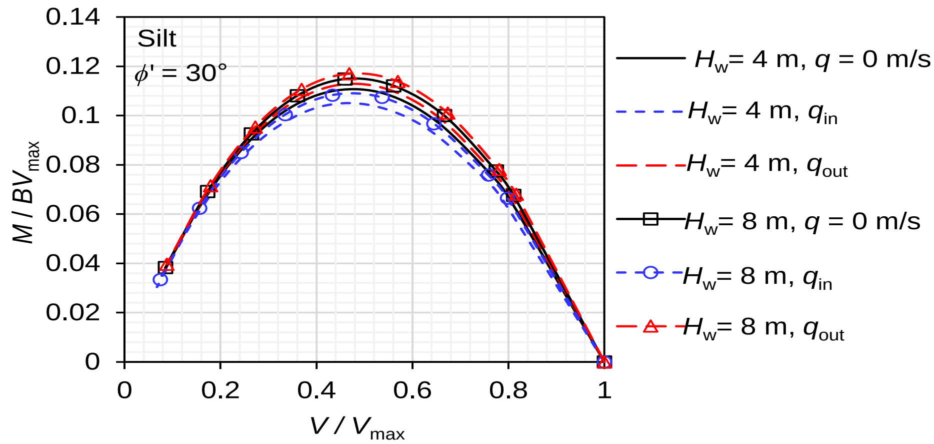

(d)

Fig. 4.12 Effect of the eccentric loading for steady state flow: (a) Effect of q and H_w on the V, M loading for clay; (b) Normalized failure envelope for clay; (c) Effect of q and H_w on the V, M loading for silt; (d) Normalized failure envelope for silt.

4.6.1.2 Effect of the soil internal friction angle

Results presented in Fig. 4.12 are generated for the clay and silt soil with the internal friction angle, $\phi' = 30°$. The influence of the ϕ' on the $V - M$ loading space is shown in Fig. 4.13. Significant increase is observed as shown in Figs. 4.13a and 4.13c for both the vertical loading and moment loading components with an increase in the internal friction angle for clay and silt. The maximum value of the moment loading for $\phi' = 30°$ is about six times in comparison for $\phi' = 10°$ for clay. This deviation is even higher for the silt, which is more than eight times. The normalized failure envelopes shown in Figs. 4.13b and 4.13d exhibits a reverse trend in shrinking the envelopes with an increasing ϕ'. These trends are consistent with that of foundation behavior subjected to inclined loading. The maximum vertical loading is greater for soil with a higher internal friction angle. The moment loading component is normalized with a greater V_{max} and therefore the M / BV_{max} is relatively small. However, the shape and size of the normalized failure envelope is almost the same between the clay and the silt.

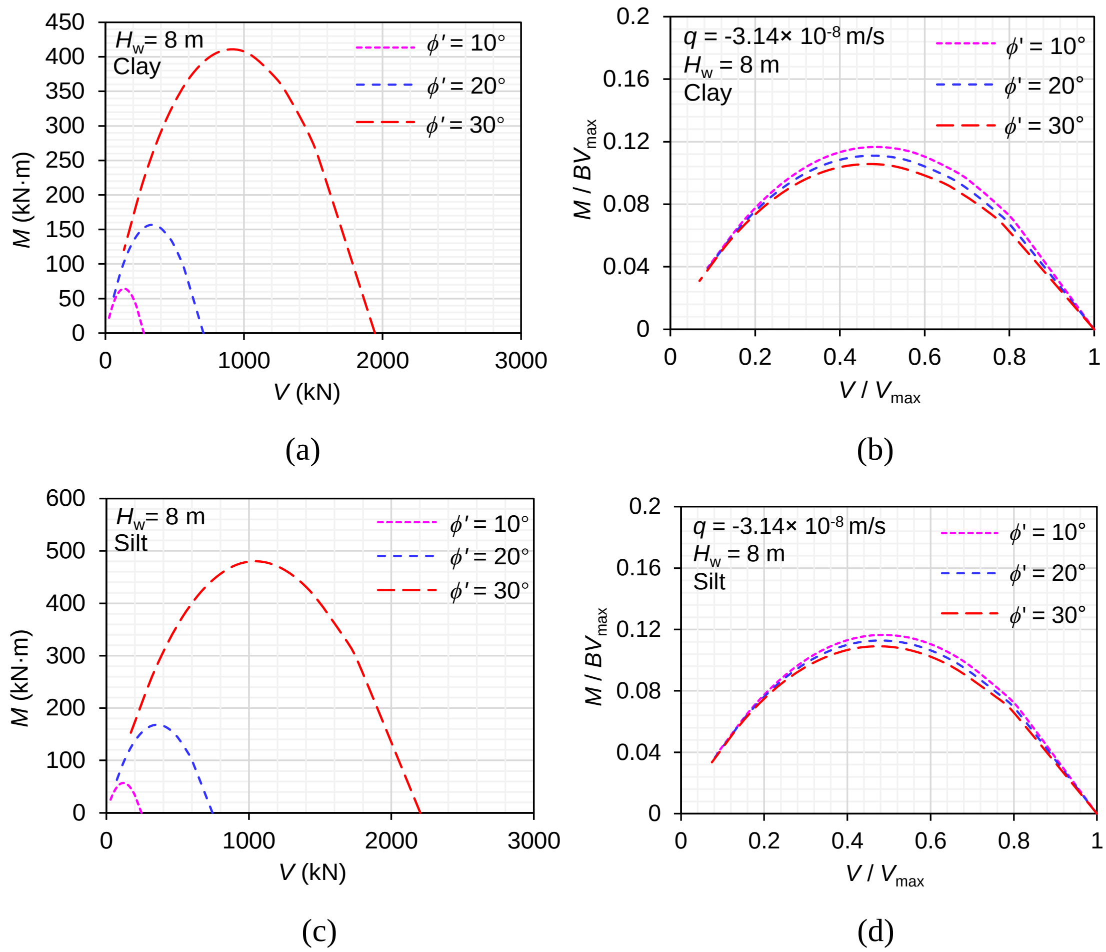

Fig. 4.13 Influence of the soil internal friction angle on the *V* – *M* loading space (q = -3.14×10^{-8} m/s): (a) *V*, *M* loading components in clay; (b) Normalized failure envelope for clay; (c) *V*, M loading components in silt; (d) Normalized failure envelope for silt.

4.6.2 Influence of transient flow on the bearing capacity

The influence of the infiltration duration combined with the foundation eccentricity ratio are investigated in this section. Fig. 4.14 summarizes the bearing capacity variation of foundation subjected to eccentric loading under unsaturated transient flow conditions. The vertical bearing capacity decreases with an increase in e / B which is consistent with the bearing capacity variation for the steady state flow condition. The main reason for this reduction is due to the decrease in the soil and foundation contact area at a large e / B. The maximum moment loading value occurs at an eccentricity ratio, e / B, between 0.2 and 0.25 as shown in the Figs. 4.14a and 4.14d for both the clay and the silt. The maximum value reduces with an increase in the infiltration duration. Shrinkage of the normalized failure envelope in Figs. 4.14b and 4.14e is also observed with an increase in the infiltration duration for e / B < 0.4. However, the variation of the normalized failure envelopes under different infiltration durations is not obvious for silt compared to clay.

The influence of the ground water table on the normalized failure envelope is summarized in Figs. 4.14b and 4.14c for clay and in Figs. 4.14e and 4.14f for silt. The normalized failure envelopes for foundation on clay subjected to infiltration duration of 5 days is close with that for steady state condition at H_w = 4 m in Fig. 4.14c. A longer infiltration duration is required for H_w = 8 m as shown in Fig. 4.14b. The influence of the infiltration duration on the normalized failure envelope for silt with different ground water table depths is consistent with that of clay.

The shrinkage of the normalized failure envelopes and the reduction in the bearing capacity are mainly due to the reduction of [S_e (u_a – u_w) tanϕ'] which was explained in an earlier section. Overall, the foundation subjected to the eccentric loading without inclination is influenced by several factors, which include the eccentricity ratio, the [S_e (u_a

– u_w) tanϕ'] variation caused by different flow rates, initial ground water table depth and the soil types.

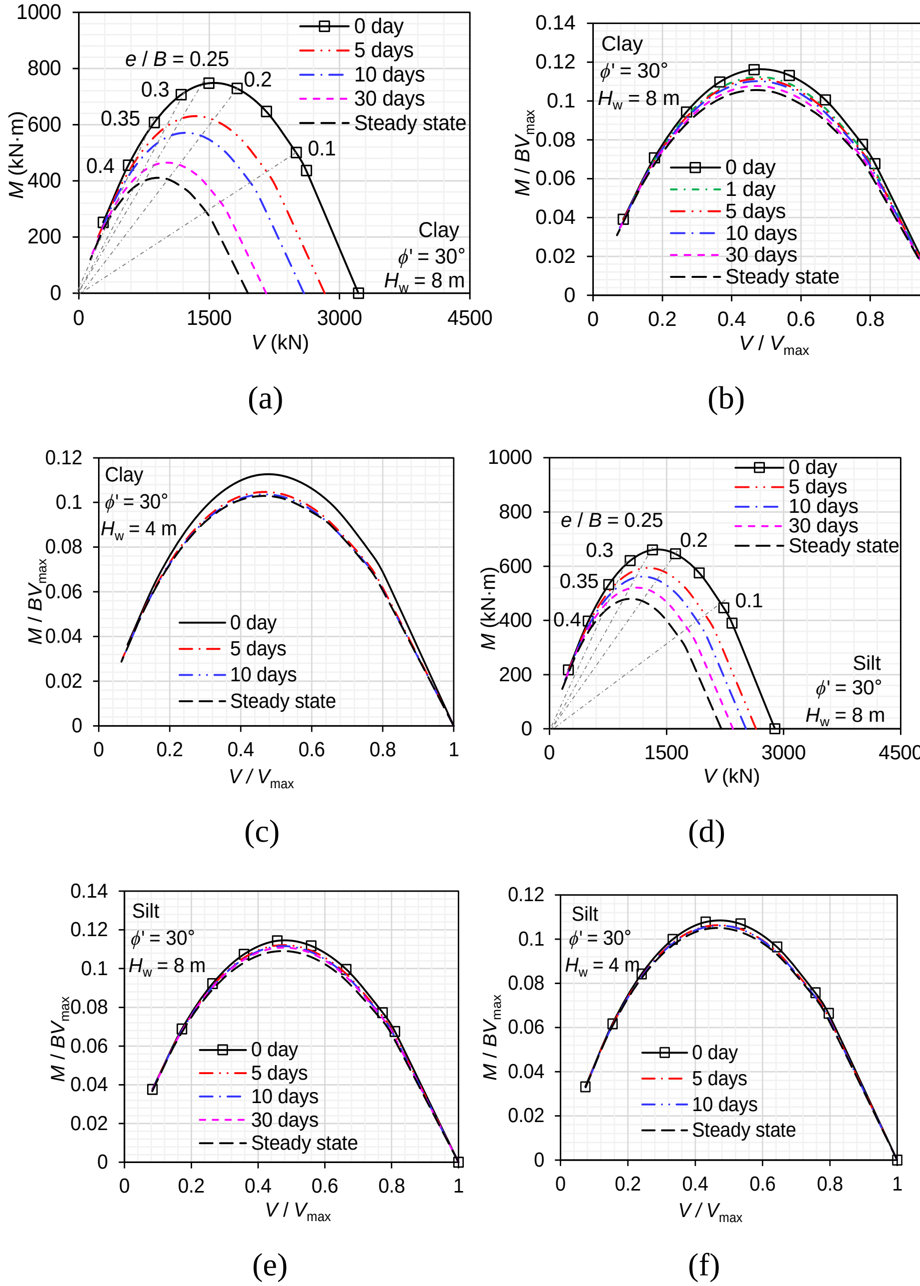

Fig. 4.14 Effect of the eccentric loading under transient flow (q_{in} = 3.14 × 10^{-8} m/s): (a) Effect of infiltration duration for clay; (b) H_w = 8 m for clay; (c) H_w = 4 m for clay; (d) Effect of infiltration duration for silt; (e) H_w = 8 m for silt; (f) H_w = 4 m for silt.

4.7 Proposed semi-empirical failure envelope equations

Based on the parametric studies results from the slip line method discussed in earlier sections, semi-empirical equations are proposed in this section to predict the shape and size of the normalized failure envelopes in the *V*- *H* and *V*- *M* loading spaces. The size of the failure envelopes is influenced by the soil properties, the matric suction distribution that results from the unsaturated flow and initial ground water table depths. The shape of the failure envelopes presented in the earlier sections are parabolic. Eqs. (4.27a) and (4.27b) are typically parabolic form equations that describe the shape and size of the failure envelope in the literature (Gottardi and Butterfield 1993, Loukidis et al. 2008, Zheng et al. 2019, Pham et al. 2019, Pham et al. 2020, 2022).

$$\left(\frac{H}{V_{\max}}\right)=\kappa\left(\frac{V}{V_{\max}}\right)\left[1-\left(\frac{V}{V_{\max}}\right)^{\lambda}\right] \tag{4.27a}$$

$$\left(\frac{M}{BV_{\max}}\right)=\kappa\left(\frac{V}{V_{\max}}\right)\left[1-\left(\frac{V}{V_{\max}}\right)^{\lambda}\right] \tag{4.27b}$$

κ typically represents the initial slope of the curve; λ typically represents the maximum point or the tangential slope of the other intercept with $V / V_{\max}$ axis. However, most of the published failure envelop equations are developed for saturated soils, which include cohesionless soils or clays under undrained conditions (i.e., $\phi = 0$). Among them, the failure envelops equations proposed by Pham et al. (2022) can be used for $c-\phi$ soils. To the best of the authors' knowledge, there are no failure envelops equations proposed for unsaturated soil in the two loading spaces ($V-H$ and $V-M$ loading spaces). Therefore, failure envelopes equations that take account the influence of the matric suction variation are developed in this study for the two loading spaces for $c-\phi$ soil in an unsaturated condition.

The equations are using the form of Eqs. (4.27a) and (4.27b). Relationship set up between the two fitting parameters and the influence parameters are shown in Table 4.6.

Table 4.6 Proposed semi-empirical equations

	Failure envelopes equations
***V* – *H* loading space**	$\left(\frac{H}{V_{\max}}\right)=\kappa\left(\frac{V}{V_{\max}}\right)\left[1-\left(\frac{V}{V_{\max}}\right)^{\lambda}\right]$ $\kappa=\frac{\left[0.53-0.199\left(\frac{c_{\mathrm{sat}}}{\gamma_{sat}B}\right)+2.22\left(\frac{c_{\mathrm{sat}}}{\gamma_{sat}B}\right)^{2}\right]^{0.27}\tan(\phi')+S_{\mathrm{e}}(u_{\mathrm{a}}-u_{\mathrm{w}})\tan(\phi')}{1+1.9\left[1+\tan(\phi')\right]^{-2.22}S_{\mathrm{e}}(u_{\mathrm{a}}-u_{\mathrm{w}})\tan(\phi')}$ $\lambda=1.78\left(\frac{c_{\mathrm{sat}}}{\gamma_{\mathrm{sat}}B}\right)^{0.2}\left(1+\tan(\phi')\right)^{\left[-3.96\left(\frac{c_{\mathrm{sat}}}{\gamma_{\mathrm{sat}}B}\right)^{0.14}\right]}\left[1+S_{\mathrm{e}}(u_{\mathrm{a}}-u_{\mathrm{w}})\right]^{0.04}$
***V* – *M* loading space**	$\left(\frac{M}{BV_{\max}}\right)=\kappa\left(\frac{V}{V_{\max}}\right)\left[1-\left(\frac{V}{V_{\max}}\right)^{\lambda}\right]$ $\kappa=0.55\tan(\phi')^{0.03}+\left(0.5-0.5\tan(\phi')^{0.00016}\right)\left[S_{\mathrm{e}}(u_{\mathrm{a}}-u_{\mathrm{w}})\right]$ $\lambda=1.11\left(\frac{c_{\mathrm{sat}}}{\gamma_{\mathrm{sat}}B}\right)^{0.14}\left(1+\tan(\phi')\right)^{\left[-0.4-2.3\left(\frac{c_{\mathrm{sat}}}{\gamma_{\mathrm{sat}}B}\right)+3\left(\frac{c_{\mathrm{sat}}}{\gamma_{\mathrm{sat}}B}\right)^{2}\right]}+0.003\tan(\phi')^{0.45}\left[S_{\mathrm{e}}(u_{\mathrm{a}}-u_{\mathrm{w}})\right]$

The values of the matric suction, (u_a – u_w) and the effective degree of saturation, S_e in the equations in Table 4.6 refer to those obtained at the ground surface. The results are likely to be underestimated when surface ponding occurs. The reasons for selecting the value at the ground surface but not the average value in the stress bulb zone beneath the foundation are: (i) for achieving conservative results; (ii) the average value may be influenced by the foundation width (Oh and Vanapalli 2013). If there is less data available directly for matric suction and the degree of saturation, the variation of the matric suction and the effective degree of saturation can also be obtained from Eqs. (4.14) and (4.15) for steady state condition and Eqs. (4.23) and (4.24) for transient state condition. The proposed equation has a smooth transition between the unsaturated soil and saturated soil. The equations are suitable for $c' - \phi'$ soil with $0 < c' \leq 20$ kPa and $0 < \phi' \leq 40°$. More studies are required to understand the influence of soil properties that do not fall in this range.

4.8 Comparison studies

Two comparison studies are conducted in this section to verify the reliability of the proposed equations: Comparison study 1: The envelopes obtained from the proposed equations are compared to that from the parametric studies presented in the earlier section. Comparison study 2: The envelopes obtained from the proposed equations are compared to that obtained from additional parameters that are not involved in parametric studies presented in the earlier section.

4.8.1 Comparison study I

Fig. 4.15 presents the results of the comparison study 1. Fig. 4.15a provides a summary of the comparison study for clay with both steady state (infiltration flow rate: -3.14×10^{-8} m/s) and transient state (infiltration flow rate: 3.14×10^{-8} m/s) in $V-H$ loading space. Fig. 4.15b shows the comparison of silt for the steady state evaporation with flow rate value of 1.15×10^{-8} m/s and the transient flow infiltration rate of 3.14×10^{-8} m/s. Fig. 4.15c and 4.15d are for the comparison in the $V-M$ loading space for clay and silt, respectively. All the results show the coefficient of determination value R^2 between the results obtained from the equation and the slip line method is above 85%.

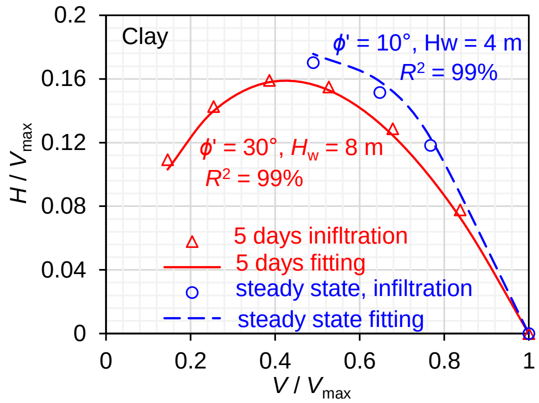

(a)

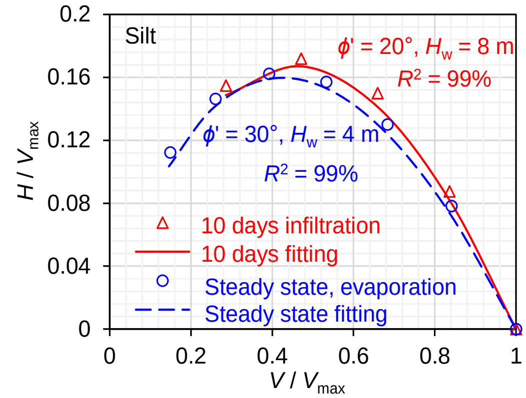

(b)

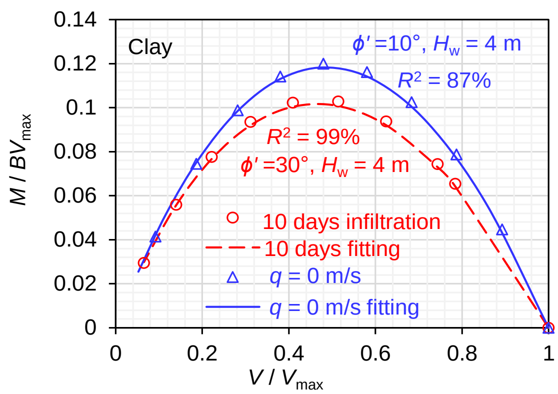

(c)

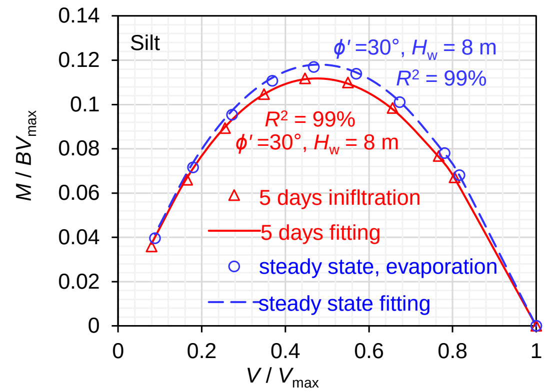

(d)

Fig. 4.15 Comparison of the proposed equation with the results obtained from the slip line method: (a) For clay in *V* – *H* loading space; (b) For silt in *V* – *H* loading space; (c) For clay in *V* – *M* loading space; (d) For silt in *V* – *M* loading space.

4.8.2 Comparison study II

Eight different cases are used to provide further comparisons for the failure envelope derived by the proposed semi-empirical equations and the slip line method for different parameters: the internal friction angle, the ground water table depths, the soil types and properties, the steady state and transient state flow rate. Table 4.7 summarizes the parameters used for the eight representative cases. In addition to the eight cases, the failure envelope predicted by the proposed equations is also compared with that obtained from the failure envelope equations proposed by Pham et al. (2022) for saturated $c' - \phi'$ soil.

Good consistency with R^2 value around 99% can be observed in Fig. 4.16 for all the eight cases between the predicted failure envelopes and that obtained using the slip line method. Similar trends with respect to consistency in results are also observed in Figs. 4.16e and 4.16f between the envelopes equations proposed in this study and that proposed by Pham et al. (2022) for saturated c- ϕ soil.

Both the comparison studies summarized in this section suggest the equations proposed in this study can provide reasonable results for the failure envelope prediction in each loading space taking account different parameters.

Table 4.7 Summary of the parameters used in various cases

	H_w (m)	c' (kPa)	ϕ' (°)	γ_{sat} (kN/m^3)	Fitting parameters, α (kPa^{-1})	Saturated hydraulic conductivity, k_s (m/s)	Saturated volumetric water content, θ_s	Residual volumetric water content, θ_r	Unsaturated flow
Case 1 Clay	2	10	30°	20	0.005	5.0×10^{-8}	0.58	0.1	$q = 0$ m/s
Case 2 Clay	3	10	20°	20	0.005	5.0×10^{-8}	0.58	0.1	Transient flow $q_{in} = 3.14 \times 10^{-8}$ m/s
Case 3 Silt	2	5	25°	20	0.01	1.0×10^{-7}	0.38	0.06	Steady state flow $q_{out} = 1.15 \times 10^{-8}$ m/s
Case 4 Silt	6	5	20°	20	0.01	1.0×10^{-7}	0.38	0.06	Transient flow $q_{in} = 3.14 \times 10^{-8}$ m/s
Case 5 Saturated soil	0	15	30°	20	–	–	–	–	–
Case 6 Saturated soil	0	20	10°	20	–	–	–	–	–
Case 7 Soil (Shahrokhabadi et al. 2019)	3[a]	1.7	30°	20	0.5	1.0×10^{-7}	0.45	0.1	Transient flow $q_{in} = 1.0 \times 10^{-7}$ m/s
Case 8 Soil (Aubertin et al. 2009)	4[a]	10[a]	25°[a]	18[a]	0.1	1.0×10^{-8}	0.38	0.06	Transient flow $q_{in} = 0.5 \times 10^{-8}$ m/s

[a]Assumed value based on typical soil properties.

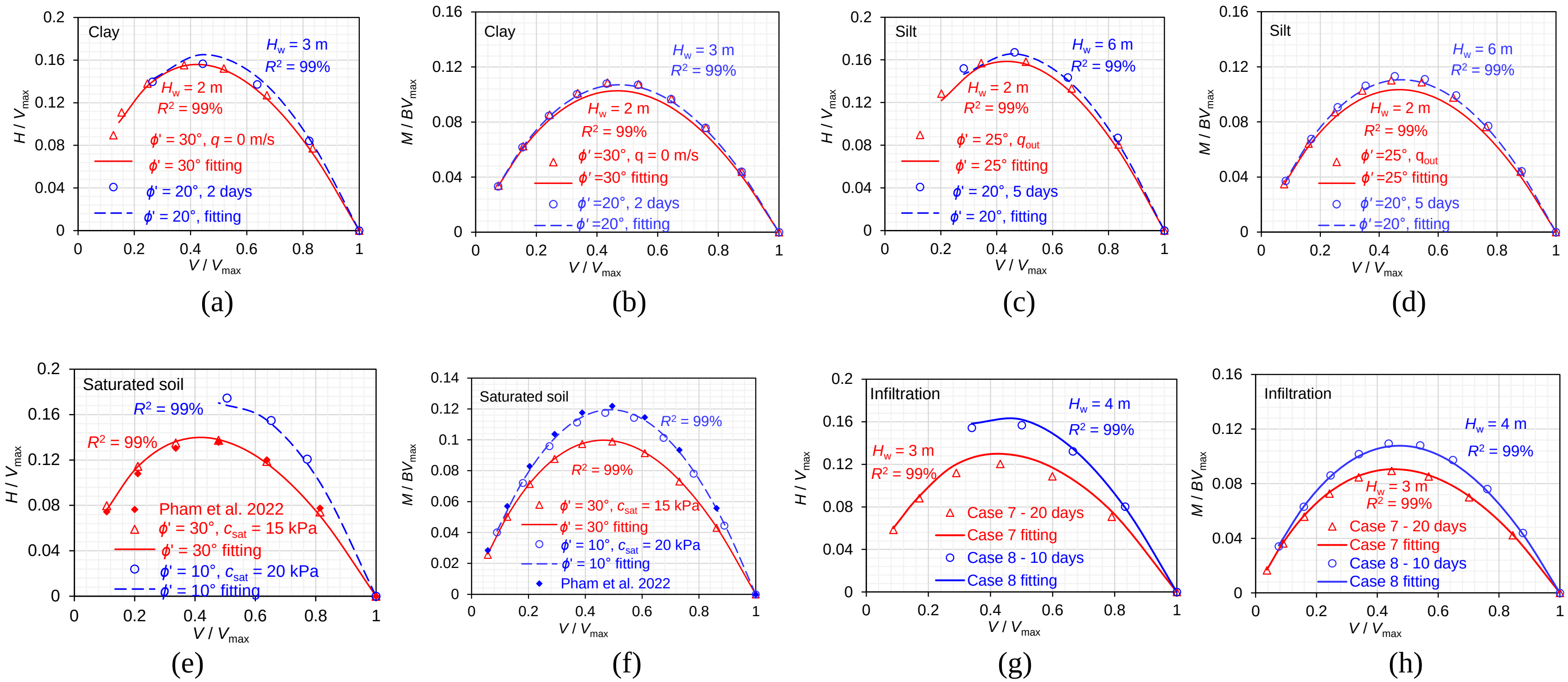

Fig. 4.16 Comparison with additional data: (a) Case 1 and 2 in $V-H$ loading space; (b) Case 1 and 2 in $V-M$ loading space; (c) Case 3 and 4 in $V-H$ loading space; (d) Case 3 and 4 in $V-M$ loading space; (e) Case 5 and 6 in $V-H$ loading space; (f) Case 5 and 6 in $V-M$ loading space; (g) Case 7 and 8 in $V-H$ loading space; (h) Case 7 and 8 in $V-M$ loading space;

4.9 Discussion

The parametric studies summarized in earlier section were conducted to highlight the influence of different flow rates, ground water table depths, internal friction angles on the bearing capacity failure envelop variation. The control variable method is used for the parametric studies which means the parameters mentioned above were set as variables; however, other parameters such as the SWCC were controlled as a constant. Similar methodology was followed in other studies (e.g., Vahedifard and Robinson 2016) for investigation of the foundation vertical bearing capacity under different unsaturated flow conditions. However, it should be noted that the SWCC typically exhibits hysteresis behavior. The hysteresis of the SWCC refers to the non-unique relationship of the soil water content and the matric suction. At the same matric suction, the wetting SWCC exhibits a lower volumetric water contents / degree of saturation compared to that of the drying SWCC. The nonuniform pore size distribution (Fredlund et al. 2012) and the presence of the entrapped air (Fredlund & Rahardjo 1993, Kristo et al. 2019) in the soil are two of the key reasons that contribute to the hysteresis. They will also influence the stress state of the soil which also impacts the soil permeability. The soil permeability function is typically estimated based on the saturated soil permeability and the SWCC. Therefore, the soil permeability also exhibits hysteresis (Fredlund 2006). Due to this reason, the soil under drying path has a relatively higher soil permeability compared to that under wetting path at the same matric suction. Several studies conclude that the hysteresis effect influences the hydro-mechanical behavior of soil which in turn has an impact on the slope stability and foundation bearing capacity (Chen et al. 2017, Tang et al. 2017, Kristo et al. 2019).

In this section, the influence of the hysteresis behavior on the normalized bearing capacity failure envelop is discussed. Comparisons are made between the bearing capacity failure envelopes obtained using the drying and wetting SWCC curve under the same infiltration condition. The soil with significant hysteresis behaviour, provided in Jeong et al. (2018) is used for analysing the results. The drying and wetting SWCC of the studied soil are shown in Fig. 4.17. The other soil properties used for the analysis are summarized in Table 4.8. The foundation width is set as 2 m. The analysis is conducted with the ground water table of 4 m and infiltration influx of 1×10^{-7} m/s.

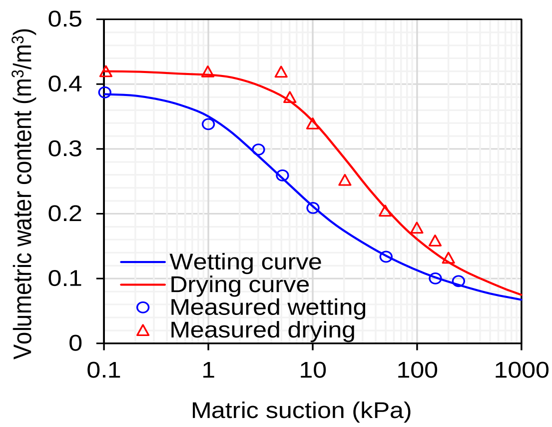

Fig 4.17 Hysteretic soil water characteristic curves (modified from Jeong et al. 2018)

Table 4.8 Soil properties used for comparison

Properties	**Value**
Specific gravity, G_s	2.71
Effective cohesion, c' (kPa)	5
Effective internal friction angle, ϕ' (°)	30
Saturated hydraulic conductivity, k_s (m/s)	4.76×10^{-7}
Saturated volumetric water content, θ_s	Drying: 0.418 Wetting: 0.387
Residual volumetric water content, θ_r	Drying: 0.032 Wetting: 0.032
Fitting parameters for Eqs. (4.12) and (4.13), α (kPa^{-1})	Drying: 0.13 Wetting: 0.51

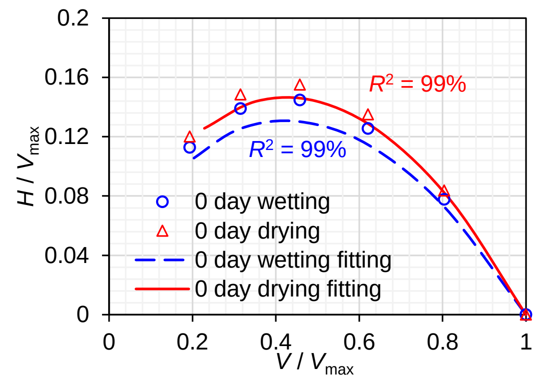

(a)

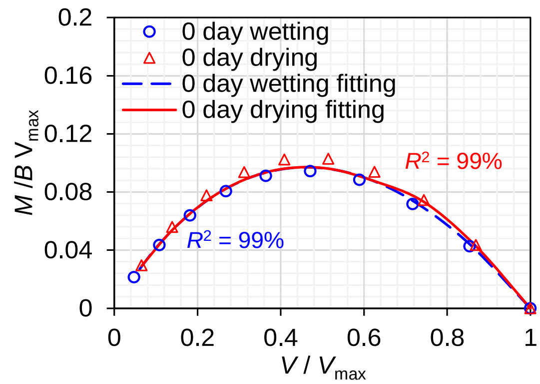

(b)

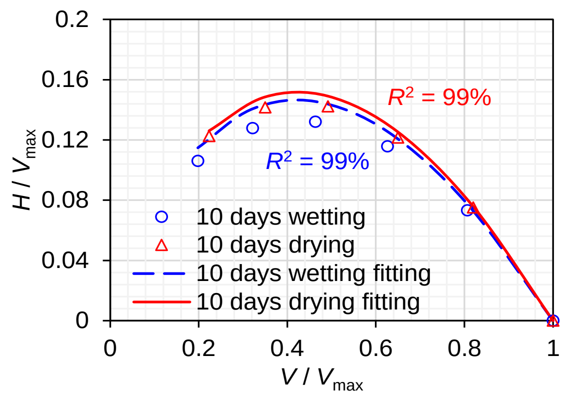

(c)

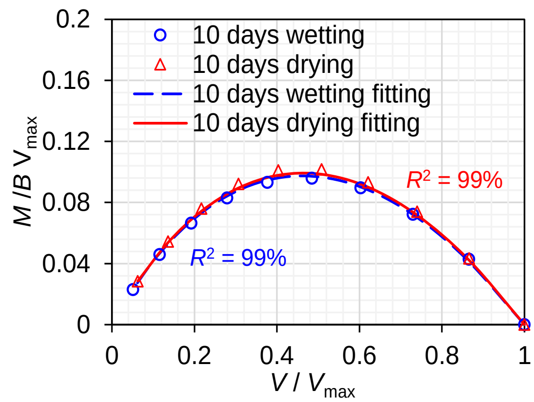

(d)

Fig 4.18 Failure envelops obtained from the drying and wetting curves (infiltration under 1×10^{-7} m/s): (a) 0 day for *V* – *H* loading space; (b) 0 day for *V* – *M* loading space; (c) 10 days for *V* – *H* loading space; (d) 10 days for *V* – *M* loading space

The results obtained from the slip line method and the proposed semi-empirical equations using the drying and wetting SWCC are presented in Fig. 4.18. The bearing capacity failure envelops in *V* – *H* loading space and *V* – *M* loading space under 0 days of rainfall is shown in Figs. 4.18a and 4.18b. The R^2 between the results obtained from slip line method using the drying and wetting SWCC is 99.9% and 98.2%, respectively in *V* –

H loading space and $V - M$ loading space. The small difference between results using drying and wetting curve is also found in Figs. 4.18c and 4.18d for rainfall of 10 days duration with R^2 of 99.4% and 99.1% for $V - H$ loading space and $V - M$ loading space, respectively. For all the cases in Fig. 4.18, the failure envelops obtained using the slip line method with drying SWCC are slightly overestimated compared to that obtained from wetting SWCC. However, the relative deviation is lower than 15%. The normalized failure envelops estimated by the proposed semi-empirical equations using the wetting and drying curves are consistent with the results obtained from the slip line method with R^2 of 99% for all the cases in Fig. 4.18.

The above results suggest that the hysteresis effect is not predominant for the normalized failure envelop. Such a behavior may be associated with the bearing capacity information that is normalized in the failure envelop. Both the maximum bearing capacity and the bearing capacity obtained at different inclination and eccentricity will be influenced by the hysteresis effect and other influence parameters (e.g., the flow rates, the ground water table depths and the internal friction angle investigated in this Chapter). The variation caused by these parameters is reduced by normalizing the bearing capacity (e.g., V / V_{max}). However, the hysteresis effect is not only an important but also a complex influence factor. More studies are required for further understanding the effects of the hysteresis on the foundation bearing capacity and other individual bearing capacity components considering combined loading conditions.

4.10 Conclusions

The slip line method coupled with the analytical solution of the matric suction profiles for unsaturated flow conditions is proposed in this Chapter to determine the bearing capacity of foundations subjected to inclined or eccentric loading. The influence of the ground water table depths, the flow rates, the infiltration duration, and soil types on the bearing capacity failure envelopes are investigated by the proposed method. In addition, semi-empirical equations are respectively proposed in the $V-H$ loading space and $V-M$ loading space for predicting the failure envelopes based on the parametric study results. Comparisons are provided between failure envelopes obtained from the proposed analytical method, the proposed semi-empirical equations, and the published studies. The main conclusions are summarized below:

(1) The proposed slip line method can provide reliable results for foundation subjected to the inclined or eccentric loading under both steady state, transient state flow conditions.

(2) The inclination angle has a negative effect on the foundation total ultimate bearing capacity and the vertical loading components. The horizontal loading components will increase with the increased inclination angle followed by a reduction. The maximum horizontal loading occurs at the inclination angle between 15° and 20° for fine-grained soils such as the clay and silt.

(3) A negative effect can be associated with the eccentricity on the vertical loading components. The moment loading increases with the eccentricity ratio and reduces after reaching a peak value. The maximum moment loading occurs at the eccentricity ratio between 0.2 and 0.25 for both clay and silt for different loading scenarios.

(4) The failure envelopes in both $V-H$ loading space and $V-M$ loading space expand under the evaporation condition and shrink under the infiltration condition. The longer infiltration duration results in the failure envelope shrinkage. In addition, the ground water table depths will influence the initial suction distribution and in turn influence

failure envelope size and variation rates. It is the [S_e ($u_a - u_w$) tanϕ'] that controls the failure envelope variation for different unsaturated flow conditions.

(5) The proposed semi-empirical equation in each loading space can provide reasonable prediction results taking account the influence of matric suction. Good agreement is found between the results from the semi-empirical equations and that from the slip line methods and published studies. The equation has smooth transition from unsaturated to saturated soil conditions and can be implemented with a calculation tool to build up the failure envelopes efficiently.

The proposed analytical method and the semi-empirical equations respectively, in this Chapter can be used in geotechnical engineering practice for the determination of the foundation bearing capacity taking account of the influence of flow conditions in unsaturated soils. The method and results in this study are useful to explain the field-measured data accurately during the foundation service life and provide a good reference in forensics studies related to foundation failures.

References

Akbari Garakani, A., Sadeghi, H., Saheb, S., and Lamei, A. 2020. Bearing capacity of shallow foundations on unsaturated soils: analytical approach with 3D numerical simulations and experimental validations. Int. J. Geomech., 20 (3), 04019181. https://doi.org/10.1061/(ASCE)GM.1943-5622.0001589.

Anand, A., and Sarkar, R. 2022. A comprehensive probabilistic investigation on bearing behavior of unsaturated fly ash deposits. Arab. J. Geosci., 15(4), 1-19. https://doi.org/10.1007/s12517-022-09535-z

Aubertin, M., Cifuentes, E., Apithy, S.A., Bussière, B., Molson, J., and Chapuis, R.P. 2009. Analyses of water diversion along inclined covers with capillary barrier effects. Can. Geotech. J., 46(10), 1146-1164. https://doi.org/10.1139/T09-050.

CGS 2006. Canadian Foundation Engineering Manual, 4th edition. Canadian Geotechnical Society.

CEN. 2004. Eurocode 7: Geotechnical design – Part 1: General rules. Standard EN 1997-1. European Committee for Standardization (CEN), Brussels, Belgium.

Chen, P., Mirus, B., Lu, N., and Godt, J. W. 2017. Effect of hydraulic hysteresis on stability of infinite slopes under steady infiltration. J Geotech. Geoenvior., 143(9), 04017041.

Cheng, X., Tan, M., and Vanapalli, S. 2021. Simple approaches for the design of shallow and deep foundations for unsaturated soils II: numerical Techniques. Indian Geotech. J., 51(1), 115-126. https://doi.org/10.1007/s40098-021-00500-3.

Du, Y., Sheng, Q., Fu, X., Chen, H., and Li, G. 2022. New Model for Predicting the Bearing Capacity of Large Strip Foundations on Soil under Combined Loading. Int. J. Geomech., 22(5), 04022055. https://doi.org/10.1061/(ASCE)GM.1943-5622.0002389.

Fathipour, H., Payan, M., Chenari, R.J., and Fatahi, B. 2022a. General failure envelope of eccentrically and obliquely loaded strip footings resting on an inherently anisotropic granular medium. Comput. Geotech., 146, 104734. https://doi.org/10.1016/j.compgeo.2022.104734.

Fathipour, H., Payan, M., Safardoost Siahmazgi, A., Jamshidi Chenari, R., and Senetakis, K. 2022b. Numerical study on the bearing capacity of strip footing resting on partially saturated soil subjected to combined vertical-horizontal-moment loading. Eur. J. Environ. Civ. Eng., 1-34. https ://doi.org/10.1080/19648189.2022.2080769.

Fredlund, D.G., 2006. Unsaturated soil mechanics in engineering practice. J. Geotech. Geoenviron. Eng., 132(3), 286-321. https://doi.org/10.1061/(ASCE)1090-0241(2006)132:3(286).

Fredlund, D.G., Rahardjo, H. 1993. Soil mechanics for unsaturated soils. John Wiley & Sons.

Fredlund, D.G Rahardjo, H., Fredlund, M.D. 2012. Unsaturated soil mechanics in engineering practice. John Wiley & Sons.

Fredlund, D.G., and Xing, A. 1994. Equations for the soil-water characteristic curve. Can. Geotech. J. 31, No. 4, 521–532. https://doi.org/10.1139/t94-061.

Ganesh, R., Khuntia, S., and Sahoo, J.P. 2017. Bearing capacity of shallow strip foundations in sand under eccentric and oblique loads. Int. J. Geomech., 17(4): 06016028. https://doi.org/10.1061/(ASCE)GM.1943-5622.0000799.

Gardner, W.R. 1958. Some steady state solutions of the unsaturated moisture flow equation with application to evaporation from a water table. Soil Sci. 85, 4, 228–232. https://doi.org/10.1097/00010694-195804000-00006.

Ghasemzadeh, H., Akbari, F. 2019. Determining the bearing capacity factor due to nonlinear matric suction distribution in the soil. Can. J. Soil Sci., 99, 4, 434-446. https://doi.org/10.1139/cjss-2019-0071.

Gottardi, G. and Butterfield, R. 1993. On the bearing capacity of surface footings on sand under general planar load. Soils Found. 33, No. 3, 68 – 79. https://doi.org/10.3208/sandf1972.33.3_68.

Gourvenec, S., and Barnett, S. 2011. Undrained failure envelope for skirted foundations under general loading. Géotechnique, 61(3), 263-270. https://doi.org/10.1680/geot.9.T.027.

Gourvenec, S., and Randolph, M. 2003. Effect of strength non-homogeneity on the shape of failure envelopes for combined loading of strip and circular foundations on clay. Géotechnique, 53(6), 575-586. https://doi.org/10.1680/geot.2003.53.6.575.

Hansen, J.B. 1970. A revised and extended formula for bearing capacity. DGI Bull., No. 28, Danish Geotechnical Institute, Copenhagen, Denmark, 5–11.

Hjiaj, M., Lyamin, A.V., and Sloan, S.W. 2004. Bearing capacity of a cohesive-frictional soil under non-eccentric inclined loading. Comput. Geotech., 31(6), 491-516. https://doi.org/10.1016/j.compgeo.2004.06.001.

Hou C.Q., Shi G.Z., Sun Z.B., and Xi, Y. 2020. Calculation of bearing capacity of unsaturated soil strip foundation based on slip line theory. J. Yangtze River Scientific Res. Inst., 37, 6. https://doi.org/10.11988/ckyyb.20190112.

Jeong, S., Kim, Y., Park, H., and Kim, J. 2018. Effects of rainfall infiltration and hysteresis on the settlement of shallow foundations in unsaturated soil. Environ. Earth. Sci., 77(13), 1-12. https://doi.org/10.1007/s12665-018-7690-1

Jin, L., Zhang, H., Luo, C., and Feng, Q. 2021. The implementation of improved radial movement optimization to calculate the ultimate bearing capacity of strip footing on unsaturated soil under inclined loading. Arab. J. Geosci., 14(17), 1-13. https://doi.org/10.1007/s12517-021-08090-3.

Khalili, N., Khabbaz, M.H. 1998. A unique relationship for χ for the determination of the shear strength of unsaturated soils. Géotechnique, 48, 5, 681-687. https://doi.org/10.1680/geot.1998.48.5.681.

Ko, J., Seo, H., and Lee, J.K. 2022. Failure Envelopes for Circular Foundations on two-layered clay under combined loading. Int. J. Geomech., 22(7), 04022085. https://doi.org/10.1061/(ASCE)GM.1943-5622.0002395.

Krabbenhoft, S., Damkilde, L., and Krabbenhoft, K. 2012. Lower-bound calculations of the bearing capacity of eccentrically loaded footings in cohesionless soil. Can. Geotech. J., 49(3), 298-310. https://doi.org/10.1139/t11-103.

Krabbenhoft, S., Damkilde, L., and Krabbenhoft, K. 2014. Bearing capacity of strip footings in cohesionless soil subject to eccentric and inclined loads. Int. J. Geomech. https://doi.org/10.1061/(ASCE)GM.1943-5622.0000332.

Kristo, C., Rahardjo, H., and Satyanaga, A. 2019. Effect of hysteresis on the stability of residual soil slope. Int. Soil Water Conserv. Res., *7*(3), 226-238.

Li, C., and Jiang, P. 2022. Oblique and eccentric bearing capacity of embedded strip footings using the method of rigorous characteristics. Int. J. Numer. Anal. Methods Geomech.https://doi.org/10.1002/nag.3363.

Li, D.Y., Guo, Y.X., and Gao, Y.F. 2013. Principle and application of pole point method of Mohr's circle. Chin J Geotech Eng, 35, 1883-1888.

Loukidis, D., Chakraborty, T., and Salgado, R. 2008. Bearing capacity of strip footings on purely frictional soil under eccentric and inclined loads. Can. Geotech. J., 45(6), 768-787. https://doi.org/10.1139/T08-015.

Lu, N., Likos, W.J. 2004. Unsaturated soil mechanics, Wiley, New York.

Lu, N., Likos, W.J. 2006. Suction stress characteristic curve for unsaturated soil. J. Geotech. Geoenviron. Eng., 132, 2, 131-142. https://doi.org/10.1061/(ASCE)1090-0241(2006)132:2(131).

Mahmoudabadi, V., Ravichandran, N. 2019. Design of shallow foundation considering site-specific rainfall and water table data: theoretical framework and application. Int. J. Geomech., 19, 7, 04019063. https://doi.org/10.1061/(ASCE)GM.1943-5622.0001432.

Meyerhof, G.G. 1951. The ultimate bearing capacity of foundations. Géotechnique, 2(4), 301–332. https://doi.org/10.1680/geot.1951.2.4.301.

Meyerhof, G.G. 1953. The bearing capacity of foundations under eccentric and inclined loads. Proc., 3rd Int. Conf. on Soil Mechanics and Foundation Engineering (ICSMFE), Vol. I, International Society of Soil Mechanics and Geotechnical Engineering, London, 440–445.

Meyerhof, G.G. 1963. Some recent research on the bearing capacity of foundations. Can. Geotech. J., 1(1), 16–26. https://doi.org/10.1139/t63-003.

Michalowski, R.L. 2001. The rule of equivalent states in limit-state analysis of soils. J. Geotech. Geoenviron. Eng., 127(1), 76-83. https://doi.org/10.1061/(ASCE)1090-0241(2001)127:1(76).

Michalowski, R.L., and You, L. 1998. Effective width rule in calculations of bearing capacity of shallow footings. Comput. Geotech., 23(4), 237-253. https://doi.org/10.1016/S0266-352X(98)00024-X.

Oh, W.T., Vanapalli, S.K. 2013. Interpretation of the bearing capacity of unsaturated fine-grained soil using the modified effective and the modified total stress approaches. Int. J. Geomech., 13, 6, 769-778. https://doi.org/10.1061/(ASCE)GM.1943-5622.0000263.

Patra, C., Behara, R., Sivakugan, N., and Das, B. 2012a. Ultimate bearing capacity of shallow strip foundation under eccentrically inclined load, Part I. Int. J. Geotech. Eng., 6(3), 343-352. https://doi.org/10.3328/IJGE.2012.06.03.343-352.

Patra, C., Behara, R., Sivakugan, N., and Das, B. 2012b. Ultimate bearing capacity of shallow strip foundation under eccentrically inclined load, Part II. Int. J. Geotech. Eng.,6(4), 507-514. https://doi.org/10.3328/IJGE.2012.06.04.507-514.

Pham, Q. N., Ohtsuka, S., Isobe, K., Fukumoto, Y., and Hoshina, T. 2019. Ultimate bearing capacity of rigid footing under eccentric vertical load. Soils Found., 59(6), 1980-1991. https://doi.org/10.1016/j.sandf.2019.09.004.

Pham, Q.N., Ohtsuka, S., Isobe, K., and Fukumoto, Y. 2020. Limit load space of rigid footing under eccentrically inclined load. Soils and Found., 60(4), 811-824. https://doi.org/10.1016/j.sandf.2020.05.004.

Pham, Q.N., Ohtsuka, S., Isobe, K., and Fukumoto, Y. 2022. Limit load space of rigid strip footing on cohesive-frictional soil subjected to eccentrically inclined loads. Comput. Geotech., 151, 104956. https://doi.org/10.1016/j.compgeo.2022.104956.

Ravichandran, N., Vickneswaran, T., Marathe, S., Jella, V.S. 2021. Numerical Analysis of Settlement Response of Shallow Footing Subjected to Heavy Rainfall and Flood Events. Int. J. Geosci., 12, 2, 138-158. https ://doi.org/10.4236/ijg.2021.122009.

Shahrokhabadi, S., Vahedifard, F., Ghazanfari, E., Foroutan, M., 2019. Earth pressure profiles in unsaturated soils under transient flow. Eng. Geol., 260, 105218. https://doi.org/10.1016/j.enggeo.2019.105218.

Shwan, B. 2015. Experimental and numerical study of the shear strength of unsaturated sand. Doctoral dissertation, University of Sheffield.

Srivastava, R., Yeh, T.C.J., 1991. Analytical solutions for one-dimension, transient infiltration toward the water table in homogeneous and layered soils. Water Resour. Res., 27, 5, 753–762. https://doi.org/10.1029/90WR02772.

Sun, D.A., Wang, L., and Li, L. 2019. Stability of unsaturated soil slopes with cracks under steady-infiltration conditions. Int. J. Geomech., 19(6), 04019044. https://doi.org/10.1061/(ASCE)GM.1943-5622.0001398.

Taiebat, H.A., and J.P. Carter. 2000. Numerical studies of the bearing capacity of shallow foundations on cohesive soil subjected to combined loading. Géotechnique 50 (4) : 409–418. https://doi.org/10.1680/geot.2000.50.4.409.

Taiebat, H.A., and J.P. Carter. 2002. Bearing capacity of strip and circular foundations on undrained clay subjected to eccentric loads. Géotechnique 52 (1): 61–64. https://doi.org/10.1680/geot.2002.52.1.61.

Tan, M., and Vanapalli, S.K. 2022. Foundation bearing capacity estimation on unsaturated soil slope under transient flow condition using slip line method. Comput. Geotech., 148, 104804. https://doi.org/10.1016/j.compgeo.2022.104804.

Tan, M., Cheng, X., Vanapalli, S.K. 2021. Simple Approaches for the Design of Shallow and Deep Foundations for Unsaturated Soils I: Theoretical and Experimental Studies. Indian Geotech. J., 51, 1, 97-114. https://doi.org/10.1007/s40098-021-00501-2.

Tang, Y., Chen, C., Qian, B., Ren, J., and Guan, Y. 2022. Plate Load Tests on an Unsaturated Sand–Kaolin Mixture with Varying Water Table. Sensors, 22(6), 2161. https://doi.org/10.3390%2Fs22062161.

Tang, Y., Taiebat, H.A. and Russell, A.R. 2017. Bearing capacity of shallow foundations in unsaturated soil considering hydraulic hysteresis and three drainage conditions. Int. J. Geomech., 17,6, 04016142. https://doi.org/10.1061/(ASCE)GM.1943-5622.0000845.

Terzaghi, K. 1943. Theoretical soil mechanics. New York: Wiley. http ://dx.doi.org/10.1002/9780470172766.

Vahedifard F., Leshchinsky B.A., Mortezai K., Lu N. 2015. Active earth pressures for unsaturated retaining structures. J. Geotech. Geoenviron. Eng. 141(11): 04015048. https://doi.org/10.1061/(ASCE)GT.1943-5606.0001356.

Vahedifard, F. and Robinson, J.D. 2016. Unified method for estimating the ultimate bearing capacity of shallow foundations in variably saturated soils under steady flow. J. Geotech. Geoenviron. Eng., 142, 4, 04015095. https://doi.org/10.1061/(ASCE)GT.1943-5606.0001445.

Vanapalli, S.K., Fredlund, D.G., Pufahl, D.E., Clifton, A.W. 1996. Model for the prediction of shear strength with respect to soil suction. Can. Geotech. J. 33, 3, 379-392. https://doi.org/10.1139/t96-060.

Vesic A. 1975. Bearing capacity of shallow foundations. In: Winterkorn HF, Fang HY, editors. Foundation engineering handbook. New York: Van Nostrand Reinhold. P. 121–47.

Vo, T., Russell, A.R. 2016. Bearing capacity of strip footings on unsaturated soils by the slip line theory. Comput. Geotech., 74, 122-131. https://doi.org/10.1016/j.compgeo.2015.12.016.

Wuttke, F., Kafle, B., Lins, Y., and Schanz, T. 2013. Macroelement for statically loaded shallow strip foundation resting on unsaturated soil. Int. J. Geomech., 13(5), 557-564. https://doi.org/10.1061/(ASCE)GM.1943-5622.0000254.

Yuan, S., Du, J. 2020. A lower-bound formulation for unsaturated soils. Géotechnique, 70(2), 123-137. https://doi.org/10.1680/jgeot.18.P.103.

Zhan, T.L., Jia, G.W., Chen, Y.M., Fredlund, D.G., Li, H. 2013. An analytical solution for rainfall infiltration into an unsaturated infinite slope and its application to slope stability analysis. Int. J. Numer. Anal. Methods Geomech., 37, 12, 1737-1760. https://doi.org/10.1002/nag.2106.

Zhan, T.L., Ng, C.W., 2004. Analytical analysis of rainfall infiltration mechanism in unsaturated soils. Int. J. Geomech., 4, 4, 273-284. https://doi.org/10.1061/(ASCE)1532-3641(2004)4:4(273).

Zheng, G., Zhao, J., Zhou, H., and Zhang, T. 2019. Ultimate bearing capacity of strip footings on sand overlying clay under inclined loading. Comput. Geotech., 106, 266-273. https://doi.org/10.1016/j.compgeo.2018.11.003

CHAPTER 5

Shallow foundation behavior on an expansive soil slope subjected to different infiltration conditions[4]

5.1 Introduction

Infrastructure construction activities that include the highways, railways, pipelines, and residential structures on hilly regions increased significantly to meet various needs of the human population growth all over the world, especially in the urban regions during the last half century. Studies by Wang et al. (2020) suggest the multiple island effects of the urbanization significantly increase both the temperature and the precipitation. For example, temperature increase accelerates the water evaporation that enhances water condensation in the atmosphere contributing to intense rainfalls (Fig. 5.1a). These hydrological events have a significant influence on the matric suction fluctuations and impact the soil hydro-mechanical behavior (i.e., hydraulic conductivity, shear strength / stiffness variation and volume change) (e.g., Rahardjo et al. 2007, Qi and Vanapalli 2015a, Khan et al. 2021).

The influence of hydrological events is more pronounced in unsaturated expansive soils that are also referred to as 'problematic soils' because the hydro-mechanical properties are sensitive to water content changes. The estimated annual costs of infrastructures damages in expansive soils are significant for around 0.15 billion in UK (Mousavi et al. 2014), 1 billion in China (Jalal et al. 2020) and 9 billion in US which includes around 5.7 billion

[4] The contents presented in this chapter are summarized as a manuscript that has been submitted to an international journal for review:

Tan, M., & Vanapalli, S. K. 2023. Shallow foundation behavior on an expansive soil slope subjected to different infiltration conditions. (*Revised version is under review*) due to problems associated with highways and houses (Amakye et al. 2021). Geohazards such as slope failures and extensive damages to highways, railways and foundations in expansive soils can be mainly attributed to swell and shrink characteristics associated with water evaporation and precipitation cycles (Day and Axten 1989, Wates and Fourie 1993, Li et al. 2011). In the past, the hydro-mechanical behavior has been typically modeled using unimodal soil-water characteristic curve (SWCC) behavior. However, in recent years there is more evidence to highlight the bimodal nature of SWCC behavior due to the influence of cracks that contributes a complex soil structure with micro and macropores (Zhang and Chen 2005, Azam et al. 2013). For this reason, the hydraulic conductivity and shear strength function are rigorously considered as bimodal in nature (Li et al. 2014). The cracks can be considered as water flow channels that increase the seepage, degree of saturation, volume change and decrease the matric suction and its contribution towards soil shear strength (Huang and Wu 2007, Zhang et al. 2020). Moreover, the crack network can widen and propagate deeper during the drying and wetting cycles. Due to this reason, SWCC changes and there will be a significant change in the hydraulic conductivity and the shear strength of the unsaturated soil. However, it is challenging to model the cracks propagation and model the SWCC and soil properties that vary due to climatic factors. Therefore, in this study, the bimodal SWCC is used in the analysis as a simplified approach to consider the influence of cracks.

In recent years, many studies focused on highlighting the performance of expansive soil slopes (Ng et al. 2003, Jiang et al. 2013, Qi and Vanapalli 2015a, 2015b, Ijaz et al. 2022) and foundation or infrastructures on expansive soils (Xu and Fu 2000, Xu 2004, Buzzi et al. 2010, Yenes et al. 2012, EI-Samea et al. 2022, Sarker and Wang 2022). These studies address the significant influence of matric suction on the slope stability and foundation behavior, respectively. The soil shear strength contribution arising from matric suction reduces due to the rainfall infiltration. The shear strength decrease leads to a drop in the slope factor of safety (FS) and the foundation bearing capacity. Besides, the matric suction variation also leads to the volume change behavior of the soil; due to this reason, differential settlement of the foundation may likely occur with water content variations (Buzzi 2010). Also, the changing geometry of the slope during the rainfall may also contribute to a lower slope factor of safety (Qi and Vanapalli 2015a). Moreover, studies by Day and Axten (1989) and Pradel and Raad (1993) suggest that the shear strength contribution arising from cohesion is typically low at normal stress values are low (i.e., at the slope surface). Therefore, a high potential of surficial failure is likely when there is rainfall infiltration into compacted clay slopes. For this reason, the various parameters that influence failure conditions in the surficial stability of the slope due to the relationship between the rainfall intensity and duration, the soil hydraulic conductivity, and the slope geometry need rigorous investigations.

Several studies in the literature provide a better understanding on the influence of the unsaturated flow on the foundation behavior in conventional soils that do not exhibit swelling characteristics (e.g., Le et al. 2013, Vahedifard and Robinson, 2016, Kim et al. 2017, Ravichandran et al. 2021, Tan and Vanapalli 2022, 2023, Fathipour et al. 2022). However, focus of most of these studies were directed to investigate the foundation behavior on a level unsaturated soil ground. Research studies for foundations on unsaturated sloping ground considering the simultaneous influence of unsaturated transient flow are limited in the literature (Anand and Sarkar 2021, Tan and Vanapalli 2022).

Moreover, the coupled influence of deformation of the slope as well as the slope factor of safety (FS) along with the foundation behavior under different rainfall conditions are not considered in these studies. The slope will no longer be able to provide support for the foundation if it is already unstable due to the rainfall infiltration. The foundation loading may accelerate the slope failure for such a scenario. However, studies that consider the influence of transient flow conditions on the combined performance of the slope and foundation are rather limited.

For the above reasons, the study summarized in this Chapter focuses on the performance of the shallow foundation-slope combined system in an unsaturated expansive soil from Regina, Canada that is subjected to rainfall infiltration (see Fig. 5.1b). The Regina clay is selected as a representative soil in this study due to the following reasons: (i) The clay is highly plastic and is typically fissured at the surface (Sauer, 1975); (ii) There are several published studies in the literature that discussed failure of embankments, highways and foundations on the Regina clay (e.g., Widger and Fredlund, 1978, Qi and Vanapalli 2015b, Liu and Vanapalli 2022) associated with water infiltration. Numerical studies were undertaken to simulate the performance of both the foundation and slope behavior considering several complex scenarios for Regina clay. The numerical model set up for the slope considered in this study is consistent with the earlier published studies (Tan and Vanapalli 2021). For rigorous analysis, bimodal SWCC has been included in the numerical model for considering the influence of soil cracks as a simplification. The influence of the rainfall intensity, duration, foundation set back distance and foundation loading on both the foundation bearing capacity and slope FS are investigated. The results summarized in this novel study are of significant interest to practicing engineers as they provide a better understanding of the foundation-slope system in unsaturated expansive soils considering different rainfall infiltration scenarios.

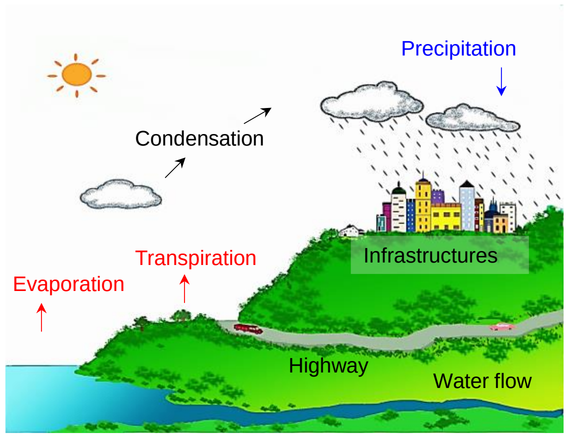

(a)

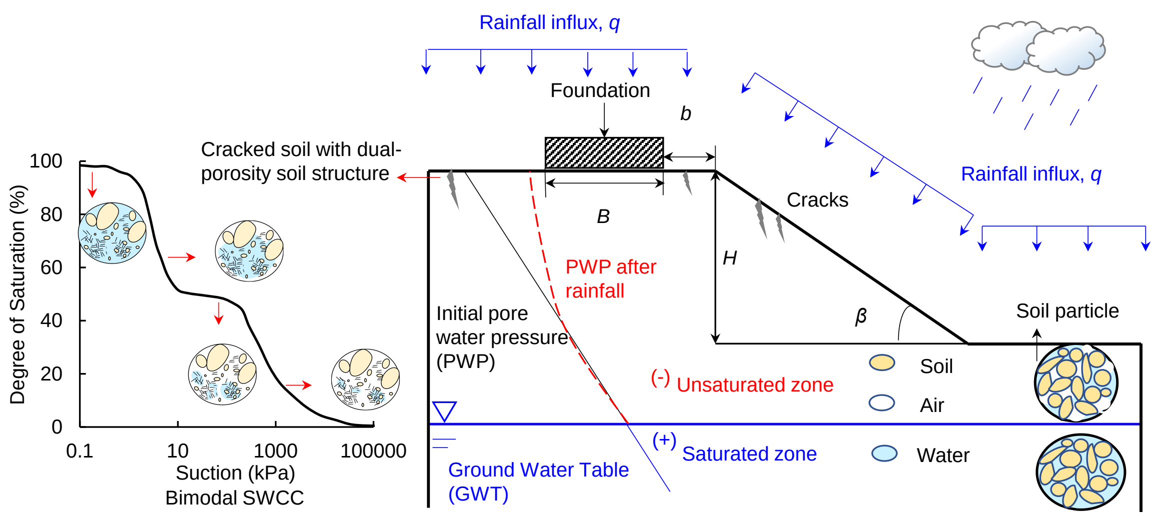

(b)

Fig. 5.1 Problem definition: (a) Water cycle; (b) Foundation on cracked soil slope

5.2 Methodology

5.2.1 Governing equations

The governing equations that describe the hydro-mechanical behavior of the unsaturated soils in the finite element analysis (FEA) are summarized as Eqs. (5.1a) and (5.1b). Eq. (5.1a) is the partial differential equation for the static equilibrium corresponding to the unsaturated soil element. Eq. (5.1b) describes the two-dimensional water flow in an unsaturated soil element assuming the water is incompressible and deformation in the soil are incrementally infinitesimal (Richards, 1931, Qi and Vanapalli, 2015a). The air phase in the unsaturated soil is typically continuous and is equivalent to the atmospheric pressure conditions; hence the negative pore-water pressure in the soil with respect to the atmospheric pressure is the matric suction.

$$\frac{\partial \sigma_{ij}}{\partial x_i} + b_j = 0 \tag{5.1a}$$

$$\frac{\partial q_i}{\partial x_i} + \frac{\partial \theta_w}{\partial t} = 0 \tag{5.1b}$$

where σ_{ij} defined as the components of total stress tensor; b_j represents components of the body force vector. θ_w is the volumetric water content and t is time; q_i are the flow velocities in *i*- directions. The flow velocity is given by Darcy's law, which relates the flow velocities with the hydraulic heads as shown in Eq. (5.2).

$$q_i = -k \frac{\partial}{\partial x_i}\left(\frac{u_w}{\gamma_w} + y\right) \tag{5.2}$$

where k is the hydraulic conductivity; u_w is the pore water pressure; γ_w is the unit weight of water; y is the vertical coordinate (elevation).

5.2.2 Constitutive relationships

The rigorous mechanical behavior of the unsaturated soil needs to be described not only by the stress-strain relationship but also using the relationship between water content and the stress state variables (Qi and Vanapalli 2015a). The net normal stress, (σ_n - u_a) and matric suction, (u_a - u_w) are the key two independent stress variables that can be used for rationally describing the unsaturated soil constitutive relationships as shown in Eqs. (5.3) and (5.4) that are consistent with the continuum mechanics principles after simplification:

$$d\varepsilon_{ij} = \frac{1+\mu}{E} d\sigma_{ij} - \frac{\mu}{E} d\sigma_{mean}\delta_{ij} - \frac{1}{H} du_{\mathrm{w}}\delta_{ij} \tag{5.3}$$

$$d\theta_{\mathrm{w}} = \frac{3}{H} d\sigma_{mean} - \frac{1}{H_w} du_{\mathrm{w}} \tag{5.4}$$

where ε_{ij} refers to the components of the strain tensor; E defines as the elastic modulus for soil; σ_{mean} is equal to the average value of the stress in each direction, (σ_x + σ_y + σ_z) / 3; δ_{ij} is the Kronecker delta, H refers to the unsaturated soil modulus for soil structure with respect to (u_a - u_w), H = E / (1-2μ). H_w represents a modulus relating the variation in volumetric water content with the variation in matric suction; μ is the Poisson's ratio and is set as constant as many numerical studies in this paper. However, it should be noted that the Poisson's ratio as well as the soil unit weight also varies with the matric suction (Sun et al. 2019, Kumar Thota et al. 2021). Results by Tan and Vanapalli (2022) and Sun et al. (2019) suggest that the deviation obtained from the variation of the soil unit weight compared to the constant soil unit weight or the saturated soil unit weight is approximately 20%.

Eq. (5.5) which describes the relationship between the variation of the volumetric water content and the corresponding soil volume variation can be obtained by substituting Eq. (5.3) into Eq. (5.4).

$$d\theta_{\mathrm{w}} = \frac{E}{H(1-2\mu)} d\varepsilon_v - \left(\frac{1}{H_{\mathrm{w}}} - \frac{3\beta}{H}\right) du_{\mathrm{w}} \tag{5.5}$$

The hydro-mechanical behavior of the unsaturated soil can be described by the unknown pore water pressure and the displacement obtained by substituting Eqs. (5.3) and (5.5) into Eqs. (5.1a) and (5.1b). The unknown pore water pressure and the displacement can be simultaneously solved with the aid of SIGMA/W, a module which is suitable for modelling the stress and deformation of the soil in Geo-studio (Geo-Slope Int. Ltd 2018) in this study.

5.2.3 Shear strength and modulus of elasticity

Soil shear strength and modulus of elasticity are two key parameters in assessing the performance of foundations and slope stability. There are many models available to predict the matric suction contribution towards the soil shear strength (e.g., Vanapalli et al. 1996, Lu and Likos 2006, Satyanaga and Rahardjo, 2019). The semi-empirical model (Eq. (5.6)) proposed by Vanapalli et al. (1996) that is built into the Geo-studio is used to predict the unsaturated soil shear strength with respect to matric suction using the SWCC, which is the relationship between the water content (i.e., gravimetric or volumetric) or degree of saturation and soil suction.

$$\tau = c' + \left(\sigma_n - u_a\right)\tan\phi' + \left(u_a - u_w\right)\left(\frac{\theta_w - \theta_r}{\theta_s - \theta_r}\right)\tan\phi' \tag{5.6}$$

where τ is the unsaturated soil shear strength, c', ϕ' are effective cohesion and effective internal friction angle, respectively; θ_s and θ_r are the saturated and residual volumetric water contents, respectively.

The modulus of elasticity of the unsaturated soil is estimated based on Eq. (5.7) proposed by Oh et al. (2009). The information of SWCC and two fitting parameters α, β are required in the prediction. α = 0.1 and β = 2 are used in this study as good estimation results were found earlier from the studies by Adem and Vanapalli (2013) and Qi and Vanapalli (2015a) for Regina expansive clay.

$$E_{\mathrm{unsat}} = E_{\mathrm{sat}}\left[1+\alpha\frac{(u_{\mathrm{a}}-u_{\mathrm{w}})}{(P_{\mathrm{a}}/101.3)}\left(S^{\beta}\right)\right] \tag{5.7}$$

where E_{unsat} and E_{sat} are the modulus of elasticity of unsaturated and saturated soil, respectively. P_{a} is the atmosphere pressure. This equation does not consider the effect of confining stress; however, it has been validated with extensive experimental investigations (Vanapalli and Oh 2010).

The Geo-studio used in the present study is not having feature for generating the variation of the modulus of elasticity with respect to the matric suction. Therefore, approximation technique (Qi and Vanapalli 2015a) has been used in the model combined with the Eq. (5.7) for the estimation of modulus elasticity. For the approximation technique, the active surface that is typically with surface cracks of the slope is divided into several layers. The modulus of elasticity of each layer is calculated and updated based on Eq. (5.7) using the matric suction distribution obtained from previous time interval. For the sloping ground, the average modulus of elasticity and average matric suction are used for each layer for the estimation and updating.

5.2.4 Slope stability

The FS of the slope has been evaluated using limit equilibrium method with the aid of SLOPE/W in the Geo-studio. The SLOPE/W is a module that can be used for the slope stability analysis. The Morgenstern-Price method with half sine side function is used in this study because it takes account of interslice shear and normal forces and provides a relative lower FS (GEO-SLOPE International Ltd. 2012a). FS of the slope can be described as the ratio of the soil shear strength (τ_f) to the shear stress (τ_s) on the slip surface that is shown as Eq. (5.8).

$$\mathrm{FS} = \frac{\tau_{\mathrm{f}}}{\tau_{\mathrm{s}}} \tag{5.8}$$

The position of the critical circular slip surface with the critical factor of safety (CFS, lowest factor of safety) can be obtained by the procedure coded in the software. The circular slip surface is assumed in this study based on the investigations by Widger and Fredlund (1978) which suggest that the slope instability failure surface in Regina area is typically circular. However, it should be mentioned that the soil is typically non-homogeneous, and the rainfall infiltration conditions are complex. Due to these reasons, the slide surface may not be circular in some scenarios. Therefore, a comparison study is conducted to evaluate the differences between the circular and non-circular slip surface and their corresponding CFS values for the problem investigated in this study. The non-circular failure mechanism is obtained by the slip surface optimization process. The optimization implemented in SLOPE/W is based on the theoretical framework proposed by Greco (1996) and Malkawi et al. (2001) in which the Monte Carlo method with the random walking procedure is used. In SLOPE/W, this approach is extended, and the slip surface is divided into several straight-line segments (GEO-SLOPE International Ltd. 2012b). The controlling parameters for the optimization are used by the default value provided in SLOPE/W. For example, a default value of 16 is used in the optimization procedure for the number of ending points, which controls the line segments numbers. This value is also higher than that mentioned in Malkawi et al. (2001) which is reliable for obtaining the actual shape of the critical slip surface. The optimization process initiates from the point on the slip surface and extends to the ground surface. The point will be moved to probe the lower safety factor along the ground surface. The optimization procedure is then applied for the next point on the slip surface for searching the lower safety factor. The vertices of each segment will move within an elliptical search area defined in SLOPE/W to probe the lower safety factor followed by moving the exit/last point along the ground surface at the end. Monte Carlo method with the random walking procedure is used for the point probe within the elliptical search area (GEO-SLOPE International Ltd. 2012b). The longest segment will then be subdivided, and the trial is repeated until the process reaches the specified limits such as the tolerance variation for the safety factor or the maximum trials numbers. In this study the default values suggested for the tolerance variation of the factor of safety is 1×10^{-7} and the maximum trial number is 2000. The circular and non-circular slide surfaces obtained in SLOPE/W for the slope with the foundation loading and without the foundation loading subjected to different rainfall intensities are compared. Results from this comparison study suggest that circular slide assumption will slightly overestimate the CFS compared to that of the non-circular failure mechanism obtained by the optimization slip surface process. For the deep-seated failure mechanism for all the cases, the maximum relative deviation between the CFS obtained from the circular and non-circular slip surface is about 8.8%.

It should also be noted that there are limitations using the Morgenstern-Price method in this study. The localized shear stress concentrations and the stress-strain behavior of the soil are not well captured in the Morgenstern-Price method. To overcome the limitation, the finite element stress-based method is also conducted for providing comparisons with the Morgenstern-Price method and presented in the discussion section. The finite element stress-based method uses the stress distribution results obtained from the finite element method (i.e., using SIGMA/W) to calculate the mobilized shear force and the resisting shear force of each slip surface slice and integrating them along the entire slip surface in SLOPE/W to calculate the FS. Therefore, the slice factor of safety is not constant using the finite element stress-based method compared to that which is constant using the Morgenstern-Price method (GEO-SLOPE International Ltd. 2012a).

5.3 Model details and validation

5.3.1 Model details

There are four key steps for assessing the bearing capacity and the slope stability for the problem shown in Fig. 5.1b. Fig. 5.2 shows a step-by-step procedure used in the present study in the form a flow chart. The in-situ analysis is performed as a first step in SIGMA/W to determine the initial PWP distribution and the initial stress distribution. The initial pore water pressure is equal 0 kPa at natural GWT level and increases linearly with respect to depth. The hydro-mechanical coupling analysis is undertaken with the rainfall infiltration in the second step. The variation of the PWP is obtained directly from this step. In the third step, the foundation bearing capacity analysis is conducted based on the updated PWP. In the final step, slope stability is evaluated with different foundation loading scenarios in SLOPE/W: (i) slope without foundation loading; (ii) slope with foundation ultimate bearing capacity loading; (iii) slope with foundation allowable bearing capacity loading. The key objective of applying the three different loading conditions is to investigate the impact of the surcharge load magnitude on the slope stability. Different yielding conditions and failure mechanisms corresponding to the slope CFS are derived from the last two steps.

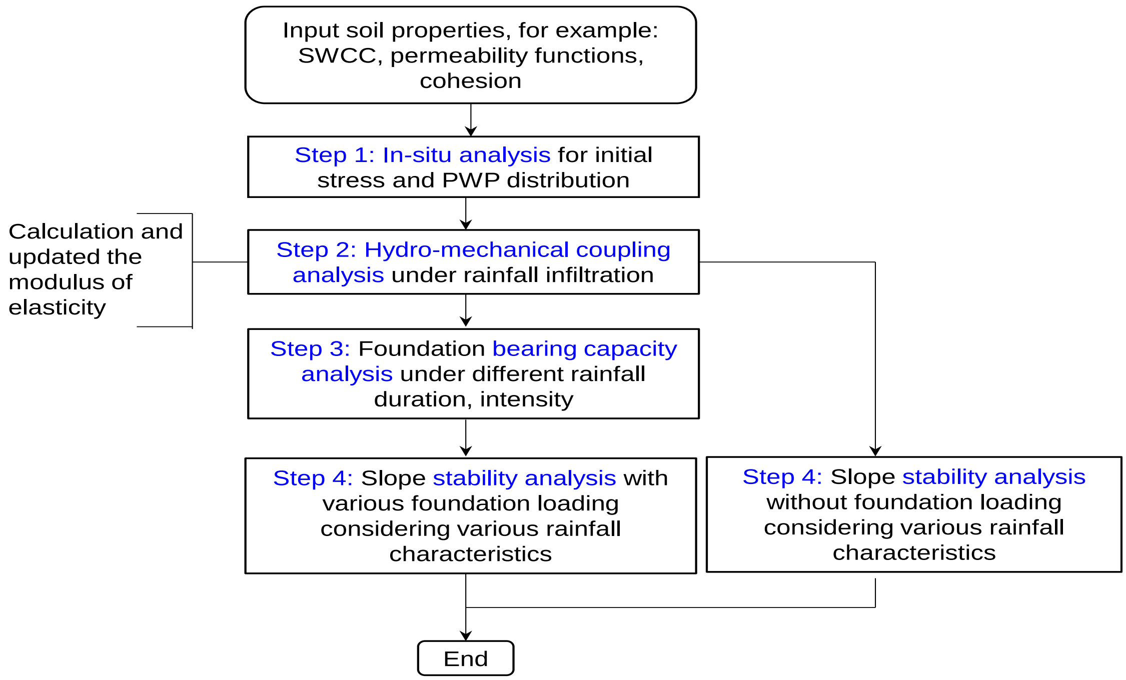

Fig. 5.2 Flow chart with details of steps of modelling

Fig. 5.3 presents the model details with the foundation setback ratio of two meters as an example. The foundation width is set as one meter following typical foundation dimensions in the published studies (Kim et al. 2017, Du et al. 2021). The height of the slope is 10 m with a slope angle of 30˚. This slope geometry is reasonable that lies in the range (i.e., 14° to 35°) reported by Widger and Fredlund (1978) for the embankment slope angle in the Regina area. The boundary of the model is also far enough to alleviate the boundary effect. The active zone of Regina clay may extend about 2.8 m depth based on the investigations by Yoshida et al. (1983). Therefore, the soil active zone depth is set as three meters in the model. Soil within the active zone depth is assumed cracked due to the environmental factors associated with evaporation and infiltration changes. The sub-soil is assumed not affected by the environmental factors. Several different yielding criterions such as the Mohr-Coulomb yield criterion, Cam-Clay model and modified Cam-Clay model that can be utilized for analysis. In this paper, the widely used Mohr-Coulomb (MC) yield criterion has been extended in the finite element analysis as the yield function assuming elastic, perfectly - plastic model for the surface soil in the active zone. Linear elastic model has been used for the sub-soil.

The soil properties of both the surface soil and sub-soil that are used in the model are gathered from Qi and Vanapalli (2015a) and Azam and Ito (2011) and are summarized in Table 5.1. The grain size distribution is shown in Fig. 5.4a. The soil is classified as CH (clay with high plasticity, Azam and Ito (2011)). The SWCC and the soil hydraulic conductivity are shown in Figs. 5.4b and 5.4c. The cracks in the surface expansive soil typically contribute to a dual porosity structure and hence exhibits a bimodal SWCC (Li et al. 2011, Qi and Vanapalli 2015a). The SWCC data used in the model is derived from experimental study performed by Azam and Ito (2011). The data was fitted with a spline function built in the software. The first air entry value is 10 kPa followed by the second air entry value of 300 kPa, which is also referred to as the air entry value of the sub-soil. The sub-soil SWCC is obtained based on the bimodal SWCC with superposition technique proposed by Li et al. (2011). The hydraulic conductivity function used in the model are obtained based on the data from Qi and Vanapalli (2015a) and Shuai (1998). The saturated hydraulic conductivity of the surface layer is 5.66×10^{-3} m/day.

The initial ground water table (GWT) is 16 m from the top surface of the slope. This depth is within the GWT range provided by Qi and Vanapalli (2015b) and is reasonable for the semi-arid to arid type climate classification of Regina area, which has the ground water table located a greater depth (Fredlund and Rahardjo 1993); in addition, the region is windy with a typically dry environment. The initial maximum surficial suction value is also less than the values reported in Qi and Vanapalli (2015b) (i.e., 200 to 300 kPa) and are in the range suggested by Widger and Fredlund (1978) (i.e., 135 to 380 kPa) for Regina clay.

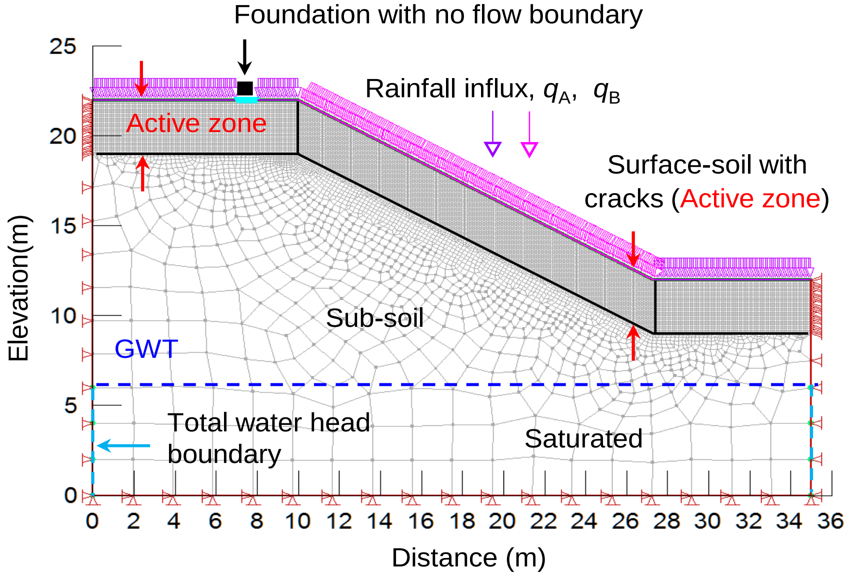

Fig. 5.3 Model details

Table 5.1 Soil properties

Soil Properties	Surface soil	Sub-soil
Liquid limit, w_L (%)	82.8	82.8
Plastic limit, w_P (%)	30.1	30.1
Plasticity Index, I_p (%)	52.7	52.7
Shrinkage limit, w_S (%)	15	15
Effective cohesion, c' (kPa)	5	10 in SLOPE/W
Effective internal friction angle, ϕ' (˚)	17.5	17.5 in SLOPE/W
Modulus of elasticity, E_{sat} (kPa)	4000	4000
Unit weight, γ (kN/m^3)	18.04	18.04
Poisson's ratio, μ	0.4	0.4

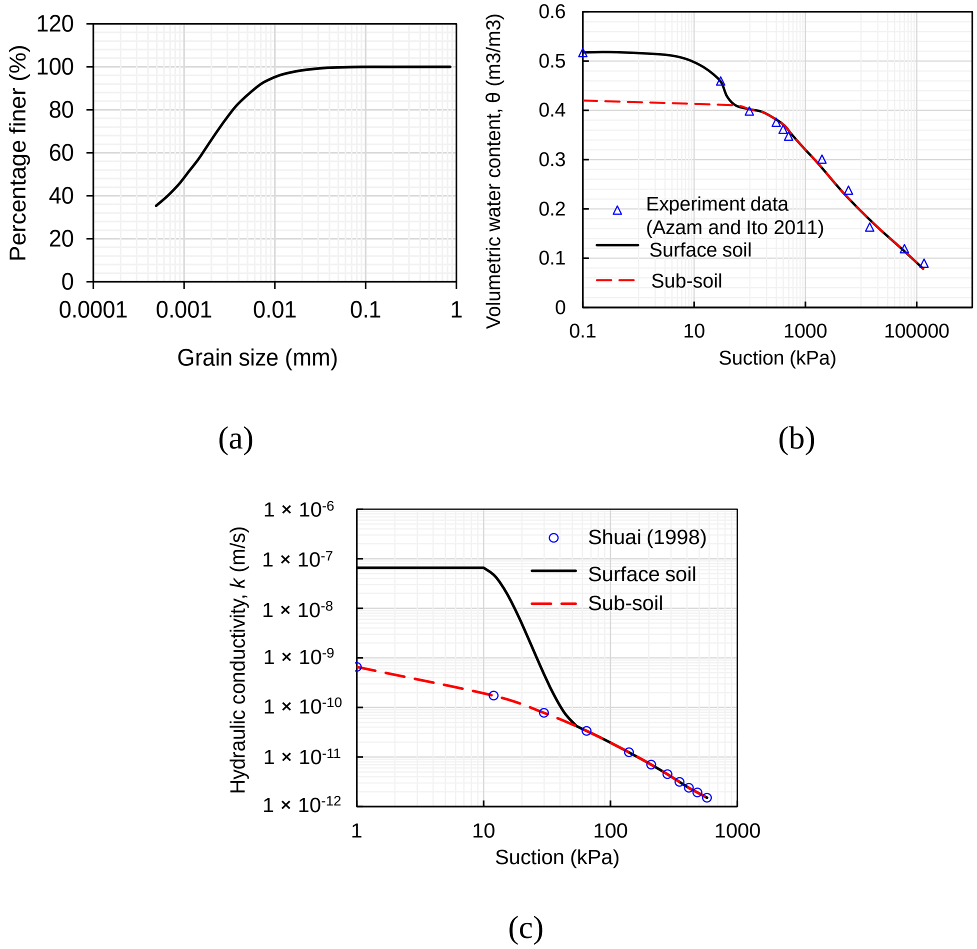

Fig. 5.4 The Regina clay soil properties: (a) Grain size distribution; (b) SWCC; (c) Soil hydraulic conductivity

Both hydraulic and mechanical boundaries have been considered and established as presented in Fig. 5.3. Displacement control is widely used in the literature for estimating the foundation bearing capacity in the numerical analysis (Loukidis et al., 2008, Tan et al. 2022); in this study, a rate of 0.1 m/day has been used for obtaining the foundation bearing capacity. The bottom boundary is fully constrained, and the lateral boundaries are implemented with roller supports. Total water head boundary has been applied at the lateral boundaries below the GWT. For the lateral boundaries above the GWT, default boundary in the software which represents the impervious boundary is applied. This is considered reasonable due to the flow under the infiltration impact is mainly in the surficial layer as the ground water table is at a greater depth. In addition, it is assumed that the effect of the lateral flow through the lateral boundary is negligible (Qi and Vanapalli, 2015a) on the foundation behavior. The rainfall influx boundary q_A has been applied along the top and toe of the slope surface. The rainfall influx boundary q_B is normal to the sloping ground and is calculated as $q_A\cos\beta$. Three rainfall influx boundaries (q_A) have been considered for the parametric studies: q_1 = 1.05×10^{-3}, q_2 = 2.60×10^{-3}, q_3 = 6.90×10^{-3} m/day. q_1 is determined based on the average monthly precipitation in the rainy season recorded in Regina, Canada shown in Fig. 5.5. q_2 is the maximum monthly precipitation of the year in Fig. 5.5. The above two influx values are slightly lower than the surface soil saturated hydraulic conductivity. q_3 is the maximum monthly precipitation during the past 10 years. This value is slightly higher than the surface soil hydraulic conductivity value. The precipitation record is selected randomly to represent a general infiltration condition and the three influx boundaries are set for comparison for the parametric studies. During the infiltration process, run-off condition at the surface soil may occur. In this run-off scenario, the influx boundary is coded to automatically change to the hydraulic head boundary of 0 kPa. 'No flow' boundary is applied below the foundation at the surface of the slope top. Besides the infiltration influx, the rainfall duration from 0 to 150 days at 30 days intervals are considered for the parametric study. The foundation setback ratio (b/B) of 0, 1, 2, 4 are also included.

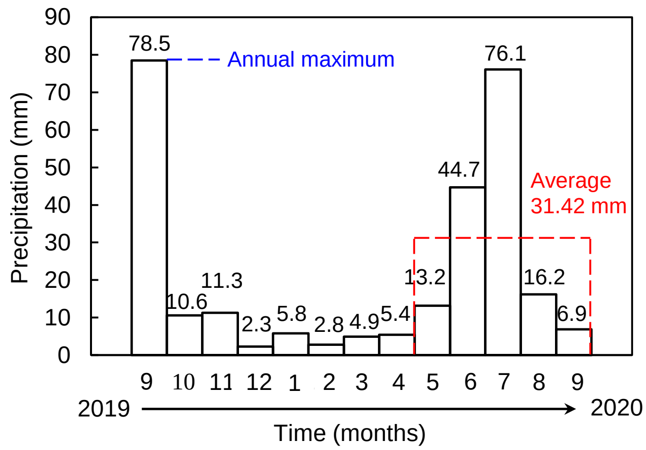

Fig. 5.5 Precipitation records in Regina, Canada

5.3.2 Model validation

Comparison studies are conducted considering two different aspects: (i) The pore water pressure distribution and elastic modulus estimation on the expansive soil slope with cracks at the surficial layer under water infiltration. (ii) The foundation bearing capacity of unsaturated soil.

The modeling method is first compared with the study conducted by Qi and Vanapalli (2015a) on Regina clay slope subjected to rainfall infiltration. A slope that is consistent with the Qi and Vanapalli (2015a) has been set up for comparison purposes using the modeling method illustrated in this study. Comparisons have been made with respect to the PWP distribution and elastic modulus distribution before and after rainfall infiltration of both studies. Fig. 5.6 presents a good agreement of the results obtained in this study after 30 days of rainfall infiltration at mid of the sloping ground with that in Qi and Vanapalli (2015a).

The bearing capacity obtained from the numerical analysis is compared to that obtained from theoretical and semi-empirical methods published in the literature for foundation on level ground (Vanapalli and Mohammed 2007, Vahedifard and Robinson 2016, Ghasemzadeh and Akbari 2019). The soil properties used in the validation model are the same as that were discussed in the previous section. Four GWTs (4 m, 8 m, 12 m, 16 m) have been included in this validation study.

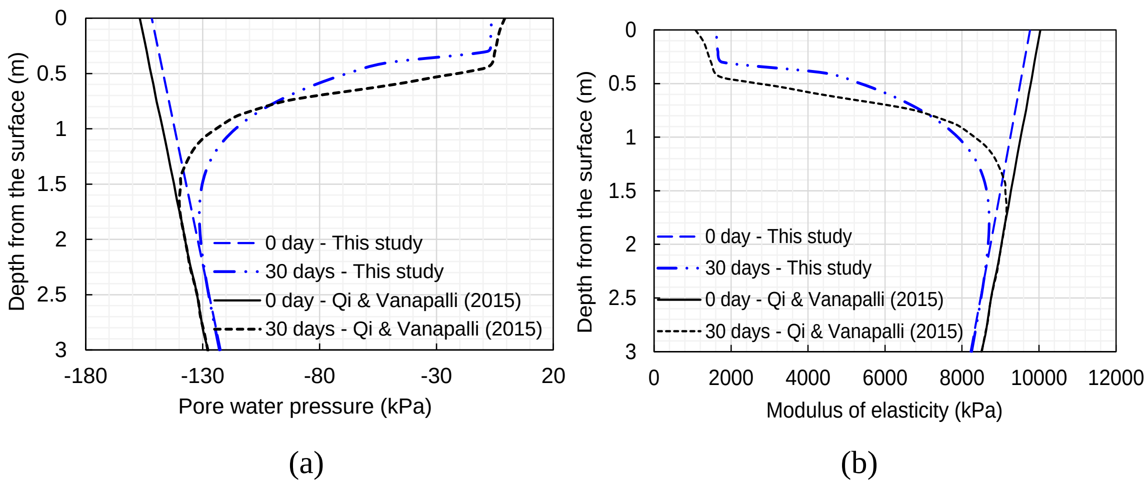

Fig. 5.6 Comparison between results of this study and Qi and Vanapalli (2015a): (a) PWP distribution; (b) Modulus of elasticity

Fig. 5.7a illustrates the foundation stress versus displacement curve under four GWTs. The bearing capacity is determined by the graphical method used in the literature (e.g., Costa et al. 2003, Oh and Vanapalli 2013). For the graphical method, the intersection of the tangents as shown in Fig. 5.7a to the initial elastic portion and the final portions of the stress versus displacement curve is considered as the ultimate bearing capacity. Fig. 5.7b presents a good agreement between the bearing capacity obtained from the numerical method in this study and that calculated with the equation proposed by Ghasemzadeh and Akbari (2019). The maximum deviation is less than 20% for different matric suction values. The bearing capacity from the present analysis is also within the range of that obtained from equations proposed by Vanapalli and Mohammed (2007) and Vahedifard and Robinson (2016). The ψ in the figure is a fitting parameter for the bearing capacity estimation and is related to the soil plasticity index. Three suggested ψ values, $\psi_1 = 1.18$, $\psi_2 = 2.5$, $\psi_3 = 3.5$ (Vanapalli and Mohammed 2007, Vanapalli and Oh 2010) have been considered for the comparison because limited data has been found for the ψ corresponding to the soil used for this study. Good agreement has been found between the present results and that obtained with $\psi = 2.5$. The summarized details in this section suggest that the numerical modeling method used in this study can provide reasonable estimation of the infiltration condition and foundation bearing capacity.

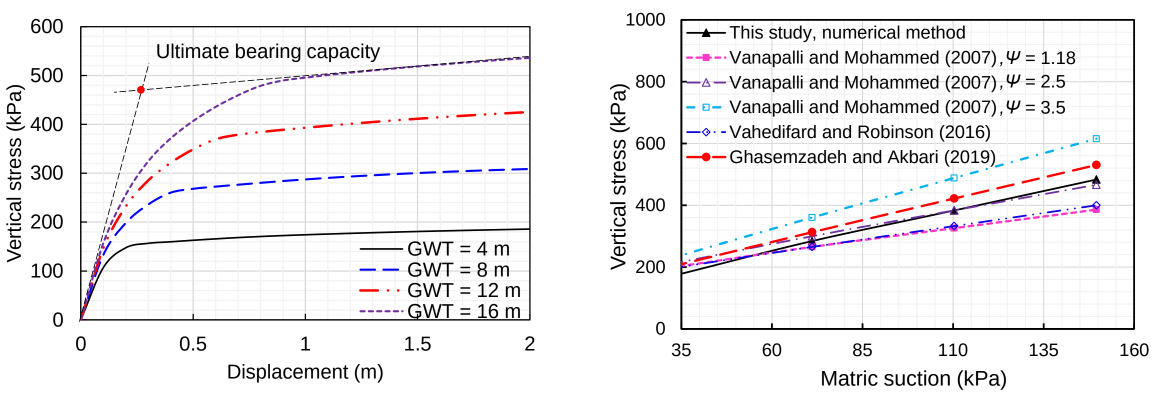

(a) (b)

Fig. 5.7 Bearing capacity comparison: (a) Bearing capacity determination; (b) Comparison with published studies

5.4 Results

5.4.1 Foundation bearing capacity

5.4.1.1 Effect of rainfall duration and intensity

Fig. 5.8a illustrates the foundation bearing capacity variation with setback ratio of one considering different rainfall scenarios. The value of the ultimate bearing capacity under rainfall intensity of q_3 after a duration of 30 days is not provided in this figure because the slope is not stable. The foundation ultimate bearing capacity decreases rapidly during the first 90 days under a rainfall intensity of q_1 = 1.05×10^{-3} m/day. The decreasing rate from then on slows down and the bearing capacity reaches approximately to a value of 100 kPa at 150 days. This is less than a third of the value for the scenario that is prior to rainfall. Similar decreasing trends have been observed under the higher rainfall intensities, q_2 and q_3. Dramatic reduction of the ultimate bearing capacity was observed during the first 30 days of rainfall with both rainfall intensities. The decrease of foundation ultimate bearing capacity is not significant after that time. Such a behavior may be attributed to the PWP changes rate that is influenced by the relationship between the rainfall intensity and the soil hydraulic conductivity. In other words, the soil hydraulic conductivity varies during rainfall infiltration. The slope cannot provide support after a certain time under a higher rainfall intensity; more details are explained in a later section.

Figs. 5.8b, 5.8c and 5.8d show the soil yield and the maximum shear strain contours in the active zone. The soil yielding contour was drawn based on the modified MC criterion discussed earlier. It should be noted that the sub soil obeys the linear elastic model and hence will not exhibit a yielding zone. However, the influence of the sub-soil is not significant, and the rainfall resulted failure is mainly occurring in the surface layer soil as shown in the Fig. 5.8b. It can be seen in Fig. 5.8b that the slope toe and the surface soil on sloping ground adjacent to the foundation are yielding after 30 days of rainfall infiltration. The yielding depth at the slope toe advances deeper with an increase in the rainfall duration. More water flows to the toe and stress accumulates and concentrates at the toe of the slope. For this reason, shear strength values will reduce significantly due to matric suction reduction. Soil adjacent to the foundation also mobilizes and the yielding zone cuts through the sloping ground surface with the increasing rainfall duration. The yielding zone also advances more towards the slope top level ground surface with the increasing rainfall duration. The above phenomenon is consistent with the shallow surface failure observed for slope under infiltration condition (Wu et al. 2015).

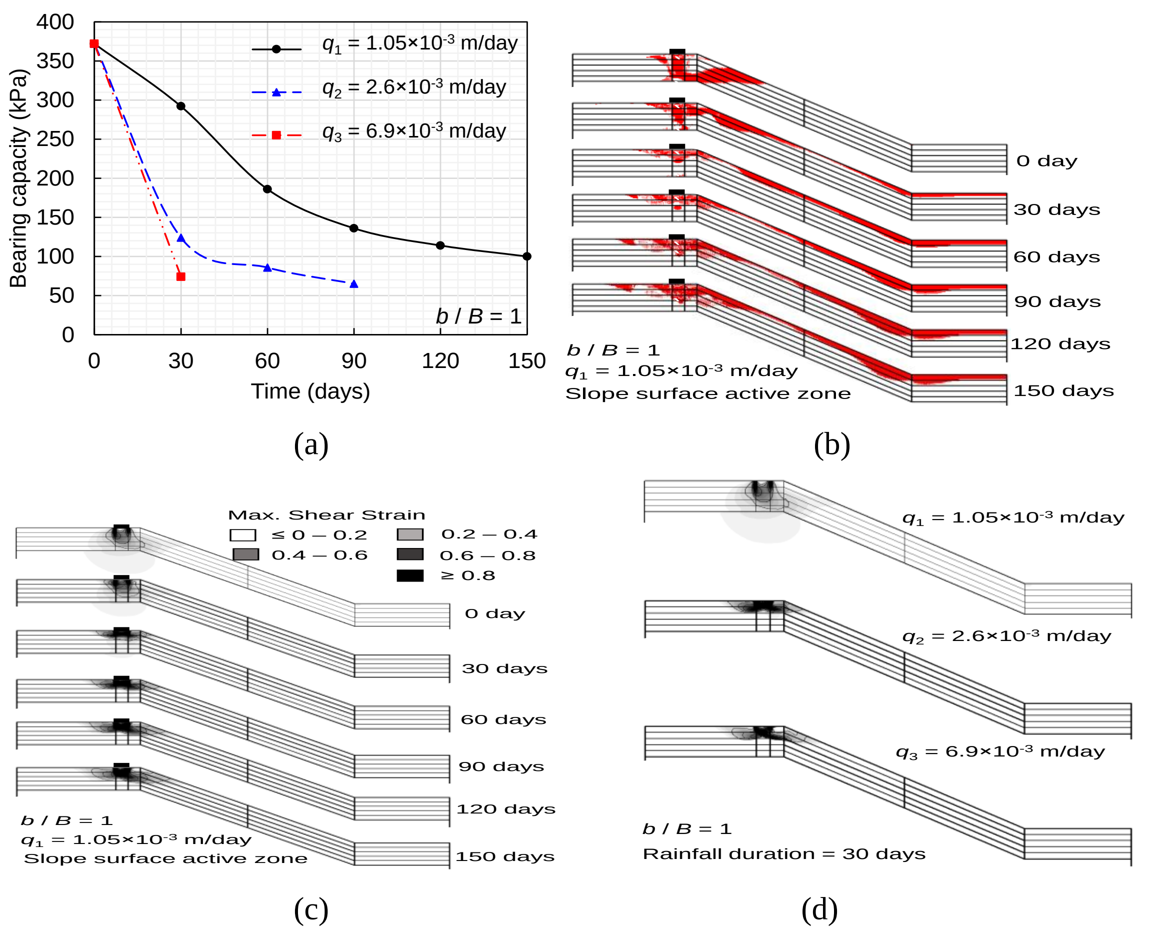

Fig. 5.8 Foundation bearing capacity for different rainfall scenarios: (a) Bearing capacity under different rainfall intensities; (b) Yielding contour corresponding to the ultimate bearing capacity; (c) Maximum shear strain contour (d) Maximum shear strain under different rainfall intensities

The maximum shear strain contour in Fig. 5.8c correlates the yielding zone in Fig. 5.8b well. Fig. 5.8c indicates that the combined influence of the slope surface failure and foundation bearing capacity failure becomes obvious with the increasing rainfall duration. It should be noted that the failure mechanism also depends on the slope stability which will be illustrated together with the slope CFS later. Fig. 5.8d presents the maximum shear strain contour obtained from the three different rainfall intensities for a rainfall duration of 30 days. Soil cuts through more on the surface of slope top-level ground and sloping ground with a higher rainfall intensity. Overall, the rainfall intensity and duration have a negative effect on the foundation bearing capacity.

5.4.1.2 Effect of foundation setback ratio

The normalized foundation bearing capacity variation with the foundation setback ratio on slope for different rainfall intensities and duration are summarized in Figs. 5.9a, 5.9b and 5.9c. The results are presented as the normalized foundation bearing capacity which is widely used in the literature to alleviate the effect of foundation width and soil unit weight. The summarized results suggest that the foundation bearing capacity increases with an increase in the foundation setback distance. Such a behavior can be attributed to the increased soil resistance associated with a large setback distance. These results also correlate well with the yield contours and the maximum shear strain contours shown in Figs. 5.9d, 5.9e and 5.9f. All the contours show more soil is mobilized and extended to the slope top-level ground with an increase in the foundation setback ratio. The yielding zone that results from the foundation loading will not be developed further to the sloping ground surface when the foundation setback ratio is large enough. Failure mechanism of foundation with lower setback ratio will cut through the slope surface.

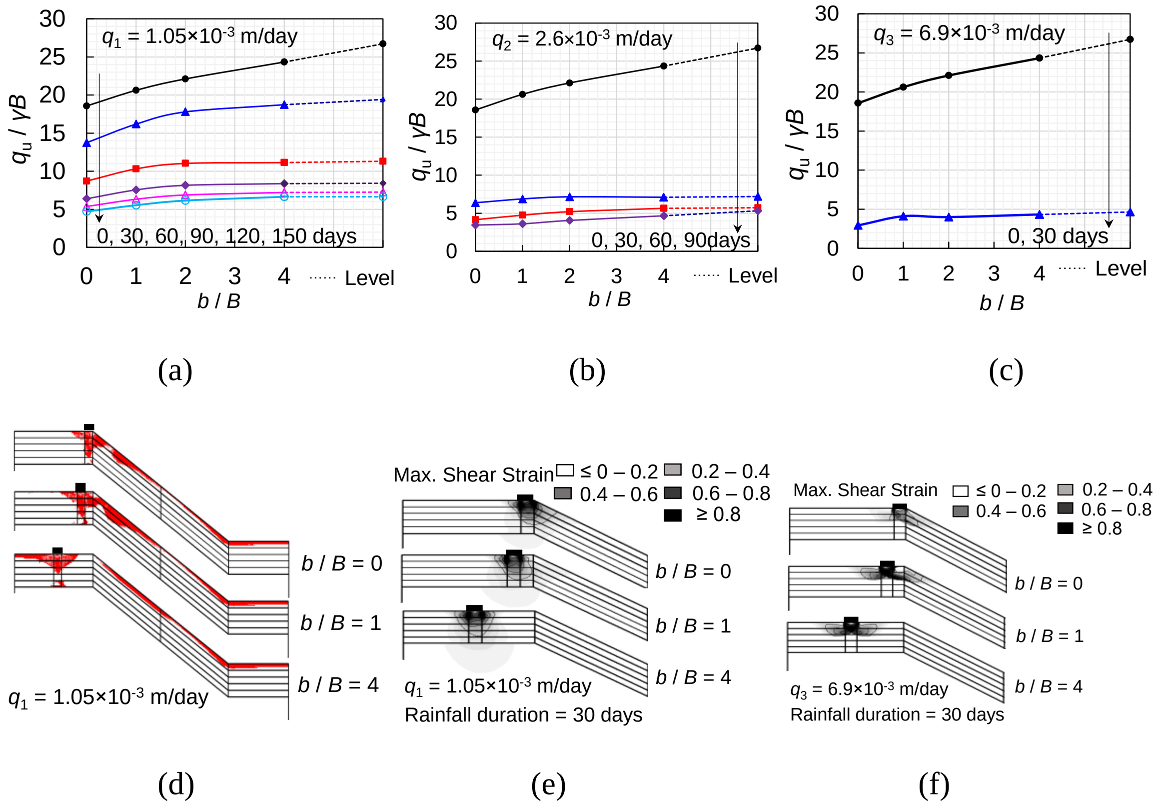

Fig. 5.9 Effect of foundation setback ratios: (a) q_1; (b) q_2; (c) q_3; (d) Yield contour; (e) Maximum shear strain contour under q_1; (f) Maximum shear strain contour under q_3

Fig. 5.9 also highlights more interesting results. Prior to rainfall, the critical foundation setback ratio (CSR), which represents the setback ratio at soil bearing capacity equals that for foundation on level ground, is greater than a value of four. The value of the CSR decreases with an increase in the rainfall duration and rainfall intensity. As shown in Fig. 5.9a, the CSR is about three during a rainfall intensity q_1 for 30 days. This value decreases to about one with the rainfall duration under rainfall intensity of q_3 as seen in Fig. 5.9c. These results suggest that the influence of the foundation setback ratio after a high rainfall intensity or a long rainfall duration is not obvious compared to without rainfall condition.

In other words, a heavy rainfall and a long rainfall duration have a significant impact on the foundations irrespective of the foundation setback ratio. However, higher foundation setback ratio facilitates a higher bearing capacity based on the results in Fig. 5.9. Therefore, it is suggested to have a greater setback distance (i.e., $b/B > 4$).

5.4.2 Slope stability

5.4.2.1. Effect of rainfall duration, intensity on the CFS

Fig. 5.10 presents the slope CFS with respect to the three different rainfall intensities and foundation loading conditions. The CFS reduces at a rapid rate with an increase in the rainfall intensity irrespective of the foundation loading (i.e., with or without loading). Fig. 5.10a illustrates the CFS variation with the rainfall duration and intensities without foundation loading condition. Significant decrease of CFS under rainfall intensity of q_3 has been found within the first 30 days. The CFS value decreases from 1.93 to 1.2 during the 30 days. The reduction of CFS is not obvious for the slope under rainfall intensity of q_1 until 120 days. A turning point has been found on each of the CFS curve. The turning point as discussed in this paper represents the point on the CFS curve that reflect the reduction rate changes obviously as shown in Fig. 5.10a. The CFS reduces rapidly after the turning point for all the three different rainfall scenarios. The turning point reflects the failure mechanisms variation shown as the failure mechanisms A and B in Fig. 5.10a. Deep seated failure (Failure mechanism A) has been observed before the turning point, while shallow surface failure or the toe failure have been found after the turning point. The shallow surface failure and the toe failure are common failure mechanisms induced by the rainfall infiltration. In other words, the slope stability mainly depends on the slope characteristic (for example, the slope original geometry and initial soil properties) before the turning point. However, after a specific rainfall duration, the rainfall characteristics are the predominant factors that affect the slope stability. This also explains why the turning point on the CFS curve under rainfall intensity of q_3 arises earlier than that under q_1. Higher rainfall intensity contributes towards a dramatic decrease in matric suction in a short time, and this in turn leads to the shear strength reduction and the CFS decrease.

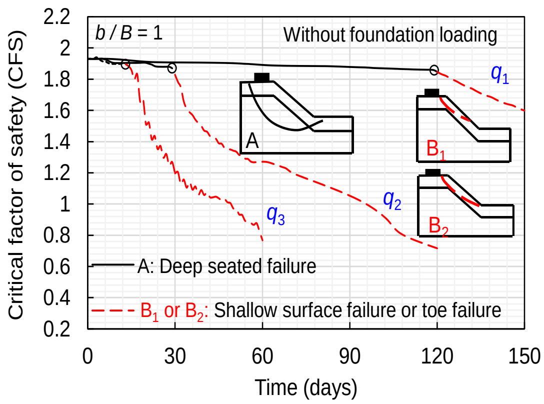

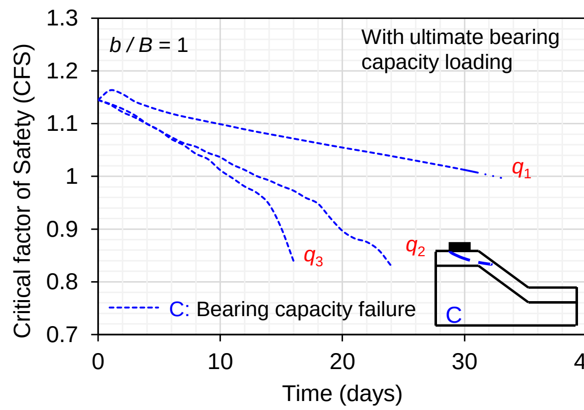

(a) (b)

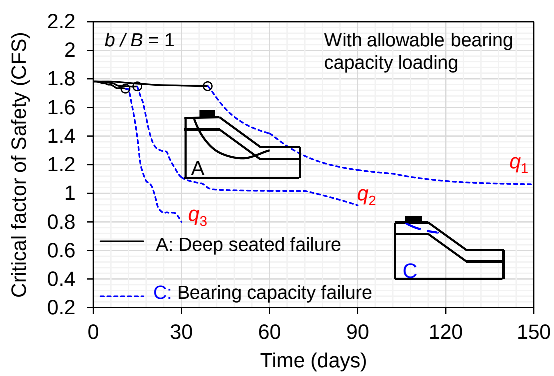

(c)

Fig. 5.10 CFS with various loading conditions for different rainfall scenarios: (a) Without foundation loading; (b) With ultimate bearing capacity loading; (c) With allowable bearing capacity loading

Figs. 5.10b and 5.10c provide CFS variation for slope under foundation ultimate bearing capacity loading and allowable bearing capacity loading. The allowable bearing capacity is determined based on the AASHTO (2014) with a FS of three. This allowable bearing capacity is only used for comparison purposes to understand the effect of different loading magnitudes on the slope. The ultimate bearing capacity prior to rainfall has been applied as surcharge load to the slope. Well-defined turning point are not found in Fig. 5.10b for slope with foundation ultimate bearing capacity loading. Only foundation bearing capacity failure (Failure mechanism C in Fig. 5.10b) has been observed for the combined foundation-slope system under this scenario. The initial CFS of 1.14 is also lower than that without foundation loading of 1.93. Moreover, CFS reduces rapidly with the increasing rainfall intensity and duration even at the early rainfall infiltration event. However, the variation trend of slope with allowable bearing capacity loading (see Fig. 5.10c), which has similar trends as in Fig. 5.10a. The reduction of CFS is not obvious at early rainfall event. Sharp drop in CFS has been observed with an increase in the rainfall duration after the turning point. Deep seated failure before the turning point has been found and bearing capacity failure has been observed after the turning point. Though the foundation bearing capacity failure mechanism has been observed for slope under both the foundation ultimate bearing capacity and the allowable bearing capacity under the longer rainfall duration, the surcharge loading magnitude results in the difference of the failure mechanisms during early rainfall duration. This means that the combined influence of the rainfall and the foundation loading has more impact on the foundation-slope system in comparison to limited or no foundation loading.

Based on the earlier discussions, it can be concluded that the deep-seated failure is predominantly dependent on the slope initial condition and soil properties that are prevalent at early rainfall condition. The CFS reduction is not significant in this stage. The foundation loading has significant influence on the CFS prior to the rainfall and during the rainfall. After a specific rainfall duration, the CFS decreases dramatically and slope surface failure, toe failure or foundation bearing capacity failure may be observed based on different foundation loading conditions. In this stage, it is the rainfall characteristics and foundation loading that predominantly controls the CFS and the corresponding failure mechanisms; and it increases the risk of the system instability.

Soil volume change also influences the slope stability, especially it is predominant in expansive soils. Fig. 5.11 presents the slope surface vertical upward displacement along with different rainfall intensities and duration. The maximum vertical upward displacement of the slope surface without foundation loading under rainfall intensity of q_1 in Fig. 5.11a is about 7 mm; this value is two times lower than rainfall intensity of q_3 in Fig. 5.11c. The vertical displacement increases with an increase in the rainfall intensity and duration. Due to the relatively large modulus of elasticity used in the model, the influence of this vertical displacement on the slope FS is relatively small compared to that caused by the shear strength reduction during rainfall. However, the differential heave can have a significant impact and contributes to damages to the foundation as well as the super-structure and should be considered in the design of foundations.

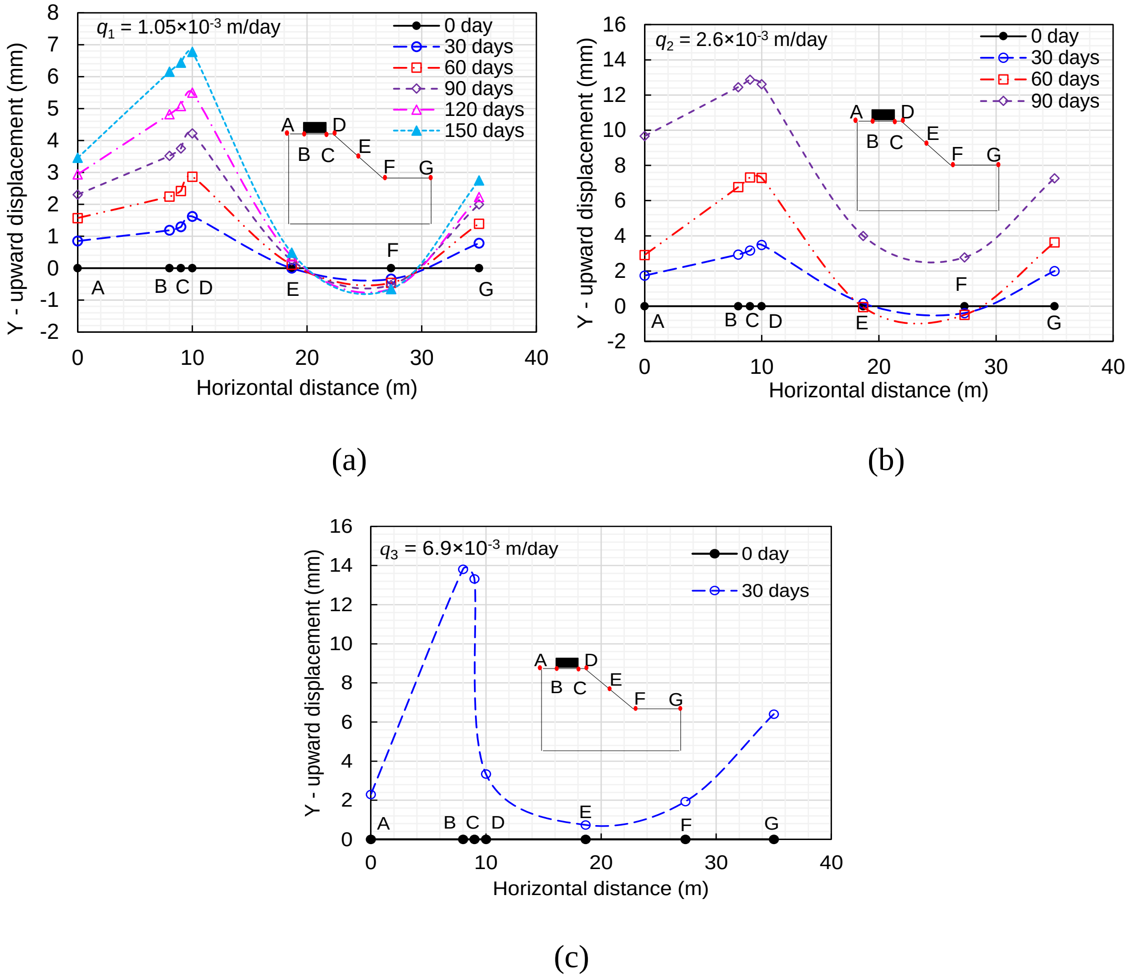

Fig. 5.11 Vertical displacement of the slope surface without foundation loading: (a) q_1; (b) q_2; (c) q_3

5.4.2.2. Effect of foundation setback ratio on the CFS

Fig. 5.12 illustrates the relationship between the CFS and the foundation setback ratio. Fig. 5.12a suggest that CFS increases with an increase in the foundation setback ratio for the ultimate bearing capacity loading condition with the same rainfall characteristic. The critical slip surface shows that only foundation with a large setback ratio may have deep seated failure associated with an early rainfall event. This means the stability of the foundation-slope system with a higher foundation setback ratio may be first controlled predominantly by the combined influence of slope initial condition, soil properties and surcharge loading. After a certain period of rainfall, bearing capacity failure caused by the foundation loading combined with the rainfall infiltration is likely arise.

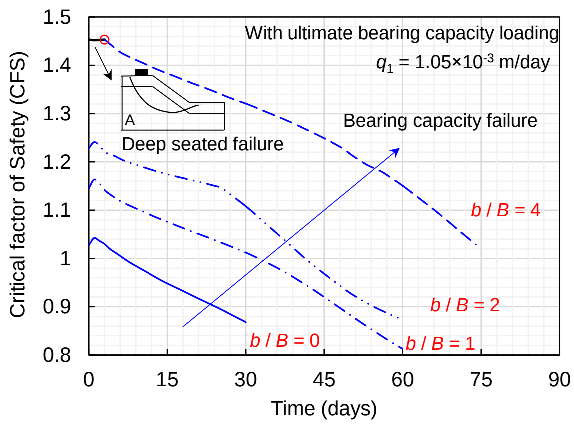

(a)

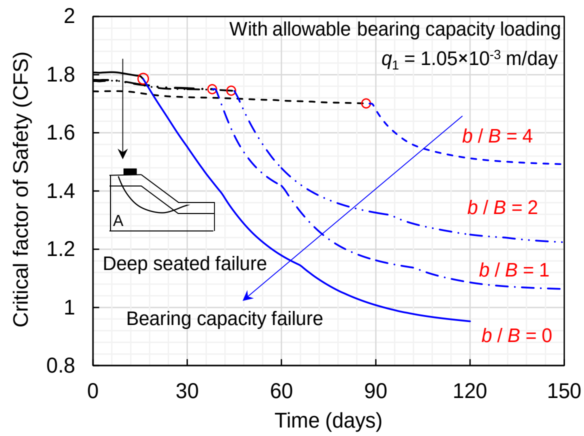

(b)

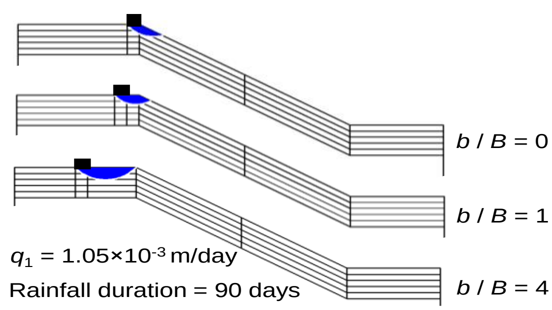

(c)

Fig. 5.12 Effect of foundation set back ratio: (a) With ultimate bearing capacity loading; (b) With allowable bearing capacity loading; (c) Critical slip surface corresponding to CFS under bearing capacity failure

Fig. 5.12b shows the CFS of the foundation-slope system under the foundation allowable bearing capacity loading for different foundation setback ratio. The deep-seated failure mechanism is found for all setback ratios before the turning point, which is different to the foundation-slope system under ultimate bearing capacity loading. Foundation with a higher setback ratio has a lower CFS compared to that with a small setback ratio at early rainfall event. This is probably because the foundation with higher setback ratio has a higher bearing capacity; the initial foundation loading applied on the slope is slightly higher than that with a small setback ratio. Moreover, the allowable bearing capacity loading is not large enough to cause the foundation bearing capacity failure directly under the combined influence of the slope, soil properties and rainfall infiltration. However, foundation with a higher setback ratio still will have a higher CFS under the same rainfall intensity and duration after the turning point as more soil provides support to the foundation. The turning point, which reflects the failure mechanisms variation, is observed at almost 90 days of rainfall as shown in Fig. 5.12b for $b/B = 4$. This means the influence of rainfall is not pronounced for the CFS of foundation-slope system with higher foundation setback ratio under a relatively small foundation loading. Therefore, higher setback ratio is recommended for the foundation design. The critical slip surfaces that contribute to bearing capacity failure mode are shown in Fig. 5.12c. The mobilized soil zone on the sloping ground reduces and extends more on the top-level ground of slope with the increasing setback ratio, which is similar to the contour shown in Fig. 5.9.

5.5 Discussion and limitation of the present study

The slope FS is determined using the Morgenstern-Price method in this study. As discussed earlier, the localized shear stress concentrations may not be rigorously captured extending this approach. Therefore, the finite element stress-based FS in SLOPE/W are obtained and compared with the FS obtained from the Morgenstern-Price method in Fig. 5.13a, 5.13b and 5.13c. The comparison of the failure mechanisms obtained from the two methods are presented in Fig. 5.13d – 5.13g. The CFS obtained by the finite element stress-based method is slightly higher than that obtained by the Morgenstern-Price method. This phenomenon is also consistent with the results provided by the Geo-Slope Int. Ltd (2012a). The reason for the higher CFS is probably related to the normal stress along the slip surface as shown in Figs. 5.13b and 5.13c. The CFS obtained by the two methods are close for the deep-seated failure (before the turning point mentioned earlier) in Fig. 5.13b. For the toe failure, higher normal stress is observed from the finite element stress-based method in Fig. 5.13c which corresponds to the slice near the foundation and the slice near the slope toe with stress concentration. This results in the relatively higher CFS as shown in Fig. 5.13a. The failure surfaces shown in Fig. 5.13d and 5.13f that are obtained from the two methods (i.e., finite element stress-based method and Morgenstern-Price method) are almost the same. Due to this reason, there are small deviations of the CFSs obtained from these two methods (see Fig. 5.13a). However, for the CFSs that exhibited a relatively large deviation, there is some difference between the failure mechanisms from the two methods as shown in Fig. 5.13g. Fig. 5.13e depicts different failure mechanisms obtained from the two methods. This behavior is consistent to the CFS curve shown in Fig. 5.13a. The turning point on the CFS curve will occur earlier than that obtained based on the finite element stress-based method. However, this turning point which represents for the failure mechanism variation is close for both the methods. In other words, the failure mechanisms from the two methods are similar and the small deviations are considered reasonable. In summary, the CFS obtained from the present study is conservative and hence can be considered reasonable for use in engineering practice applications.

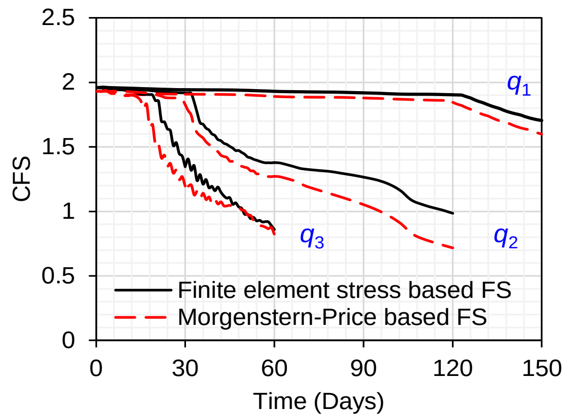

2.5
2
1.5
1
0.5
0
CFS
0
30
60
90
120
150
Time (Days)
q1
q2
q3
Finite element stress based FS
Morgenstern-Price based FS

(a)

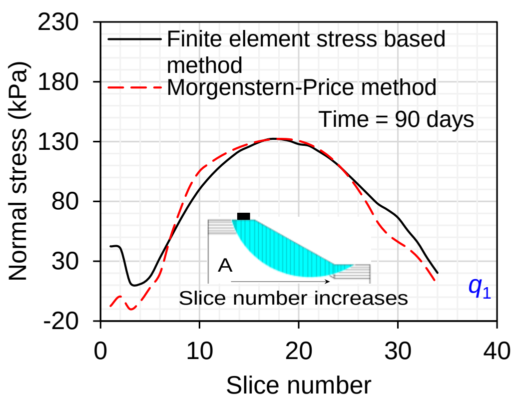

230
180
130
80
30
-20
Normal stress (kPa)
0
10
20
30
40
Slice number
Finite element stress based method
Morgenstern-Price method
Time = 90 days
A
Slice number increases
q1

(b)

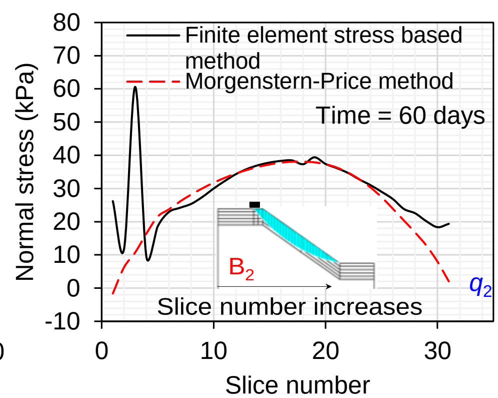

80
70
60
50
40
30
20
10
0
-10
Normal stress (kPa)
0
10
20
30
Slice number
Finite element stress based method
Morgenstern-Price method
Time = 60 days
B2
Slice number increases
q2

(c)

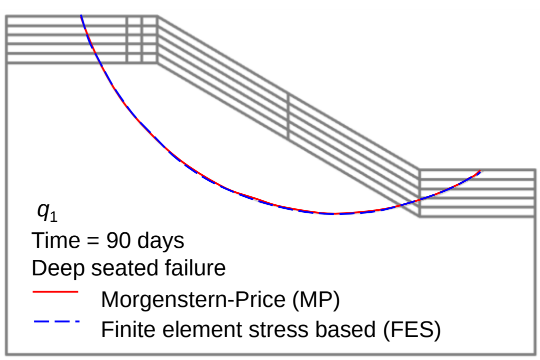

q1
Time = 90 days
Deep seated failure
Morgenstern-Price (MP)
Finite element stress based (FES)

(d)

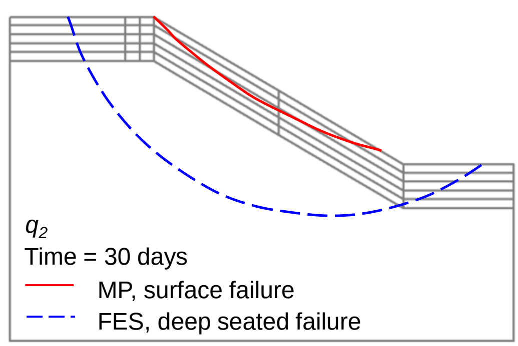

q2
Time = 30 days
MP, surface failure
FES, deep seated failure

(e)

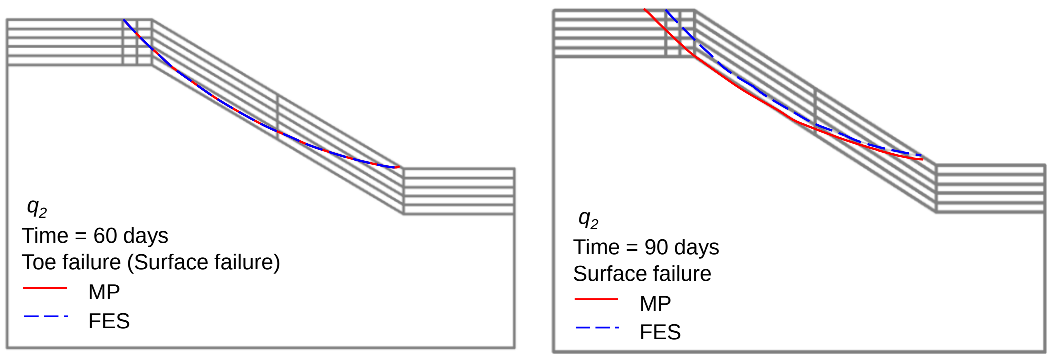

(f) (g)

Fig. 5.13 Comparison of the finite element stress based method and Morgenstern-Price method: (a) CFS, (b) Normal stress along the deep seated failure surface, (c) Normal stress along the surface/toe failure surface, (d) Deep seated failure comparison, (e) Comparison at 30 days of rainfall, (f) comparison at 60 days of rainfall, (g) Comparison at 90 days of rainfall

The measured properties of Regina clay were mainly used in present study. In addition, the different relationships between the influence parameters and the soil properties were also investigated such that more comprehensive information can be derived from this study. For example, the rainfall intensity that is higher and lower than the soil saturated hydraulic conductivity is considered. The amount of the water that infiltrates into the soil depends mainly on the relationship between the rainfall intensity and the soil hydraulic conductivity. The soil hydraulic conductivity will be changing during the rainfall. The initial conditions (i.e., the initial ground water table depths or the initial surface seepage) will influence the soil initial hydraulic conductivity as shown in Fig. 5.14. Fig. 5.14d shows different soil initial hydraulic conductivities of points on different position of the slope surface. A higher soil hydraulic conductivity and lower matric suction are found for Point F compared to those for Point D. This results in the deviation of pore water pressure variation during the rainfall as shown in Fig. 5.14a, 5.14b and 5.14c. Studies by Vahedifard and Robinson (2016) and Tan and Vanapalli (2022) show that it is the combination of the soil properties and the contribution of the matric suction that will influence the effect of the rainfall infiltration on the foundation bearing capacity. It can be seen from Fig. 5.14d that the initial soil hydraulic conductivity at all points on the slope surface are lower than any of the three rainfall intensities used in this study. Therefore, the surface ponding occurred at early rainfall under the three rainfall intensities. At this moment, it is the relationship between the hydraulic gradient, the saturated soil hydraulic conductivity and the rainfall intensity that controls the water infiltration rates. This will influence matric suction variation and in turn influence the bearing capacity fluctuation and slope stability. For rainfall intensity higher than the saturated soil hydraulic conductivity, the surface ponding keeps occur during the rainfall as shown in Fig. 5.14c. Therefore, it is suggested to have the drainage system or other treatment for the slope. The most conservative bearing capacity is the bearing capacity of the soil in saturated condition. If the rainfall intensity is lower than the soil saturated hydraulic conductivity, the final bearing capacity depends on the combination of the rainfall intensity, duration, and the variation of the soil hydraulic conductivity. However, it should be noted that if the rainfall duration is long enough or if the ground water table is shallow, or in certain cases when there is a rise in the water table, final foundation bearing capacity is significantly influenced. The scenarios considered in this study includes different infiltration conditions. These results provide as a reference to understand other soils behavior that have similar soil properties and are subjected to different infiltration conditions.

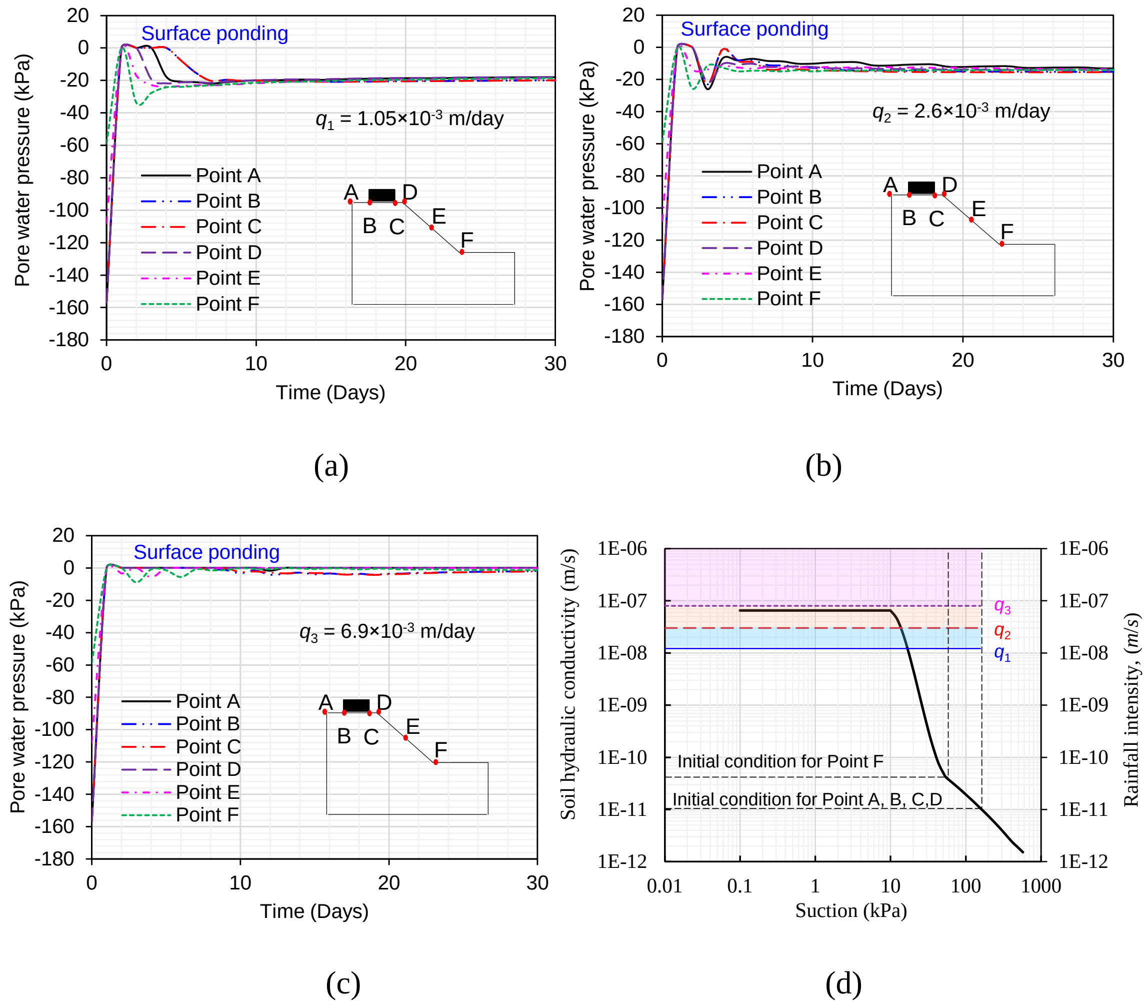

Fig. 5.14 PWP variation at the surface of the slope under rainfall infiltration: (a) q_1; (b) q_2; (c) q_3; (d) Relationship between the soil hydraulic conductivity and rainfall intensity

The shear strength equation applicable for reliable estimation of the shear strength using the bimodal SWCC with two air entry values (for example, Satyanaga and Rahardjo, 2019, Satyanaga et al. 2022) is not considered in the study. This is because convergence problems are likely due to highly non-linear behaviour from the numerical simulation using the bimodal soil shear strength. For more rigorously addressing this problem, a more complex model and advanced numerical techniques are required to be considered in future studies.

There are other parameters that will also influence the foundation and slope system. For example, the slope height and the slope angle. Higher slope angle will yield a relatively lower FS (Rahardjo et al. 2007) and relatively lower bearing capacity of the foundation under the rainfall condition (Tan and Vanapalli, 2022). Results by Rahardjo et al. (2007) suggest that the slope with lower slope height is more stable due to the relatively higher initial slope FS under the rainfall. However, reduction in the FS of a slope with a greater height is relatively small and the reduction rate is slower compared to the slope with lower height; the failure of a higher slope is probably caused by the loss of matric suction. This may influence the foundation bearing capacity variation during the rainfall that require further investigations.

5.6 Conclusions

In the present study, hydro-mechanical coupled analyses have been performed for Regina clay expansive soil to investigate the bearing capacity and stability of foundation-slope system subjected to rainfall infiltration. The bimodal SWCC has been used in the study for understanding the influence of cracks that have a significant impact on the bearing capacity of shallow foundation on sloping ground. Parametric studies were undertaken considering the influence of the rainfall intensity, rainfall duration, foundation setback ratio and foundation loading. Based on the parametric studies' results, several conclusions have been obtained as follows:

(1) A higher rainfall intensity contributes to higher reduction rate in the bearing capacity when other parameters are same. However, the influence of the setback ratio on the

bearing capacity is not obvious with a higher rainfall intensity and longer rainfall duration. The foundation setback ratio has a positive effect on the foundation bearing capacity and it is suggested that the foundation setback ratio should be at least greater than four based on the present study for the Regina clay.

(2) The rainfall intensity and its duration have a negative effect on the critical factor of safety of the slope. For the combined foundation-slope system, the CFS reduction decreases slowly when the foundation loading is small in the early rainfall event. The CFS reduces rapidly under the combined influence of a higher foundation loading and rainfall intensity. The foundation setback ratio typically has a positive effect on the CFS of the combined system. Drainage measures are suggested to be considered in the design of foundation and slope system for the rainfall intensity that is greater than the soil saturated hydraulic conductivity.

(3) The rainfall intensity, rainfall duration, foundation setback ratio and foundation loading have combined impact on the foundation-slope failure mechanisms. The slope surface failure, toe failure, foundation bearing capacity failure and deep-seated failure are observed in the present study. Deep seated failure is mainly caused by the slope geometry and soil properties; it also can be observed when the foundation loading is relatively small and setback ratio is large enough during early rainfall event. The slope surface failure and toe failure are mainly caused by the rainfall infiltration. Such a behavior is obvious for higher rainfall intensities that extend for a longer rainfall duration. Different foundation failure mechanisms have been observed with various foundation setback ratios for different rainfall scenarios.

The study presented in this Chapter provides a better understanding of the bearing capacity and stability of foundation-slope combined system for a typical expansive soil subjected to rainfall infiltration. It is important to understand the combined influence of the rainfall characteristics, foundation loading and setback ratio in the engineering design because of uncertainties associated with the climate factors. The approaches presented in this study facilitate the evaluating of foundations on slopes combined behavior during the entire service life of the infrastructure. Moreover, they can be used in forensics studies for assessing foundation and slope failures.

References

AASHTO (American Association of State Highway and Transportation Officials) 2014. LRFD Bridge Design Specifications, Seventh Edition.

Adem, H.H. and Vanapalli, S.K. 2013. 'Constitutive modeling approach for estimating 1-D heave with respect to time for expansive soils.' Int. J. Geotech. Eng., 7(2), 199-204.

Amakye, S.Y. and Abbey, S.J. 2021. 'Understanding the performance of expansive subgrade materials treated with non-traditional stabilisers: A review.' Cleaner Eng. Technol., 4, 100159.

Anand, A., Sarkar, R., 2021. 'A comprehensive investigation on bearing capacity of shallow foundations on unsaturated fly ash slopes adopting finite element limit analysis.' Eur. J. Environ. Civ., 1-27. https://doi.org/10.1080/19648189.2021.1967200.

Azam, S. and Ito, M. 2011. 'Unsaturated soil properties of a fissured expansive clay.' In 14th Pan-American Conf. Soil Mech. Geotech. Eng., Toronto, Ontario, Canada.

Azam, S., Ito, M., and Chowdhury, R. 2013. 'Engineering properties of an expansive soil.' In Proceedings of the 18th International Conference on Soil mechanics and Geotechnical Engineering (pp. 199-202).

Buzzi, O., Fityus, S., and Sloan, S.W. 2010. 'Use of expanding polyurethane resin to remediate expansive soil foundations.' Can. Geotech. J., 47(6), 623-634.

Costa, Y.D., Cintra, J.C. and Zornberg, J.G., 2003. 'Influence of matric suction on the results of plate load tests performed on a lateritic soil deposit.' Geotech. Test. J., 26(2), 219-227.

Day, R.W., and Axten, G.W. 1989. 'Surficial stability of compacted clay slopes.' J. Geotech. Eng., 115(4), 577-580.

Du, D., Zhuang, Y., Sun, Q., Yang, X., and Dias, D. 2021. 'Bearing capacity evaluation for shallow foundations on unsaturated soils using discretization technique.' Comput. Geotech., 137, 104309.

El-Samea, A., Hassan, W., Mowafy, Y.M., El-Naiem, A., Abdo, M., and Towfeek, A.R. 2022. 'Numerical analysis of shallow foundation on expansive soil.' J. Al-Azhar University Eng. Sector, 17(63), 480-501.

Fathipour, H., Payan, M., Safardoost Siahmazgi, A., Jamshidi Chenari, R. and Senetakis, K. 2022. 'Numerical study on the bearing capacity of strip footing resting on partially saturated soil subjected to combined vertical-horizontal-moment loading.' Eur. J. Environ. Civ. Eng., 1-34.

Fredlund, D.G. and Rahardjo, H. 1993. Soil mechanics for unsaturated soils. John Wiley & Sons.

Geo-Slope Int. Ltd 2018, Geo-studio 2018 R2.

Geo-Slope Int. Ltd. 2012a. Stability modeling with SLOPE/W, An Engineering Methodology. Calgary, Alberta, Canada.

Geo-slope Int. Ltd. 2012b. Stability modeling with Geostudio. GEO-SLOPE International, Ltd.

Ghasemzadeh, H. and Akbari, F. 2019. 'Determining the bearing capacity factor due to nonlinear matric suction distribution in the soil.' Can. J. Soil Sci., 99(4), 434-446.

Greco, V.R. 1996. Efficient Monte Carlo technique for locating critical slip surface. J. Geotech. Eng., 122(7), 517-525.

Huang, R., and Wu L.Z. 2007. 'Stability analysis of unsaturated expansive soil slope.' Earth Sci. Front., 14(6), 129-133.

Ijaz, N., Ye, W., ur Rehman, Z., Dai, F. and Ijaz, Z. 2022. 'Numerical study on stability of lignosulphonate-based stabilized surficial layer of unsaturated expansive soil slope considering hydro-mechanical effect.' Transp. Geotech., 32, 100697.

Jalal, F.E., Xu, Y., Jamhiri, B. and Memon, S.A. 2020. 'On the recent trends in expansive soil stabilization using calcium-based stabilizer materials (CSMs): a comprehensive review.' Adv. Mater. Sci. Eng., 2020, 1-23.

Jiang, H., Wang, B., Inyang, H.I., Liu, J., Gu, K. and Shi, B. 2013. 'Role of expansive soil and topography on slope failure and its countermeasures, Yun County, China.' Eng. Geol., 152(1), 155-161.

Khan, M.S., Nobahar, M., Stroud, M., Amini, F., and Ivoke, J. 2021. 'Evaluation of rainfall induced moisture variation depth in highway embankment made of Yazoo clay.' Transp. Geotech., 30, 100602.

Kim, Y., Park, H. and Jeong, S. 2017. 'Settlement behavior of shallow foundations in unsaturated soils under rainfall.' Sustainability, 9(8), 1417.

Kumar Thota, S., Duc Cao, T., and Vahedifard, F. 2021. 'Poisson's ratio characteristic curve of unsaturated soils.' J. Geotech. Geoenviron. Eng., 147(1).

Le, T.M.H., Gallipoli, D., Sanchez, M., Wheeler, S., 2013. 'Rainfall-induced differential settlements of foundations on heterogeneous unsaturated soils.' Géotechnique, 63(15), 1346-1355. https://doi.org/10.1680/geot.12.P.181.

Li, J. H., Zhang, L.M. and Li, X. 2011. 'Soil-water characteristic curve and permeability function for unsaturated cracked soil.' Can. Geotech. J., 48(7), 1010-1031.

Li, X., Li, J.H., and Zhang, L.M. 2014. 'Predicting bimodal soil–water characteristic curves and permeability functions using physically based parameters.' Comput. Geotech., 57, 85-96.

Liu, Y., and Vanapalli, S.K. 2022. 'Modified shear displacement method for analysis of piles in unsaturated expansive soils considering influence of environmental factors.' Int. J. Geomech., 22(6), 04022069.

Loukidis, D., Chakraborty, T., and Salgado, R. 2008. ‘Bearing capacity of strip footings on purely frictional soil under eccentric and inclined loads.’ Can. Geotech. J., 45(6), 768-787.

Lu, N., Likos, W.J., 2006. ‘Suction stress characteristic curve for unsaturated soil.’ J. Geotech. Geoenviron. Eng. 132 (2), 131–142. https://doi.org/10.1061/(ASCE)1090-0241(2006)132:2(131).

Malkawi, A.I.H., Hassan, W.F., and Sarma, S.K. 2001. Global search method for locating general slip surface using Monte Carlo techniques. J. Geotech. Geoenviron. Eng., 127(8), 688-698.

Mousavi, F., Abdi, E., and Rahimi, H. 2014. Effect of polymer stabilizer on swelling potential and CBR of forest road material. KSCE J. Civ. Eng., 18, 2064-2071.

Ng, C.W.W., Zhan, L.T., Bao, C.G., Fredlund, D.G. and Gong, B.W. 2003. ‘Performance of an unsaturated expansive soil slope subjected to artificial rainfall infiltration.’ Geotechnique, 53(2), 143-157.

Oh, W.T. and Vanapalli, S.K. 2013. ‘Interpretation of the bearing capacity of unsaturated fine-grained soil using the modified effective and the modified total stress approaches.” Int. J. Geomech., 13(6), 769-778.

Oh, W.T., Vanapalli, S.K. and Puppala, A.J. 2009. ‘Semi-empirical model for the prediction of modulus of elasticity for unsaturated soils.’ Can. Geotech. J., 46 (8), 903-914.

Pradel, D., and Raad, G. 1993. ‘Effect of permeability on surficial stability of homogeneous slopes.’ J. Geotech. Eng., 119(2), 315-332.

Qi, S. and Vanapalli, S.K. 2015a. ‘Hydro-mechanical coupling effect on surficial layer stability of unsaturated expansive soil slopes.’ Comput. Geotech., 70, 68-82.

Qi, S., and Vanapalli, S.K. 2015b. ‘Stability analysis of an expansive clay slope: a case study of infiltration-induced shallow failure of an embankment in Regina, Canada.’ Int. J. Georesources Environ., 1(1), 1-1.

Rahardjo, H., Ong, T.H., Rezaur, R.B. and Leong, E.C. 2007. ‘Factors controlling instability of homogeneous soil slopes under rainfall.’ J. Geotech. Geoenviron. Eng., 133(12), 1532-1543.

Ravichandran, N., Vickneswaran, T., Marathe, S. and Jella, V.S., 2021. ‘Numerical analysis of settlement response of shallow footing subjected to heavy rainfall and flood events.’ Int. J. Geosci., 12(2), 138-158. https://doi.org/10.4236/ijg.2021.122009.

Richards, L. A. 1931. ‘Capillary conduction of liquids through porous mediums.’ Physics, 1(5), 318-333.

Sarker, D. and Wang, J.X. 2022. ‘Moisture influence on structural responses of pavement on expansive soils.’ Transp. Geotech., 35, 100773.

Satyanaga, A., Bairakhmetov, N., Kim, J.R. and Moon, S.W. 2022. ‘Role of bimodal water retention curve on the unsaturated shear strength.’ Applied Sciences, 12(3), 1266.

Satyanaga, A. and Rahardjo, H. 2019. ‘Unsaturated shear strength of soil with bimodal soil-water characteristic curve.’ Géotechnique, 69(9), 828-832.

Sauer, E.K. 1975. ‘Urban fringe development and slope instability in southern Saskatchewan.’ Can. Geotech. J., 12(1), 106-118.

Shuai, F. 1998. ‘Simulation of swelling pressure measurements on expansive soils.’ Doctor of Philosophy thesis.

Sun, D. A., Wang, L. and Li, L. 2019. ‘Stability of unsaturated soil slopes with cracks under steady-infiltration conditions.’ Int. J. Geomech., 19(6), 04019044.

Tan, M., and Vanapalli, S.K. 2021. ‘Performance estimation of a shallow foundation on an unsaturated expansive soil slope subjected to rainfall infiltration.’ In MATEC Web of Conferences (Vol. 337, p. 03009). EDP Sciences.

Tan, M. and Vanapalli, S.K. 2022. ‘Foundation bearing capacity estimation on unsaturated soil slope under transient flow condition using slip line method.’ Comput. Geotech., 148, 104804.

Tan, M. and Vanapalli, S.K. 2023. ‘Failure envelops for foundation subjected to inclined and eccentric loading considering steady state and transient flow conditions in unsaturated soils. Comput. Geotech., 157, 105315.

Tan, M., Li, Y., Yi, P., and Liu, J. 2022. ‘Vertical Bearing Capacity of Foundations with Large Embedment Depth in Normally Consolidated Clay.’ J. Geotech. Geoenviron. Eng., 148(11), 06022012.

Vahedifard, F. and Robinson, J.D. 2016. ‘Unified method for estimating the ultimate bearing capacity of shallow foundations in variably saturated soils under steady flow.’ J. Geotech. Geoenviron. Eng., 142(4), 04015095.

Vanapalli, S.K. and Mohamed, F.M. 2007. ‘Bearing capacity of model footings in unsaturated soils.’ In Experimental Unsaturated Soil Mechanics, 483-493. Springer, Berlin, Heidelberg.

Vanapalli, S.K. and Oh, W.T. 2010. ‘A model for predicting the modulus of elasticity of unsaturated soils using the soil-water characteristic curve.’ Int. J. Geotech. Eng., 4(4), 425-433.

Vanapalli, S.K., Fredlund, D.G., Pufahl, D.E. and Clifton, A.W. 1996. ‘Model for the prediction of shear strength with respect to soil suction.’ Can. Geotech. J. 33 (3), 379-392.

Wang, W., Wang, L., Miao, Y., Cheng, C., and Chen, S. 2020. ‘A survey on the influence of intense rainfall induced by climate warming on operation safety and service life of urban asphalt pavement.’ J. Infrastruct. Preserv. Resilience, 1(1), 1-14.

Wates, J.A., and Fourie, A.B. 1993. ‘Surficial stability of embankments: a case history.’ J. S. Afr. Inst. Civ. Eng., 35(1), 1-8.

Widger, R.A. and D.G. Fredlund, 1978. ‘Stability of swelling clay embankments.’ Can. Geotech. J., 16(1): 140 – 151.

Wu, L.Z., Huang, R.Q., Xu, Q., Zhang, L.M. and Li, H.L. 2015. ‘Analysis of physical testing of rainfall-induced soil slope failures.’ Environ. Earth Sci., 73, 8519-8531.

Xu, Y. 2004. ‘Bearing capacity of unsaturated expansive soils.’ Geotech. Geol. Eng., 22, 611-625.

Xu, Y.F., Fu, D. and Zhang, G.J. 2020. ‘On the bearing capacity of an unsaturated expansive soil basement.’ In Unsaturated Soils for Asia (pp. 763-767). CRC Press.

Yenes, M., Nespereira, J., Blanco, J. A., Suárez, M., Monterrubio, S. and Iglesias, C. 2012. ‘Shallow foundations on expansive soils: a case study of the El Viso Geotechnical Unit, Salamanca, Spain. Bull.’ Eng. Geol. Environ., 71, 51-59.

Yoshida, R.T., Fredlund, D.G. and Hamilton, J.J. 1983. ‘The prediction of total heave of a slab-on-grade floor on Regina clay.’ Can. Geotech. J., 20 (1), 69-81.

Zhang, L. and Chen, Q. 2005. ‘Predicting bimodal soil–water characteristic curves.’ J. Geotech. Geoenviron., 131(5), 666-670.

Zhang, J., Zhu, D. and Zhang, S. 2020. ‘Shallow slope stability evolution during rainwater infiltration considering soil cracking state.’ Comput. Geotech., 117, 103285.

CHAPTER 6

Numerical studies on foundation behavior in unsaturated soils subjected to vertical and inclined and eccentric loading

6.1 Introduction

Foundations are widely used in geotechnical engineering practice applications to provide support to different types of loads from the superstructure. For example, foundations of various structures such as the dams, retaining walls, bridges, and transmission towers are subjected to different combination of loadings. Many researchers investigated the combined effects such as the inclined and eccentric loads both for onshore and offshore structures extending the principles of saturated soil mechanics (Martin 1994, Gourvenec and Randolph, 2003; Krabbenhoft et al., 2012, 2014; Vulpe et al., 2014; Mehravar 2016; Ganesh et al., 2017; Fathipour et al., 2022a; Hosseini et al. 2023). However, soil above the natural groundwater level which is typically at a greater depth in semi-arid and arid regions is typically in a state of unsaturated condition. In addition, soil conditions in this unsaturated zone fluctuate due to the influence of hydrological events such as the rainfall, snow melt and water evaporation. In other words, the matric suction which is an independent stress state variable required for rational interpretation of unsaturated soils is sensitive to the changes in water content and has a significant influence on the flow behavior. In addition, the soil shear strength and volume change behavior are also influenced due to water content changes. As a result, the bearing capacity and the settlement of the foundation are also influenced by the water flow behavior in unsaturated soils. Therefore, a comprehensive understanding of the shallow foundation behavior is required considering the influence of flow behavior in unsaturated soils.

In recent years, a few researchers (Wuttke et al., 2013; Jin et al., 2021; Afsharpour et al., 2022, Fathipour et al., 2022b, 2023, Tan and Vanapalli, 2023) investigated the foundation behavior under the combined loading (i.e., inclined and eccentric loadings) on different soils that are in a state of unsaturated condition. Most of these studies focus only on the influence of matric suction considering homogeneous soil conditions. Typically, soils are heterogeneous, and their properties are spatially variable due to geomorphological and geological processes such as the sedimentation, the soil weathering, and the soil mineral components variation (Cho 2012, Jiang et al. 2014, Ng et al. 2022). Several investigators (Srivastava et al. 2010, Cho 2012, 2014, Zhu et al. 2013, Jiang et al. 2014, Gholampour and Johari, 2019, Liao and Ji, 2021, Gu et al., 2023) have investigated the influence of the spatial variability in unsaturated soils for geotechnical problems such as the slope stability subjected to rainfall infiltration. However, only a few studies have been reported in the literature (Le et al. 2013, 2019, Tan et al. 2017, 2020, Ravichandran et al. 2017, Fei et al. 2021, Mahmoudabadi and Ravichandran, 2023) that are related to the behavior of shallow foundations considering the spatial variation of soil properties associated with flow conditions in unsaturated soils. Most of these studies focus on the behavior of foundations in homogeneous soils that are subjected to vertical loading only. To the best of the authors' knowledge there are no studies in literature that have investigated the foundations behavior under combined (i.e., inclined and eccentric) loading taking account the soil spatial variability and the unsaturated flow conditions.

For this reason, the focus of this Chapter is directed towards analyzing the foundation behavior subjected to combined loading considering different scenarios of flow conditions in unsaturated soils in addition to considering spatial variability of soil properties. Investigations based on laboratory or field studies can be extremely time consuming and expensive; in addition, reliable interpretation is not possible to control and consider the influence of many factors from field studies. Besides, investigations by analytical methods are typically based on several assumptions or simplifications. Due to this reason, finite element methods are widely used for the investigation of the foundation behavior under combined loading (Taiebat and Carter 2000; Gourvenec and Randolph 2003; Gourvenec and Mana 2011; Shen et al. 2017). Moreover, it is easier to interpret the failure mechanisms from visual contours that are generated from numerical modeling studies. Therefore, in this Chapter, the finite element (FE) analyses were performed to provide a better understanding of the problem with the aid of the commercial ABAQUS software. A subroutine USDFLD is developed and called into the ABAQUS software to incorporate the variation of the soil properties with respect to matric suction into the FE model. The spatial variability of the soil properties is characterized by applying the random fields that is consistent with other published studies from the literature (Cho 2012, 2014, Zhu and Zhang, 2013, Liao and Ji, 2021, Ng et al. 2022). Fig. 6.1 summarizes how the USDFLD and soil spatial variability are considered in the numerical analysis in this study. Code is developed with the midpoint method based on the Cholesky decomposition technique for generating the random field in the MATLAB. In addition, Python script is written to incorporate the generated random field into the FE model that can be used in the analysis. The numerical results are first compared with the results obtained from the experimental and analytical studies for homogeneous soils. Comparisons are then made between the FE results obtained from FE models considering the soil spatial variability for heterogeneous soils and homogeneous soils.

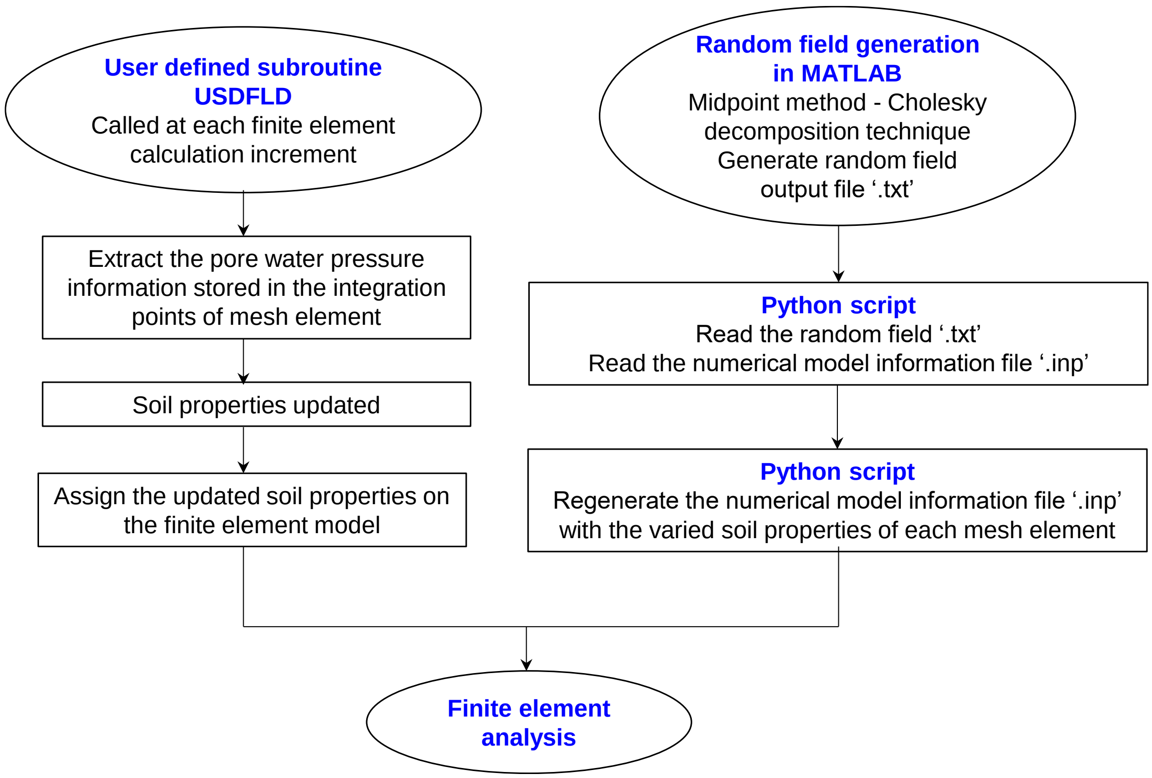

Fig. 6.1 Flow chart of developed USDFLD and the random field generation

6.2 Methodology

The failure envelope method is widely used for the investigation of the foundation behavior in saturated soils subjected to combined loading (e.g., Gottardi and Butterfield, 1993, Gouvenec and Randolph 2003, Taiebat and Carter 2000, 2002; Pham et al. 2019, 2020, 2022, Liu et al. 2023). In this method, the failure envelope is developed for foundation subjected to the inclined loading in the vertical (V) and horizontal loading (H) space and for eccentric loading in the vertical and moment loading (M) space. The foundation is unsafe if the combined loading value is located outside the failure envelop. In this section, the FE model details combined with the failure envelop methods will be first illustrated followed by the realization of the soil spatial variability in the model. Later, details related to the numerical procedure framework based on the user developed subroutine USDFLD will be presented.

6.2.1 Finite element model details

Small-strain finite element plane strain model was developed as shown in Fig. 6.2 to simulate the foundation located on the unsaturated soil subjected to combined loading. The foundation was simulated as a rigid body. The horizontal distance from the foundation edge to the soil domain external boundary was prescribed as 4*B* based on preliminary numerical investigations; based on these studies it was found that the distance is sufficiently remote and has no influence on the results associated with the foundation behavior or soil response. The foundation and soil interface surface pairs were defined to simulate the interaction between the foundation and the soil. Hard contact was defined for the normal interface behavior; while for the tangential interface behavior, the interface friction angle was assumed to be equal to the soil effective internal friction angle, ϕ'.

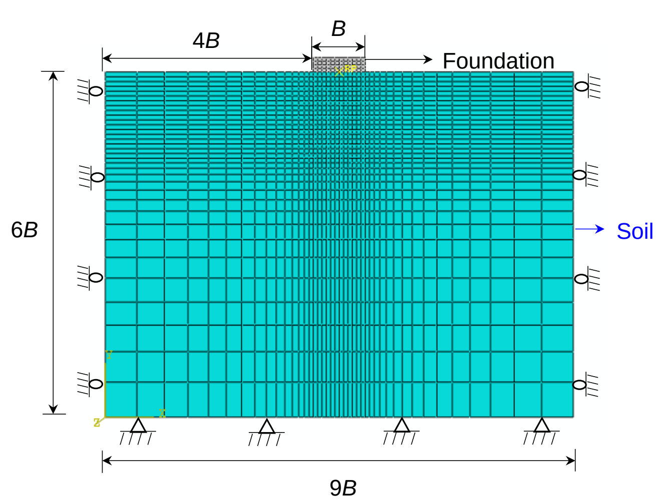

Fig. 6.2 Details of the numerical model

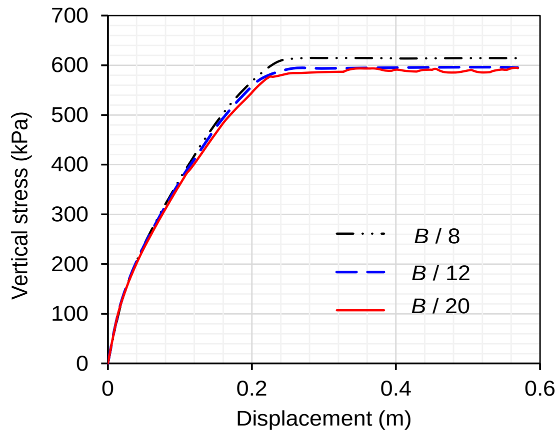

Fig. 6.3 Mesh sensitivity results

The soil was represented as an elastic-perfectly plastic material following the modified Mohr-Coulomb (M-C) model considering the influence of matric suction. The relationship between the soil shear strength and stiffness with matric suction were based on Eq. (6.1) and Eq. (6.2), respectively.

$$\tau = c' + (\sigma_{\mathrm{n}} - u_{\mathrm{a}}) \tan \phi' + (u_{\mathrm{a}} - u_{\mathrm{w}}) S_{\mathrm{e}} \tan \phi' \tag{6.1}$$

$$E_{\mathrm{unsat}} = E_{\mathrm{sat}} \left[1 + \alpha_E \frac{(u_{\mathrm{a}} - u_{\mathrm{w}})}{P_{\mathrm{a}} / 101.3} \left(S^{\beta} \right) \right] \tag{6.2}$$

where E_{unsat} and E_{sat} are the modulus of elasticity for unsaturated soil and saturated soil, respectively. α_{E} and β are respectively the fitting parameters that are related to the soil types and plasticity index (Oh et al. 2009). The above relationship was achieved through user subroutine USDFLD. Code has been developed in the subroutine and is called into the ABAQUS to incorporate the contribution of the matric suction (or pore water pressure) in the soil properties into the finite element model. Details of the USDFLD procedure will be illustrated along with the implemented numerical framework in a later section of this Chapter. In ABAQUS, the ratio of the unsaturated soil hydraulic conductivity over the saturated soil hydraulic conductivity (i.e., $k_r = k / k_s$, k and k_s are the soil hydraulic conductivity for unsaturated soil and saturated soil, respectively) along with the degree of saturation information must be provided. Such a relationship can be expressed by different models such as the Gardner's model (1958) and the macroscopic models (Averjanov 1950, Yuster 1951, Irmay 1954, 1971, Mualem 1986) as shown in Eq. (6.3) and Eq. (6.4), respectively.

$$k = k_s e^{-\alpha\psi} \tag{6.3}$$

$$k_r = S_e{}^P \tag{6.4}$$

where a represents for the soil water characteristic curve (SWCC) reduction rate (Zhan and Ng, 2004). Ψ noted as the suction head. P is a constant and is set as 3 by default in ABAQUS, which is also supported by the experiment results by Irmay (1971). There are several models that can be used in the numerical analysis (e.g., van Genuchten, 1980; Fredlund and Xing, 1994); however, Gardner's (1958) model is used in the present study because of its simplicity and to make it possible for the comparison between the numerical methods and analytical methods that are typically proposed based on the model.

The CPE4H mesh (4-node plane strain quadrilateral, bilinear displacement, bilinear pore pressure, hybrid constant pressure element) was generated in the model. This type of mesh is typically used for investigating the hydro-mechanical behavior of soils. Mesh refinement was undertaken (see Fig. 6.2) near the foundation edge to ensure reasonable results. A minimum mesh size of $B/12$ was set based on the mesh sensitivity analysis results which is shown in Fig. 6.3. A linear increase in the pore water pressure distribution is set at the lateral boundaries below the ground water table. The bottom boundary and the lateral boundary above the ground water table is set as default as zero flux boundary following the published literature (Qi and Vanapalli 2015, Wu et al. 2017, Tan and Vanapalli 2021). This boundary setting is reasonable since it is far from the foundation; the lateral flow at the lateral boundary has little or no influence on the vertical flow behavior at the shallow surface soil near the foundation. Mesh nodes around the lateral boundaries were constrained with roller supports to restrain the out-of-plane displacement. The bottom boundary was fixed. No flow boundary is set on the soil boundary beneath the foundation and the rainfall influx boundary is set along the upper soil boundary when considering the infiltration conditions.

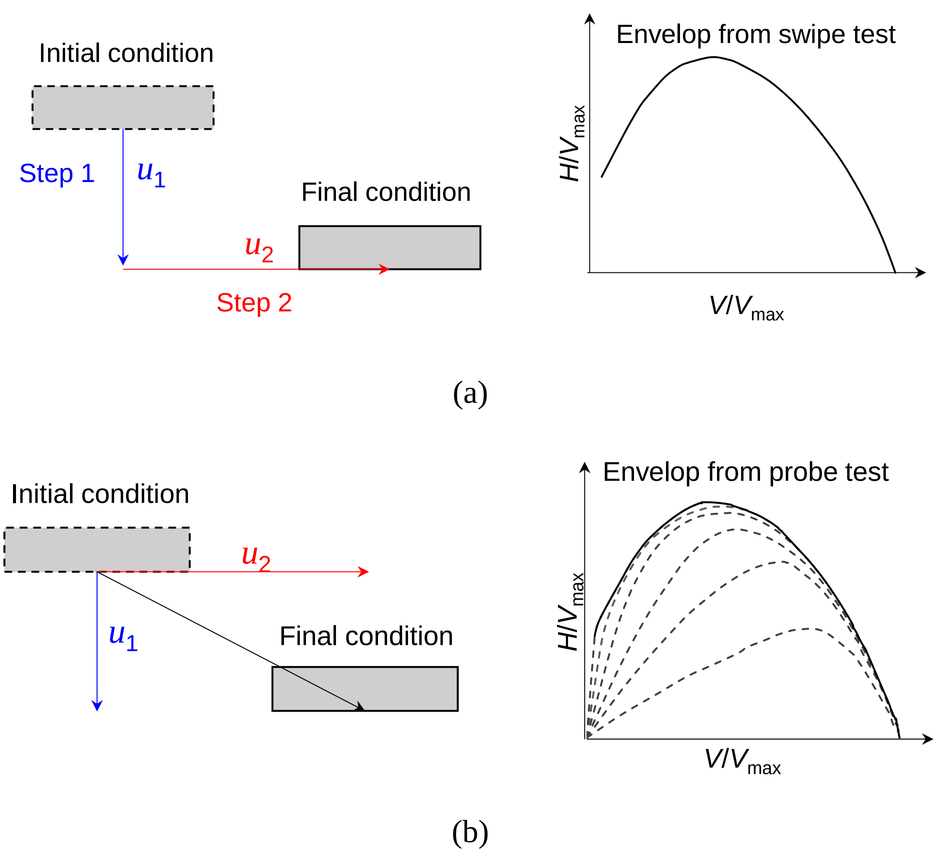

Fig. 6.4 Loading paths and failure envelopes: (a) Swipe test; (b) Probe test

The failure envelopes are typically investigated by the 'swipe' test and the 'probe' test shown in Fig. 6.4. These two types of tests are based on the displacement control in the FE analyses. The swipe test allows the foundation to firstly achieve the ultimate load in one direction (e.g., vertical direction) with a given displacement u_1, then u_1 is held constant and displacement u_2 is subsequently imposed on the foundation in the second direction until the corresponding bearing capacity is achieved as shown in Fig. 6.4a. The failure envelop in the loading space can be obtained by a single swipe test (Gourvenec and Randolph 2003). The probe test keeps the ratio of the displacements in the two directions constant until there is no more variation in stress with further displacement. One point located on the failure envelope is obtained for one displacement ratio. The entire failure envelope can be obtained by changing different displacement ratio as illustrated in Fig. 6.4b. The approach used in the literature is based on failure envelop normalization technique such that the results are presented in an independent manner without the influence of parameters such as the foundation width (Tang et al. 2015). In this study, the failure envelop is normalized with the ultimate vertical bearing capacity V_{max}. The normalized vertical, horizontal and moment loading can be expressed as V / V_{max}, H / V_{max} and M / BV_{max} with foundation width for dimensional homogeneity.

6.2.2 Soil spatial variability

The soil in nature is typically heterogeneous, and the soil properties are spatially variable which are often characterized by the random field. The random field generation can be simulated by discretization techniques such as the midpoint method, the Karhunen – Loeve (K-L) expansion method and the spatial average method. The midpoint method based on the Cholesky decomposition technique is used in this study because it is simple to implement; this approach has also been used by many scholars for the discretization of the random fields (Srivastava et al. 2010, Li et al. 2015, Liu et al. 2017).

In this Chapter, the effective shear strength parameters of the saturated soils and the saturated hydraulic conductivity are assumed to be log-normally distributed based on the published studies and field investigation reports (Ali et al. 2014, Jiang et al. 2014). The log-normal assumption is considered reasonable as the soil properties are not negative (Griffiths and Fenton, 2007). The soil properties can be characterized statistically by a mean, μ and a standard deviation, σ or the coefficient of variation (COV) which represents the ratio of the σ to the μ. A cross-correlated non-Gaussian random field can be generated to consider the soil properties autocorrelation and cross-correlation.

The autocorrelation function (ACF) describes the soil properties autocorrelation extent between soil at two different positions in the space within the framework of random field (Vanmarcke 1983, Jiang et al. 2014). There are several widely used ACFs; for example, the single exponential, the squared exponential, the cosine exponential, and binary noise ACFs. The single exponential ACF shown as Eq. (6.5) is used in this study because it is simple and widely used in the investigation of various geotechnical problems (Griffiths and Fenton 2004, Cho 2012, 2014, Li et al. 2014, 2015):

$$\rho\left(\tau_{\mathrm{x}},\tau_{\mathrm{y}}\right)=\exp\left[-2\left(\frac{\tau_{\mathrm{x}}}{\delta_{\mathrm{h}}}+\frac{\tau_{\mathrm{y}}}{\delta_{\mathrm{v}}}\right)\right] \tag{6.5}$$

where the scale of fluctuations, δ_{h}, δ_{v} respectively represent the spatial fluctuation range in the horizontal and vertical direction of soil properties that showing the highly correlation, which is twice the autocorrelation distance. (Phoon and Kulhawy 1999, Jiang et al. 2014). τ_{x} and τ_{y} are respectively describe the absolute horizontal and vertical distances between the two random field elements centroid point coordinates (x_{i}, y_i) and (x_{j}, y_{j}), $\tau_{\mathrm{x}} = |\, x_{\mathrm{i}} - x_{\mathrm{j}} \,|$, τ_{y}

$= | y_i - y_j |$, i and j represent the random field element numbers. An autocorrelation matrix $\boldsymbol{A}$ can be generated based on the random field elements as shown in Eq. (6.6):

$$\boldsymbol{A} = \begin{bmatrix} 1 & \rho\left(\tau_{x12}, \tau_{y12}\right) & \cdots & \rho\left(\tau_{x1n}, \tau_{y1n}\right) \\ \rho\left(\tau_{x21}, \tau_{y21}\right) & 1 & \cdots & \rho\left(\tau_{x2n}, \tau_{y2n}\right) \\ \vdots & \vdots & \ddots & \vdots \\ \rho\left(\tau_{xn1}, \tau_{yn1}\right) & \rho\left(\tau_{xn2}, \tau_{yn2}\right) & \cdots & 1 \end{bmatrix} \tag{6.6}$$

A cross-correlation matric $\boldsymbol{R} = (\rho_{q,l})_{m\times m}$ can be supposed with m represented the number of random fields and $\rho_{q,l}$ represented the cross-correlation coefficient. The cross-correlation between different soil properties is not considered in this study to focus only on the influence of the independent soil properties spatial variability. The Cholesky decomposition algorithm can be used to factor the two matrices, $\boldsymbol{A}$ and $\boldsymbol{R}$, to obtain the lower triangular matrices $\boldsymbol{L_1}$ and $\boldsymbol{L_2}$, respectively:

$$\boldsymbol{L}_1 \boldsymbol{L}_1^T = \boldsymbol{A} \tag{6.7}$$

$$\boldsymbol{L}_2 \boldsymbol{L}_2^T = \boldsymbol{R} \tag{6.8}$$

Then the cross-correlated standard Gaussian random fields $\boldsymbol{H}^{CG}(x, y)$ can be obtained as Eq. (6.9),

$$\boldsymbol{H}^{CG}(x, y) = \boldsymbol{L}_1 \boldsymbol{\xi} \boldsymbol{L}_2^T \tag{6.9}$$

where ξ is an independent standard normal sample matrix which can be obtained by the Latin hypercube sampling method; CG is the cross-correlated standard Gaussian random fields. Then the cross-correlated non-Gaussian random fields can be obtained as Eq. (6.10) by an isoprobabilistic transformation (Li et al. 2011):

$$\boldsymbol{H}(x, y) = G^{-1}\left\{\Phi\left[\boldsymbol{H}^{CG}(x, y)\right]\right\} \tag{6.10}$$

where G^{-1} represents the inverse function of marginal cumulative distribution of the non-Gaussian vector random field. Φ denotes the standard Gaussian cumulative distribution function.

6.2.3 Numerical modeling framework

The step-by-step procedure of the numerical modeling framework is explained in this section with the aid of flow chart shown in Fig. 6.5. The first step is to build the FE model based on the model details discussed earlier. A steady state analysis is then performed as a next step to obtain the initial stress and pore water pressure distribution based on the ground water table and the gravity of the soil. The obtained soil stress and pore water pressure are then incorporated into the model to conduct the geostatic analysis with the application of the gravity on both soil and the foundation. The model now is ready to investigate the influence of the unsaturated flow and the foundation bearing capacity analysis. For hydrostatic case, the displacement control for obtaining the foundation bearing capacity will be applied directly after the geostatic step. For the case considered the steady state or transient flow, the displacement control step will be applied after the water infiltration simulation.

The developed user subroutine USDFLD discussed in earlier sections is loaded with modeling input file prior to initiating the calculations. The key details of the subroutine USDFLD and its working procedure is summarized below:

(i) The developed subroutine USDFLD will be called at the beginning of every calculation increment (i.e., at the end of the previous increment) for updating the soil properties.

(ii) The developed code is capable to extract the pore water pressure information, which is stored in the integration points of CPE4H mesh. As a next step, the soil properties can be updated based on Eqs. (6.1) and (6.2) using the obtained pore water pressure from the previous calculation increment.

(iii) The updated soil properties from step (ii) will then be assigned on the finite element model for the next calculation increment.

(iv) Step (i) to (iii) will be repeated until the calculation is terminated.

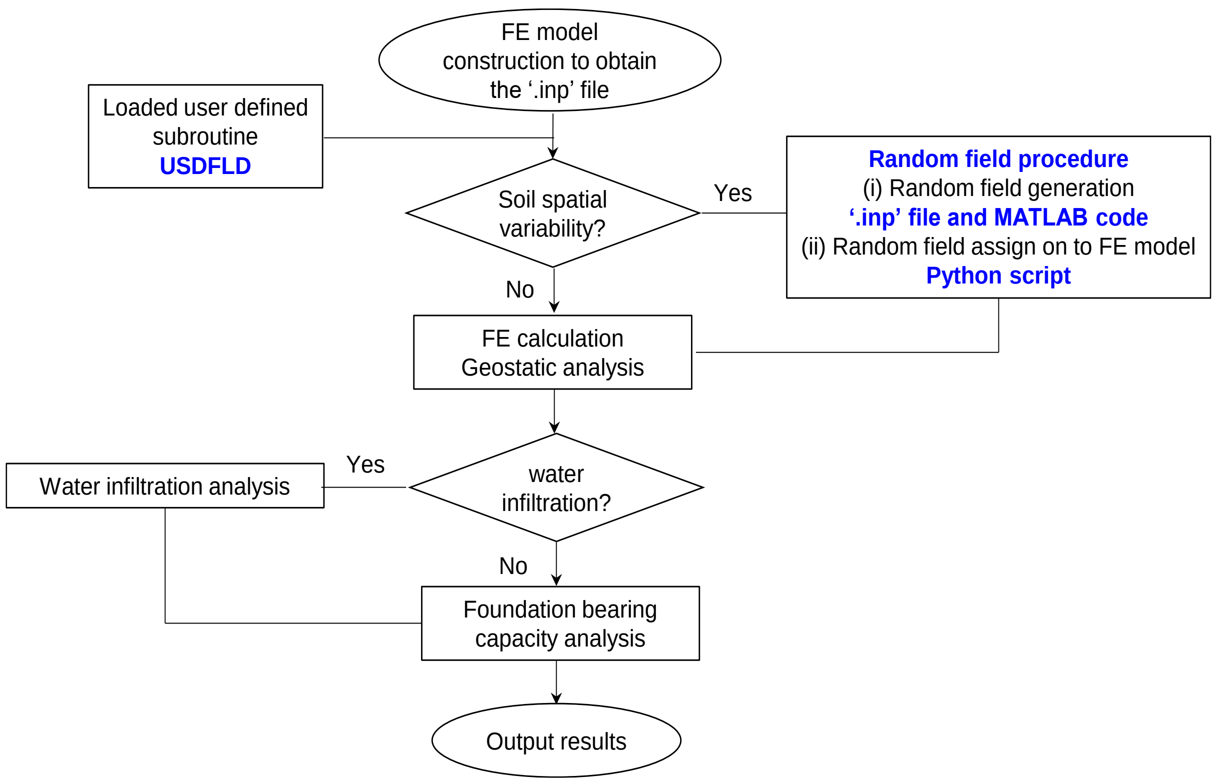

Fig. 6.5 Flow chat of the numerical modeling framework

The random field generation code and python procedure are also developed for incorporating the spatially variable soil properties into the model and performing the FE modeling. The random field generation code is developed with the aid of MATLAB to extract the mesh elements and elements numbers of the FE model that facilitate in the random field generation. The midpoint method based on the Cholesky decomposition technique discussed earlier is involved in the developed code as a next step to generate the random field based on the obtained elements. The obtained elements with the corresponding random value of the soil properties will then be stored in a file that will be called by the developed code interpreted by Python. ABAQUS provides a Python interface which make it efficient to customize the calculation requirements with Python script. The developed Python script will assign the spatial variable properties onto the FE model to replace the original homogeneous soil properties. The FE analysis is then conducted with the initial stress calculation, the geostatic analysis, the infiltration simulation, and foundation bearing capacity analysis.

6.3 Comparison studies for foundations on homogeneous soils

Comparison studies are summarized in this section between the results obtained from the performed numerical study and that from experimental data, the slip line method and the semi-empirical equations. First, results from the FE analysis for foundation subjected to vertical loading under hydrostatic state are compared with a physical model test conducted by Shwan (2015). The results obtained from the FE analysis for the foundation subjected to combined loading are used to provide comparisons with the other methods.

6.3.1. Comparison study I

Shwan (2015) conducted physical model tests for a steel strip footing on a commercial fine sand from the David Ball Group, UK. The strip footing dimension used in their study is 25 mm × 15 mm×138 mm (width × thickness × length) is placed on the surface of fine sand sample with an average particle size of 0.18 mm. The sand is placed in a chamber with dimensions of 140 mm × 400 mm (length × width) with glass side walls. In this physical model test approximate plane strain conditions are achieved due to the reduced friction of the glass walls (see Fig. 6.6a). A layer of porous plastic was placed at the bottom of the chamber that was covered with a thin layer of silt such that suction is transmitted smoothly. The matric suction in the soil placed in the test chamber is controlled by extending the hanging water column technique as shown in Fig. 6.6a. More details about the suction control method are available in Shwan (2015). The model footing test is conducted using a loading piston with a constant displacement rate of 0.6 mm/min. The test terminated when the load that is monitored by a loading cell has limited change with the settlement. The numerical model that is based on the model details summarized earlier is set up for comparison with the experiment and is shown in Fig. 6.6b.

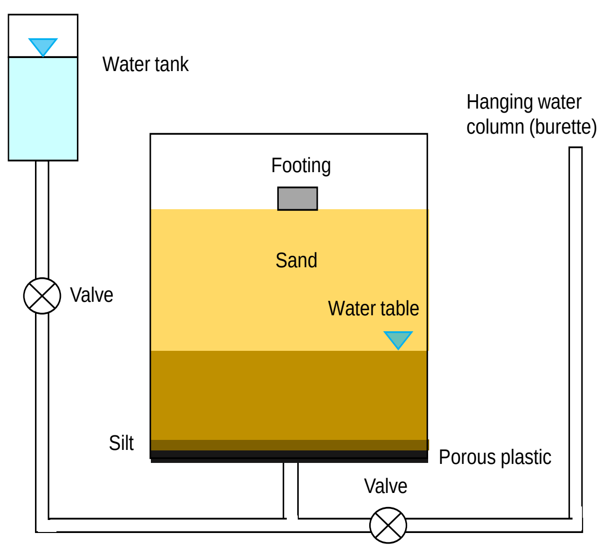

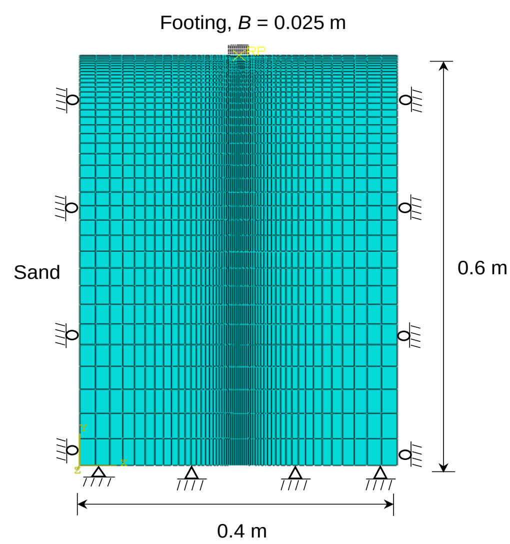

Fig. 6.6 Strip footing model test setup and the corresponding numerical model: (a) Test rig; (b) Numerical model

The SWCC was obtained from the hanging column technique and is shown in Fig. 6.7. The sand properties are presented in Table 6.1. The relationship between the soil hydraulic conductivity and matric suction is assumed based on Eq. (6.4) with p equal 3. The fitting parameters for the estimation of elastic modulus for unsaturated soil is based on the suggestion provided by Oh et al. (2009). The saturated elastic modulus is estimated from experimental data of the stress and displacement curve. It should be noted that a small value of cohesion must be assumed in the numerical model in ABAQUS by using the Mohr-Colomb model. Shwan (2015) provided comprehensive discussions about the bearing capacity determined from experimental results and that from the discontinuity layout optimization procedure. The results show that a cohesion value of 2 kPa and 3 kPa provides good comparison results for GWT = 0.2m, GWT = 0.55m, respectively. Therefore, the 2 kPa and 3 kPa are used in the numerical model for comparison purposes.

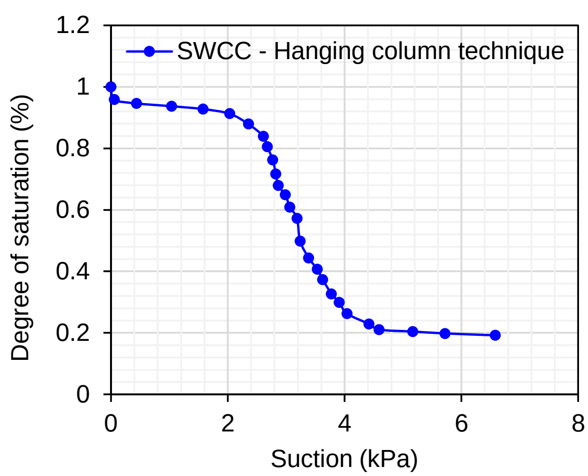

Fig. 6.7 SWCC for the sand used in the numerical model

Two different ground water tables (GWT) (i.e., H_w = 0.2m and H_w = 0.55m) are considered for providing comparison studies. The comparison results between the FE analysis and the experimental study are shown in Fig. 6.8. Good agreement is found for the stress and settlement curves for both conditions. The bearing capacity value is the measured stress value that has no significant variation with the increasing settlement.

Table 6.1 Soil properties for the sand

Properties	Sand
Specific gravity, G_s	2.65
Effective cohesion, c'	0
Effective internal friction angle, ϕ' (°)	36.8
Dry unit weight, γ_{dry} (kN/m^3)	15.3
Saturated soil elastic modulus, E_{sat} (kPa)	8000
Fitting parameter for E_{unsat}, α_E	1.5
Fitting parameter for E_{unsat}, β	0.8
Saturated hydraulic conductivity, k_s (m/s)	1.0×10^{-5}

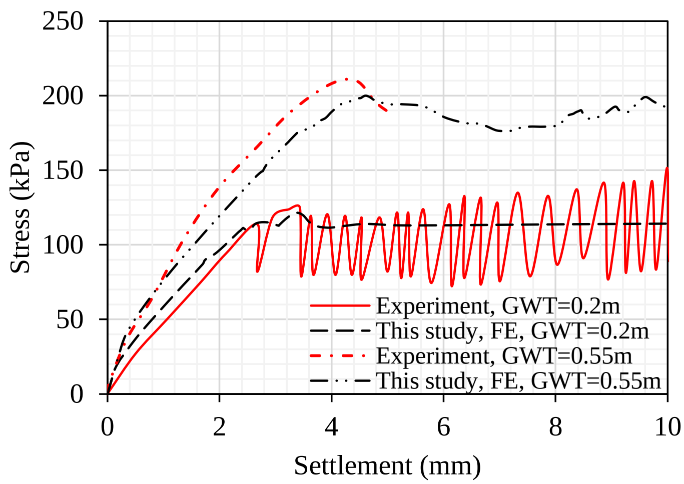

Fig. 6.8 Comparison results between the FE analysis and the experimental study

6.3.2 Comparison study II

Foundation subjected to inclined and eccentric loading is analyzed in this section using the problem illustrated in Fig. 6.9. Comparison is made between the bearing capacity failure envelop obtained from the FE analysis, the slip line method and the semi-empirical equations proposed by Tan and Vanapalli (2023). The numerical model that is comprehensively described is shown in Fig. 6.2. It should be noted that the foundation and soil interface is considered rough that facilitate in providing a good comparison. Indian Head till is used for the comparison and the properties used in the numerical model are summarized in Table 6.2. The soil data that is used in present study is gathered from the published studies (Oh and Vanapalli 2018). The SWCC is shown in Fig. 6.10. Eq. (6.3) is used to estimate the relationship between k_r and the effective degree of saturation. The swipe test and probe test are both conducted for obtaining the failure envelopes in the $V – H$ loading space and $V – M$ loading space. The failure envelopes obtained under the hydrostatic condition and the transient infiltration with $q_{in} = 0.5 \times 10^{-7}$ m/s for 20 days are used for comparison purposes.

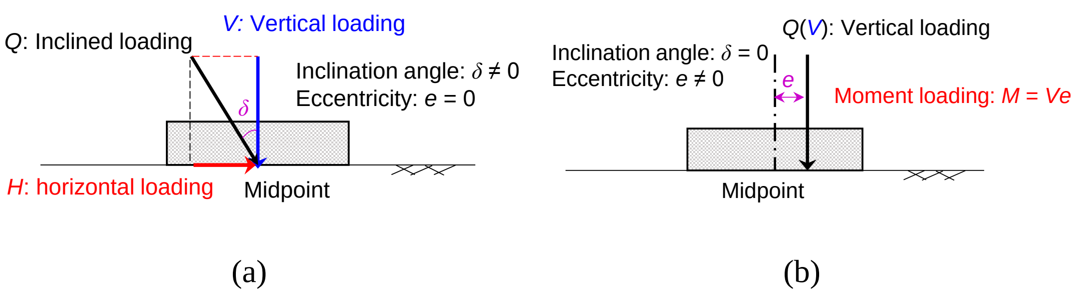

Fig. 6.9 Foundation subjected to inclined and eccentric loading: (a) Inclined loading; (b) Eccentric loading

Table 6.2 Soil properties used in the numerical model

Properties	Indian Head till
Specific gravity, G_s	2.71
Effective cohesion, c' (kPa)	9
Effective internal friction angle, ϕ' (°)	23
Dry unit weight, γ_{dry} (kN/m^3)	14.37
Saturated soil elastic modulus, E_{sat} (kPa)	7000
Fitting parameter for E_{unsat}, α_E	0.1
Fitting parameter for E_{unsat}, β	2
Saturated hydraulic conductivity, k_s (m/s)	1.0×10^{-7}

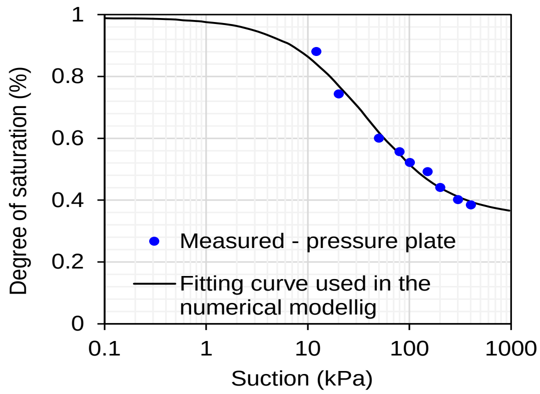

Fig. 6.10 SWCC of the Indian Head till

Fig. 6.11 shows the failure envelopes obtained by the FE analyses (Swipe test and Probe test), the slip line method and the semi-empirical equations proposed by Tan and Vanapalli (2023). The failure envelopes obtained from the slip line method and the equations located in between that obtained from the Swipe test and the Probe test in the $V-H$ loading space in Figs. 6.11a and 6.11c. This is because the failure envelopes obtained from the Swipe test is typically conservative as the elastic-plastic yielding that occurs within the failure locus and can be considered as the lower bound solution for the $V-H$ loading space (Gourvenec and Randolph 2003, Supachawarote et al. 2004). However, for the $V-M$ loading space, it can be seen the slip line method and the equation provide conservative results at higher eccentricity ratio (for example, $e / B > 0.3$ in Figs. 6.11b and 6.11d) compared to that obtained from the swipe test. This is due to the effective width method that is used for the bearing capacity calculation in the $V-M$ loading space in the slip line method and the semi-empirical equation in Tan and Vanapalli (2023). Results by Michalowski and You (1998) also suggest that the effective width rule method may underestimate the bearing capacity with a large eccentricity ratio. For cohesive-frictional soils, the underestimated bearing capacity value (i.e., deviation value) may decrease as the soil internal friction angle increases. Nevertheless, the results of the finite element method and other methods show relatively good agreement in Fig. 6.11.

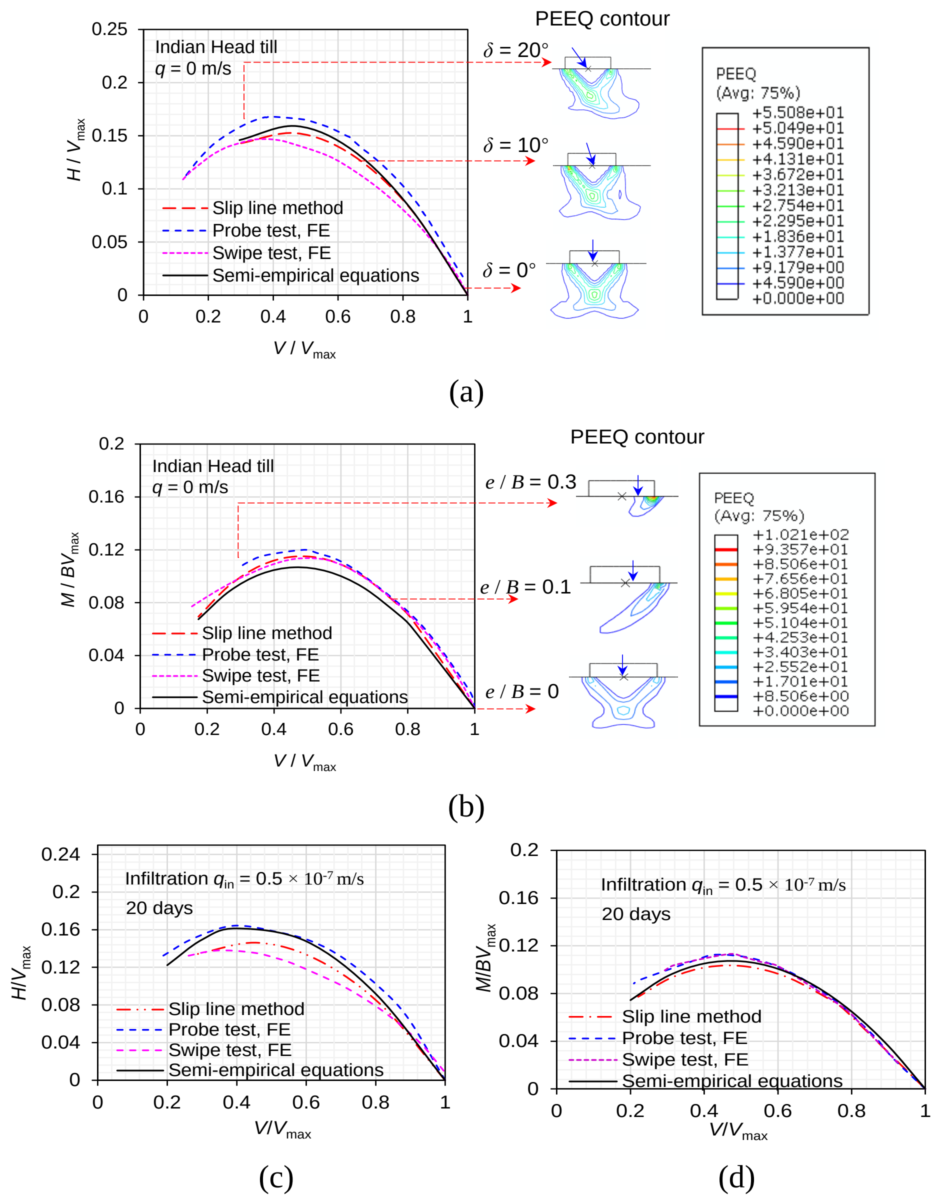

Fig. 6.11 Comparison of the failure envelope obtained from various methods: (a) *V*- *H* loading space for hydrostatic condition; (b) *V*- *M* loading space for hydrostatic condition; (c) *V*- *H* loading space for transient condition; (d) *V*- *M* loading space for transient condition.

The equivalent plastic strain (PEEQ) contour which shows the yielding zone is also shown in Figs. 6.11a and 6.11b to highlight the failure mechanism of the soil for different loading inclination angle and eccentricity values. The failure zone becomes shallower and smaller with an increase in the inclination angle and eccentricity ratio respectively in Fig. 6.11a and Fig. 6.11b, which is consistent with the trends observed in saturated soils (Pham et al. 2022). The sliding trend is observed as the inclination angle increases. The PEEQ contour in Fig. 6.11b shows that soil mobilized mostly at the right corner of the foundation edge with a higher eccentricity ratio. Influence of the inclination and the eccentricity loading under the infiltration condition on the failure mechanism have less difference compared to the hydrostatic condition for the above case.

6.4 Comparison studies for foundation on soil with spatial variable properties

Comparison studies are conducted between the bearing capacity failure envelop obtained from numerical model results with and without considering the soil spatial variability. The spatial variability associated with soil saturated hydraulic conductivity, k_s, soil saturated effective cohesion, c' and soil effective internal friction angle, ϕ' are considered for providing comparisons. For each soil parameter, two independent random fields examples were generated and are compared with the results without considering the random field. The soil parameters statistics are summarized in Table 6.3. The statistics (i.e., COV, δ_h, δ_v) in this study are determined based on the statistics' range provided in the published studies Cho (2012), Jiang et al. (2014) and Liu et al. (2017).

Table 6.3 Summary of soil properties statistics

Soil properties	Mean	COV	δ_h	δ_v
Effective cohesion, c' (kPa)	9	0.3	30	2
Effective internal friction angle, ϕ' (°)	23	0.2	30	2
Saturated hydraulic conductivity, k_s (m/s)	1×10^{-7}	1	20	0.5

6.4.1 Soil saturated hydraulic conductivity

Figs. 6.12 shows two examples of random fields generated for the soil saturated hydraulic conductivity. The random fields are generated based on the mid-point method with the Cholesky decomposition technique discussed earlier. The random fields were assigned to the FE model for evaluating the foundation behavior under the combined loading. A transient infiltration with $q_{in} = 5 \times 10^{-7}$ m/s for half day is considered in this section.

The pore water pressure distribution profiles after half a day of water infiltration are compared in Figs. 6.13b and 6.13c at two sections (see Fig. 6.13a). There are differences in the water pressure profiles obtained from the numerical model results with and without considering the hydraulic conductivity spatial variability. The results with respect to the variation of the normalized bearing capacity failure envelops in the $V – H$ loading space and $V – M$ loading space are not obvious as shown in Fig. 6.14. This is also supported by the equivalent plastics strain (PEEQ) contours which exhibits slight or negligible difference in the failure mechanisms. PEEQ value obtained from the model is higher when the soil spatial variability is considered in comparison to neglecting the soil spatial variability; relative deviation PEEQ values are 29.5% and 39.3% respectively for the $V – H$ loading space and $V – M$ loading space. One more possible reason for the slight differences in the failure envelopes than typically expected values may be associated with the rainfall intensity and duration. The pore water pressure variation below the foundation is not significant for the rainfall characteristics considered in this study. The rainfall characteristics in this Chapter are set considering the limitations associated the ABAQUS software that the run-off condition cannot be considered.

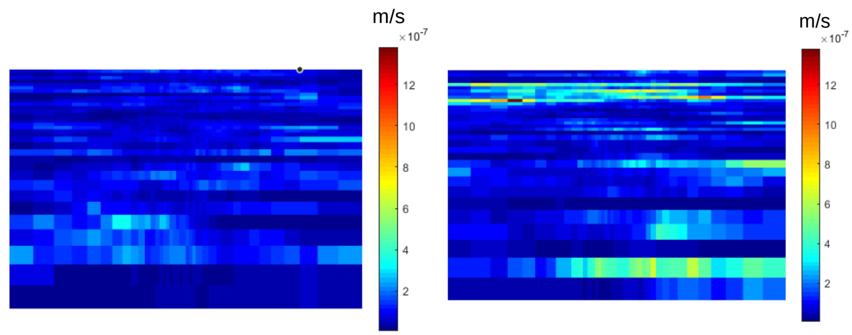

(a) (b)

Fig. 6.12 Random fields of k_s: (a) Random field 1; (b) Random field 2

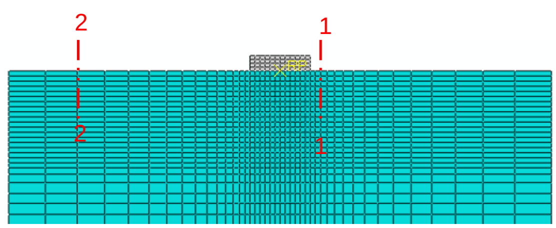

(a)

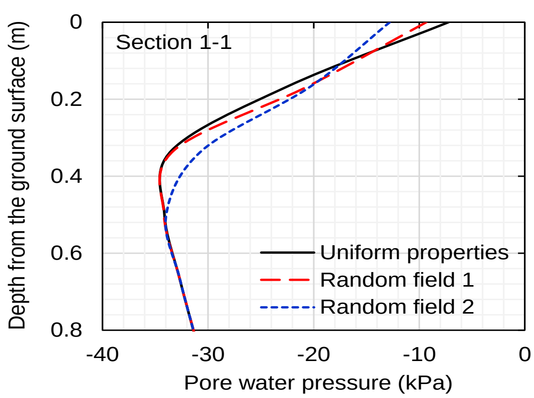

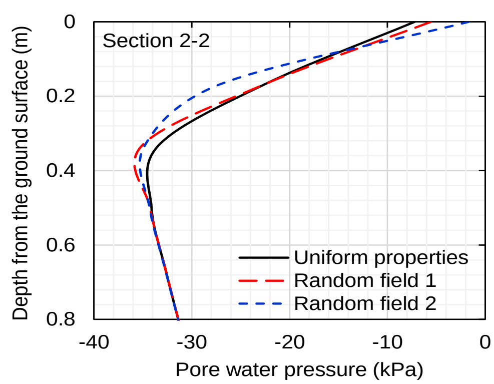

(b) (c)

Fig. 6.13 Results comparison: (a) Section diagram; (b) Pore water pressure profile at section 1-1; (c) Pore water pressure profile at section 2-2

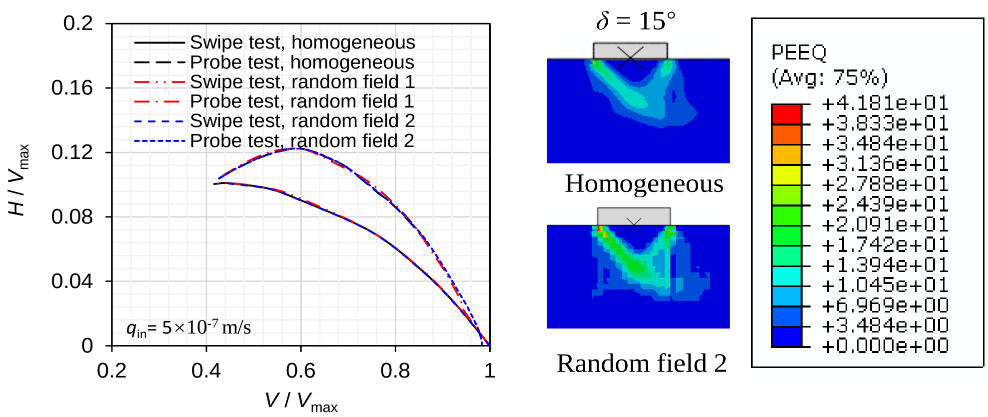

(a)

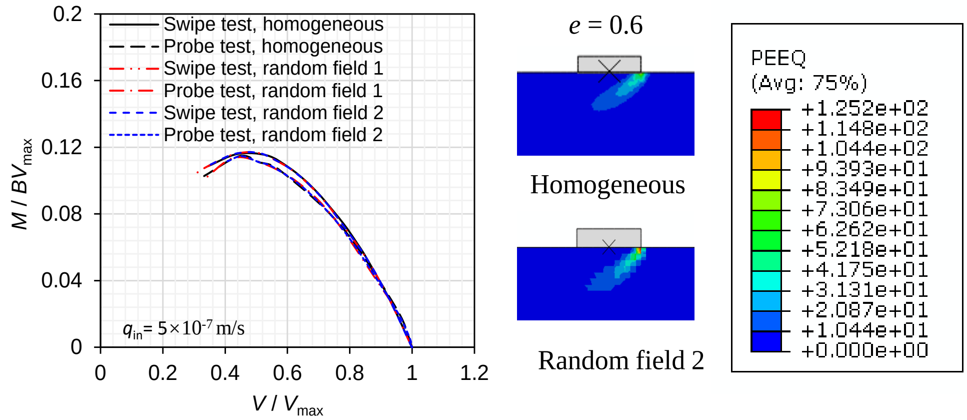

(b)

Fig. 6.14 Comparison of normalized failure envelopes: (a) Normalized failure envelopes in *V-H* loading space (b) Normalized failure envelopes in *V-M* loading space

The above summarized results are obtained based on the random fields that are limited to two. Different random fields can be generated with other assumed statistics (i.e., COV, δ_h, δ_v). Compared to large δ_h and δ_v, there will be less correlation between two values of the soil properties at different positions with a relatively lower δ_h and δ_v. Different random fields of the soil hydraulic conductivity results in significantly different pore water pressure distributions. Therefore, the deviations in the pore water profile or the normalized failure envelop may be influenced by different random field with various assumed statistics. This behavior can also be supported by a probability analysis study conducted by Cho (2014). In this study, Cho (2014) investigated the influence of the COV and the scale of fluctuations/autocorrelation distance on the probability of failure of slope subjected to rainfall. Results show that different combination of the COV and the autocorrelation distance will result in the difference of the slope critical failure surface range. For the autocorrelation distance that is higher than 4, the probability of failure of the slope will increase with an increase in the autocorrelation distance. However, for the autocorrelation distance that is lower than 4, the variation of the probability of failure are influenced by many parameters such as the COV, the infiltration duration. Therefore, probability analyses are proposed to be undertaken for investigating the foundation bearing capacity and the failure envelope subjected to rainfall infiltration with the varied statistics for generating the random fields. However, investigations and discussions related to probability studies are beyond the scope of the present study.

6.4.2 Soil effective cohesion and internal friction angle

The influence of the spatial variability of the effective shear strength parameters on the foundation behavior is also investigated. Fig. 6.15 shows the examples of the random fields of the soil saturated effective cohesion, c' and the effective internal friction angle, ϕ'. The foundation bearing capacity failure envelop obtained from the numerical model with and without considering the spatial variability of soil effective shear strength parameters are shown in Fig. 6.16. Significant differences can be observed in Fig. 6.16a and 6.16c for the failure envelopes in V – H loading space. These modeling results suggest the spatial variability of soil has a significant impact on foundations subjected to inclined loading; however, the deviation is comparatively less in the case of eccentric loading. The deviation of the failure envelopes is more obvious when the spatial variability of the effective internal friction angles is considered as shown in Fig. 6.16c and 6.16d compared to the effective cohesion (i.e., Fig. 6.16a and 6.16b). The maximum relative deviation is 18.2% at the maximum H/V_{max} value between the failure envelops obtained from the model considered random field 2 and that from the model with constant soil internal friction angle in Fig. 6.16c. This is also consistent with the conclusion reported by Tan and Vanapalli (2023) that the internal friction angle has significant influence on the foundation bearing capacity failure envelop.

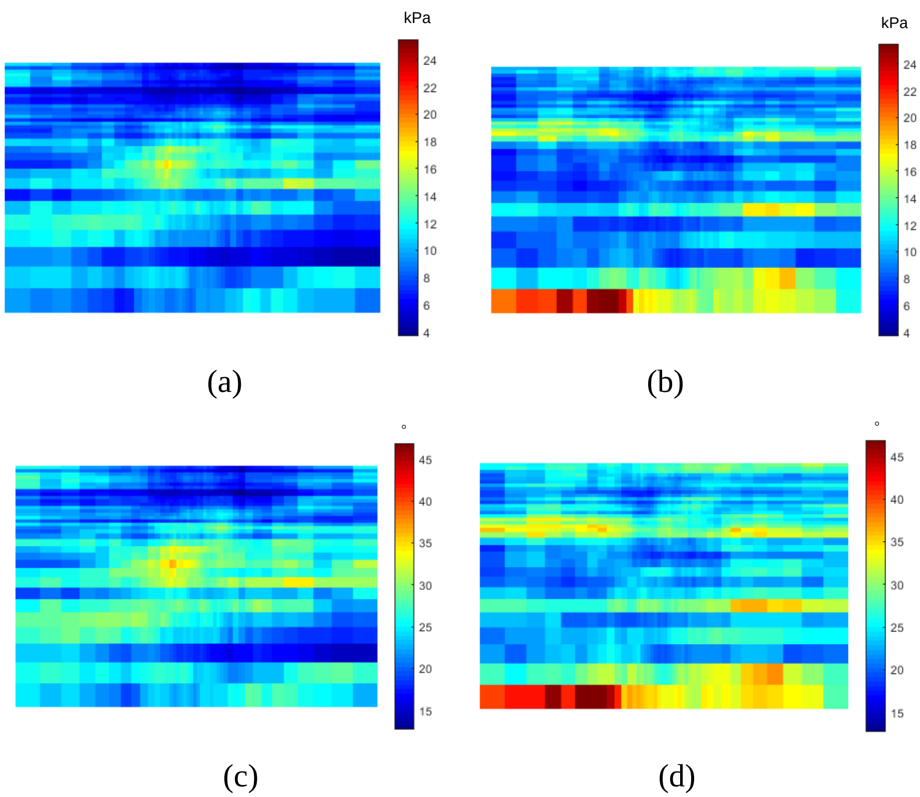

Fig. 6.15 Random fields of c' and ϕ': (a) Random field 1 of c'; (b) Random field 2 of c'; (c) Random field 1 of ϕ'; (d) Random field 2 of ϕ'

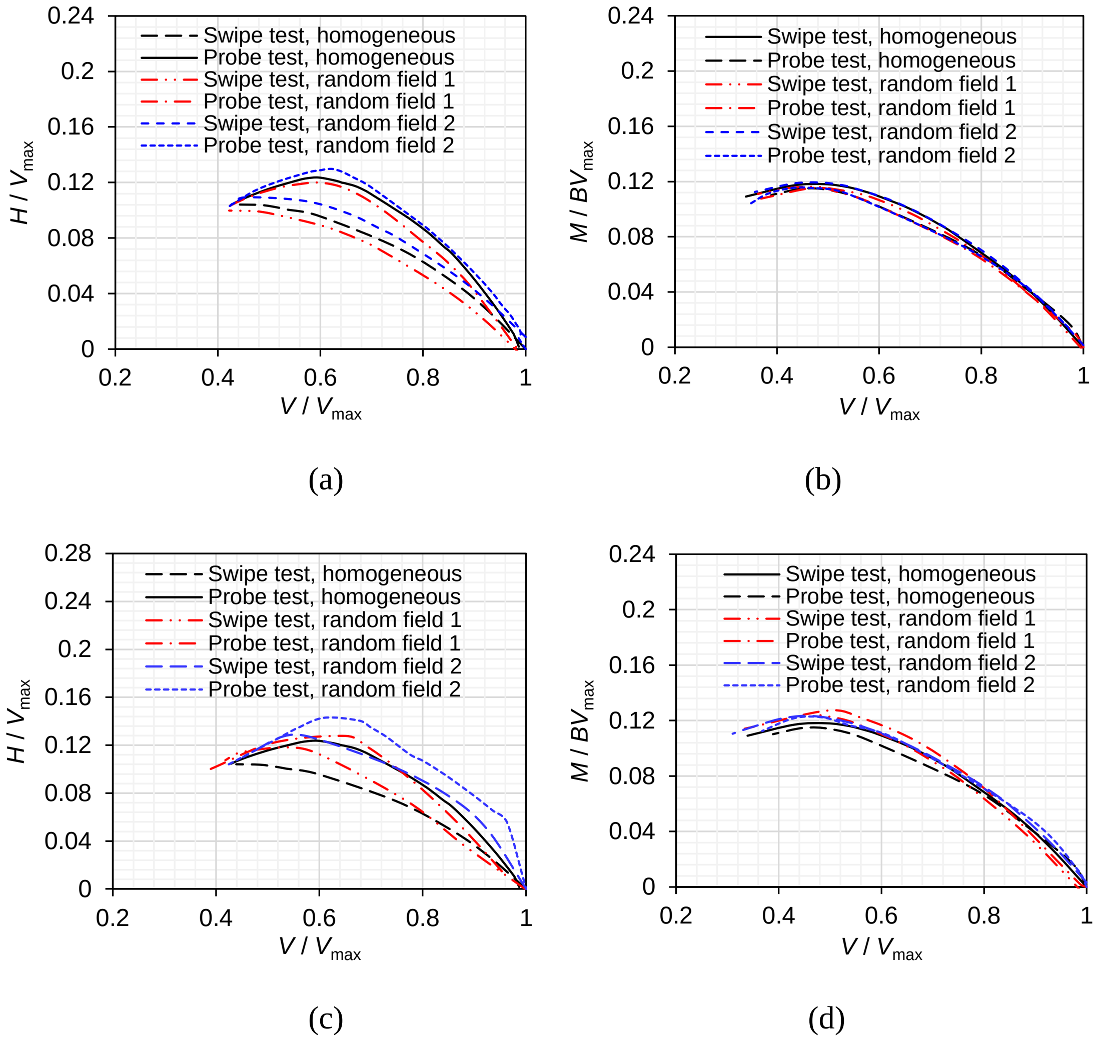

Fig. 6.16 Comparison of normalised failure envelopes: (a) Spatial variability of c' in V – H loading space; (b) Spatial variability of c' in V – M loading space; (c) Spatial variability of ϕ' in V- H loading space; (d) Spatial variability of ϕ' in V- M loading space

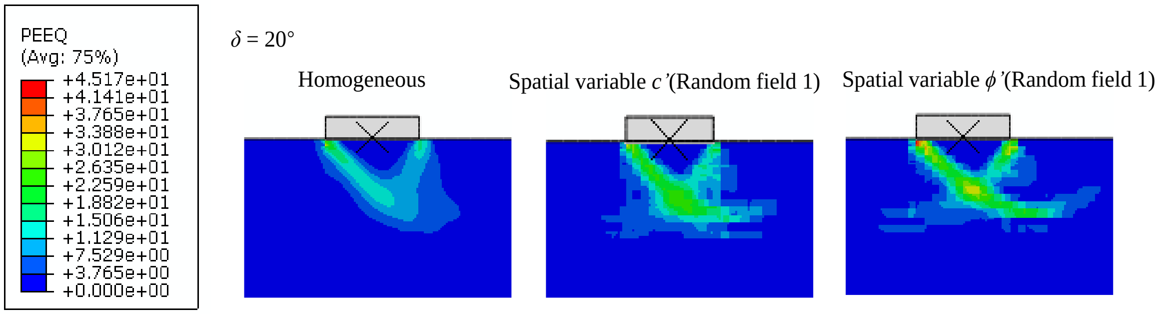

(a)

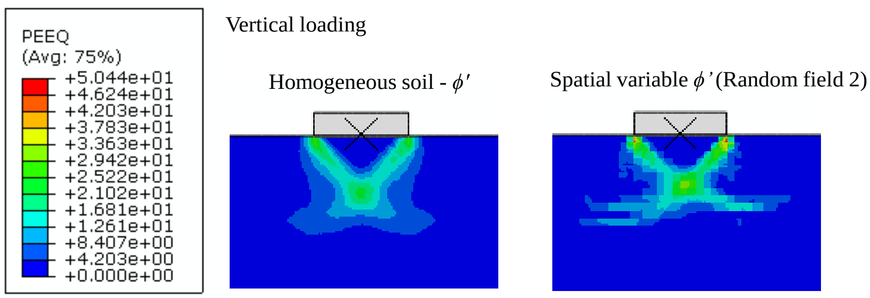

(b)

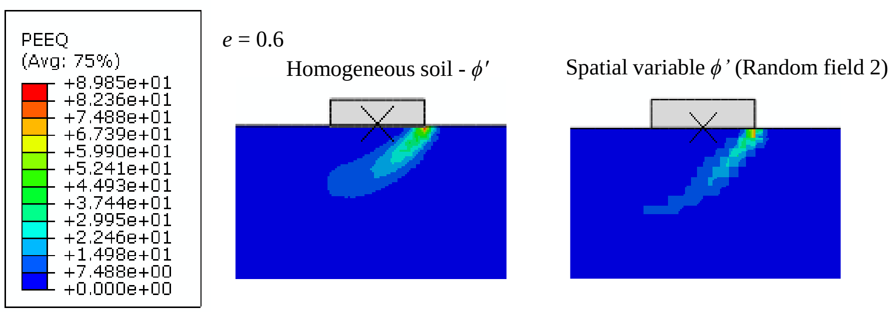

(c)

Fig. 6.17 Comparison of PEEQ obtained from models with and without consideration of soil spatial variability: (a) Inclined loading (δ = 20°); (b) Vertical loading; (c) Eccentric loading (Eccentricity e = 0.6)

Comparison of the failure mechanisms for foundation subjected to inclined and eccentric loading for different soil properties considerations is conducted and shown in Fig. 6.17. The equivalent plastics strain (PEEQ) contour of the foundation subjected to the inclined loading under the hydrostatic condition is shown in Fig. 6.17a. One-side failure mechanism is found for the model that considers homogeneous soil properties. However, the shear plane develops along the weak soil beneath the foundation for models considered the spatial variability of c' and ϕ', respectively. The failure mechanism is not totally developed only one side. This phenomenon is more obvious when considering the spatial variability of ϕ', which is also consistent with the bearing capacity failure envelop in Fig. 6.16c. It is interesting to see in Fig. 6.17b that the failure shear plane extended more towards the soil near the surface when considering the spatial variability of ϕ' for foundation subjected to central vertical loading. The failure mechanism exhibits asymmetric pattern compared to the results obtained in the homogeneous soil. For soil subjected to eccentric loading, the failure mechanisms obtained from models with different soil properties considerations are similar, which corresponds to the less deviation of the failure envelopes in Fig. 6.16d. However, it can be seen in Fig. 6.17c that the failure shear plane extends relative deeper in soil considered the spatial variability.

6.5 Summary and conclusion

In this study, a numerical technique is proposed to investigate the foundation bearing capacity subjected to vertical, inclined and eccentric loading considering the influence of variations in the unsaturated flow conditions (i.e., hydrostatic and transient flow conditions). A user defined subroutine USDFLD is developed for incorporating the variation of the soil properties with the varied matric suction in an unsaturated soil. Code procedure that is developed as a part of this study facilitates to incorporate the soil spatial variability into the FE model. The obtained results from the FE model are used for providing comparisons between the failure envelopes obtained in homogeneous soil and that in soil with spatial variable properties. Several conclusions from these investigations are summarized below:

(1) There is a good agreement between the proposed numerical framework results and the experimental data, the slip line method and semi-empirical equations for predicting the foundation bearing capacity and failure envelops.

(2) One side failure mechanism is observed with an increase in the foundation loading inclination angle and the eccentricity in homogeneous soils for both hydrostatic and transient flow conditions.

(3) The spatial variability of soil effective shear strength parameters: cohesion and internal friction angle have a significant impact on the failure envelop in the *V*- *H* loading space. The effect of spatial variability of the soil saturated hydraulic conductivity on the failure envelope variation is not as obvious as the effective internal friction angle in this study. However, variation of the pore water pressure distribution is observed in the numerical model that consider the soil saturated hydraulic conductivity spatial variability.

(4) Significant variation of the failure mechanism is found between the results obtained from the model with and without considering the spatial variability. The failure mechanism of foundation subjected to central vertical loading exhibits asymmetric pattern when considering the soil spatial variability. For foundation subjected to inclined loading, the yielding zone may extend to both sides of the soil beneath the foundation which is different from the one-side failure mechanism that typically observed for foundation on homogeneous soil subjected to inclined loading; such a

behavior is more distinct in models that consider the spatial variability of the effective internal friction angle.

The results in this study are valuable to understand the influence of the soil spatial variability on the foundation bearing capacity and its failure envelops. It should also be noted that the results presented in this Chapter are obtained considering only a limited number of random fields. Probability analysis for foundation bearing capacity and the bearing capacity failure envelops would provide a more comprehensive information based on more random fields. More random fields can also be generated by considering other assumed COV and scale of fluctuations. The influence of these varied statistics for generating the random field on the foundation bearing capacity in unsaturated soil is also deserves further investigation. Probability analysis combined with the Monte Carlo simulations, Kriging model, random forest technique or other artificial intelligence methods can be used in further investigation studies with large quantity random fields. Such methods can be more efficient and can provide more rigorous and reliable results. In addition, the existing semi-empirical equations for describing the bearing capacity failure envelop in the literature can be modified for incorporating soil spatial variability based on the probability analysis.

Reference

Afsharpour, S., Payan, M., Chenari, R.J., Ahmadi, H., and Fathipour, H. 2022. Bearing capacity of strip footings on unsaturated soils under combined loading using LEM. Geomech. Eng., 31(2), 223. https://doi.org/10.12989/gae.2022.31.2.223

Ali, A., Huang, J., Lyamin, A.V., Sloan, S.W., Griffiths, D.V., Cassidy, M.J., and Li, J.H. 2014. Simplified quantitative risk assessment of rainfall-induced landslides modelled by infinite slopes. Eng. Geol., 179, 102-116.

Averjanov, S.F. 1950. About permeability of surface soils in case of incomplete saturation. *English Collection*, 7, 19-21.

Cho, S.E. 2012. Probabilistic analysis of seepage that considers the spatial variability of permeability for an embankment on soil foundation. Eng. Geol., 133, 30-39.

Cho, S.E. 2014. Probabilistic stability analysis of rainfall-induced landslides considering spatial variability of permeability. Eng. Geol., 171, 11-20.

Fathipour, H., Payan, M., Chenari, R.J., Fatahi, B., 2022a. General failure envelope of eccentrically and obliquely loaded strip footings resting on an inherently anisotropic granular medium. Comput. Geotech. 146, 104734. https://doi.org/10.1016/j.compgeo.2022.104734.

Fathipour, H., Payan, M., Safardoost Siahmazgi, A., Jamshidi Chenari, R., and Senetakis, K. 2022b. Numerical study on the bearing capacity of strip footing resting on partially saturated soil subjected to combined vertical-horizontal-moment loading. Eur. J. Environ. Civ. Eng., 1-34. https ://doi.org/10.1080/19648189.2022.2080769.

Fathipour, H., Tajani, S.B., Payan, M., Chenari, R.J., and Senetakis, K. 2023. Impact of transient infiltration on the ultimate bearing capacity of obliquely and eccentrically loaded strip footings on partially saturated soils. Int. J. Geomech. 23(2), 04022290.

Fei, S., Tan, X., Gong, W., Dong, X., Zha, F., and Xu, L. 2021. Reliability analysis of strip footing under rainfall using KL-FORM. Geomechanics and Engineering, 24(2), 167.

Ganesh, R., Khuntia, S., Sahoo, J.P., 2017. Bearing capacity of shallow strip foundations in sand under eccentric and oblique loads. Int. J. Geomech. 17 (4), 06016028. https://doi.org/10.1061/(ASCE)GM.1943-5622.0000799.

Gardner, W.R. 1958. Some steady state solutions of the unsaturated moisture flow equation with application to evaporation from a water table. Soil Sci. 85, 4, 228–232. https://doi.org/10.1097/00010694-195804000-00006.

Gholampour, A., and Johari, A. 2019. Reliability-based analysis of braced excavation in unsaturated soils considering conditional spatial variability. Comput. Geotech., 115, 103163.

Gottardi, G., and Butterfield, R. 1993. On the bearing capacity of surface footings on sand under general planar loads. Soils and Found., 33(3), 68–79.

Gourvenec, S., and M. Randolph. 2003. Effect of strength nonhomogeneity on the shape of failure envelopes for combined loading of strip and circular foundations on clay. Géotechnique 53 (6): 575–586. https://doi.org/10.1680/geot.2003.53.6.575

Gourvenec, S.M., and Mana, D. S.K. 2011. Undrained vertical bearing capacity factors for shallow foundations. Géotechnique Lett., 1(4), 101-108. https://doi.org/10.1680/geolett.11.00026.

Griffiths, D.V., Fenton, G.A., 2004. Probabilistic slope stability analysis by finite elements. J. Geotech. Geoenviron. 130 (5), 507–518.

Griffiths, D.V., Fenton, G.A., 2007. Probabilistic Method in Geotechnical Engineering. Springer, p. 346.

Gu, X., Ou, Q., Zhang, W., Fu, J., and Hao, S. 2023. A novel subroutine for estimating unsaturated slope stability considering water fluctuation in spatially variable soils. Bull. Eng. Geol. Environ., 82(1), 6.

Hosseini, M., Yaghoobi, B., Ranjbar, P.Z., Payan, M., and Chenari, R.J. 2023. Stability analysis of geosynthetic-reinforced shallow foundations with a lower-bound fela approach adopting the non-associated plastic flow rule. Int. J. Geomech., 23(2), 04022280.

Irmay, S. 1954. On the hydraulic conductivity of unsaturated soils. Trans. Am. Geophys. Union 35:463-467.

Irmay, S. 1971. A model of flow of liquid-gas mixtures in porous media and hysteresis of capillary potential. *In Symposium on mathematical modeling of transport processes in porous media.* Houston, TX. 28 February-4 March. AICHE, New York.

Jiang S.H., Li D.Q., Zhou C.B., and Fang G.G. 2014. Slope reliability analysis considering effect of autocorrelation functions. Chin. J. Geotech. Eng., 36(3), 508-518.

Jin, L., Zhang, H., Luo, C., and Feng, Q. 2021. The implementation of improved radial movement optimization to calculate the ultimate bearing capacity of strip footing on unsaturated soil under inclined loading. Arab. J. Geosci., 14(17), 1-13. https://doi.org/10.1007/s12517-021-08090-3.

Krabbenhoft, S., Damkilde, L., Krabbenhoft, K., 2012. Lower-bound calculations of the bearing capacity of eccentrically loaded footings in cohesionless soil. Can. Geotech. J. 49 (3), 298–310. https://doi.org/10.1139/t11-103.

Krabbenhoft, S., Damkilde, L., Krabbenhoft, K., 2014. Bearing capacity of strip footings in cohesionless soil subject to eccentric and inclined loads. Int. J. Geomech. https://doi.org/10.1061/(ASCE)GM.1943-5622.0000332.

Le, T.M.H., Gallipoli, D., Sanchez, M., and Wheeler, S. 2013. Rainfall-induced differential settlements of foundations on heterogeneous unsaturated soils. Géotechnique, 63(15), 1346-1355.

Li D.Q., Chen Y.F., Lu W.B., Zhou C.B. 2011. Stochastic response surface method for reliability analysis of rock slopes involving correlated non-normal variables. Comput. Geotech.; 38(1):58–68.

Li, D.Q., Jiang, S.H., Cao, Z.J., Zhou, W., Zhou, C.B., and Zhang, L.M. 2015. A multiple response-surface method for slope reliability analysis considering spatial variability of soil properties. Eng. Geol., 187, 60-72.

Li, D.Q., Qi, X.H., Phoon, K.K., Zhang, L.M., and Zhou, C.B. 2014. Effect of spatially variable shear strength parameters with linearly increasing mean trend on reliability of infinite slopes. Struct. Saf., 49, 45-55.

Liao, W., and Ji, J. 2021. Time-dependent reliability analysis of rainfall-induced shallow landslides considering spatial variability of soil permeability. Comput. Geotech., 129, 103903.

Liu, J., Guo, X., and Yi, P. 2023. Probabilistic approach to the stability analysis of caisson foundations under combined loading in spatially variable soil. Appl. Ocean Res., 134, 103509.

Liu, L.L., Cheng, Y.M., and Zhang, S.H. 2017. Conditional random field reliability analysis of a cohesion-frictional slope. Comput. Geotech., 82, 173-186.

Mahmoudabadi, V., and Ravichandran, N. 2023. Reliability-based optimization in climate-adaptive design of embedded footing. Georisk: Assessment and Management of Risk for Engineered Systems and Geohazards, 17(2), 287-309.

Martin, C.M. 1994. Physical and numerical modelling of offshore foundations under combined loads. Doctoral dissertation, Oxford University, UK.

Mehravar, M., O. Harireche, and A. Faramarzi. 2016. Evaluation of undrained failure envelopes of caisson foundations under combined loading. Appl. Ocean Res. 59: 129–137. https://doi.org/10.1016/j.apor.2016.05.001.

Michalowski, R.L., and You, L. 1998. Effective width rule in calculations of bearing capacity of shallow footings. Comput. Geotech., 23(4), 237-253. https://doi.org/10.1016/S0266-352X(98)00024-X.

Mualem, Y. 1986. Hydraulic conductivity of unsaturated soils: prediction and formulas. Methods of soil analysis. Part I, Physical and mineralogical methods.2nd Ed., Agronomy, A. Klute, ed., Am. Soc. Of Agronomy, Inc., and Soil Sci. Soc. Of Am., Inc., Madison, Wis.,799-823.

Ng, C.W., Qu, C., Ni, J., and Guo, H. 2022. Three-dimensional reliability analysis of unsaturated soil slope considering permeability rotated anisotropy random fields. Comput. Geotech., 151, 104944.

Oh, W.T., Vanapalli, S.K., and Puppala, A.J. 2009. Semi-empirical model for the prediction of modulus of elasticity for unsaturated soils. Can. Geotech. J., 46(8), 903-914.

Oh, W.T., Vanapalli, S.K. 2018. Modeling the stress versus settlement behavior of shallow foundations in unsaturated cohesive soils extending the modified total stress approach. Soils Found., 58, 2, 382-397. https://doi.org/10.1016/j.sandf.2018.02.008.

Pham, Q.N., Ohtsuka, S., Isobe, K., Fukumoto, Y., and Hoshina, T. 2019. Ultimate bearing capacity of rigid footing under eccentric vertical load. Soils Found., 59(6), 1980-1991.

Pham, Q.N., Ohtsuka, S., Isobe, K., and Fukumoto, Y. 2020. Limit load space of rigid footing under eccentrically inclined load. Soils Found., 60(4), 811-824.

Pham, Q.N., Ohtsuka, S., Isobe, K., and Fukumoto, Y. 2022. Limit load space of rigid strip footing on cohesive-frictional soil subjected to eccentrically inclined loads. Comput. Geotech., 151, 104956.

Phoon, K.K., and Kulhawy, F.H. 1999. Characterization of geotechnical variability. Can. Geotech. J., 36(4), 612-624.

Qi, S., and Vanapalli, S.K. 2015. Hydro-mechanical coupling effect on surficial layer stability of unsaturated expansive soil slopes. Comput. Geotech., 70, 68-82.

Ravichandran, N., Mahmoudabadi, V., and Shrestha, S. 2017. Analysis of the bearing capacity of shallow foundation in unsaturated soil using Monte Carlo simulation. Int. J. Geosci., 8(10), 1231-1250.

Shen, Z., Bie, S., and Guo, L. 2017. Undrained capacity of a surface circular foundation under fully three-dimensional loading. Comput. Geotech., 92, 57-67. https://doi.org/10.1016/j.compgeo.2017.07.018.

Shwan, B. 2015. Experimental and numerical study of the shear strength of unsaturated sand. Doctoral dissertation, University of Sheffield.

Srivastava, A., Babu, G.S., and Haldar, S. 2010. Influence of spatial variability of permeability property on steady state seepage flow and slope stability analysis. Eng. Geol., 110(3-4), 93-101.

Supachawarote, C., Randolph, M., and Gourvenec, S. 2004, May. Inclined pull-out capacity of suction caissons. *In The Fourteenth International Offshore and Polar Engineering Conference.*

Taiebat, H.A., and J.P. Carter. 2000. Numerical studies of the bearing capacity of shallow foundations on cohesive soil subjected to combined loading. Géotechnique 50 (4): 409–418. https://doi.org/10.1680/geot.2000.50.4.409.

Taiebat, H.A., and J.P. Carter. 2002. Bearing capacity of strip and circular foundations on undrained clay subjected to eccentric loads. Géotechnique 52 (1): 61–64. https://doi.org/10.1680/geot.2002.52.1.61.

Tan X., Dong X., Fei S., Gong W., Xiu L., Hou X., and Ma H. 2020. Reliability analysis method based on KL expansion and its application. Chin. J. Geotech. Eng., 42(5), 808-816.

Tan, M., and Vanapalli, S.K. 2021. Performance estimation of a shallow foundation on an unsaturated expansive soil slope subjected to rainfall infiltration. In MATEC Web of Conferences. Vol. 337, p. 03009. EDP Sciences. https://doi.org/10.1051/matecconf/202133703009.

Tan, M., and Vanapalli, S.K. 2023. Failure envelops for foundation subjected to inclined and eccentric loading considering steady state and transient flow conditions in unsaturated soils. Comput. Geotech., 157, 105315.

Tan, X.H., Xie, Y., Hou, X.L., Li, P., and Wang, X. 2017. Reliability Analysis of Shallow Foundations on Unsaturated Soils under Rainfall Infiltration. In Geo-Risk 2017, pp. 588-597.

Tang, C., Phoon, K.K., and Toh, K.C. 2015. Effect of footing width on N_γ and failure envelope of eccentrically and obliquely loaded strip footings on sand. Can. Geotech. J., 52(6), 694-707.

Vanmarcke, E.H., 1983. Random Fields: Analysis and Synthesis. The MIT Press, Cambridge, MA.

Vulpe, C., S. Gourvenec, and M. Power. 2014. A generalised failure envelope for undrained capacity of circular shallow foundations under general loading. Géotechnique Lett. 4 (3): 187–196. https://doi.org/10.1680/geolett.14.00010.

Wu, L.Z., Xu, Q., and Zhu, J.D. 2017. Incorporating hydro-mechanical coupling in an analysis of the effects of rainfall patterns on unsaturated soil slope stability. Arab. J. Geosci., 10(17), 1-11. https://doi.org/10.1007/s12517-017-3147-1.

Wuttke, F., Kafle, B., Lins, Y., and Schanz, T. 2013. Macroelement for statically loaded shallow strip foundation resting on unsaturated soil. Int. J. Geomech., 13(5), 557-564. https://doi.org/10.1061/(ASCE)GM.1943-5622.0000254.

Yuster, S.T. 1951. Theoretical considerations of multiphase flow in idealized capillary systems. Proc. World Pet. Congr., 3rd 2:437-445.

Zhan, T.L., Ng, C.W., 2004. Analytical analysis of rainfall infiltration mechanism in unsaturated soils. Int. J. Geomech., 4, 4, 273-284. https://doi.org/10.1061/(ASCE)1532-3641(2004)4:4(273).

Zhu, H., and Zhang, L.M. 2013. Characterizing geotechnical anisotropic spatial variations using random field theory. Can. Geotech. J., 50(7), 723-734.

Zhu, H., Zhang, L. M., Zhang, L.L., and Zhou, C.B. 2013. Two-dimensional probabilistic infiltration analysis with a spatially varying permeability function. Comput. Geotech., 48, 249-259.

CHAPTER 7

Conclusions and suggestions for future work

7.1 Major Conclusions

Comprehensive studies are reported in the literature for the design of shallow foundations based on saturated soil mechanics. However, there is still limited understanding related to behavior of shallow foundations in unsaturated soils. The studies that have been undertaken to-date suggest that the matric suction is sensitive to the changes in water content; in addition, it influences other soil properties. The unsaturated flow has a significant impact on the foundation behavior. For this reason, the focus of this thesis has been directed to investigate the foundation behavior considering various scenarios of unsaturated flow conditions that include the hydrostatic state, steady state and transient flow conditions.

In this thesis: analytical methods, semi-empirical equations and numerical method were developed to incorporate the unsaturated flow into the foundation behavior. Comprehensive investigation studies are undertaken to investigate: (i) bearing capacity of foundation on the sloping ground in different types of soils including cracked expansive soils, and (ii) bearing capacity of foundation under the inclined and eccentric loading conditions with homogeneous soil properties and considering spatial variation of soil properties. The proposed method can be incorporated into the calculation tools for rational evaluation of the foundation bearing capacity on both level and sloping unsaturated soil ground. Moreover, the proposed method and the results presented in this thesis provide reliable interpretation and explanation of the foundation behavior at any state during its service life span. The proposed methods also can be used as a forensic tool for providing rigorous back evaluation of the failed foundation or slope.

Major conclusions drawn from the research undertaken in this thesis are summarized below.

7.1.1 State-of-the-art review

Foundation on level ground subjected to vertical loading are extensively investigated in the literature in recent years. These studies highlight that the matric suction is a key parameter that significantly influences the foundation behavior. However, studies related to foundation behavior considering the influence of inclined and eccentric loading in the literature is rather limited. More importantly, there are limited studies related to the foundation behavior under combined (i.e., inclined and eccentric) loading taking account of the flow behavior in unsaturated soil and the spatial variability of the soil properties.

The foundation behavior on slopes in saturated soils have been studied by many scholars comprehensively. The slope geometry, soil properties, foundation position, and foundation loading conditions all have influence on the foundation and slope system. However, limited understanding is found for foundation on sloping ground considering the unsaturated flow.

For the above reasons, innovative models have been developed in this thesis that can provide a better understanding for foundation behavior under different unsaturated flow conditions taking account influence of several parameters.

7.1.2 Foundation bearing capacity estimation on unsaturated soil slope under transient flow condition

An analytical method is proposed for evaluating the foundation bearing capacity on sloping ground of unsaturated soil under the transient flow condition. The method extends the slip line method and incorporates a closed-form solution taking account the transient unsaturated vertical flow conditions. The framework is a first attempt in the literature to combine the slip line method with the transient flow condition towards the evaluation of the foundation bearing capacity. The proposed code procedure was considered reliable for the three comparison studies related to: (i) foundation bearing capacity calculation on sloping ground in saturated soil; (ii) matric suction and effective degree of saturation profiles along with depth; (iii) foundation bearing capacity calculation on level ground in unsaturated soil. Comprehensive parametric studies including the rainfall characteristics, the slope angle, the foundation setback ratio and ground water table depth for different types of soils were conducted with the proposed method. Results suggest that the matric suction and the effective degree of saturation contribution is the predominant factors that influence the foundation bearing capacity. These factors varied during the transient flow conditions depending on the rainfall characteristics, type of soil, soil properties and the initial ground condition. The proposed method can be used as an efficient tool for the estimation of foundation bearing capacity on level and sloping ground of saturated and unsaturated soil.

7.1.3 Failure envelopes for foundation subjected to inclined or eccentric loading considering steady and transient state flow.

An improved and modified analytical method is proposed for evaluating the bearing capacity of foundation subjected to the inclined and eccentric loading. The proposed method extended the slip line theory incorporating with the steady state and transient flow conditions in unsaturated soils; it also included the variation of the soil unit weight variation with the changing water content. Comparison is first conducted between the foundation bearing capacity subjected to inclined and eccentric loading in saturated soil and that from the proposed method. Then the proposed method is further validated with the analytical and experimental results in obtaining the foundation bearing capacity under the hydrostatic, steady state and transient flow conditions. Good agreements had been found for each comparison study. Failure envelopes are then obtained by parametric studies in the $V – H$ and $V – M$ loading spaces using the proposed method, respectively. The influence of the ground water table depths, the flow rates, the infiltration duration, and soil types on the bearing capacity failure envelopes are investigated. The loading inclination angle or the eccentricity have negative effect on the total bearing capacity. The failure envelops in both loading spaces expand during the evaporation condition and shrink under the infiltration condition.

Semi-empirical equations for describing the failure envelops are proposed based on the parametric studies results. Good agreement is found between the results from the proposed equations and that from the slip line methods and published studies. The equation has smooth transition from saturated to unsaturated soil conditions and can be implemented into a calculation tool to build up the failure envelopes efficiently. The two methods proposed in this reasearch can be used in geotechnical engineering practice for the determination of foundation bearing capacity under different loading scenarios and unsaturated flow conditions.

7.1.4 Foundation on cracked expansive soil slope subjected to rainfall infiltration

Numerical technique is used for evaluating the foundation bearing capacity and expansive soil slope stability combined performance. A semi-empirical model which considers the variation of elastic modulus with the matric suction was implemented in the numerical model. The bimodal SWCC is considered in the model for best describing the cracked expansive soil. The numerical model was considered to provide relatively reasonable results based on the comparison studies related to the matric suction profile under the rainfall infiltration, and the bearing capacity evaluation using different methods. Parametric studies were conducted and reveal that higher rainfall intensity contributes to higher reduction rate in the bearing capacity when other parameters are kept constant. The critical factor of safety reduces rapidly under the combined influence of a higher foundation loading and rainfall intensity. The slope surface failure, toe failure, foundation bearing capacity failure and deep-seated failure are observed in the present study based on different combination of the foundation position and rainfall characteristics. It is suggested that the foundation setback ratio should be at least greater than four for the Regina clay and similar types of soils. Moreover, results suggested that when the rainfall intensity is higher than the soil saturated hydraulic conductivity, the drainage measures or other slope stabilization treatments are essential for a stable slope and infrastructures.

7.1.5 Numerical studies on foundation behavior in unsaturated soils subjected to vertical and inclined and eccentric loading

A numerical procedure is developed to simulate the foundation bearing capacity and the bearing capacity failure envelops in the V - H and V - M loading spaces taking account the unsaturated flow. User defined subroutine USDFLD is developed for incorporating the variation of the soil properties with the varied matric suction in unsaturated soil. MATLAB

Code procedure and Python scripts are developed to generate the random field considering the influence of the effective shear strength parameters and saturated hydraulic conductivity and incorporate them into the finite element model, respectively. The proposed procedure for the bearing capacity estimation and failure envelops prediction is compared with the experimental data, slip line method and the semi-empirical equations which achieved good comparison results. The results of the comparison study between the numerical model with and without the soil spatial variability reveal that the soil saturated effective cohesion and effective internal friction angle has significant impact on the failure envelop in the *V*- *H* loading space. The influence of the spatial variability of the soil saturated hydraulic conductivity is not as obvious as the internal friction angle. However, it influences the matric suction distributions. The failure mechanism of foundation subjected to central vertical loading exhibits asymmetric pattern when considering the effective soil shear strength parameters spatial variability. For foundation subjected to inclined loading, the yielding zone may extend to both sides of the soil below the foundation which is different from the one-side failure mechanism that typically observed for foundation on homogeneous soil subjected to inclined loading; this phenomenon is more obvious for the results obtained from models that consider the spatial variability of the effective internal friction angle.

7.2 Suggestions for future work

Suggestions for future research are summarized below:

(1) Extend the proposed analytical method for foundation on layered soils

The soil in nature is typically heterogeneous with different layers or spatial variability due to geomorphological and geological processes such as the sedimentation, the soil weathering, and the soil mineral components variation. Therefore, more comprehensive research for foundations on layered soils is required extending the mechanics of unsaturated soils.

(2) Probability analysis of foundation bearing capacity considering different rainfall characteristics

Though the spatial variability of the soil properties is considered in this thesis, there are still uncertainties for different combination of the soil properties random field and the rainfall characteristics. The numerical techniques proposed in the thesis can be further improved to combine with other high efficiency model such as the Kriging Model, random forest or other artificial intelligence techniques for the probability analysis. The proposed semi-empirical equations for the failure envelop prediction can be modified to fit the probability analysis results.

(3) Investigation of the soil and foundation behavior including the high suction range

The suction range investigation in this study is within the boundary effect zone and transition zone to consider only the influence of matric suction (i.e., capillary stresses) associated with changes in water content in the liquid phase. However, suction can reach high values in expansive soil in arid and semi-arid regions. Therefore, both the influence of capillarity and adsorption should be considered for more rigorous analysis for assessing the foundation behavior over a large range of suction.